Etude de l'implication des cellules microgliales et de l'α-synucleine dans la maladie neurodégénérative de Parkinson

Simon Moussaud

UNIVERSITÉ DE BOURGOGNE

ENVIRONNEMENTS, SANTÉ, STIC
ÉCOLE DOCTORALE DE L'UNIVERSITÉ DE BOURGOGNE

THESE

MICROGLIES ET α-SYNUCLEINE DANS LA MALADIE DE PARKINSON

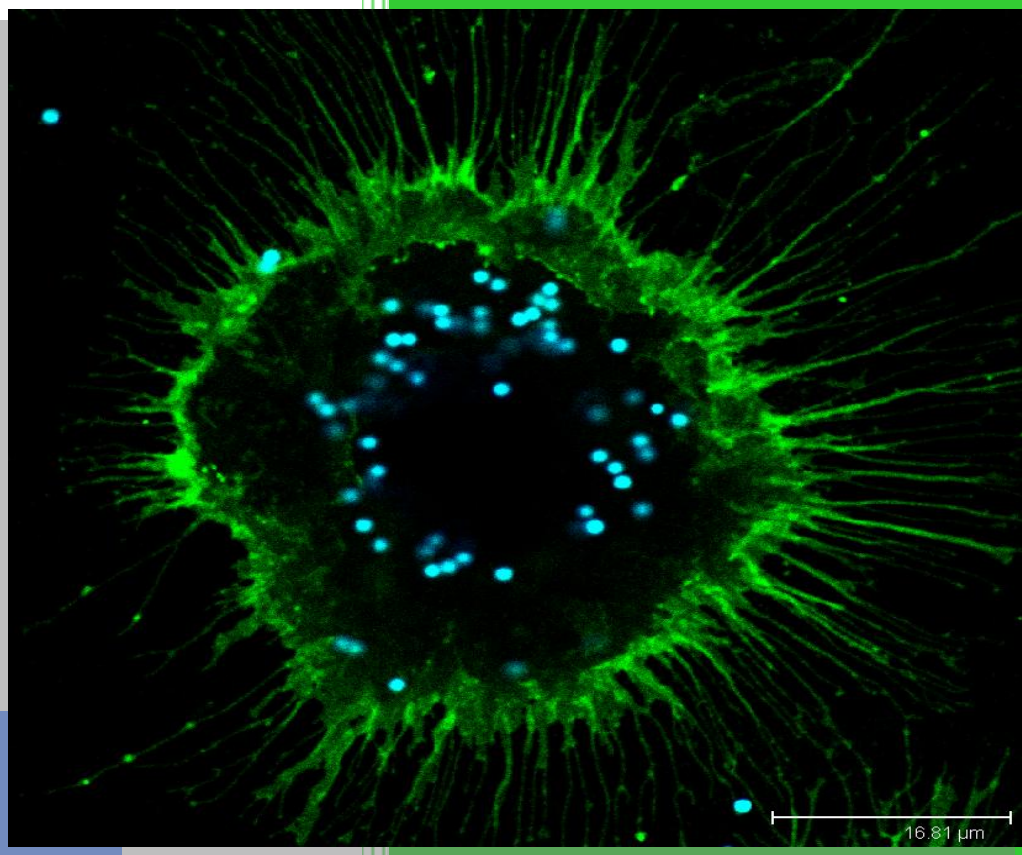

Présentée et soutenue publiquement en 2011 par

Simon Moussaud

Avec le soutien de

Boehringer Ingelheim

Instituts thématiques Inserm
Institut national de la santé et de la recherche médicale

« La vérité scientifique sera toujours plus belle que les créations de notre imagination et que les illusions de notre ignorance. »
Claude Bernard

« On fait la science avec des faits, comme on fait une maison avec des pierres: mais une accumulation de faits n'est pas plus une science qu'un tas de pierres n'est une maison. »
Henri Poincaré

« La science est une chose merveilleuse... tant qu'il ne faut pas en vivre ! »
Albert Einstein

Université de Bourgogne - UFR Sciences de la vie
Ecole doctorale Environnement Santé STIC

THESE pour l'obtention du diplôme de
Docteur en Sciences de l'Université de Bourgogne
Discipline : Biochimie, biologie moléculaire et cellulaire

ETUDE DE L'IMPLICATION DES CELLULES MICROGLIALES ET DE L'α-SYNUCLEINE DANS LA MALADIE NEURODEGENERATIVE DE PARKINSON.

Présentée et soutenue publiquement le 25 février 2011 par

Simon Moussaud

Direction et encadrement de la thèse :

Pr. Johanna Chluba et **Dr. Henning J. Draheim**
INSERM U866,
Lipides Nutrition Cancer,
Equipe mort cellulaire et cancer
Boehringer Ingelheim,
CNS Research,
Parkinson's disease Group

Jury :

Rapporteurs :	Dr. Nancy J. Grant	et
	Dr. Alain Bessis	
Examinateurs :	Pr. Johanna Chluba	et
	Dr. Philippe Garnier	

Contacts

Simon Moussaud
Zeughausgasse 2,
88400 Biberach, Germany
Phone: ++49-151-5535-2741
and
13 avenue du Château
21800 Quetigny, France
Phone: ++33-3.80.46.36.11
Email: moussaudsimon@hotmail.fr

Pr. Johanna Chluba
UFR Sciences de la vie,
Lipides Nutrition Cancer,
Equipe mort cellulaire et cancer,
INSERM U866,
Bâtiment Gabriel
6 boulevard Gabriel
21000 Dijon, France
Phone/Fax: ++33-3.80.39.62.23
Email: johanna.chluba@u-bourgogne.fr

Dr. Henning Joerg Draheim
Boehringer Ingelheim Pharma GmbH & Co. KG
CNS Research
Birkendorfer Strasse 65
88397 Biberach, Germany
Phone: ++49-7351-54-2856
Fax: ++49-7351-54-98928
Email: henning.draheim@boehringer-ingelheim.com

Acknowledgments

First of all, I want to express my gratitude to the CNS research department of Boehringer Ingelheim Pharma GmbH & Co. KG for the financial support and to Pr. Bastian Hengerer for having given me the opportunity to prepare my PhD in his department.

A very special thank you goes to my supervisor at Boehringer Ingelheim, Dr. Henning Draheim, and my supervisor at the University of Burgundy, Pr. Johanna Chluba, for their support, advice and guidance during the three years of my thesis.

I also sincerely thank all my colleagues from the laboratory 6, Doris Linn, Ute Beyrle, Jessica Schad, Ramona Amann, Catherine Savage and Thomas Longden for their excellent assistance and friendship.

I also gratefully acknowledge all the other persons from Boehringer Ingelheim and the University of Burgundy I worked with and without whom my PhD would not have been possible, in particularly Pr. Alain Pugin, Dr. Marcus Kostka, Dr. Karin Danzer, Dr. Stephan Schuster, Elisabeth Lamodière, Patrick Oeckl, Peter Anding, Sabine Finger and Monika Palchaudhuri.

Finally, I would like also to thank Dr. Philippe Garnier and Dr. Valérie Laurens-Callin for having accepted to be part of my progress committee and all the members of the jury for their efforts and time spend.

Abstract

Age-related neurodegenerative disorders like Parkinson's disease take an enormous toll on individuals and on society. Despite extensive efforts, Parkinson's disease remains incurable and only very limited treatments exist. Indeed, Parkinson's pathogenesis is still not clear and research on its molecular mechanisms is ongoing.

In this study, we focused our interest on two abnormal events occurring in Parkinson's patients, namely α-synuclein aggregation and microglial activation.

We first investigated α-synuclein and its abnormal polymerisation. For this purpose, we developed novel methods, which allowed the *in vitro* production of different types of α-synuclein oligomers. Using highly sensitive biophysical methods, we characterised these different oligomers at a single-particle level. Then, we tested their biological effects on neurons.

Afterwards, we studied microglial activation. We concentrated our efforts on two axes, namely age-related changes in microglial function and K^+ channels in microglia. We showed that Kv1.3 and Kir2.1 K^+ channels are involved in microglial activation.

In parallel, we developed a new approach, which allows the effective isolation and culture of primary microglia from adult mouse brains. Adult primary microglia presented subtle but crucial differences in comparison to microglia from neo-natal mice, confirming the hypothesis of age-related changes of microglia.

Taken together, our results support the hypotheses that microglial modulation or inhibition of α-synuclein oligomerisation are possible therapeutic strategies against Parkinson's disease.

Character number: 1592

Key words :

Aging - Neurodegenerative disorders - Parkinson's disease - Neurodegeneration - α-synuclein - Oligomers - Toxicity - Dopamine - Neurons - Neuroinflammation - Microglia - Brain macrophages - Brain immunity - C8-B4 cell line - Primary culture - In vitro *isolation method - Patch-clamp - Electrophysiology - Potassium channels - Kv1.3 - Kir2.1 - Nitric oxide - Cytokines*

Résumé en français

Les maladies neurodégénératives liées à l'âge, telle celle de Parkinson, sont un problème majeur de santé publique. Cependant, la maladie de Parkinson reste incurable et les traitements sont très limités. En effet, les causes de la maladie restent encore mal comprises et la recherche se concentre sur ses mécanismes moléculaires.

Dans cette étude, nous nous sommes intéressés à deux phénomènes anormaux se produisant dans la maladie de Parkinson : l'agrégation de l'α-synucléine et l'activation des cellules microgliales.

Pour étudier la polymérisation de l'α-synucléine, nous avons établi de nouvelles méthodes permettant la production *in vitro* de différents types d'oligomères d'α-synucléine. Grâce à des méthodes biophysiques de pointe, nous avons caractérisé ces différents oligomères à l'échelle moléculaire. Puis nous avons étudié leurs effets toxiques sur les neurones.

Ensuite, nous nous sommes intéressés à l'activation des microglies et en particulier à leurs canaux potassiques et aux changements liés au vieillissement. Nous avons identifié les canaux Kv1.3 et Kir2.1 et montré qu'ils étaient impliqués dans l'activation des microglies.

En parallèle, nous avons établi une méthode originale qui permet l'isolation et la culture de microglies primaires issues de cerveaux adultes. En comparaison à celles de nouveaux-nés, les microglies adultes montrent des différences subtiles mais cruciales qui soutiennent l'hypothèse de changements liés au vieillissement.

Globalement, nos résultats suggèrent qu'il est possible de développer de nouvelles approches thérapeutiques contre la maladie de Parkinson en modulant l'action des microglies ou en bloquant l'oligomérisation de l' α-synucléine.

Nombre de caractères : 1695

Mots-clés :

Vieillissement - Maladies neurodégénératives - Maladie de Parkinson - Neurodégénération - α-synucléine - Oligomères - Toxicité - Dopamine - Neurones - Neuroinflammation - Microglies - Immunité du cerveau - Lignée cellulaire C8-B4 - Cultures primaires - Méthode d'isolation in vitro *- Patch-clamp - Electrophysiologie - Canaux potassiques - Kv1.3 - Kir2.1 - Oxyde nitrique - Cytokines*

Résumé substantiel en français

La recherche contre les maladies neurodégénératives est un enjeu de santé publique car ces maladies touchent une part importante et croissante de la population des pays occidentaux. En effet, la maladie de Parkinson est la deuxième maladie neurodégénérative la plus fréquente après la maladie d'Alzheimer. Aux vues du vieillissement de la population et de l'augmentation de la durée de vie moyenne, ces deux maladies, qui ont l'âge pour principal facteur de risque, vont fortement progresser dans les décennies à venir (www.who.int).

Malheureusement, les causes exactes de la maladie de Parkinson restent encore mystérieuses et bien que très fréquente, la maladie de Parkinson est actuellement encore incurable et les traitements disponibles sont très limités.

La maladie de Parkinson provoque des tremblements et des raideurs musculaires chroniques, des problèmes de contrôle des mouvements et d'équilibre ainsi que divers autres symptômes neuromoteurs et neurologiques. L'origine de ces symptômes est liée à la dégénération des neurones dopaminergiques présents dans une zone précise du cerveau, appelée *substantia nigra pars compacta*. Cette perte anormale et inexpliquée de neurones induit une chute de la stimulation dopaminergique dans le *striatum* et par conséquent une dérégulation des réseaux neuraux du contrôle des fonctions motrices. Quand les symptômes apparaissent, plus de la moitié des neurones dopaminergiques de la *substantia nigra* ont déjà disparu, ce qui rend la rémission difficile. Actuellement, il n'existe d'ailleurs que des traitements palliatifs et aucun traitement curatif ou préventif (Jakobsen and Jensen, 2003).

Les causes exactes de la dégénération des neurones dopaminergiques de la *substantia nigra* restent encore à établir. Un déterminisme génétique est identifié dans seulement 5% des cas (Dauer and Przedborski, 2003; Weintraub *et al.*, 2008). Ces cas héréditaires ont permis la découverte de gènes-cibles impliqués dans la maladie, tels que l'α-synucléine, une petite protéine de 14,5 kDa. Des mutations du gène codant pour l'α-synucléine sont à l'origine de formes héréditaires, autosomiques, dominantes et juvéniles de la maladie de Parkinson (Polymeropoulos *et al.*, 1997; Kruger *et al.*, 1998; Zarranz *et al.*, 2004). L'α-synucléine est essentiellement retrouvée dans les neurones et sa fonction semble être liée au transport vésiculaire synaptique (Bennett, 2005). Cependant, fait étonnant, chez tous les malades de Parkinson, l'α-synucléine forme de grosses inclusions protéiques dans les neurones appelées corps de Lewy (Lewy, 1912; Spillantini *et al.*, 1997). Cette agrégation anormale de l'α-synucléine est observée dans la maladie de Parkinson, mais aussi d'autres maladies neurodégénératives, toutes réunies sous le nom de synucléinopathies (Lavedan, 1998).

En conséquence, la recherche sur l'α-synucléine est cruciale dans la compréhension de la maladie de Parkinson. Bien que très étudiés actuellement, les mécanismes provoquant l'agrégation anormale de l'α-synucléine comportent encore de nombreuses interrogations. Il a été montré que les polymères d'α-synucléine avaient une structure β-amyloïde et qu'ils étaient toxiques pour les neurones. De plus, les polymères d'α-synucléine sont présents sous de nombreuses formes de différentes tailles. Ces différentes formes ne sont pas encore caractérisées dans le détail mais il semble que, contrairement à ce qui était supposé auparavant, ce soient les formes de petite taille nommées oligomères qui soient les plus pathogènes et non pas les fibrilles formant les corps de Lewy (Lashuel *et al.*, 2002; Dev *et al.*, 2003).

Cela étant, pour les cas non héréditaires, c'est-à-dire dans 95% des cas, les causes de la neurodégénération ne sont pas directement liées à un déterminant génétique et restent encore mal comprises (Dauer and Przedborski, 2003; Weintraub *et al.*, 2008). Dans la maladie de Parkinson aussi bien que dans celle d'Alzheimer, une inflammation des tissus cérébraux est observée. Pendant longtemps, la neuroinflammation a été considérée comme étant une conséquence peu importante de la neurodégénération. Mais depuis peu, plusieurs découvertes ont montré que la neuroinflammation avait en réalité un impact important sur la neurodégénération (Whitton, 2007). Dans le cerveau, un type de cellules gliales, les cellules microgliales joue un rôle central dans la régulation de l'immunité et de l'inflammation.

Les cellules microgliales, ou microglies, sont des cellules immunitaires cérébrales d'origine myéloïde. Elles sont 4 à 5 fois plus concentrées dans la *substantia nigra* que dans les autres parties du cerveau. Une fois activées, elles changent de forme et se transforment en macrophages amiboïdes capables de phagocytose. Cette activation est suivie par la sécrétion de radicaux oxygénés comme l'oxyde nitrique et le peroxyde d'hydrogène, de cytokines pro-inflammatoires et pro-apototiques comme l'interleukine 1β et le TNF-α, de chimiokines et d'autres facteurs inflammatoires comme les prostaglandines (Block *et al.*, 2007). Chez les personnes touchées par la maladie de Parkinson, ainsi que chez les modèles animaux utilisés pour la recherche, un nombre anormalement élevé de microglies activées et une forte concentration de marqueurs de l'inflammation sont observés (Croisier *et al.*, 2005). De plus, l'inhibition des processus inflammatoires provoque une résistance accrue à la neurodégénération alors que l'injection dans le cerveau d'un puissant activateur des microglies, le lipopolysaccharide bactérien, induit une forte neurodégénération qui touche particulièrement les neurones dopaminergiques (Liu, 2006). En effet, les microglies semblent être impliquées dans une sorte de cercle vicieux qui aboutit à la neurodégénération massive des neurones dopaminergiques ; une fois activées, les microglies provoquent la mort des neurones et en mourant, les neurones dopaminergiques activent les microglies (Kim and Joh, 2006).

Dans cette étude, nous nous sommes donc intéressés à ces deux phénomènes anormaux se produisant dans la maladie de Parkinson qui sont d'une part l'agrégation de l'α-synucléine et d'autre part l'activation des microglies.

Premièrement, nous nous sommes focalisés sur les oligomères d'α-synucléine et plus généralement sur la faculté qu'a cette protéine de se polymériser pour former différents types de structures (voir article 1). Afin d'étudier la polymérisation de l'α-synucléine, nous avons établi de nouvelles méthodes permettant la production *in vitro* d'oligomères d' α-synucléine. Grâce à des méthodes biophysiques de pointe comme la microsopie à force atomique et l'analyse de distribution d'intensité de fluorescence (FIDA), nous avons caractérisé à l'échelle moléculaire nos différentes préparations d'oligomères d' α-synucléine. Nous avons observé que chacune contenait un mélange hétérogène de différents types d'oligomères d'α-synucléine, certaines formes n'étant présentent que dans certaines préparations.

Puis nous avons étudié les effets biologiques de ces oligomères sur des cultures de neurones. Nous avons ainsi pu observer que les différentes préparations d'oligomères se distinguaient aussi dans leurs effets biologiques. Certains oligomères sont capables d'induire des influx de calcium dans les neurones ainsi que de provoquer une perte du potentiel membranaire, une activation de la caspase 3 et finalement une mort cellulaire, alors que d'autres ont montré l'étonnante capacité de pouvoir se transloquer dans les neurones où, par un effet d'ensemencement, ils étaient en mesure de provoquer l'agrégation massive et rapide de l'α-synucléine intracellulaire (voir article 1). Nos résultats suggèrent que l'α-synucléine est cytotoxique sous forme d'oligomères. Par conséquent, l'inhibition de la formation d'oligomères d'α-synucléine pourrait permettre de bloquer la neurotoxicité induite par l'α-synucléine.

Ensuite, nous nous sommes intéressés aux microglies et à leur rôle dans la neurodégénération. Nous avons ainsi cherché à étudier *in vitro* les microglies et leur activation.

Nous nous sommes concentrés sur les changements liés au vieillissement que semblent subir les microglies et qui pourraient être un élément central dans l'instauration de la neuroinflammation dans les maladies neurodégénératives liées à l'âge. La culture *in vitro* de microglies isolées de tissus adultes n'ayant, à notre connaissance, encore jamais été réalisée, nous avons déjà dû établir une nouvelle méthode pour arriver à ce but (voir article 3). Après un long travail d'optimisation, nous avons réussi à mettre au point un protocole original et efficace, et qui plus est relativement simple, qui permet l'isolation et la culture de microglies primaires issues de cerveaux de souris adultes.

En utilisant des techniques comme l'immunofluorescence, la cytométrie de flux, les tests de phagocytose mais aussi le patch-clamp, l'essai de Griess et l'ELISA multiplexé, nous avons soigneusement comparé ces microglies adultes à leurs homologues issus de nouveaux-nés ainsi qu'à la lignée cellulaire microgliale C8-B4 (voir article 3). En comparaison à celles de nouveaux-nés, les microglies adultes montrent des différences dans leur activation. Bien que subtiles, ces différences n'en sont pas moins cruciales et soutiennent l'hypothèse de changements délétères liés au vieillissement. En effet, chez les microglies adultes, nous avons noté une augmentation de l'activité pro-inflammatoires et pro-apoptotiques et une diminution des effets anti-inflammatoires et neuroprotecteurs.

En parallèle, nous avons étudié les courants et canaux potassiques présents chez les microglies dans le but de mieux comprendre le lien entre leurs caractéristiques électrophysiologiques et le processus d'activation, mais aussi dans le but de chercher une cible moléculaire possible en vue de moduler pharmacologiquement les microglies (voir articles 2 et 3). Grâce à la technique du patch-clamp, mais aussi en utilisant des techniques de biologie moléculaire et de pharmacologie, nous avons réussi à exactement identifier deux canaux voltage-dépendants, Kv1.3 et Kir2.1, comme étant à l'origine des courants potassiques entrant et sortant respectivement. De plus, nous avons caractérisé ces canaux et montré que leur activité était liée à l'activation des microglies.

En conclusion, dans la présente étude, nous apportons de nouvelles données sur la protéine α-synucléine et les microglies et sur leurs impacts respectifs sur la neurodégénération. Nos résultats suggèrent que la modulation de l'activité des microglies ou l'inhibition de l'oligomérisation de l' α-synucléine sont des pistes intéressantes en vue de développer de nouvelles approches thérapeutiques contre la maladie de Parkinson.

Abbreviations

%	(percent or percentage),
±	(plus/minus),
°C	(degrees Celcius),
α	(alpha),
β	(beta),
Δ	(delta or difference),
γ	(gamma),
K	(kappa),
λ	(lambda or wavelength),
µ	(micro),
Ω	(omega or ohm),
4-AP	(4-aminopyridine),
AFM	(atomic force microscopy),
BSA	(bovine serum albumin),
Ca^{2+}	(calcium),
CD	(cluster of differentiation),
CI	(interval of confidence),
Cl^-	(chloride),
CNS	(central nervous system),
COMT	(cathechol-O-methyl transferase),
DC-EBIO	(5,6-dichloro-1-ethyl-1,3-dihydro-2H-benzimidazole-2-one),
DIV	(days *in vitro*),
DMEM	(Dulbecco's modified Eagle's medium),
DMSO	(dimethyl-sulphoxide),
DNA	(desoxyribonucleic acid),
EDTA	(ethylene diamine tetraacetate),
EGTA	(ethylene glycol-bis(2-amino ethylether)-N,N,N′,N′-tetraacetate),
FBS	(foetal bovine serum),
FCS	(fluorescence correlation spectroscopy),
FIDA	(fluorescence intensity distribution analysis),
FLIPR	(fluorescent imaging plate reader),
GalC	(galactocerebroside),
GAPDH	(glyceraldehyde 3-phosphate dehydrogenase),
GFAP	(glial fibrillary acidic protein),
GM-CSF	(granulocyte and macrophage colony stimulating factor),
H-7	(1-(5-isoquinolinesulfonyl)-2-methylpiperazine),
HBSS	(Hank's balanced salt solution),
HEPES	(4-(2-hydroxyethyl)piperazine-1-ethanesulfonic acid),
Genistein	(4',5,7-trihydroxyisoflavone),
IB_4	(isolectin B_4 from *Griffonia simplicifolia*),
IFN-γ	(interferon gamma),
IK	(intermediate conductance calcium-activated channels),
IL	(interleukin),
iNOS or NOS2	(inducible nitric oxide synthase),
K^+	(potassium),
KC	(keratinocyte chemoattractant),
Kir	(inwardly-rectifying K^+ channel),
Kv	(voltage-dependent K^+ channel),
L-DOPA	(L-3,4-dihydroxyphenylalanine),
LRRK2	(leucin-rich repeat kinase 2),
LPS	(bacterial lipopolysaccharides),
M	(molar or mega),
m	(meter or milli),
MAO	(monoamine oxidase),
MHC	(major histocompatibility complex),
MFI	(mean of fluorescence),
MPP^+	(1-methyl-4-phenylpyridinium),
MPTP	(1-methyl-4-phenyl-1,2,3,6-tetrahydropyridine),
MWCO	(molecular weight cut-off),
n	(nano),
Na^+	(sodium),
NeuN	(neuron nuclei),
NO	(nitric oxide),
PBS	(phosphate-buffered saline),
PET	(positron emission tomography),
RFU	(relative fluorescence unit),
RNA	(ribonucleic acid),
RT	(room temperature),
ROS	(reactive oxygen species),
SD	(standard deviation),
SEM	(standard error of the mean),
SK	(small conductance calcium-activated channels),
TGF-β	(transforming growth factor beta),
TH	(tyrosine hydroxylase),
TNF-α	(tumour necrosis factor alpha),
TRAM-34	(1-[(2-chlorophenyl)diphenylmethyl]-1H-pyrazole),
wt	(wild-type = non-mutated),

Tables of contents

I. Foreword - 18 -

II. General introduction - 20 -

1. Parkinson's disease - 20 -
   - *1.1. Opening remarks on neurodegenerative diseases* - 20 -
   - *1.2. Parkinson's disease: an increasing society burden* - 20 -
   - *1.3. History of the research on Parkinson's disease* - 21 -
   - *1.4. Clinical symptoms of Parkinson's disease* - 23 -
   - *1.5. Aetiology and pathophysiology of Parkinson's disease* - 24 -
   - *1.6. Therapeutic strategies and research axes* - 28 -
   - *1.7. The α-synuclein pathoprotein* - 31 -
2. Glia and brain immunity - 35 -
   - *2.1. Opening remarks on glial cells* - 35 -
   - *2.2. Discovery and renaissance of glial cells* - 36 -
   - *2.3. Immunity of the brain* - 37 -
   - *2.4. Origins, characteristics and functions of microglia* - 38 -
   - *2.5. Microglial activation* - 40 -
   - *2.6. Electrophysiological characteristics of microglial cells* - 42 -
   - *2.7. Involvement of microglia in neurodegeneration* - 45 -
3. Problematic, strategies and aims - 49 -
   - *3.1. Aim 1: To study α-synuclein oligomerisation and its biological effects.* - 49 -
   - *3.2. Aim 2: To define the electrophysiological characteristics of microglia.* - 49 -
   - *3.3. Aim 3: To determine age-related changes in microglial activation.* - 50 -
   - *3.4. Aim 4: To investigate the link between microglial activation and Parkinson's disease.* - 50 -

III. Results and discussion - 51 -

1. α-synuclein oligomers (article 1) - 51 -
   - *1.1. Résumé en français* - 51 -
   - *1.2. Foreword* - 52 -
   - *1.3. Summary* - 52 -
   - *1.4. Introduction* - 53 -
   - *1.5. Materials and Methods* - 54 -
   - *1.6. Results* - 60 -
   - *1.7. Discussion* - 74 -
   - *1.8. Supplemental materials* - 78 -
     - 1.8.1. Supplemental figures - 78 -
     - 1.8.2. Supplemental videos - 80 -
   - *1.9. Acknowledgments* - 80 -
2. Electrophysiological characterisation of microglia (article 2) - 81 -
   - *2.1. Résumé en français* - 81 -
   - *2.2. Foreword* - 82 -
   - *2.3. Abstract* - 82 -
   - *2.4. Introduction* - 83 -
   - *2.5. Materials and Methods* - 85 -
   - 2.6. *Results* - 87 -
   - *2.7. Discussion* - 95 -
   - *2.8. Acknowledgments* - 99 -
3. A new method to isolate microglia of aged animals (article 3) - 101 -
   - *3.1. Résumé en français* - 101 -
   - *3.2. Foreword* - 102 -

3.3. Abstract _____ *- 102 -*
3.4. Introduction _____ *- 103 -*
3.5. Materials and Methods _____ *- 105 -*
3.6. Results _____ *- 109 -*
3.7. Discussion _____ *- 119 -*
3.8. Acknowledgments _____ *- 122 -*
3.9. Supplemental materials _____ *- 122 -*
3.9.1. Supplemental material 1 _____ - 122 -
3.9.1. Supplemental material 2 _____ - 122 -

IV. Final conclusions and perspectives _____ - 125 -

1. α-synuclein _____ - 126 -
2. Electrophysiology of microglia _____ - 128 -
3. *In vitro* modelling of aged microglial functions _____ - 130 -
4. Microglia and Parkinson's disease _____ - 132 -
5. Future directions _____ - 136 -

V. References _____ - 138 -

VI. Appendices _____ - 146 -

List of figures

II. General introduction - 20 -

Figure 1: Two centuries of research on Parkinson's disease. - 22 -
Figure 2: Brain areas and neural networks affected in Parkinson's disease. - 25 -
Figure 3: Disease's progression into the brain. - 26 -
Figure 4: Dopaminergic synapse and dopamine metabolism. - 29 -
Figure 5: Lewy bodies and Lewy neurites. - 31 -
Figure 6: α-synuclein structures. - 33 -
Figure 7: Glia are composed of different cell types. - 35 -
Figure 8: Glia cells represented by earlier investigators. - 36 -
Figure 9: Distribution of microglia in the brain. - 40 -
Figure 10: Electrophysiology and patch-clamp. - 42 -
Figure 11: Microglia express different ion currents. - 44 -
Figure 12: PET imaging of microglial activation. - 46 -
Figure 13: Neuroinflammation and neurodegeneration draw a self-propelling vicious circle. - 47 -

III. Results and discussion - 51 -

- Article 1: α-synuclein oligomers - 51 -

Figure 1: Characterization of long-term incubation of α-syn oligomers (types A1 and A2). - 61 -
Figure 2: Characterization of α-syn oligomer types B1 and B2 generated with stirring bars. - 62 -
Figure 3: Characterization of α-syn oligomers (types C1 and C2). - 62 -
Figure 4: [Ca^{2+}] elevation by α-syn oligomer types A1 and A2 in SH-SY5Y cells. - 65 -
Figure 5: [Ca^{2+}] elevation by α-syn oligomer types A1 and A2 in primary neurons. - 65 -
Figure 6: Depolarization of membrane potential induced by oligomer types A1 and A2. - 67 -
Figure 7: α-Syn oligomer types A1 and A2 induced intracellular [Ca^{2+}] increase *via* influx of extracellular [Ca^{2+}] sources. - 68 -
Figure 8: Toxicity of α-syn oligomer types A1 and A2. - 70 -
Figure 9: Seeding effect of α-syn oligomer types B1 and B2. - 72 -
Figure 10: Seeding effect of α-syn oligomer types C1 and C2. - 73 -
Supplemental figure 1: AFM image of monomeric α-syn. - 78 -
Supplemental figure 2: Expression levels of α-syn in SH-SY5Y cells. - 78 -
Supplemental figure 3: [Ca^{2+}] elevation by α-syn oligomers type A1 and A2 in SH-SY5Y cells. - 79 -
Supplemental figure 4: [Ca^{2+}] elevation by α-syn oligomers type A1 and A2 in primary cortical neurons. - 79 -
Supplemental figure 5: α-syn fibrils. - 80 -

- Article 2: Electrophysiological characterisation of microglia - 81 -

Figure 1: Comparison of voltage-dependent K^+ currents in primary microglia and the C8-B4 cell line. - 87 -
Figure 2: Characterisation of the voltage-dependent inward rectifying K^+ current. - 88 -
Figure 3: Pharmacological characterisation of the voltage-dependent outward K^+ current. - 89 -
Figure 4: The outward K^+ current of C8-B4 cells is cumulatively inactivated. - 91 -
Figure 5: Molecular characterisation of K^+ channels in C8-B4 microglia. - 92 -
Figure 6: Inward and outward rectifying K^+ currents are modulated in response to cell activation and protein kinase activity. - 94 -

- Article 3: A new method to isolate microglia of aged animals - 101 -

Figure 1: Schematic procedure workflow for isolation of microglia from an adult mouse. - 110 -
Figure 2: Quantity and purity of the collected cells. - 111 -
Figure 3: Immuno-fluorescence pictures of adult primary microglia (A-F) performed with a confocal microscope. - 113 -
Figure 4: Functional characterisation of the adult microglia in comparison with other microglial models. - 116 -
Figure 5: Electrophysiological and pharmacological characterisation of voltage-dependent K^+ currents in adult microglia. - 118 -
Supplemental material 1: Immuno-phenotype characterisation by flow cytometry. - 123 -

IV. Final conclusions and perspectives - 125 -

Figure 1: Microglia and α-synuclein oligomers. - 133 -
Figure 2: Is α-synuclein able to activate microglial cells? - 135 -
Figure 3: LRRK2 and microglia: a novelty. - 135 -

List of tables

II. General introduction - 20 -

Table 1: List of the *park* genes. - 27 -

III. Results and discussion - 51 -

- Article 1: α-synuclein oligomers - 51 -

Table 1: Different types of α-syn oligomers. - 74 -

- Article 2: Electrophysiological characterisation of microglia - 81 -

Table 1: Primers used in reverse transcription PCR. - 86 -

Table 2: Comparison of activated and unstimulated C8-B4 microglia. - 97 -

- Article 3: A new method to isolate microglia of aged animals - 101 -

Table 1: Immuno-phenotype characterisation by flow cytometry. - 108 -

I. Foreword

My PhD thesis has been conducted from 2007 to 2010 under the direction of Dr. Henning Draheim, Laboratory head at Boehringer Ingelheim Pharma GmbH & Co. KG in the central nervous system (CNS) department, and Pr. Johanna Chluba, Laboratory head at the University of Burgundy, INSERM U866. The major part of my research work took place in the CNS research department of the pharmaceutical company Boehringer Ingelheim in Biberach an der Riss (Germany).

The CNS research department of Boehringer Ingelheim is composed of three groups, each one focusing on a major therapeutic area, namely Parkinson's disease, Alzheimer's disease and chronic pain. With a view to developing new treatments, the CNS department is working on new therapeutic strategies. To dynamise innovation and to explore new therapeutic areas, the CNS department is actively interested in basic research. Consequently, the CNS department has developed numerous collaborations with universities and welcomes PhD students in many of its own research teams.

I was integrated in the Parkinson's disease research department headed by Pr. Bastian Hengerer and more precisely in the laboratory 6 headed by Dr. Henning Draheim. The laboratory 6 is specialised in *in vitro* basic research, particularly in cell culture and electrophysiology. Additionally, during my PhD, I had the chance to get free access to the other laboratories of the department and I have to say that it was great to have such an easy access to powerful, rare and expensive devices, innovating techniques and competent experts.

My PhD project was focused on two major topics: α-synuclein and microglia. I first worked in collaboration with Dr. Karin Danzer on the α-synuclein protein and its role on Parkinson's disease. Our aims were to control *in vitro* α-synuclein oligomerisation, to characterise the different forms of α-synuclein oligomers and finally to examine their biological

effects on neurons. During this period, our interests shifted from neurons to microglial cells and we decided to explore the implications of microglia on Parkinson's pathogenesis and more generally in neurodegenerative processes. Our aims were first to establish an *in vitro* microglial model and then to study microglial activation. We were particularly interested in the electrophysiological characterisation of microglial cells and the regulation of their ion channels according to their activation state.

During the last three years, I strove to achieve a better understanding and additional know-how but also a real expertise in these fields. The present manuscript exposes and highlights the results of my PhD work. It is composed of three major parts:

- Firstly, in a comprehensive introduction, I will provide an overview of the scientific background and the current knowledge about Parkinson's disease, α-synuclein and microglia and I will introduce the problematic and research approaches of my PhD thesis.

- Secondly, I will present and discuss the results of experiments on α-synuclein oligomerisation and toxicity, and on *in vitro* experiments on microglia in the form of three peer-reviewed publications.

- Finally, I will summarize and discuss the novel original data that we have gained regarding these topics and the possible next steps of this interesting project.

II. General introduction

1. Parkinson's disease

1.1. Opening remarks on neurodegenerative diseases

Neurodegenerative disorders constitute a group of severe neurological diseases characterised by progressive nervous system dysfunctions. These nervous system dysfunctions are directly linked to the loss of neurons in specific brain areas. Depending on the brain area and the affected neuron type, different impairments of particular body activities occur. For example, loss of memory and cognitive function are the hallmark of Alzheimer's disease, whereas involuntary tremors and the loss of control of motor activities are the main symptoms of Parkinson's disease. Additionally to these two principal neurodegenerative disorders, numerous different others syndromes exist: Huntington's disease, amyotrophic lateral sclerosis, multiple sclerosis, corticobasal degeneration, multiple system atrophy, progressive supranuclear palsy, dementia with Lewy bodies... At present, there are no disease-modifying treatments available for most of the above listed diseases.

1.2. Parkinson's disease: an increasing society burden

Age-related neurodegenerative disorders - and in particular Parkinson's disease - are an increasing public health problem. After Alzheimer's disease, Parkinson's disease is the second most frequent neurological disease but to date, there is no cure for both diseases. In France, the incidence of Parkinson's disease is between 16 and 19 per 100 000 people per year while the prevalence is estimated to be around 160 per 100 000 people per year. Worldwide, around 65 million Parkinson's cases are estimated and the WHO has predicted that by 2040 neurodegenerative diseases will overtake cancer to be the world's second cause of disease after cardiovascular diseases (www.who.int).

The overwhelming progression of Parkinson's and Alzheimer's diseases incidences is directly linked with the demographic aging and the augmentation of the life expectancy. Indeed for both diseases, the major risk factor is aging. The usual age of onset is the early 60's and the incidence and prevalence of Parkinson's disease increase with age, occurring in more than 1% of the people over the age of 65 and increasing to 4-5% by the age of 85 (deRjik *et al.*, 2000; Weintraub *et al.*, 2008).

Furthermore, Parkinson's disease is generally long-lasting and disabling. It highly affects the quality of life, the mobility and the self-sufficiency of the patients. Consequently, this disease requires constant medical accompaniment, which leads to substantial healthcare expenses. Taking all these facts together and considering the demographic projections and the constant increase of life expectancy, neurodegenerative disorders will pose a significantly increasing burden for society and represent a real challenge for the future.

1.3. *History of the research on Parkinson's disease*

Scientific research on Parkinson's disease started with the following milestone: "An Essay on the Shaking Palsy" published in 1817 by the english physician Dr James Parkinson (Figure 1). Indeed, this essay is the first precise description of the parkisonian syndrome in the scientific and medical literature. But it is only one century later that the french neurologist Jean-Martin Charcot defined the shaking palsy observed by James Parkinson as a distinct syndrome and named it "Parkinson's disease". Later, in the 1950's the biochemical and molecular mechanisms of neurotransmission in the brain were unraveled. In particular, the 2000 Nobel prize laureate Pr. Arvid Carlsson largely contributed to the discovery of the dopamine-mediated neurotransmission and the development of L-DOPA (L-3,4-dihydroxyphenylalanine) for symptomatic treatment of Parkinson's disease. L-DOPA is a dopamine precursor (Figure 4) and is still the gold standard for symptomatic Parkinson's treatment. L-DOPA was firstly marketed in 1973 by Roche under the commercial name "modopar". Subsequently, L-DOPA entered in the composition of other dopamine replacement drugs, such as levodopa, atamet, stalevo, sinemet and duodopa. Interestingly, in the ancient traditional ayurvedic indian medicine, seeds from the

plant *Mucuna pruriens* were used to efficiently treat Parkinson's disease (Kampatava in sanskrit). Surprisingly, it has been recently discovered that this beans contain large amounts of L-DOPA (Manyam and Sánchez-Ramos, 1999)!

However, although Parkinson's disease has been known worldwide since ages, and although it has been the object of intense research during the two last centuries, this disease is still incurable and far away from being fully understood.

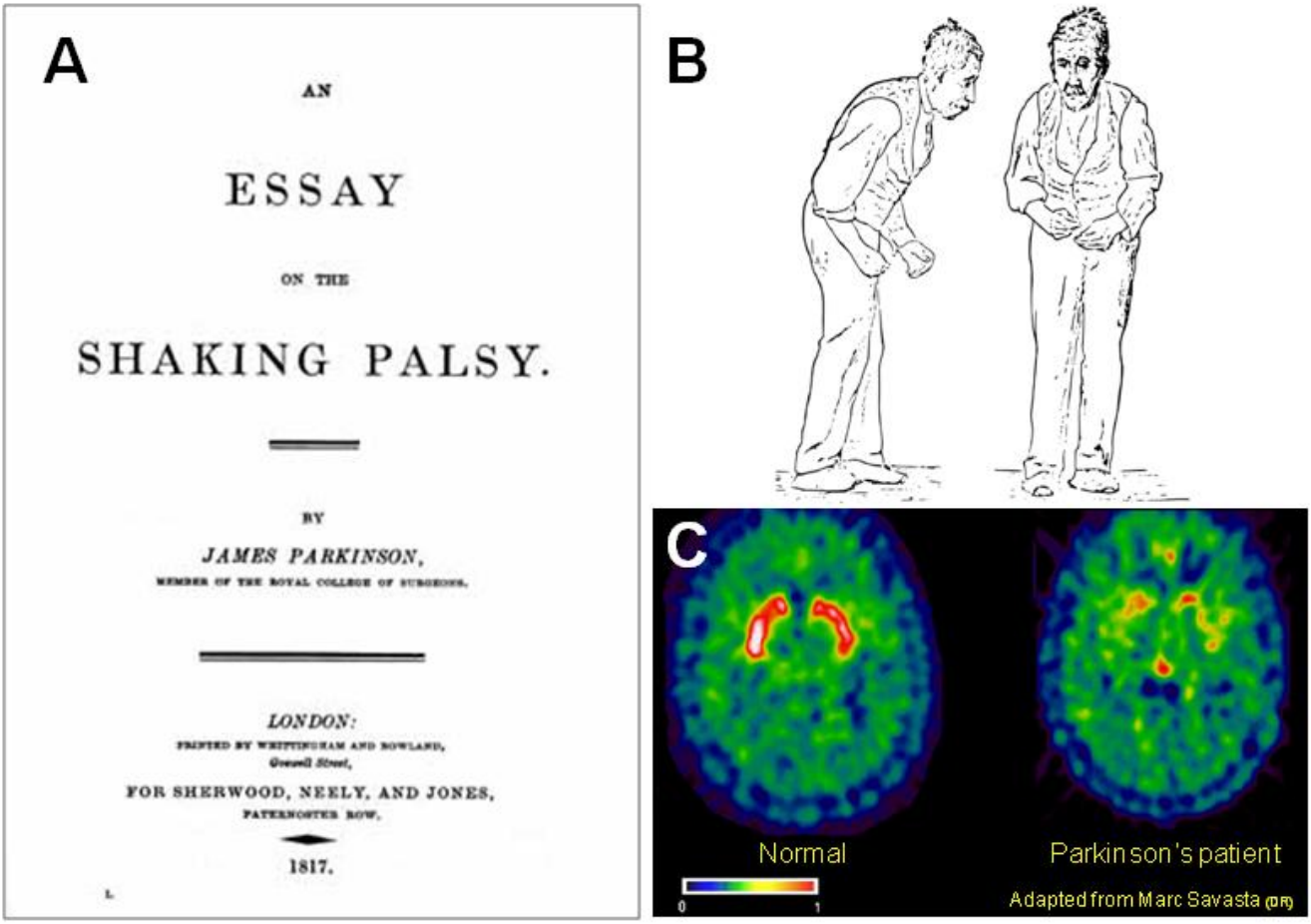

Figure 1: Two centuries of research on Parkinson's disease.
A) The first scientific description of Parkinson's disease was performed by James Parkinson in 1817. ***B)*** Illustration extracted from "A manual of disease of the nervous system" by Sir William Richard Gowers in 1886 representing a Parkinson's patient in a characteristic disease-induced posture. ***C)*** Pictures of transverse brain sections, captured by positron emission tomography and with the [^{18}F]-DOPA marker, showing dopaminergic neuron loss in the brain of a Parkinson's patient (right panel) in comparison to a healthy person (left panel). A pseudocolour rainbow scale is used to represent dopaminergic neurones presence; warmer colours correspond to high dopaminergic neuron density (image adapted from Marc Savasta).

1.4. *Clinical symptoms of Parkinson's disease*

The manifestation and progression of the clinical symptoms of Parkinson's disease are variable in function of the individual and the disease stage and can be spread over decades. Generally, Parkinson's disease causes progressive and asymmetrical impairment of the motor capacities by affecting control of the muscles. These disabling motor disorders are termed "parkinsonism" (Lang and Lozano, 1998; Dauer and Przedborski, 2003; Weintraub *et al.*, 2008). Commonly, they consist in resting muscle tremor, such as head and arm tremor, but also rigidity, slowness (bradykinesia), absence of normal unconscious movement, inability to initiate movement (akinesia), gait disturbances, loss of postural reflexes, balance problems, a characteristic postural position (Figure 1 B) and a reduced facial expression (hypomimia).

These primary symptoms can also be accompanied by secondary non-motor symptoms, which are significant contributors to disability and to life quality worsening. The non-motor symptoms may vary according to the individual and the disease stage and are not always directly linked with Parkinson's pathology. Comorbid non-motor symptoms include mood alterations, such as depression, anxiety, apathy but also cognitive impairments, such as confusion, speech problems, dementia, and also various other disorders, such as freezing, swallowing difficulties, sleep perturbations, sexual dysfunction, bladder dysfunction, constipation, blood pressure problems, pain signalling impairment and loss of olfactory sense (Lang and Lozano, 1998; Weintraub *et al.*, 2008). Interestingly, the loss of olfactory sense is used as test for diagnosis because is it one of the first clinical symptoms that appears even before tremors (Doty *et al.*, 1995).

The diagnosis for Parkinson's disease is based on the observation of clinical symptoms, neurological examinations and responsiveness to anti-parkisonism drugs. However, misdiagnoses and confusion with other illnesses, such as essential tremor, progressive supra nuclear palsy, medication induced parkinsonism, normal pressure hydrocephalus are frequent. Moreover, Parkinson's disease includes different forms and other neurological impairments, such as Alzheimer's disease, multiple system atrophy can coexist. For all the aforementioned

reasons and due to the lack of early, objective and unerringly diagnosis tests, Parkinson's disease is still difficult to diagnose.

Although it is not possible to halt or slowdown progression of the disease, symptomatic palliative treatments against parkinsonism can provide efficient relief from the various symptoms and significantly improve the quality of life. However, some drugs also induce problematic secondary effects. For example, L-DOPA treatment induces with time motor complications, such as motor fluctuations or wearing-off effect (succession of periods of good mobility control followed by periods of severe motor dysfunction), dyskinesia (involuntary movements) and sometimes hallucinations. Dopaminergic agonists can induce nausea, insomnia and compulsive/obsessive cravings, such as pathological gambling, hypersexuality, impulsive shopping or eating. Part of these secondary effects can be prevented by medication optimization or by additional pharmacological treatments.

Although Parkinson's patients have a shortened life expectancy, Parkinson's disease is only seldom directly lethal because death is typically caused by secondary complications, such as pneumonia or cardiovascular problems. Furthermore, Parkinson's disease is a slow-progressing disease and its onset starts in advance-aged persons.

1.5. Aetiology and pathophysiology of Parkinson's disease

The primary parkisonian symptoms are directly linked to the abnormal neurodegeneration of the pigmented dopaminergic neurons (Figure 1 C) localised in a midbrain area called the *substantia nigra pars compacta* or "black substance" (Figure 2) (Jakobsen and Jensen, 2003). These dopaminergic neurons project their axons into the striatum, thus forming the dopaminergic nigrostriatal pathway. The nigrostriatal pathway is divided into direct and indirect pathways. Both together form a kind of balance, which is crucial in movement control. The disappearance of dopaminergic neurons of the *substantia nigra* induces a decline of striatal dopamine stimulation. This reduction of dopaminergic stimulation increases the excitation of the indirect pathway while it increases the inhibition of the direct pathway. This imbalance finally leads to an increased inhibition of the ventral anterior nucleus of the thalamus and a decreased excitation of the motor cortex (Figure 2).

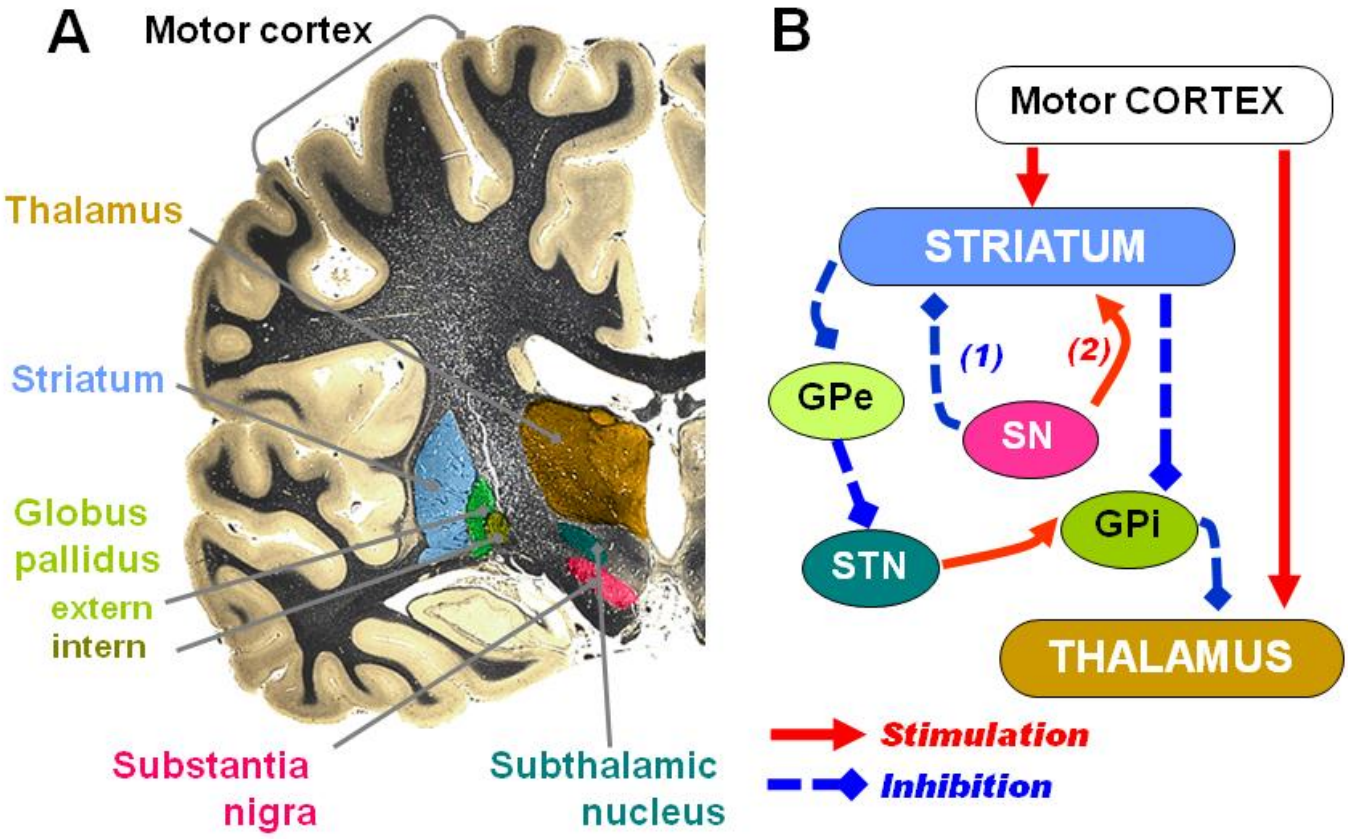

Figure 2: Brain areas and neural networks affected in Parkinson's disease.
A) Coronal slice of a human brain highlighting the major brain areas involved in movement control. ***B)*** Schematic cartoon illustrating the connectivity between the different brain areas involved in the control of motor functions. In the brain of a Parkinson's patient in comparison with a healthy person, the *substantia nigra* (SN) has degenerated leading to the reduction of indirect pathway (1) and the direct pathway (2). STN: *subthalamic nucleus*, GPe and GPi: *globus pallidus* extern and intern, respectively.

Parkinson's disease is characterised by a prolonged asymptotic phase (Figure 3). Indeed, when the tremor appears, more than half of the dopaminergic neurons of the *substantia nigra* have already disappeared. However, the *substantia nigra* is not the only brain area affected by Parkinson's disease (Braak *et al.*, 2003 and 2004). Actually, an ascending disease progression in the brain is hypothesised (Figure 3). In the early stages of the disease, the olfactory bulbs and the lower brain stem are the first affected regions. Then, the basal forebrain, transentorhinal cortex and CA2 region of the hippocampus are also affected. In later stages, almost all regions seem to be affected (Figure 3). This generalisation of neurodegeneration leads to the aforementioned non-motor secondary symptoms.

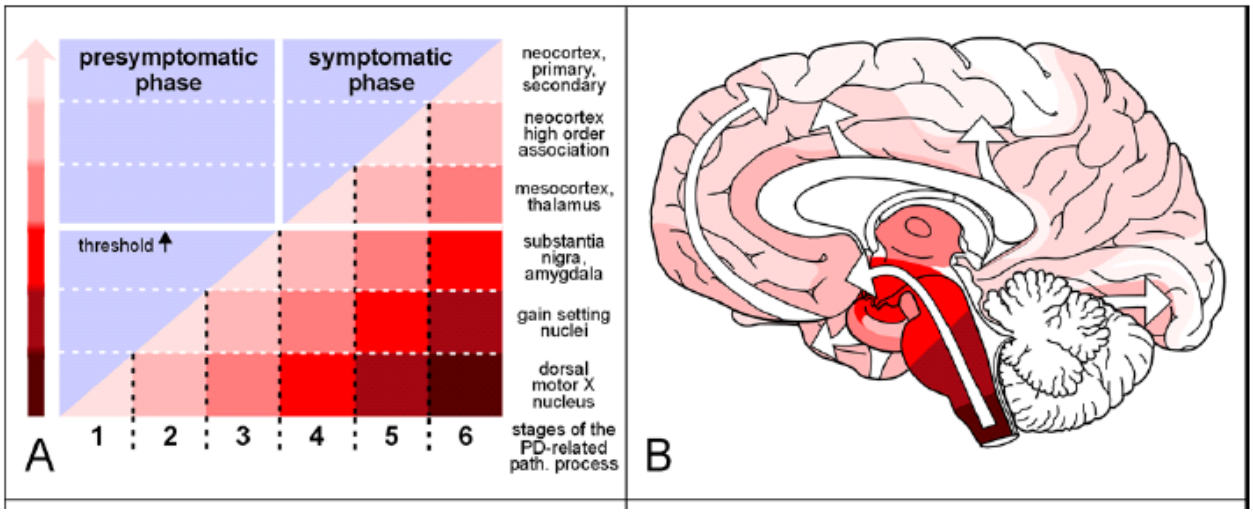

Adapted from Braak *et al.*, 2004 (DR)

Figure 3: Disease's progression into the brain.

A) Parkinson's disease progression can be divided in two phases namely the presymptomatic and the postsymptomatic phase and subdivided in different stages. The presymptomatic period is spread over years and when tremors appear around the half of the dopaminergic neurons of the *subtantia nigra* have already disappeared. ***B)*** Diagram showing the ascending pathological process with white arrows and shading intensity variations. Each phase correlates with the Lewy bodies and neurites progression into the different brain regions. Remark how the pathology progresses by diffusing from the brain stem to the rest of the CNS.

Nonetheless, in Parkinson's disease, the loss of dopaminergic neurons of the *substantia nigra pars compacta* is most acute and the reasons of this abnormal cell death are still unexplainable. However, in around 5% of the cases, parkinsonism is hereditary and different responsible genetic mutations have been identified (see Table 1). For instance, mutations in the coding genes for *α-synuclein*, *UCH-L1*, *HTRA2/Omi* and *LRRK2* provoke autosomal dominant inherited parkinsonism, whereas mutations in the coding genes for *Parkin*, *PINK1*, *DJ1*, and *ATP13A2* induce autosomal recessive inherited parkinsonism. However, familial parkinsonisms are not completely identical to the normal idiopathic and sporadic Parkinson's disease. The familial forms often appear at younger ages and present differences in the range of symptoms and in the response to treatments.

Name	Gene	Chromosomal locus	Inheritance	Age of onset	Protein function	Presence in Lewy bodies	References
park 1	*α-synuclein* (*SNCA*) mutation	4q21	AD	40	synaptic vesicles processing and traficking	+	Polymeropoulos *et al.*, 1997
park 2	*Parkin* (*PRKN*)	6q25	AR	20	Ubiquitin ligase	-	Kitada *et al.*, 1998
park 3	?	2pl3	AD	60	?	+	Gasser *et al.*, 1998
park 4	*α-synuclein* gene multiplication in the genome	4q21	AD	30	See above	+	Singleton *et al.*, 2003 Chartier-Harlin *et al.*, 2004
park 5	*UCH-L1*	4p15	AD	50	Ubiquitin-hydrolase/ligase	+	Leroy *et al.*, 1998
park 6	*PINK-1*	Lp35-36	AR	30	Mitochondrial protein kinase	+	Valente *et al.*, 2004; Gandhi *et al.*, 2006
park 7	*DJ-1*	Lp36	AR	30	Oxaditiv stress response	?	Bonifati *et al.*, 2003
park 8	*LRRK2* or *dardarin*	12p	AD	/	Protein kinase	+/-	Paisan Ruiz *et al.*, 2004; Zimprich *et al.*, 2004
park 9	*P-type ATPase* (*ATP13A2*)	1p36	AR	/	Lysosomale typ 5 P-ATPase	?	Ramirez *et al.*, 2006; Najim al-Din *et al.*, 1994;
park 10	?	Ip32	AD	/	?	?	Hicks *et al.*, 2002
park 11	?	2q36-q37	AR	/	?	?	Pankratz *et al.*, 2003
park 12	?	Xq21-q25	AD	/	?	?	Pankratz *et al.*, 2003
park 13	*HTRA2/Omi*	2p12	AD	/	Stress induced serin endoprotease	+	Strauss *et al.*, 2005

AR = autosomal recessive, AD = autosomal dominant, ? = unknown

Table 1: List of the *park* genes.
Over the years different genes and loci have been identified to be linked to familial parkinsonism. All these genes are invoved in Parkinson's pathogenesis and in dopaminergic cell death.

In non-familial parkinsonism – i. e. in the remaining 95% of the cases – the causes and modalities whereby the disease starts and progresses are still mysterious. The disease occurs in all ethnic groups and socioeconomic classes. Men have a slightly higher risk compared to women (deRjik *et al.*, 2000; Weintraub *et al.*, 2008; Wooten *et al.*, 2004). Moreover, geographic localisation, profession and life-style only induce minor risk factor variations in the prevalence. For instance, epidemiological studies have shown that head trauma and rural living slightly increase the risk, whereas caffeine and tobacco consumption slightly decrease it (Hernan *et al.*, 2002; Goldman *et al.*, 2006).

Some environmental toxins have also been identified to be risk factors. For example, in Guadeloupe, the consumption of the tropical fruit *Annona muricata*, which contains a toxin

called annonacin, was identified to increase the risk factor for Parkinson's disease (Lannuzel *et al.*, 2008). Annonacin, herbicides and pesticides, such as rotenone, paraquat and maneb, can induce dopaminergic neuron cell death and the subsequently parkinsonism through complex I inhibition (Ascherio *et al.*, 2006). However, for the aforementioned toxins, only repeated and prolonged contacts induce an increased incidence of Parkinson's disease. On the other hand, another toxin, called MPTP (1-methyl-4-phenyl-1,2,3,6-tetrahydropyridine), is able to induce parkinsonism in a very efficient manner and after a single injection. MPTP effects were discovered in California in the 1980's by elucidating a strange case of intoxication; a series of illicit drug addicts developed a dazzling parkinsonism after consumption of a synthetic opoid drug contaminated with MPTP. After investigation, researchers found that MPTP itself was not toxic but was metabolised in MPP^+ (1-methyl-4-phenylpyridinium) by action of the monoamine oxidase enzyme once in the brain (Langston, 2002). Then, MPP^+ is actively pumped into dopaminergic neurons by the dopamine transporter, wherein it potently blocks the mitochondrial complex I, leading to a selective toxicity against dopaminergic neurons. Hence, aside from 6-hydroxydopamine, MPTP is used as research tool to experimentally induce *in vivo* or *in vitro* dopaminergic depletion (Dauer and Przedborski, 2003).

However, the real causes normal of sporadic Parkinson's disease in humans are still elusive. A complex combination of genetic, epigenetic, aging processes and environmental factors may account for sporadic Parkinson's disease.

1.6. *Therapeutic strategies and research axes*

No treatments currently exist to cure or at least to slow down Parkinson's disease. However, several drugs and therapeutics are commonly used to attenuate the symptoms of Parkinson's patients (Weintraub *et al.*, 2008). Among them, the large majority targets the dopaminergic neurotransmitter system (Figure 4). For example, dopamine agonists (pramipexole, ropinirole, bromocriptine, rotigotine and apomorphine) bind directly to dopaminergic receptors and increase the dopaminergic signalling. The most prescribed drug for Parkinson's disease, L-DOPA, is a dopamine precursor which increases dopamine production. In contrast, monoamine

oxidase (MAO) inhibitors (selegiline and rasagiline) and cathecol-O-methyl transferase (COMT) inhibitors (entacapone and tolcapone) inhibit dopamine catabolism. In addition, amantadine and anticholinergic substances, but also surgery, such as pallidotomy and implantation of electrodes for deep brain stimulation, are used to reduce the symptoms (Weintraub *et al.*, 2008).

As a consequence, with a combination of paramedical and rehabilitive measures, it is possible to manage the symptoms and achieve a better quality of life for the patient at least during the first stages of the disease.

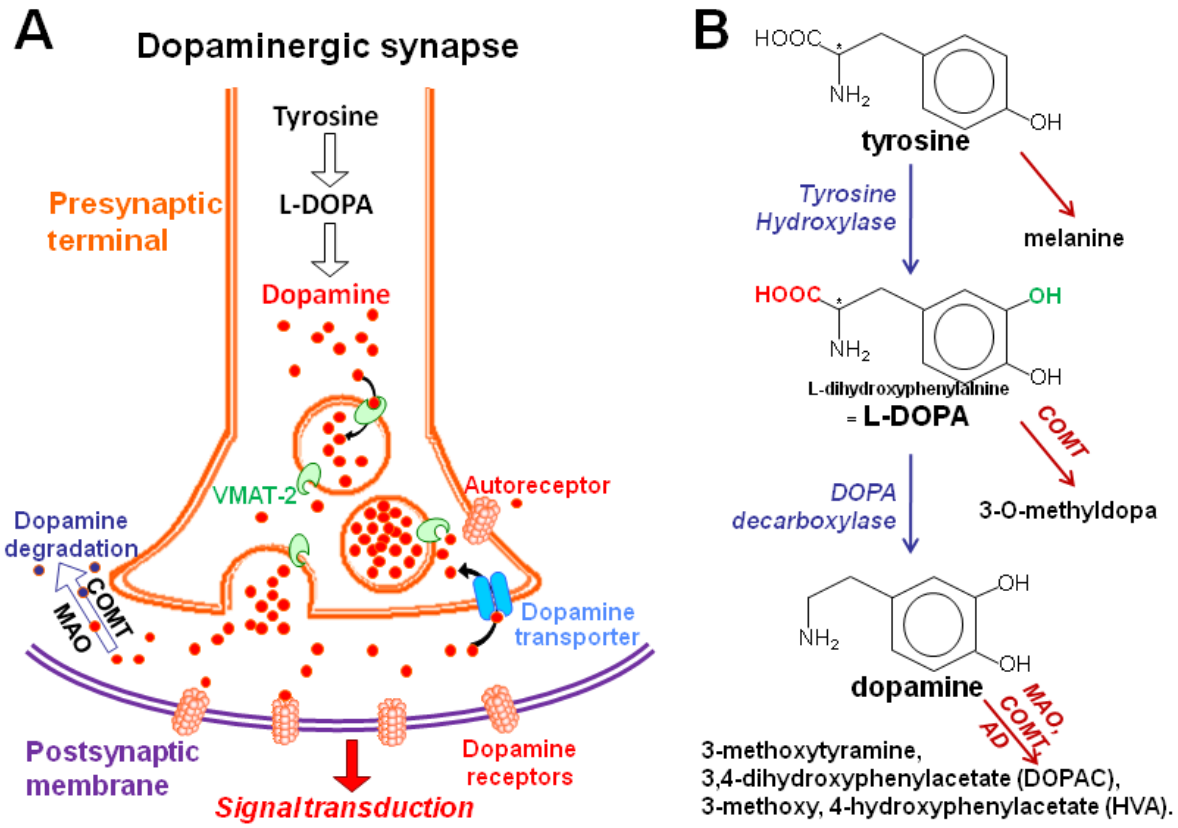

Figure 4: Dopaminergic synapse and dopamine metabolism.
A) Cartoon representing a dopaminergic synapse. In the presynaptic terminal of dopaminergic neurons, tyrosine is transformed in L-DOPA by the action of the tyrosine hydroxylase and L-DOPA is subsequently transformed to the neurotransmitter dopamine by action of the DOPA decarboxylase. Dopamine is then transferred in vesicles by the vesicular monoamine transporter 2 (VMAT-2). After exocytosis of the dopamine vesicles, dopamine binds to dopamine receptors on the postsynaptic membrane, leading to the transduction of the signal in the postsynaptic neuron. Dopamine is then recycled by reuptake *via* the dopamine transporter or catabolised by the action of the monoamine oxidase (MAO), the cathecol-O-methyl transferase (COMT) and the aldehyde deshydrogenase (AD) enzymes. ***B)*** Biochemical structures and pathways of dopamine synthesis and its metabolites.

Nonetheless, over time, the disease irreversibly progresses, the symptoms worsen and, in parallel, the efficiency of the treatments diminishes.

As a consequence, development of more efficient palliative and symptomatic treatments against these motor and neuropsychatric symptoms with less debilitating side effects is still a focal point of research.

To date, a major problem concerning the research on new treatments to cure Parkinson's disease is the absence of an early diagnostic test for Parkinson's disease. Indeed, when the disease is diagnosed - with the appearance of the first symptoms - around 70% of the dopaminergic neurons of the *substantia nigra* have already disappeared (Jakobsen and Jensen, 2003). As a result, neurodegeneration is active long before the patients become aware of the disease and, after diagnosis, possibilities for preventive and curative therapeutic strategies are limited. Thus, development of reliable tests for early diagnosis of Parkinson's disease is a crucial point and an important aim of research.

Hence, a large part of the basic research on Parkinson's disease is focused on the identification and the understanding of the keys molecular events that provoke neurodegenerative mechanisms. Different axes are being explored, including the role of proteins involved in familial parkinsonism (DJ-1, LRRK2 or α-synuclein), the role of mitochondrial dysfunction (especially complex I), the regulation of neuron apoptosis, the effect of oxidative stress, the mechanisms of proteinopathy (autophagy, proteasome and lysosome dysfunction, protein misfolding, aggregation and accumulation) and the involvement of the immune response and neuroinflammation (Dauer and Przedborski, 2003; Jenner and Olanow, 2006).

Finally, in order to restore the neural transmission failures, the implantation of pluripotent stem cells differentiated in neurons has stimulated great interest and discussion among the scientific community.

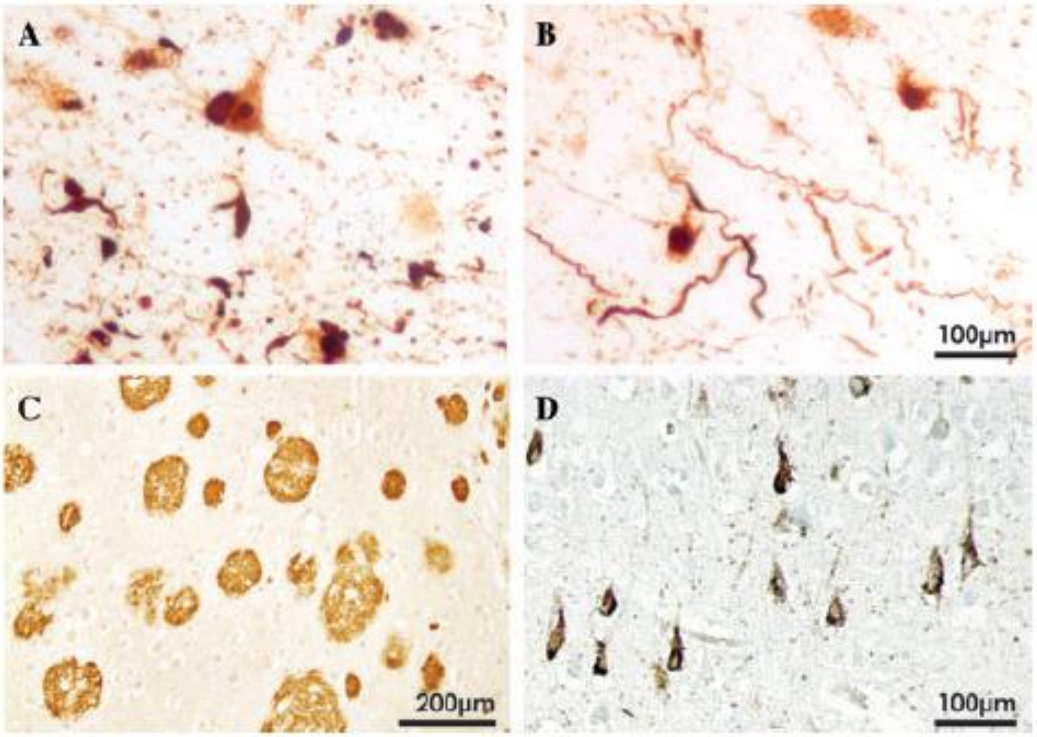

Adapted from Halliday and McCann, 2009 (DR)

Figure 5: Lewy bodies and Lewy neurites.
Lewy bodies and neurites are found in the neurons of Parkinson's patients. Patients with older onset ***(A)*** have a higher density than those with younger onset ***(B)*** because these abnormal proteinous inclusions accumulate with time. Age-related Aβ plaques ***(C)*** and tau immunopositive neurofibrillary tangles ***(D)*** also occur more frequently in older-onset cases and may be significantly contribute to the clinical heterogeneity observed in Parkinson's patients.

1.7. The α-synuclein pathoprotein

Abnormal intracellular deposits of aggregated protein, called Lewy bodies and Lewy neurites, are found in the brain of Parkinson's patients (Lewy, 1912; Spillantini *et al.*, 1997). As their respective names indicate, Lewy bodies and Lewy neurites are proteinous cytoplasmic inclusions localised in the cell body and neurites of neurons, respectively (Figure 5). They can be histologically detected by eosin staining or by anti-ubiquitin or anti-α-synuclein immunohistochemistry. Indeed, the main components of these intracellular deposits are aggregated α-synuclein as well as ubiquitin and other proteasomal proteins, but also chaperon proteins and cytoskeleton proteins (Spillantini *et al.*, 1997; Jensen *et al.*, 2000; Bennett, 2005). Actually, the detection of Lewy bodies and neurites allow post-mortem diagnosis for α-synucleinopathies (Goedert, 2001). This term encompasses Parkinson's disease but also dementia

with Lewy body (=diffuse Lewy Body disease) and in some cases, Pick's disease, multiple system atrophy, amyotrophic lateral sclerosis and Alzheimer's disease (Lavedan, 1998).

In neurons of Parkinson's cases, dysfunctions in protein catabolism, particularly in autophagy and in the ubiquitin proteasome systems, have shown to participate to Lewy body formation (McKnaught and Olanow, 2003). Consequently, it is believed that Lewy bodies and neurites are the consequence of an aggrosomal response that neurons develop to cope with the abnormal cytoplasmic protein accumulation.

The α-synuclein protein is the major component of Lewy bodies and neurites and, as previously mentioned, mutations in the *α-synuclein* gene induce inheritated parkinsonism (Table 1). Indeed, three point mutations consisting of single amino acid substitutions, A53T, A30P and E46K, are responsible for rare, severe, juvenile and autosomal dominant genetic forms of parkinsonism (Polymeropoulos *et al.*, 1997; Kruger *et al.*, 1998; Zarranz *et al.,* 2004). Additionally, the duplication or triplication of the number of gene copies of the wild-type form of *α-synuclein* gene induce an important genetic risk factor for development of Parkinson's disease (Table 1) (Singleton *et al.*, 2003; Chartier-Harlin *et al.*, 2004). Taken together, these facts are striking pieces of evidence indicating that α-synuclein is critically involved in the Parkinson's pathogenesis.

The synuclein family is composed of α-, β- and γ-synucleins. α-, β- and γ-synucleins are small proteins (127 to 140 amino acids) that share an intermediate homology (55 to 62%) and that are highly expressed in the brain (Lavedan, 1998). α-synuclein is encoded by the *SNCA* gene in humans and has a homologue in rodents (with 95.3% homology). It was first localised in presynaptic nerve terminals and nuclei of neurons and was consequently named synuclein (Maroteaux *et al.*, 1988). It was later observed that α-synuclein is not only expressed in the synaptic and nuclear regions but throughout the neuron. Moreover, α-synuclein was found in almost all brain regions and was even detected in other tissues, such as muscle and kidney (Ueda *et al.*, 1993; Lavedan, 1998). Nonetheless, α-synuclein is particularly abundant in the presynaptic terminals of neurons and is involved in synaptic transmission. Although its exact function is still elusive, α-synuclein has been implicated to neurotransmitter secretion, Golgi apparatus and vesicle trafficking, cytoskeleton interactions, apoptosis, neuroplasticity, fatty acid

binding, protein-protein interactions, chaperon and scaffold functions (Abeliovich *et al.*, 2000; Cabin *et al.*, 2002; Liu *et al.*, 2004; Yavich *et al.*, 2004).

The full length α-synuclein protein has a molecular mass of 14,5kDa and is composed of 140 amino acid residues. It contains several repeated domains of 11 residues, which display variations of the consensus sequence KTKEGV (Maroteaux *et al.*, 1988). The protein can be divided in three regions (Figure 6). The N-terminal region, from residues 1 to 60, is able to bind to biological membranes by adopting an amphipathic α-helical conformation (Davidson *et al.*, 1998). The intermediate region, from residues 61 to 95, is a key hydrophobic region for α-synuclein polymerisation. It was first identified in amyloid plaques of Alzheimer's patients and was also called NAC region for "non-amyloid component" (Ueda *et al.*, 1993). Finally, the C-terminal region, from residues 96 to 140 is a random coiled region with no apparent secondary structure. This highly acidic region is also rich in proline residues and presents four putative phosphorylation sites.

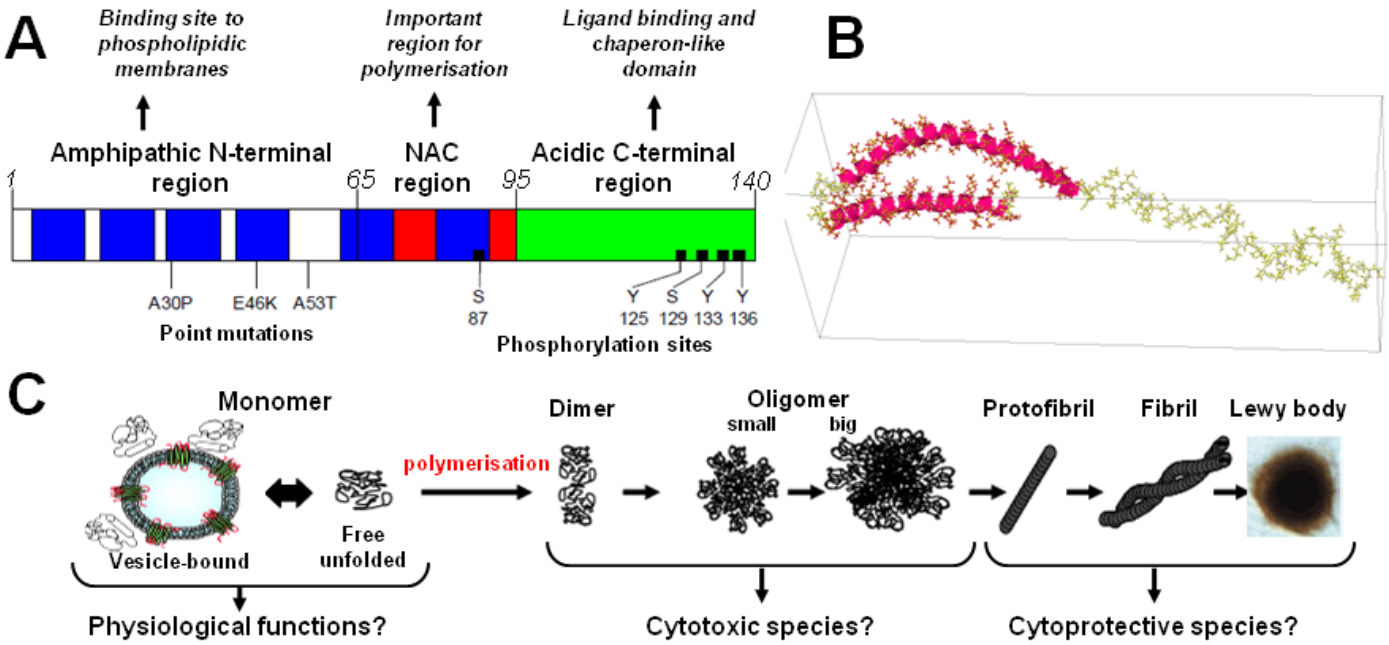

Figure 6: α-synuclein structures.

A) Schematic organisation of the primary structure of α-synuclein protein. The 140 amino acid chain is divided in 3 major regions. ***B)*** Three dimensions reconstitution of α-synuclein secondary structure. The N-terminal region can form two α-helical regions, whereas the rest of the protein is unfolded. ***C)*** Cartoon representing α-synuclein polymerisation. α-synuclein polymers can adopt different tertiary structures; small oligomers, pore forming structures, big oligomers, protofibrils, fibrils and Lewy bodies and neurites.

α-synuclein is normally found in the form of soluble unstructured monomers and of membrane-bound monomers with two α-helices secondary structure (Bennett, 2005). In pathological conditions, α-synuclein forms different polymers of various sizes with β-sheet structures (Figure 6 C).

Oligomer formation is increased by the point mutations A53T, A30P and E46K (Wood *et al.*, 1999; Conway *et al.*, 2000) or by post-transcriptional modifications, such as phosphorylation by kinases (Ser129), truncation by proteases, oxidation by reaction with reactive oxygen species, ubiquitination, and glycosylation (Okochi *et al.*, 2000; McLean *et al.*, 2002; Takahashi *et al.*, 2002). In addition, binding to lipids, to metallic cations (Mn^{2+}, Cu^{2+}, Co^{3+}, Al^{3+} and Fe^{3+}) or to other proteins and nucleation effect are suspected to be involved in polymerisation (Uversky *et al.*, 2001; Dev *et al.*, 2003; Bennett, 2005).

α-synuclein aggregation is a major hallmark of Parkinson's disease. However, the mechanisms of this abnormal process are still unclear. It is assumed that Lewy bodies and neurites are probably the last stage of α-synuclein aberrant accumulation. But it is not certain whether big aggregates of α-synuclein mediate toxicity or whether they are just a way for the cell to handle with α-synuclein aberrant accumulation (Goldberg and Lansbury, 2000). Indeed, mounting evidence point at a toxic role of oligomeric forms of α-synuclein (Lashuel *et al.*, 2002). Reports have shown that α-synuclein oligomers have membrane disrupting properties (Volles *et al.*, 2001 and 2002; Lashuel *et al.*, 2002; Demuro *et al.*, 2005). This feature can lead to endoplasmic reticulum and Golgi apparatus stress and fragmentation, to vesicle trafficking dysregulation, to mitochondrial stress and subsequently to energy production impairment, oxidative stress and apoptosis (Gosavi *et al.*, 2002, Jakobsen and Jensen, 2003). α-synuclein accumulation affects the complete proteome by blocking the proteasome system, inducing protein misfolding stress and by sequestration of other proteins. Finally, α-synuclein is suspected to be an elicitor of immune reactions in the brain, responsible for chronic neuroinflammation (Croisier *et al.*, 2005; Zhang *et al.*, 2005; Gao *et al.*, 2008).

2. Glia and brain immunity

2.1. Opening remarks on glial cells

Historically, scientists in neuroscience have focused their interest almost completely on neurons and largely ignored the other cell types. In addition to neurons, other brain cells, grouped under the common term "glia" or "neuroglia", are present. However, the term "glia" encompasses various cell types of different origins (Figure 7). Actually, glial cells are constituted of microglia, which are derived from a mesodermic cell population, and of "macroglia", which are derived from neurodermic cells. The "macroglia" class is itself divided in different cell types, such as astrocytes, Schwann cells and oligodendrocytes but also ependemyal cells, radial and enteric glia.

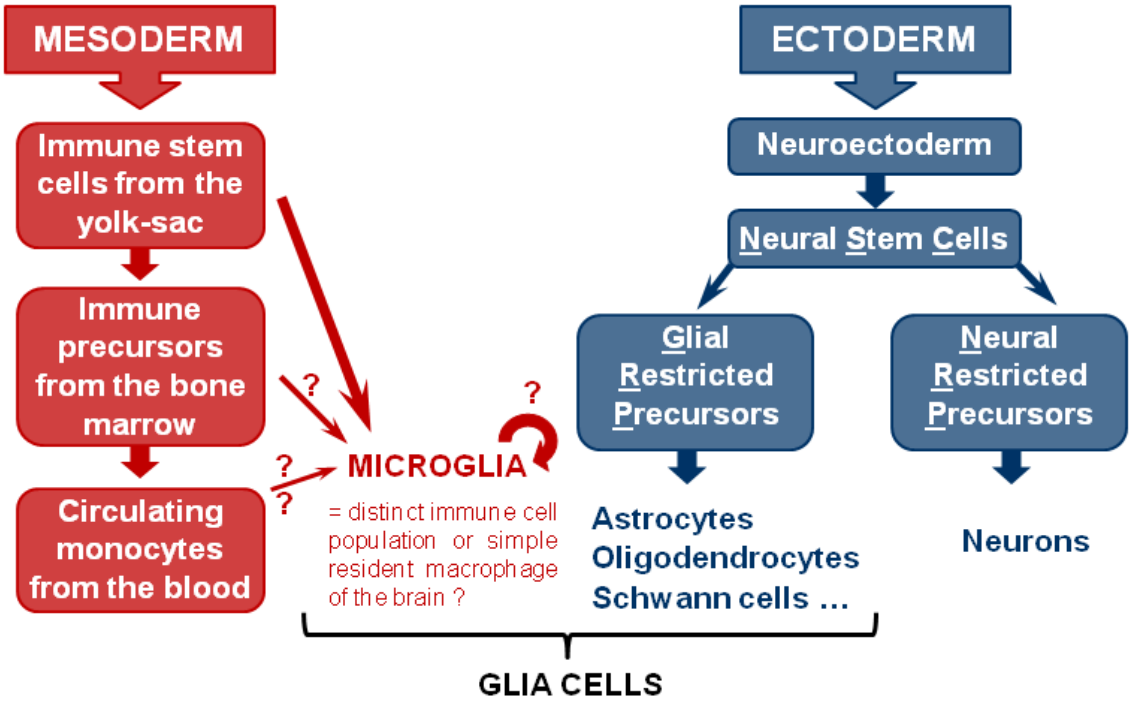

Figure 7: Glia are composed of different cell types.
On one hand, astrocytes, oligodendrocytes and Schwann cells (sometimes grouped under the term of "macroglia") have a neuroectodermic origin and derive from the same precursors than neurons. On the other hand, microglia derive from the mesoderm and belong to the same lineage as immune cells. Nowadays, the mechanisms of microglial replenishment during adulthood are still under debate.

2.2. *Discovery and renaissance of glial cells*

In 1839, Theodore Schwann theorized that cells are the basis of all living tissues and described the “Schwann cells”. In 1858, Rudolph Virchow designated the sheath around stained axons as "myelin” and introduced for the first time the term of “neuroglia” to define the connective tissue in the brain. In 1865, Otto Friederich Karl Deiters first provided definitive illustrations of astrocytes. In 1873, Camillo Golgi developed a silver impregnation staining and visualised neurons and astrocytes (Figure 8). Camillo Golgi clearly described astrocytes as "roundish oval or star shaped cells from which numerous, long, fine and never arborized prolongations originate”. But it is only in 1893 that Mihály Lenhossék introduced the term of "astrocyte“(Kettenmann and Verkhratsky, 2008).

Oligodendrocytes and microglia cells were described later due to their resistance to metal impregnation staining. In 1913, Santiago Ramón y Cajal called these cells resistant to Golgi staining the "third element”. In 1919, Cajal’s disciple Pío del Río-Hortega improved Golgi staining by silver carbonate and described two new cell types belonging to the "third element”. One cell type had few processes and was consequently named "oligodendroglia“, whereas the other cell type had short processes and was consequently named "microglia” (Figure 8 C). Additionally, del Río-Hortega recognized the role of microglia in pathology as well as their mesodermic origin. However, despite the early observations by Franz Nissl in 1899 and Ludwig Merzbacher in 1909 that microglia were able to rapidly transform from a ramified to an ameboid state, the function of microglia remained obscure until the end of the 20th century.

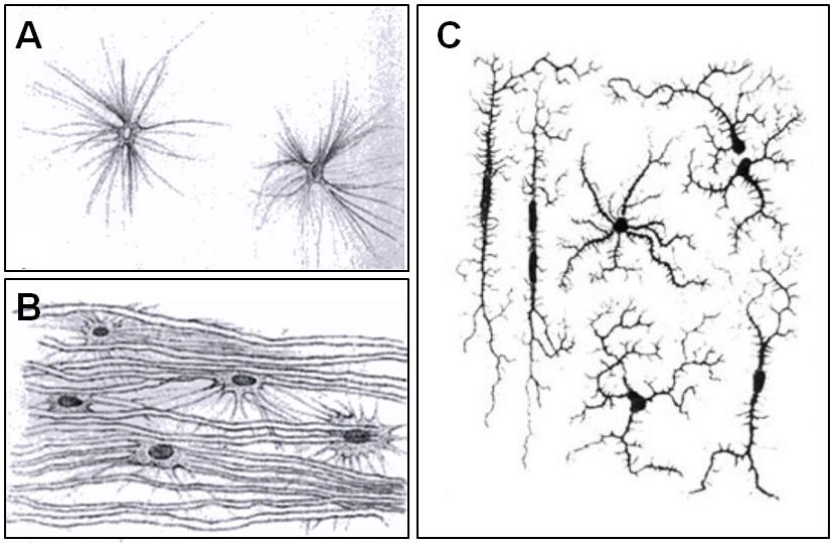

Figure 8: Glia cells represented by earlier investigators.
A and B) Illustrations of neuroglial cells extracted from Golgi’s work (1894). ***A)*** Neuroglia from the cerebral cortex and the cerebellum of a 2-month-old child. ***B)*** Longitudinal section of white matter showing axons and neuroglia in close contact. ***C)*** Illustrations of microglia with different morphologies issued from del Río-Hortega work (1932).

Glial cells were long erroneously considered as passive bystanders in the CNS. But after the second World War, calcium imaging resurrected the astrocyte and demonstrated that astrocytic activity was critical for regulation of blood flow in the brain, neurovascular coupling, modulation of synaptic activity *via* the "tripartite synapse", clearance of synaptic neurotransmitters and release of "gliotransmitters".

Meanwhile, the function of oligodendrocytes producing the myelin sheath remained hypothetical until the definite proof provided in 1962 by Richard Bunge. Chemical analysis of myelin started in the 1950's and was followed up by sequencing of myelin proteins in the 1970's. A decade later, Helmut Kettenmann showed that oligodendrocytes were more than just insulators for neurons.

In the late 1980's, research on microglial function made a breakthrough by the work of Georg Kreutzberg who demonstrated that activated microglia expressed immunological markers. Nowadays, microglia are considered as the first effectors of the brain immunity.

In conclusion, history shows that the concept of glial cells has slowly moved from "space-fillers" to key players in neural function and the future will unveil the full extent of their functions (Kettenmann and Verkhratsky, 2008).

2.3. *Immunity of the brain*

In human, the brain receives up to 20% of the cardiac output. Human brain vascularisation is so colossal that the estimated total length of capillaries is about 650 km and that nearly every neuron has its own capillary (Zlokovic, 2008). Moreover, in contrast to the other organs, the brain parenchyma is separated from the circulating blood by a highly specialised biological barrier that enwraps all capillaries and blood vessels. It is formed by the vascular basal membrane, tight layers of endothelial cells, pericytes and microglial and astrocytic projections. This barrier is named the blood-brain or hematoencephalic barrier and its role is to restrict the diffusion of damaging factors from the circulating blood to the cerebrospinal fluid (Davson, 1976). To protect the vulnerable neurons, it actively filters molecules and blocks the

entry of toxins, pathogens, plasma components and blood cells. The blood-brain barrier is known to actively pump metabolites, such as glucose or amino acids from the blood into the brain and to block the access of large and/or hydrophilic molecules. The blood-brain barrier is in turn a major and redundant obstacle to every drug discovery and delivery programmes (Abbott *et al.*, 2009).

Given that neurons are an almost postmitotic and non-proliferative cell type, it is obvious that the brain is a relatively endangered organ. In fact, the brain is an "immune privileged" organ that have no lymph nodes and where immune reactions are strongly regulated to avoid irretrievable collateral damages. In addition to the blood-brain barrier, the brain environment contains immunosuppressive molecules, such as TGF-β, and healthy neurons have inhibitory effects on microglia (Kiefer *et al.*, 1993). Under normal conditions, the blood-brain barrier prevents peripheral immune cells from entering the brain and consequently, the only immune cells in the brain parenchyma are microglia. However, after events, such as trauma and ischemia, peripheral immune cells can infiltrate the brain.

2.4. *Origins, characteristics and functions of microglia*

Contrary to neurons and the other glial cells which are derived from the neuroectoderm, microglia are of mesodermic origin (Figure 7). Indeed, microglia share common precursors with the immune cells and are derived from a hemapoetic stem cell population of the myeloid-monocytic lineage primarily localised in the yolk sac and that colonises the brain. Different waves of colonisation have been described during the embryonic and post-natal development (Davoust *et al.*, 2008). In the embryonic brain, microglia display an ameboid morphology and express activation markers, such as CD68. Microglia actively contribute to organogenesis of the brain and neuroplasticity. However, after birth, microglia change, adopting a ramified morphology and down regulating the expression of several activated/myeloid cell markers.

The origin of embryonic microglia is now well accepted but the origin of microglia during the adult life is still actively debated (Davoust *et al.*, 2008). It is not clear whether microglia are replenished by an input of bone marrow-derived progenitors originating from outside of the

CNS like monocytes/macrophages do, or whether microglia are able to proliferate and maintain the resident population, like Langerhans cells do in the skin.

In animal models and in humans, it has been observed that monocytes and hemapoetic stem cells were able to infiltrate into the brain and differentiate into microglia-like cells (Hickey *et al.*, 1992; Kennedy and Abkowitz, 1997; Djukic *et al.*, 2006) suggesting that microglia might be replenished by an input of precursors from the bone marrow and/or by a specific monocyte population. However, this invasion of peripheral cells seemed to occur only when the blood-brain barrier was altered or when bone marrow-derived progenitor cells were artificially transplanted in the blood stream (Ajami *et al.*, 2007). In healthy adults, under normal conditions, no replenishment of microglia by peripheral cells is observed and microglia form a distinct immune cell population which resides in the brain and have the rare ability for an immune cell to self-renew by direct cellular division.

Microglia account for about 10-20% of the glial cells (Raivich *et al.*, 1999). They are located throughout the brain (Figure 9), in addition to the spinal cord and optic nerves. Intriguingly, microglia are 4 to 5 times more dense in the *substantia nigra pars compacta* than anywhere else in the brain (Lawson *et al.*, 1990). In the CNS, microglia are involved in neuroplasticity, synaptogenesis, host defense, homeostasis, wound healing, debris scavenging, recruitment of peripheral immune cells and immune response regulation (Aloisi, 2001). Under physiological conditions, microglia have a ramified morphology and continually survey their surrounding micro-environment (Nimmerjahn *et al.*, 2005). As seen in Figure 9, each cell covers a defined area of around 50 to 60 µm diameter with its numerous and extremely motile processes. It has been calculated that microglia completely screen the brain parenchyma once every few hours (Nimmerjahn *et al.*, 2005). In the literature, despite their frenetic activity, these ramified surveying microglia are often wrongly designated as "resting" or "quiescent" in opposition to the ameboid “activated” or "reactive" microglia.

Actually, in response to a multitude of stressors, they have the remarkable capacity to rapidly divide, migrate and undergo morphological, functional and immunophenotypical changes; this process is called “microglial activation” or “microgliosis” (Figure 9 A).

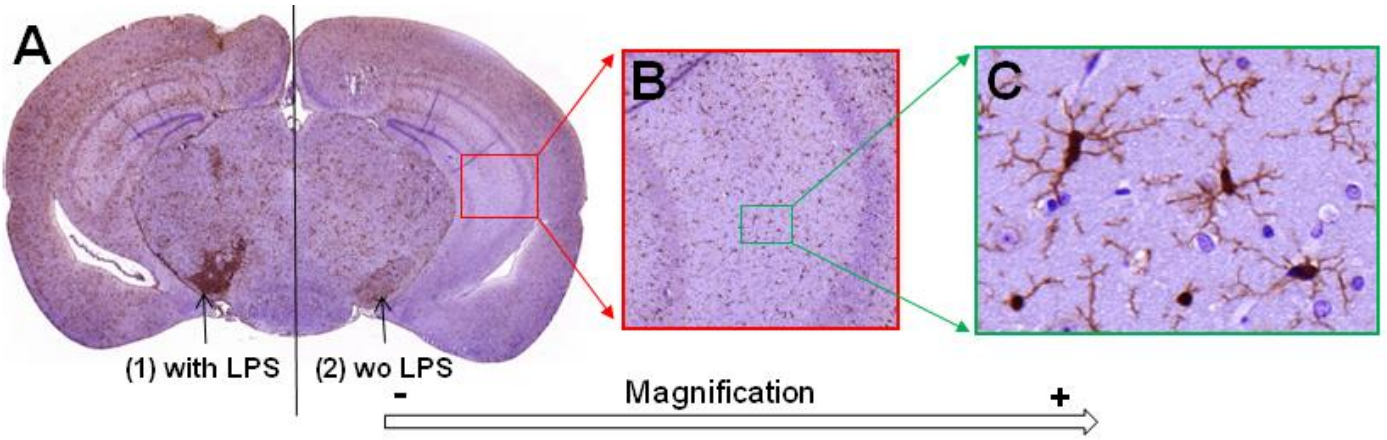

Patrick Oeckl, unpublished observations (DR)

Figure 9: Distribution of microglia in the brain.

A) Coronal brain section of a mouse brain viewed with three different magnifications. Microglia (stained in brown with anti-Iba1 antibodies) are present in all brain regions but are more dense in the *substantia nigra* (2). After injure or stereotactic LPS injection microgliosis occurs at the damaged area (1). ***B and C)*** Under normal conditions, microglia have a non-overlapping territorial distribution, their cell bodies stay immotile in the center of a surveying area, whereas the numerous fine and highly motile processes screen the area permanently.

2.5. *Microglial activation*

In reaction to abnormal stimuli, for instance after CNS injure, microglia can adopt an "activated" ameboid phenotype and migrate quickly to the injured area (Kreutzberg, 1996). Microglial activation is characterised by local microglial accumulation through direct proliferation and recruitment of the surrounding microglia by chemotaxis (Figure 9) (Block *et al.*, 2007).

As previously mentioned, microglia steadily survey their environment. Thanks to a broad spectrum of sensors, they are able to sense a lot of different stimuli, such as the presence of damaged cells and cell debris, serum factors, aberrant and misfolded proteins or bacterial, fungal and viral infection. Actually, microglia do express intracellular pattern recognition receptors, toll-like receptors, formyl peptide receptors, protease activated-receptors, scavenger receptors, various polysaccharide receptors, phosphatidylserine recognizing receptors, sphingosine 1 phosphate receptors and hypoxia sensors (Hanisch and Kettenmann, 2007).

In addition, each microglial cell is able to communicate with its bystander cells - including other microglia but also neurons, astrocytes and even cells from the peripheric

immune system – by secreting a broad panel of cytokines and chemokines, and by expressing cytokine receptors, MHC class I and II molecules, immunoaccessory glycoproteins, chemokine receptors, growth factor receptors, antibody Fc fragment receptors, complement receptors, thrombine receptors, various integrins and adhesion molecules, prostanoid receptors, cannabinoid receptors, neurotransmitters receptors and various cell-to-cell contact receptors (e.g. phosphatidylserine receptors, semaphorin receptors, CD45-CD22, CD172a-CD47, CD200R-CD200 and CX3CR1-CX3CL1) (Aloisi, 2001; Block *et al.*, 2007; Tambuyzer *et al.*, 2008).

The role of activated microglia is to scavenge pathogens, toxins, unwanted cells and cellular debris by phagocytosis (Kreutzberg, 1996). As gardians of the brain, microglia can recruit other cells and orchestrate the inflammation by producing pro-inflammatory and pro-apoptotic cytokines and chemokines (e.g. IL-1β, -6, -8, -12, -15, -18, -23, CCL-2, -3, -5, CXCL-1, -2, TNF-α…) but also prostanoids (e.g. PGE_2, PGD_2, thromboxane B_2…), reactive oxygen and nitrogen species by the action of the cycloxygenase, the NADPH oxidase and the inducible nitric oxide synthase (iNOS) enzymes, respectively. On the other side, microglia can resorb inflammation by secreting anti-inflammatory cytokines (e.g. TGF-β, soluble TNF-α receptor, IL-1 receptor antagonist, IL-4, IL-10…). They are actively implicated in wound healing processes and promote neuron survival. They elicit neuroplasticity and extracellular matrix remodeling by producing proteases (e.g. fibrinogen, cathepsins, heparanase, metalloproteases…) and by secreting growth factors (e.g. neurotrophins, nerve growth factor, brain-derived neurotrophic factor, glial cell-derived neurotrophic factor, insulin-like growth factor 1…) (Aloisi, 2001; Block *et al.*, 2007; Tambuyzer *et al.*, 2008).

In addition to morphological and functional changes, microglial activation is accompanied by striking electrophysiological changes.

2.6. *Electrophysiological characteristics of microglial cells*

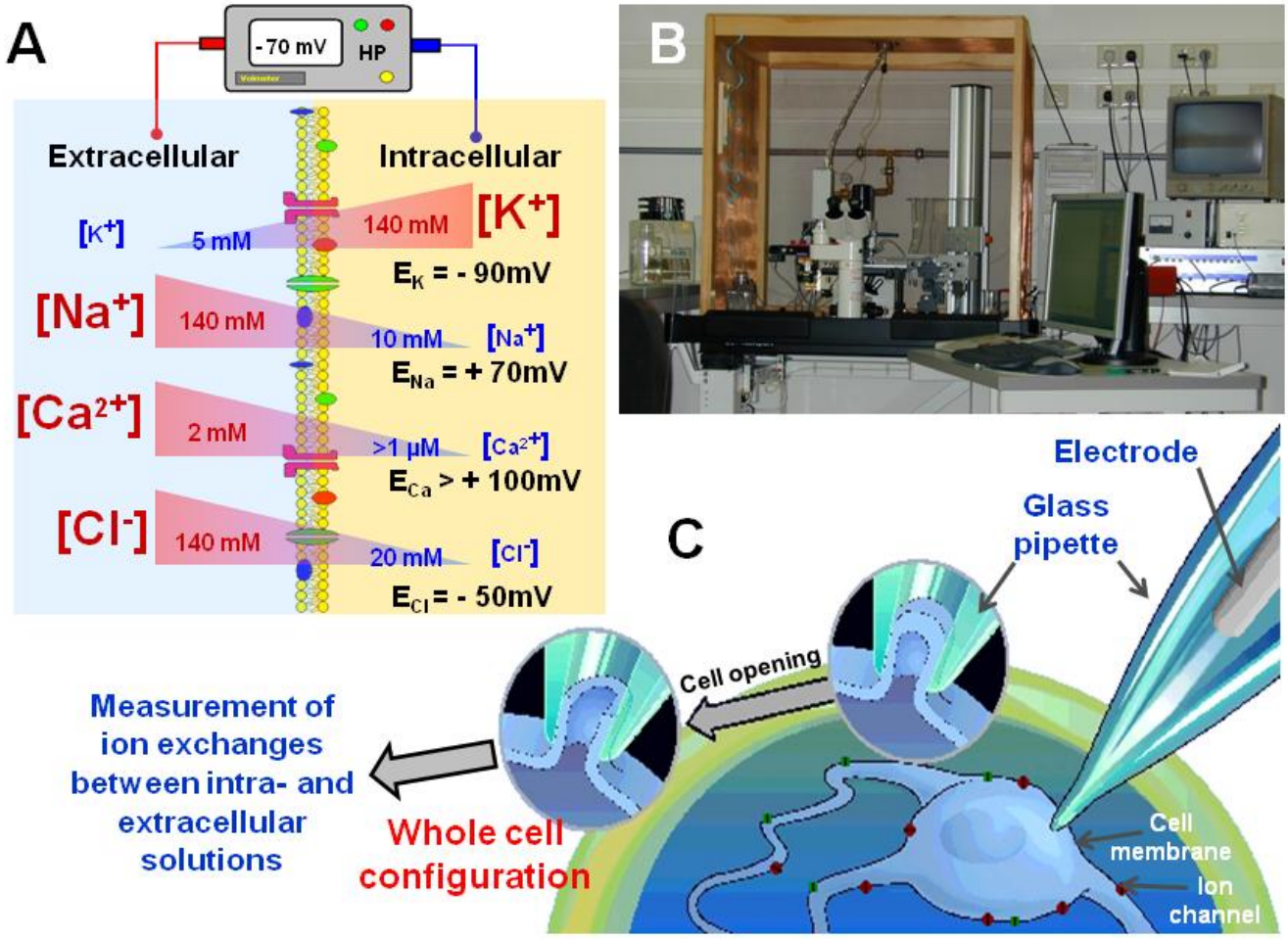

Figure 10: Electrophysiology and patch-clamp.

A) The cell membrane acts as a lipophilic semipermeable barrier. Ions cannot freely cross the cell membrane. Thanks to ion channels and ion pumps, ion concentrations and fluxes are highly regulated in cells. The unequal ion distribution between the extra- and the intracellular spaces is at the origin of the holding potential (around -70mV). With the patch-clamp technique, it is possible to measure ion fluxes across the membrane from single cells using two small electrodes and a micropipette. ***B)*** Classical patch-clamp setup consists in a Faraday cage, an antivibration table, a microscope, a robotic micromanipulator with its remote, an amplifier and a computer with a special interphase and software. ***C)*** The micropipette is clamped at a single cell and forms a tight junction with the cytoplasmic membrane, termed "gigaseal". Then, to achieve the "whole cell configuration", the cell is opened by application of an electric impulse and an underpression. One electrode is in the bath solution and measures the extracellular potential, whereas the second electrode is inside the glass micropipette and is in direct contact with the intracellular compartment.

Physiological characteristics of microglia were first established by neurologists and electrophysiologists, such as Georg Kreutzberg and Helmut Kettenmann. These first electrophysiological studies were performed using the patch-clamp technique (Hamill *et al.*, 1981) (Figure 10). This highly sensitive technique enables the measurement of ion fluxes across the membrane of single cells using two thin electrodes; one is in contact with the extracellular space, whereas the second is inserted into a micropipette which is patched to a cell. Using this technique, a wide variety of microglial ion currents were revealed and characterised with respect to their kinetic and pharmacological properties but the exact molecular correlates for some of these currents are still not completely defined (Kettenmann *et al.*, 1993; Eder, 1998).

As immune cells of the brain, microglia present particular electrophysiological characteristics. The presence of a wide variety of ion currents has been reported in microglia (Figure 11). For example, voltage-dependent proton currents, Cl^- currents, purino-dependent cation currents, Ca^{2+} currents, such as iCRAC, HERG-like currents, sodium voltage-dependent currents, and voltage-dependent and Ca^{2+}-dependent K^+ currents are listed in the literature (Eder, 1998; Inoue, 2008).

Interestingly, in microglia, K^+ current properties differ drastically depending on the functional state of the microglia (Figure 11 A and B) (Norenberg *et al.*, 1994; Fischer *et al.*, 1995; Eder, 1998; Draheim *et al.*, 1999; Prinz *et al.*, 1999; Schilling *et al.*, 2000; Pannasch *et al.*, 2006). K^+ channels are involved in the regulation of membrane potential, cell volume and intracellular ion concentrations. Moreover, K^+ channels are linked to microglial activation processes like proliferation, motility, phagocytosis, cytokine release and production of reactive oxygen species (Eder, 1998 and 2005; Khanna *et al.*, 2001; Fordyce *et al.*, 2005; Kaushal *et al.*, 2007; Li *et al.*, 2008; Wu *et al.*, 2009). Furthermore, in lymphocytes, K^+ channels are known to be involved in cell activation processes (Chandy *et al.*, 2004). Thus, K^+ channels are a potential target for pharmacological immunomodulation in autoimmune or neurodegenerative diseases.

Although the presence of voltage-dependent and Ca^{2+}-activated K^+ currents in microglia has been documented in the past, the function and modulation of these currents in microglia are still not fully understood and the molecular identities of the K^+ channels involved remain

unclear. The Kir2.1 channel is suspected to be responsible for voltage-dependent inward rectifying currents, whereas Kv1 voltage-gated channels are most frequently proposed for the voltage-dependent outward K^+ currents (Eder, 1998; Kotecha and Schlichter, 1999; Pannasch *et al.*, 2006). However, the identification of the exact Kv1 channel is difficult to unravel because Kv1 channels have close biophysical and pharmacological characteristics and are also able to form heteromers with hybrid properties (Vincente *et al.*, 2006; Villalonga *et al.*, 2007; Menteyne *et al.*, 2009).

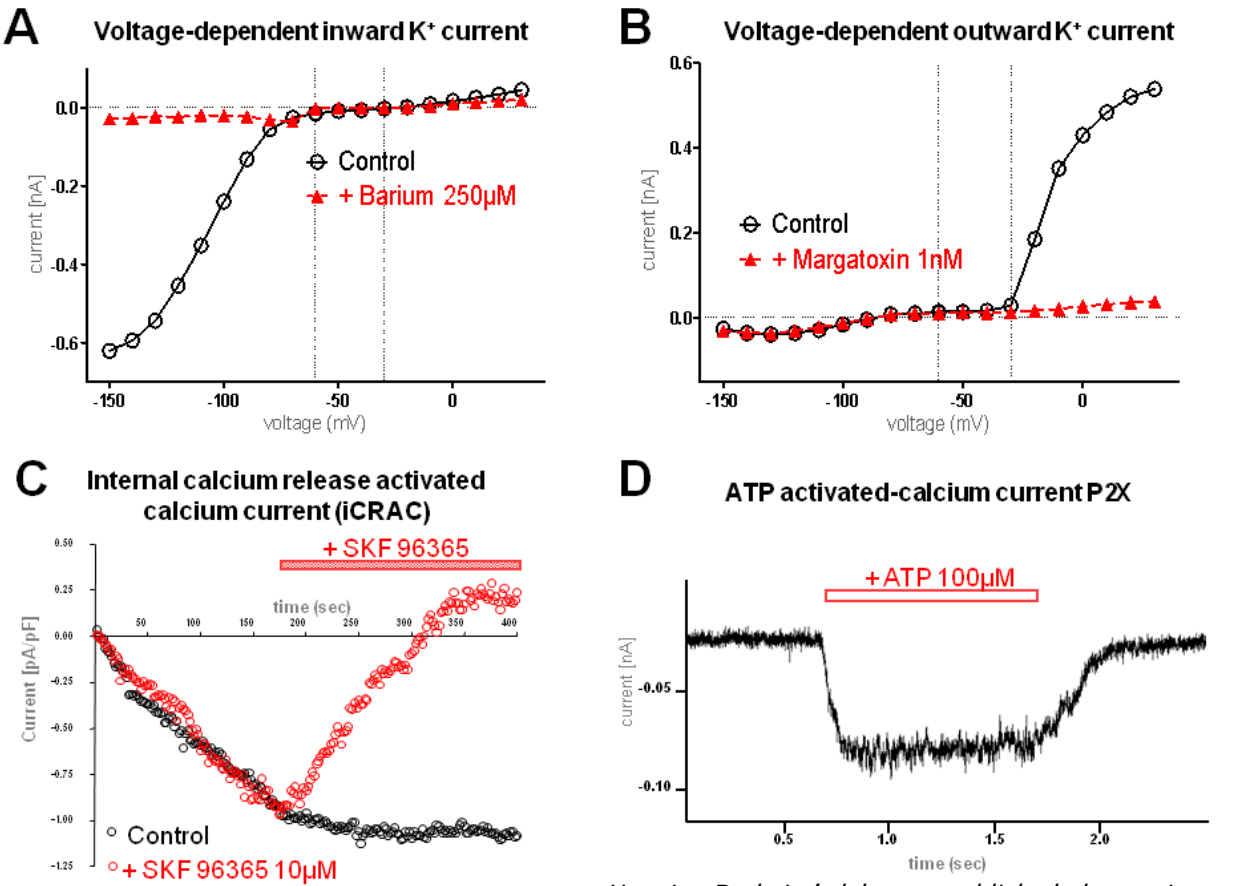

Henning Draheim's labor, unpublished observations (DR)

Figure 11: Microglia express different ion currents.

A wide variety of ion currents are present in microglia. These ion currents are controlled by ion channels, which are crucial for microglia activity. ***A)*** For example, resting microglia display a large voltage-dependent inward K^+ current. This current can be blocked by barium ions and is supposed to be elicited by the action of Kir2.1 channels. ***B)*** Activated microglia exhibit an additional voltage-dependent K^+ current. This current is an outward K^+ current induced by the opening of Kv channels and can be blocked by margatoxin. ***C)*** Microglia also have iCRAC currents, which allow them to refill their intracellular Ca^{2+} stores. ***D)*** Extracellular ATP binds to P2X channels present on microglia membrane and induce a non-selective cation influx.

2.7. *Involvement of microglia in neurodegeneration*

Neuroinflammation and activated microglia are observed in numerous neuropathologies (e.g. ischemia, hypoxia, AIDS dementia, chronic pain, brain tumours) and in neurodegenerative diseases (e.g. Alzheimer's disease, Parkinson's disease, multiple sclerosis, amyotrophic lateral sclerosis, Huntington's disease, Creutzfeldt-Jacob disease) (Tambuyzer *et al.*, 2008) (Figure 12). Despite accumulating evidence of a microglial role in Parkinson's disease, little is known about the exact contribution of microglia to the onset and progression of the neurodegenerative process.

In *post mortem* and in *in vivo* studies, widespread microglial activation in almost all brain areas and increased levels of cytokines were closely correlated to neurodegenerative diseases, and in particular to Parkinson's disease (Figure 12) (McGeer *et al.*, 1988; Hunot *et al.*, 1999; Hirsch *et al.*, 2003; Gerhard *et al.*, 2005; Long-Smith *et al.*, 2005; Block *et al.*, 2007). Whether microglial activation is a symptom or a cause of Parkinson's disease is subject to a longstanding debate. However, microglial activation has been shown to take place even before the appearance of any symptoms (Block *et al.*, 2007). In addition, after a discrete MPTP intoxication, activated microglia and abnormal neuroinflammation remain present in the brain for years, in human (Langston *et al.*, 1999) and monkeys (McGeer *et al.*, 2003). It has been also observed that stereotactic injection of LPS into the *substantia nigra* induced parkinsonism in rodents (Liu, 2006; Dutta *et al.*, 2008) and that IL-1 played a central role in this process (Godoy *et al.*, 2008). Moreover, emergence of parkinsonism-like features is sometimes linked with sequelae of infectious diseases, such as influenza, West Nile viral encephalitis or Japanese encephalitis (Long-Smith *et al.*, 2005; Weintraub *et al.*, 2008). Interestingly, the results of some epidemiological studies add weight to the possible link between the immune system and Parkinson's disease. For instance, a relationship between IL-1 polymorphisms and Parkinson's and Alzheimer's disease risk factor was demonstrated (McGeer *et al.*, 2002; Schulte *et al.*, 2002). Another study revealed that a common genetic variation in the human leukocyte antigen (HLA) region was associated with late-onset sporadic Parkinson's disease (Hamza *et al.*, 2010). Other epidemiological studies have shown that the long-term consumers of non-steroidal anti-inflammatory drugs presented a lower risk of developing Parkinson's or Alzheimer's disease (Esposito *et al.*, 2007; Imbimbo, 2009).

Taken together, these observations suggest that, in Parkinson's disease, microglia are likely to have a deleterious effect on neuron survival rather than a beneficial role (Figure 13) (Kim and Joh, 2006). Dopaminergic neurons from the *substantia nigra* are particularly vulnerable to oxidative stress and inflammation because of their dopaminergic metabolism, high concentration in iron and low content in gluthatione (Jenner and Olanow, 2006). Furthermore, activation of microglia, present in a high proportion in the *substantia nigra*, may exaggerate the inflammatory effects on dopaminergic neurons. Due to the plethora of toxic factors released by microglia, their inappropriate and chronic pro-inflammatory activity can elicit neurotoxicity and neuroinflammation. The secretion of abnormal amounts of pro-inflammatory and pro-apoptotic cytokines and chemokines (e.g. IL-1β, IL-6, IL-12, TNF-α) and the production of excitatory amino acids, eicosanoids, reactive oxygen species and nitric oxide are suspected to be harmful to neurons (Block *et al.*, 2007). In particular, IL-1 α and β is known to contribute to Alzheimer's and Parkinson's pathologies (Schulte *et al.*, 2002; Griffin, 2006).

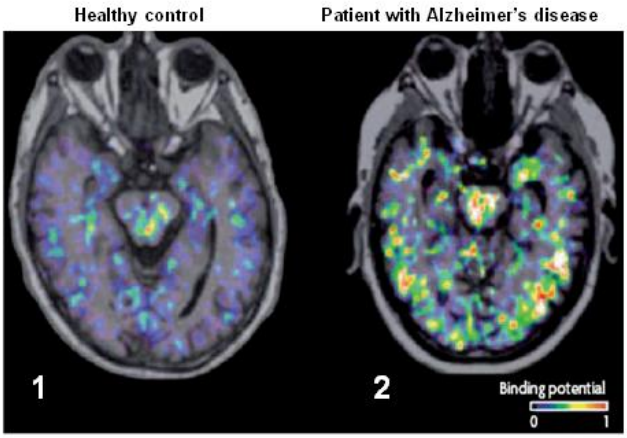

Adapted from Block *et al.*, 2007 and Gerhard *et al.*, 2005 (DR)

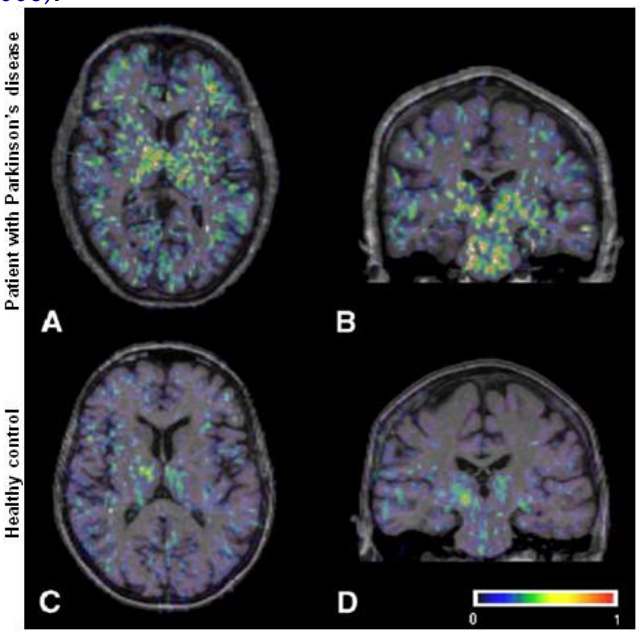

Figure 12: PET imaging of microglial activation.

Microglial activation can be monitored in human using the non-invasive positron emission tomography technology (PET). Activated microglia, which selectively overexpressed the peripheral benzodiazepine receptor, can be visualised by the binding of [^{11}C](R)-PK11195 ligand. The binding of the [^{11}C](R)-PK11195 marker is shown according to a rainbow pseudocolour scale. On the left panel, transverse brain sections of a healthy 74-year old man ***(1)*** in comparison with the same section of a 65-year old Alzeihmer's patient ***(2)***. On the right panel, transverse and coronal brain sections of a Parkinson's patient ***(A and B)*** in comparison to a healthy control ***(C and D)***. In comparison with the healthy controls, a significant increased binding is obsious in the brains from Alzheimer's and Parkinson's patients, indicating that microglia are activated in these pathologies.

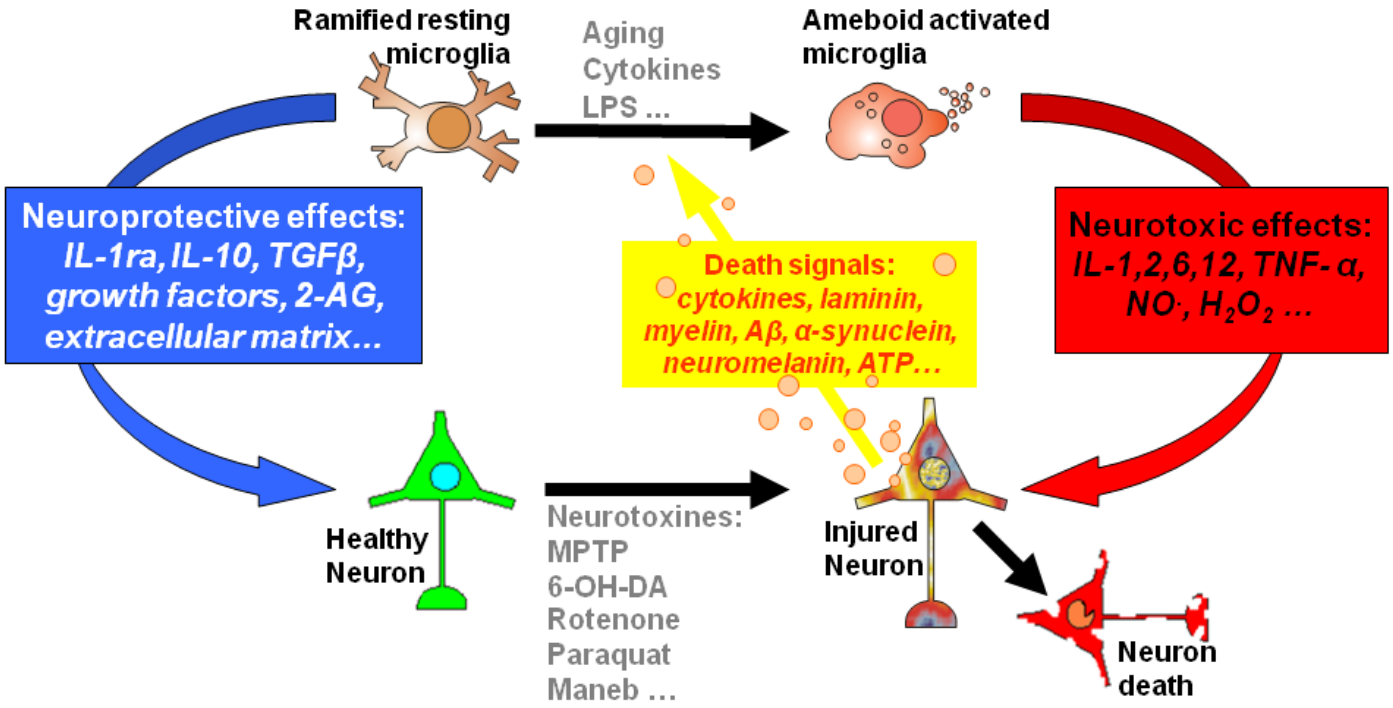

Figure 13: Neuroinflammation and neurodegeneration draw a self-propelling vicious circle.
As the major immuno-competent cells of the brain, microglia are critically involved in neuroprotection as well as in neurodegeneration. Microglia are usually beneficial and protect neurons through secretion of anti-inflammatory cytokines and growth factors (in blue). However, once activated, microglia can be deleterious through an exaggerated pro-inflammatory activity (in red). Environmental (in grey) or endogenous (in yellow) factors are suspected to promote the deleterious effect of microglia.

The reasons why inflammation is chronic and inappropriate in Parkinson's patients are still enigmatic. It is presumed that a kind of self-propelling vicious circle exists, wherein neuronal death activates microglia and that microglial activation sustains neurodegeneration (Figure 13). However, it is still unclear how this vicious circle occurs and works. Compelling evidence highlights a link between aging, microglial and neural dysfunction, increased neuroinflammation, oxidative stress and neurodegenerative pathologies (Gao and Hong, 2008; Tansey *et al.*, 2008). Aging provokes microglial senescence and the loss of beneficial microglial effects on neurons (Streit and Xue, 2009). Moreover, aged microglia release increased amounts of pro-inflammatory cytokines and lower levels of the anti-inflammatory cytokine IL-10 (Ye and Johnson, 2001; Xie *et al.*, 2003; Sierra *et al.*, 2007). In addition, microglia were recently shown to be activated by the main component of the Lewy bodies, namely α-synuclein (Croisier *et al.*, 2005; Zhang *et al.*, 2005; Gao *et al.*, 2008).

Like a double-edge sword, microglial activation is primarily a defense reaction designed to protect neurons, but, in pathological conditions, it can provoke uncontrolled collateral damages. This has led to the notion of protective autoimmunity and the development of immunomodulatory therapies which specifically increase neuroprotective aspects of microglia and thereby prevent dopaminergic neuron death (Liu, 2006).

Initial encouraging experimental results on Parkinson's animal models suggest that in fact immunomodulation can induce neuroprotection (Long-Smith *et al.*, 2005). Thus, it is imperative to achieve a better understanding of the mechanisms of microglial activation and dysfunction with regard to age and neurodegenerative conditions. To do so, the development of validated *in vitro* models are needed to clarify the basic mechanisms of age-related changes in microglia function and to search for approaches to enhance the neuroprotective effect of microglia.

3. Problematic, strategies and aims

3.1. Aim 1: To study α-synuclein oligomerisation and its biological effects.

As previously mentioned, α-synuclein is a key component of Parkinson's pathology and its aggregation is a histological hallmark of the disease. However, substantial work is required to uncover the exact involvement of α-synuclein in Parkinson's pathogenesis. In particular, the identification of the different oligomeric forms of α-synuclein protein, their molecular dissection and their biological effects are essential to clarify their contribution, if any, to neurotoxicity. As a consequence, we decided to study α-synuclein polymerisation *in vitro*. To do so, we developed new methods to produce and isolate different preparations of α-synuclein oligomers. Subsequently, we sought to characterise these different preparations and to test their biological effects on neurons.

3.2. Aim 2: To define the electrophysiological characteristics of microglia.

Microglia are a putative target for developing immune-based therapeutic strategies against neurodegenerative disorders. A common and efficient way to modulate the action of a specific cell type is to target its ion channels. Therefore, we focused our interest on the electrophysiological characteristics of microglia, with a particular interest in K^+ channels. We set out to identify the type of K^+ channels that were expressed in microglia and study their regulation after microglial activation. In addition, we compared the electrophysiological characteristics of different *in vitro* microglial models.

3.3. Aim 3: To determine age-related changes in microglial activation.

Aging and/or pathological conditions are suspected to induce microglial dysfunction, exacerbating of their deleterious effects and, in parallel, reducting of their protective effects on neurons. However, age-related changes in microglia are poorly studied and are still not well understood. One major obstacle is the lack of a suitable microglial *in vitro* model for studying microglial activation in an aged environment. Indeed, for practical reasons, most studies presently use primary microglia from neo-natal rodents or microglial cell lines, although these models do not mimic the age-dependent changes in microglial function. Consequently, our primary aim was to develop a new method for isolating and culturing primary microglia from aged mice and compare these mature primary microglia with the commonly used neo-natal microglia, as well as a microglial cell line.

3.4. Aim 4: To investigate the link between microglial activation and Parkinson's disease.

The final aim of my PhD thesis project was to achieve a better understanding of the link between microglia, neurodegeneraton and Parkinson's disease. We were interested in finding out the mechanism underlying abnormal microglial activation and the influence of microglia on neuronal death. We were also interested in finding elicitors or targets for microglial modulation with a view to developing potential therapeutic strategies against Parkinson's pathogenesis.

Thus, we meant to combine the two axes of my research - α-synuclein and microglia - to take a closer look at the potential cross-connections between them, as recently suggested in the literature (Croisier *et al.*, 2005; Zhang *et al.*, 2005; Gao *et al.*, 2008).

III. Results and discussion

1. α-synuclein oligomers (article 1)

9220 • The Journal of Neuroscience, August 22, 2007 • 27(34):9220–9232

Neurobiology of Disease

Different Species of α-Synuclein Oligomers Induce Calcium Influx and Seeding

Karin M. Danzer,[1] Dorothea Haasen,[2] Anne R. Karow,[1] Simon Moussaud,[1] Matthias Habeck,[3] Armin Giese,[3] Hans Kretzschmar,[3] Bastian Hengerer,[1] and Marcus Kostka[1]

[1]Central Nervous System Research and [2]Integrated Drug Discovery, Boehringer Ingelheim Pharma, 88397 Biberach, Germany, and [3]Zentrum für Neuropathologie und Prionforschung, Ludwig-Maximilians Universität München, 81377 München, Germany

1.1. *Résumé en français*

L'agrégation anormale de la protéine α-synucléine (α-syn) est liée à la maladie de Parkinson ainsi qu'à d'autres maladies neurodégénératives. Il semble que ce soient les agrégats d'α-syn de petite taille, tels que les oligomères préfibillaires et les protofibrilles, et non les grosses fibrilles qui soient à l'origine des effets pathologiques de l'α-syn dans la maladie de Parkinson. Malgré les efforts conséquents investis dans l'étude de l'agrégation anormale de l'α-syn, encore aucune étude n'a réussi à isoler, comparer et caractériser les différentes formes d'oligomères à l'échelle moléculaire, ainsi qu'à étudier leurs effets biologiques sur les neurones. Pour cet article, nous avons utilisé une nouvelle technique d'analyse des particules à l'échelle moléculaire. Cette technique nous a permis d'identifier, d'analyser et de comparer les différentes formes d'oligomères d'α-syn. Nous avons ainsi développé trois nouveaux protocoles pour la production *in vitro* de différentes formes d'oligomères d'α-syn. Ces préparations d'oligomères d'α-syn ont été utilisées en culture cellulaire afin d'étudier leurs effets sur les neurones. Nous avons observé que nos trois protocoles d'oligomérisation produisaient différentes formes d'oligomères présentant des effets biologiques variés. Certains d'entre eux, à la manière de porines, perturbent l'homéostasie ionique des cellules en détruisant l'intégrité de leurs membranes biologiques, provoquant ainsi la mort cellulaire. D'autres oligomères diffusent dans les cellules et y induisent la formation de gros agrégats protéiques intracellulaires similaires à des corps de Lewy. A la lumière de nos données, nous pensons que dans les

conditions physiologiques, les différentes formes d'oligomères d'α-syn décrites ici coexistent probablement dans une forme d'équilibre dynamique. Ces différents oligomères induisent de manière directe et indirecte des dommages cellulaires aux neurones. Par conséquent, nos résultats suggèrent que l'inhibition de la formation d'oligomères d'α-syn pourrait permettre de bloquer la neurotoxicité induite par l'α-syn. Ceci est une piste intéressante en vue du développement de nouvelles substances pharmacologiques pour traiter la maladie de Parkinson ainsi que les autres synucléinopathies.

1.2. Foreword

This substantial work has been performed by several scientists – including me – from Boehringer Ingelheim. Furthermore, additional persons from the Neuropathology and Prion research department from the Ludwig-Maximilians University Munich were involved in this article: Matthias Habeck, Armin Giese and Hans Kretzschmar who performed the FIDA experiments.

1.3. Summary

Aggregation of α-synuclein (α-syn) has been linked to the pathogenesis of Parkinson's disease and other neurodegenerative diseases. Increasing evidence suggests that prefibrillar oligomers and protofibrils, rather than mature fibrils of α-syn, are the pathogenic species in Parkinson's disease. Despite extensive effort on studying oligomerization of α-syn, no studies have compared different oligomer species directly on a single-particle level and investigated their biological effects on cells. In this study, we applied a novel highly sensitive single molecule detection system that allowed a direct comparison of different oligomer types. Furthermore, we studied biological effects of different oligomer types on cells. For this purpose, we developed new oligomerization protocols, that enabled the use of these different oligomers in cell culture. We found that all of our three aggregation protocols resulted in heterogeneous populations of oligomers. Some types of oligomers induced cell death *via* disruption of cellular ion homeostasis by a presumably pore-forming mechanism. Other oligomer types could directly enter the cell resulting in increased α-syn aggregation. Based on our results, we propose that under various physiological conditions, heterogeneous populations of oligomeric forms will coexist in an equilibrium. These different oligomer types lead directly or indirectly to cell damage. Our data indicate that inhibition of early α-syn aggregation events would consequently prevent all α-syn oligomer related toxicities. This has important implications for the development of disease-modifying drugs for the treatment of Parkinson's disease and other synucleinopathies.

1.4. Introduction

Parkinson's disease is pathologically characterized by a selective loss of dopaminergic neurons in the *substantia nigra* and aggregated protein deposits termed Lewy bodies (Dauer and Przedborski, 2003). The main component of these intracellular deposits is aggregated α-synuclein (α-syn) (Goedert, 2001). Gene multiplication in the α-*syn* gene (Singleton *et al.*, 2003; Chartier-Harlin *et al.*, 2004) and missense mutations (Polymeropoulos *et al.*, 1997; Kruger *et al.*, 1998; Zarranz *et al.*, 2004) are linked to familial forms of Parkinson's disease. This supports the importance of α-syn in the pathogenesis of Parkinson's disease.

In vitro studies revealed that α-syn aggregation is a nucleation-dependent process that occurs in a process ranging from monomer *via* oligomers to fibrils (Wood *et al.*, 1999; Conway *et al.*, 2000).

There is a growing body of evidence suggesting that the prefibrillar oligomers and protofibrils, rather than mature fibrils of α-syn, are the pathogenic species (Conway *et al.*, 2000; Goldberg and Lansbury, 2000; Masliah *et al.*, 2000; Auluck *et al.*, 2002; Bucciantini *et al.*, 2002, 2004; Gosavi *et al.*, 2002; Kayed *et al.*, 2003, 2004; Park and Lansbury, 2003; Bodner *et al.*, 2006; El-Agnaf *et al.*, 2006).

To date there are several protocols on oligomer preparation existing (Kayed *et al.*, 2003; Lashuel and Grillo-Bosch, 2005). Whether these methods end up in the same type of oligomers is currently not clear. If and how oligomers differ structurally from each other on a single-particle level is not known. More importantly, biological effects of different types of oligomers on cells have not been studied directly. More importantly, the question arises whether different types of oligomers induce different biological effects on cells.

To address these questions, we developed novel standardized methods of α-syn oligomer generation and compared the samples directly on a single-particle level. We applied fluorescence intensity distribution analysis (FIDA) (Kask *et al.*, 1999, 2000; Zemanova *et al.*, 2004; Levin *et al.*, 2005) in a confocal single-molecule detection system and compared our results with the fluorescence-independent method atomic force microscopy (AFM).

We exposed these differently generated oligomers to cells to investigate whether different types of oligomers have various biological effects on cells. We examined their respective actions on cytosolic calcium levels and their ability to seed intracellular aggregation of α-syn in SH-SY5Y cells [overexpressing α-syn and SH-SY5Y cells with endogenous α-syn as well as in primary neurons]. This study aims to elucidate the biological effects that might also occur in patients with Parkinson's disease or other synucleinopathies. The identification of pathologically relevant α-syn oligomer species therefore forms the basis for the identification of structural targets for antiaggregatory compounds that will be of great importance to prevent these amyloidogenic diseases.

1.5. Materials and Methods

Materials

All chemicals used were purchased from Sigma (Munich, Germany) unless stated otherwise.

Expression and purification of recombinant wild-type α-syn

Expression and purification was performed as described previously by Nuscher *et al.* (2004). Briefly, pET-5a/α-syn wild-type (wt) plasmid (a kind gift from Christian Haas and Philipp Kahle, LMU Munich, Munich, Germany) was used to transform *Escherichia coli* BL21(DE3) pLysS (Novagen, Madison, WI). Expression was induced with isopropyl-ß-D-thiogalactopyranose (Promega, Mannheim, Germany) for 4h. Cells were harvested, resuspended in 20mM Tris and 25mM NaCl, pH 8.0, and lysed by freezing in liquid nitrogen followed by thawing. After 30min of boiling, the lysate was centrifuged at 17600 x *g* for 15 min at 4°C. Supernatant was filtered through a 0.22µm filter (Millex-GV; Millipore, Bedford, MA) before being loaded onto a HiTrap Q HP column (5 ml; Amersham Biosciences, Munich, Germany) and eluted with a 25 to 500mM NaCl salt gradient. The pooled α-syn peak was passed over a Superdex 200 HR 10/30 size exclusion column (Amersham Biosciences) using 20mM Tris and 25mM NaCl, pH 8.0, as running buffer. The pooled α-syn peak was concentrated using Vivaspin columns [molecular weight cutoff (MWCO), 5kDa; Vivascience, Stonehouse, UK] and equilibrated to water. The protein concentration was determined using a BCA protein-quantification kit (Pierce, Rockford, IL). Aliquots were lyophilized and stored at -80°C.

Fluorescent labeling of α-syn

Protein labeling with the aminoreactive fluorescent dye Alexa Fluor-488-O-succinimidylester (Alexa-488; Invitrogen, Eugene, OR) was performed according to the manufacturer's manual. Unbound fluorophores were separated by filtration steps in PD10 columns (Sephadex G25; Amersham Biosciences) equilibrated with 50mM sodium phosphate, pH 7.0. Quality control of labeled α-syn was performed by mass spectrometry and by fluorescence correlation spectroscopy (FCS) measurements on an Insight Reader (Evotec Technologies, Hamburg, Germany). The typical labeling ratio, was approximately two dye molecules per α-syn molecule. To remove preformed aggregates, the stock solution of labeled α-syn was subjected to size exclusion chromatography (Sephadex 200; Amersham Biosciences).

Preparation of α-syn oligomers

- Long incubation protocol (types A1 and A2).

Type A oligomers were prepared by dissolving lyophilized protein in 50mM sodium phosphate buffer, pH 7.0, containing 20% ethanol to a final concentration of 7µM. In case of type A2 oligomers, 10µM $FeCl_3$ (J.T. Baker, Griesheim, Germany) were additionally added, whereas type A1 oligomers were prepared without addition of $FeCl_3$. After 4h of shaking (GFL, Burgwedel, Germany), both types of oligomers were relyophilized and resuspended with one-half of starting volume in 50mM sodium phosphate buffer, pH 7.0, containing 10% ethanol. This was followed by shaking for 24 h (stage 5, thermomixer 5436; Eppendorf, Wesseling-Berzdorf, Germany) at room temperature (RT) with open lids to evaporate residual ethanol. After 6 days incubation of both oligomers types at RT with closed lids, oligomers were used for characterization studies (e.g., calcium influx and

toxicity experiments). Alexa Fluor-488-O-succinimidylester-labeled oligomers were prepared in the same manner as nonlabeled oligomers by using Alexa-488 conjugated monomers.

- Stirring incubation protocol (types B1 and B2).

Type B oligomers were prepared similarly to type A oligomers by dissolving lyophilized protein in 50mM sodium phosphate buffer, pH 7.0, containing 20% ethanol to a final concentration of 7µM. In case of type B2 oligomers, 10µM $FeCl_3$ was additionally added, whereas type B1 oligomers were prepared without addition of $FeCl_3$. After 4h of shaking (GFL), both oligomer types were relyophilized and resuspended with one-half of starting volume of 50mM sodium phosphate buffer, pH 7.0, containing 10% ethanol. Additionally, after this procedure, oligomers were stirred (RCT basic; IKA Labortechnik, Staufen, Germany) with open lids using a Teflon-coated microstirrer bar (Fisher, Pittsburgh, PA) for 24h at RT. Alexa-488-labeled oligomers were prepared in the same manner as nonlabeled oligomers by using Alexa-488 fluorescent monomer.

- Spin concentration protocol (types C1 and C2).

Type C oligomers were also prepared similarly to type A oligomers by dissolving lyophilized protein in 50mM sodium phosphate buffer, pH 7.0, containing 20% ethanol to a final concentration of 7µM. In case of type C2 oligomers, 10µM $FeCl_3$ was additionally added, whereas oligomers type C1 were prepared without addition of $FeCl_3$. After overnight incubation at room temperature under continuously shaking (GFL), oligomers were concentrated using ultracentrifugation (VivaSpin 500 columns; Vivascience). The oligomers were separated from monomer using a MWCO 30kDa filter. The oligomers were retained while the monomeric protein passed through the filter as verified by FCS. Alexa-488-labeled oligomers were prepared in the same manner as nonlabeled oligomers by using Alexa-488-conjugated monomers.

Atomic force microscopy

Sample preparation for AFM was performed at RT. Typically, 3-6µl of different oligomers diluted in corresponding buffers to a working concentration of 1µM were applied to a freshly cleaved muscovite mica substrate (Ted Pella, Redding, CA) and incubated for 1min. The mica surface was then rinsed with 7x 200µl of double-processed tissue culture water (Sigma) to remove salts and loosely bound proteins. AFM images were recorded on a MultiModeTM SPM (Digital Instruments, Santa Barbara, CA) equipped with an E-Scanner using etched silicon NanoProbes (model RTESP; Veeco Instruments, Mannheim, Germany). All measurements were performed in the tapping mode with scan rates of ≃0.5Hz. Images were processed using NanoScope software (Digital Instruments).

Confocal single-particle analysis

FIDA measurements were performed on an Insight Reader (Evotec Technologies) with dual-color excitation at 488 and 633nm, using a 40x 1.2 numerical aperture microscope objective (Olympus, Tokyo, Japan) and a pinhole diameter of 70µm at the FIDA setting. Excitation power was 200µW at 488nm. Measurement time was 10s. Scanning parameters were set to 100µm scan-path length, 50Hz beam-scanner frequency, and 2000µm positioning-table movement. This is equivalent to ≃10mm/s scanning speed. All measurements were performed at RT. The fluorescence signal was analyzed by FIDA using FCSPP evaluation software version 2.0 (Evotec Technologies). Fluorescence from the fluorophore Alexa-488 was recorded with a single-photon detector. Photons were summed over time intervals of constant length (bins) using a bin length of 40µs (Kask *et al.*, 1999, 2000). Based on

previous results, the obtained data were analyzed by a three-component fit with two components fixed to a particle brightness Q of 20 and 50, respectively. For the threshold setting, nonaggregated reference samples were used. This single-molecule detection technology allows highly sensitive analysis of protein aggregation by slight changes in the brightness of individual particles. FIDA is able to distinguish between differently bright species and, as such, gives indirect information about particle sizes.

Cell culture

SH-SY5Y human dopaminergic neuroblastoma cells were maintained at 37°C in 5% CO_2 in high-glucose DMEM (PAA Laboratories, Pasching, Austria) supplemented with 15% fetal bovine serum (Invitrogen) and 4mM glutamine (Invitrogen).

To generate stable cell lines, SH-SY5Y cells were transfected using Metafectene (Cambio, Cambridge, UK) with pcDNA 3.1neo encoding α-syn[wt], α-syn[A30P], or α-syn[A53T] (plasmids were a kind gift from C. Haas and P. Kahle). As mock vector controls, SH-SY5Y cells were transfected with plasmid pUHD15.1 encoding the transactivator protein for the tetracycline inducible expression system (Clontech, Saint-Germain-en-Laye, France). Mock-transfected cells served as cells with endogenous level of α-syn.

Transfected cells were selected with 1000µg/ml G418 (PAA Laboratories) for 2-3 weeks until colonies emerged. Stable transfectants established from these colonies were tested for their α-syn expression levels using immunofluorescence and Western blot analyses.

Cortical cell culture

Neuron-enriched cerebral cortical cells were prepared from embryonic brains (embryonic day 14) of mice. Cortices were dissected from embryonic brain and the meninges were removed. The cells were dissociated by trypsinization and tituration. The dissociated cells were resuspended in serum-free B27/neurobasal medium (Invitrogen) and plated at a density of 1.25 x 10^5 cells/cm^2 on dishes precoated with poly-D-lysin/laminin. Cells were maintained at 37°C in the presence of 10% CO_2/90% air in a humidified incubator. The medium was changed every third day.

Measurement of intracellular Ca^{2+} using FLIPR.

For intracellular Ca^{2+} measurements using fluorescence imaging with a fluorescent imaging plate reader (FLIPR), primary cortical neurons were seeded at a density of 1.25 x 10^5 cells/cm^2 on 384-well, black clear-bottom microtiter plates (BD Biosciences, Heidelberg, Germany) precoated with poly-D-lysin/laminin and cultured as described above. After 7 days, cortical neurons were used for Ca^{2+} measurements. Mock-transfected SH-SY5Y cells and α-syn[wt], [A30P], or [A53T] mutants were seeded into collagen I coated 384-well, black clear-bottom microtiter plates (BD Biosciences) at a density of 6000 cells/well and cultured overnight. At the day of experiment, cells were washed with Ringer buffer [containing (in mM) 130 NaCl, 5 KCl, 1 $CaCl_2$, 1 $MgCl_2$, 2 KH_2PO_4, 5 glucose, and 20 HEPES] and loaded for 60 min with 2 µM the cell-permeable Fluo-4 AM (Teflabs, Austin, TX) in Ringer buffer containing 0.1% (w/v) pluronic acid F127 (Invitrogen). After removal of the fluorophore loading solution, cell layers were washed with Ringer buffer, incubated at room temperature for 30min, and washed again. The cell plates were then loaded into an FLIPR (TETRA TM; Molecular Devices, Wokingham, UK) together with a separate 384-well plate containing oligomers and controls. Treatment of cells was performed with the following final concentrations: 7µM oligomer types A1 and A2 (referring to moles of monomer starting concentration), 500µg/ml gramicidin D, and 1.5µM ionomycin as positive controls. Test

compounds were distributed in a randomized pattern to minimize any cell plating effects caused by well position. The FLIPR was programmed to transfer the test compounds and solvents simultaneously to all 384 wells 10s after commencement of recording of fluorescence [expressed as relative fluorescence units (RFUs)]. Fluorescence was excited at 488nm and emission was measured at 510–560nm. The duration of recording was 10min. Data are displayed as negative control-corrected values, meaning signal response to oligomers including subtraction of corresponding solvent controls. The resulting signals were quantified by taking the maximum peak height of recording duration using Screenworks 1.2.0.73 software and are expressed as mean ± SEM. Treatment effects were analyzed by unpaired *t* test for each cell line. For the SH-SY5Y cell lines, *p* values were additionally adjusted for multiple testing using the Bonferroni correction method. A *p* value <5% was considered statistically significant. Differences (Δ) between treated and untreated cell lines were quantified by differences of mean values and corresponding 95% confidence intervals (CIs). All cell lines were separately analyzed. For investigation of calcium source, calcium was omitted from the Ringer buffer and experiments were performed as described above. To demonstrate a calcium ion channel-independent effect of oligomers, 20μM cobalt, a nonspecific calcium-channel blocker, was applied to cells 5min before the application of oligomers. Experimental setup was the same as described above.

Fluorescence imaging with confocal microscopy.

SH-SY5Y cells overexpressing α-syn[wt] were seeded into collagen I-coated 96-well, black μ-clear-bottom microtiter plates (Greiner Bio-One, Frickenhausen, Germany) at a density of 7500 cells/well and cultured overnight. Cortical neurons were seeded at a density of 6 x 10^4 cells/cm^2 on 96-well, black μ-clear-bottom microtiter plates (Greiner Bio-One) precoated with poly-D-lysin/laminin and cultured as described above. After 7 days, cortical neurons were used for Ca^{2+} measurements.

Cells were washed with Ringer buffer [containing (in mM) 130 NaCl, 5 KCl, 1 CaCl2, 1 $MgCl_2$, 2 KH_2PO_4, 5 glucose, and 20 HEPES] and loaded with 2μM the cell-permeable Fluo-4 AM (Teflabs) in Ringer buffer containing 0.1% (w/v) pluronic acid (Invitrogen) at 37°C for 60min. After removal of the fluorophore loading solution, the cells were washed with Ringer buffer, incubated at room temperature for 30min, and washed again. The imaging system consisted of an inverted confocal microscope (DM IRBE; Leica, Wetzlar, Germany) equipped with a Leica 63x objective. Fluorescence excitation was performed with a 488nm argon ion laser and emitted fluorescence (505nm <λ< 530nm) was imaged by a scan head (Leica TCS SP). Time-lapse pictures (one frame per 2.5s) were captured using the Leica confocal software package and fluorescence intensities were measured from regions of interest centered on individual cells. Signals were expressed in RFUs. Treatment of cells was performed with the following final concentrations: 7μM monomer, 7μM oligomer types A1 and A2 (referring to moles of monomer starting concentration), and 6μM ionomycin as a positive control. Treatments were applied by pipetting a fixed aliquot of 50μl into the recorded well directly above the objective. The duration of recording was 150 or 300s. The 10-fold accelerated time-lapse videos were made using Windows Movie Maker software (Microsoft, Redmond, WA).

Measurement of membrane potential changes using FLIPR

Primary cortical neurons were seeded at a density of 1.25 x 10^5 cells/cm^2 on 384-well, black clear-bottom microtiter plates (BD Biosciences)

precoated with poly-D-lysin/laminin and cultured as described above. After 7 days, cortical neurons were used for measurements of membrane potential. FLIPR membrane potential assay kit was performed according to the manufacturer's instructions. Briefly, cells were washed one time with assay buffer (1x HBSS with 20mM HEPES, pH 6). Twenty microliters of loading buffer (catalog #8034; Molecular Devices) reconstituted as described in the product insert (final concentration, 20µM) was added to each well. Cell plates were incubated for 30min at 37°C. The cell plates were then loaded into an FLIPR (TETRA TM; Molecular Devices) together with a separate 384-well plate containing oligomers and controls. Treatment of cells was performed with the following final concentrations: 7µM oligomer types A1 and A2 (referring to moles of monomer starting concentration), and 500µg/ml gramicidin D as positive control. The FLIPR was programmed to transfer the test compounds and solvents simultaneously to all 384 wells 15s after commencement of recording of fluorescence (expressed as RFUs). Fluorescence was excited at (510nm < λ< 545nm) and emission was measured at (565nm <λ< 625nm). Duration of recording was 10min. Data are displayed as negative control corrected values, meaning signal response to oligomers including subtraction of corresponding solvent controls. The resulting signals were quantified by taking the maximum peak height of recording duration using Screenworks 1.2.0.73 software and are expressed as mean ± SEM. Treatment effects for primary neurons were analyzed by one-sample *t* tests versus the hypothetical value 0 and quantified by mean values of differences (Δ) and corresponding 95% CIs.

Cell treatment and immunofluorescence staining

To investigate toxic effects or seeding properties of different oligomer preparations, SH-SY5Y cells overexpressing mutant α-syn[A53T] were seeded at 5000 cells/well using collagen I-coated 384-well, black clear-bottom microtiter plates (BD Biosciences). On the next day, cells were treated with 7µM (referring to moles of monomer) of different oligomers and the same volume of the corresponding solvent controls. After 2h treatment, oligomers were diluted 1:2 in culture medium for subsequent overnight treatment.

The treatment was stopped after overnight incubation using 2% formaldehyde and 1µM Hoechst 33342 (Invitrogen) in PBS as fixation solution. After washing, the cells were permeabilized and unspecific binding sites were blocked using 0.05% saponin and 1% bovine serum albumin in PBS. After washing, the primary antibody [rabbit antibody against activated caspase-3 (Asp175; Cell Signaling Technology, Beverly, MA) or rabbit antibody against α-syn (ASY-1; a kind gift from Poul Henning Jensen, University of Aarhus, Denmark); described by Jensen *et al.* (2000)] was added for 1h at 37°C, followed by another washing step and incubation with the secondary antibody (anti-rabbit antibody labeled with Alexa-Fluor 647; Invitrogen) for 1h at RT. After a final washing step, 50µl/well remained as residual volume.

Western blotting of SH-SY5Y cell extracts

SH-SY5Y cells were scraped from 100mm dishes and washed by centrifugation and resuspension in cold PBS. The cells were resuspended in lysis buffer (250mM Tris, 750mM NaCl, 10mM EDTA, 1% NP-40, 25µg/ml leupeptin, protease inhibitor mixture, pH 7.4) and incubated on ice for 30min. After centrifugation at 1500 x *g* for 10min, protein concentrations of supernatants were quantified using the BCA assay (Pierce, Rockford, IL). Lysates (30µg of protein) were resolved by electrophoresis on a 4-12% Bis-Tris gradient gel (NuPAGE; Novex Bis-Tris Gel; Invitrogen) according to manufacturer's instructions using NuPAGE MES buffer. After transfer to nitrocellulose membrane (Protran; Whatman, Dassel, Germany) the blot was

blocked for 1h at RT with blocking buffer (I-block; Tropix, Bedford, MA). The blot was probed with ASY-1 antibody (1:500; a kind gift from Poul Henning Jensen) or anti-GAPDH (1:1000; HyTest, Turku, Finland) for 1h at RT. Bands were detected using alkaline phosphatase-conjugated secondary antibodies (1:5000; Tropix) and imaged with VersaDoc imaging system (Bio-Rad, Munich, Germany).

Measurement of the assay plates in the IN Cell Analyzer 3000

Automated confocal fluorescence microscopy using the IN Cell Analyzer 3000 (GE Healthcare Bio-Sciences, Little Chalfont, UK) has been described in detail (Haasen *et al.*, 2006; Wolff *et al.*, 2006). For our experiments, we used the 364 laser line combined with a 450BP25 emission filter for Hoechst 33342, the 647nm laser line combined with a 695BP55 emission filter for Alexa Fluor 647, and the 488nm laser line with a 535BP45 emission filter for Alexa Fluor 488. Fluorescence emission was recorded separately in the blue, red, and green channels, applying a flat-field correction for inhomogeneous illumination of the scanned area for each of the three channels.

Image analysis

Images stained for activated caspase-3 were analyzed using the nuclear trafficking (TRF2) algorithm of the IN Cell Analyzer 3000. Briefly, the algorithm identified the nuclei as pixel accumulations above a specified intensity threshold in the blue (nuclear) channel image. The number of nuclei corresponds to the absolute cell number. In a specified dilated "cytoplasmic" mask region around these nuclei, the algorithm then searched for cells above a defined threshold in the red channel image, identifying cells stained for activated caspase-3. The percentage of positive cells for each image was calculated as follows: the percentage of positive cells = (number of positive cells in signal channel/number of total cells in nuclear channel) x 100. For each treatment, the percentage of positive cells and the number of total cells were normalized to the respective solvent controls to give the percentage of control values. The mean and SEM for each analysis were calculated from the indicated number of images. Statistical significance was determined by unpaired *t* test with $p < 0.05$.

Statistical analysis

Statistical analysis was performed as indicated as mentioned in the respective sessions for calcium measurements, measurement of membrane potential, and image analysis using IN Cell Analyzer3000.

1.6. Results

Aggregation of α-syn plays an important role in the pathogenesis of Parkinson's disease and other synucleinopathies. To characterize oligomers on a single particle level and to investigate their biological effects on both human neuroblastoma SH-SY5Y cells and primary cortical neurons, we developed three novel protocols for oligomer generation based on published observations. For the first time we compared the oligomers directly in shape, morphology, and size using two single-particle analysis methods. Finally, we investigated their bioactivity on cultured human cells.

The combination of ethanol and iron is sufficient to induce α-syn oligomerization at very low protein concentrations (M. Kostka, T. Högen, K. Danzer, and A. Giese, unpublished observation). To reduce ethanol concentrations that would interfere with subsequent cell-culture experiments and to increase the oligomer yield, the aggregation conditions have been adapted and optimized. In the experiments described here, we compared three different approaches.

First, we incubated oligomers for a period of 6 days after lyophilization and resuspension in sodium phosphate buffer. This type of oligomers was termed type A. Second, based on the oligomer preparation protocol of Kayed *et al.* (2003), we used stirring bars to accelerate the aggregation process and to minimize ethanol concentrations concurrently. We termed this oligomer type B. In the third approach, we used ultrafiltration to concentrate oligomers for use in cell culture. This oligomer type was named type C. Based on a finding that iron increases particle size of ethanol-induced oligomers (M. Kostka, T. Högen, K. Danzer, and A. Giese, unpublished observation), we investigated the influence of iron on all three oligomer types (A, B, and C). Iron-free oligomers were termed type 1 oligomers and iron-containing oligomers type 2.

To quantify and characterize the differently prepared oligomers, we used fluorescently labeled α-syn in nanomolar concentrations and applied FIDA with a confocal single-molecule detection system.

Characterization of α-syn type A oligomers

Applying FIDA to characterize our oligomers, we found in the type A oligomers that nearly half of the overall particles appeared as monomers, whereas the other half was composed of small oligomeric particles. Although type A oligomers were incubated for several days, we found only small amounts of large oligomeric particles. There was no influence of iron on the particle size observed (Fig. 1 A). To confirm our FIDA results, we used AFM as a fluorescence-

independent single-molecule detection system.

AFM analysis showed that oligomers in the type A preparation appeared as a heterogeneous population with globular and protofibrillar structures. Iron seemed to influence the aggregation process resulting in more extended protofibrillar structures (A2), whereas the iron-free preparation (A1) favors the generation of spherical structures (Fig. 1 B). Thus, small oligomer particles observed with FIDA could be confirmed with AFM analysis when compared with section analysis of monomers. As also described by Lashuel *et al.* (2002b), we observed annular structures 40-45nm in diameter in both preparations. Importantly, these annular structures were not found in monomer preparations (supplemental Fig. 1). In contrast to FIDA analysis, almost no monomers were observed in type A oligomer preparations with our experimental AFM setup.

Together, using the complementary biophysical techniques FIDA and AFM, type A oligomers generated by long-term incubation of low α-syn concentrations appeared as small, globular and annular structures.

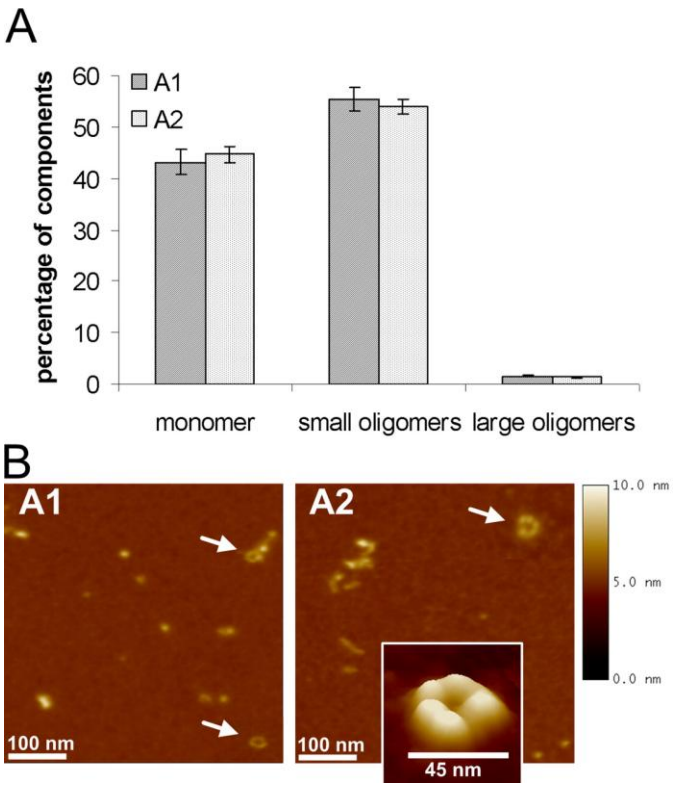

Figure 1: Characterization of long-term incubation of α-syn oligomers (types A1 and A2). ***A)*** FIDA analysis of two oligomeric α-syn forms generated after long-term incubation (6 days) in 50mM sodium phosphate buffer. The influence of ferrous chloride has been worked out (type A1 without ferrous chloride and type A2 with ferrous chloride). The mean ± SEM of five measurements are shown. ***B)*** AFM images (500 x 500nm) of type A1 and A2 oligomeric α-syn forms generated after long-term incubation (6 days) in 50mM sodium phosphate buffer. Section analysis revealed globular or protofibrillar oligomers from 2 to 6nm in height. Also, annular structures (arrows) were found in both oligomer types A1 and A2. AFM images are representative examples of several AFM images of independent oligomer preparations.

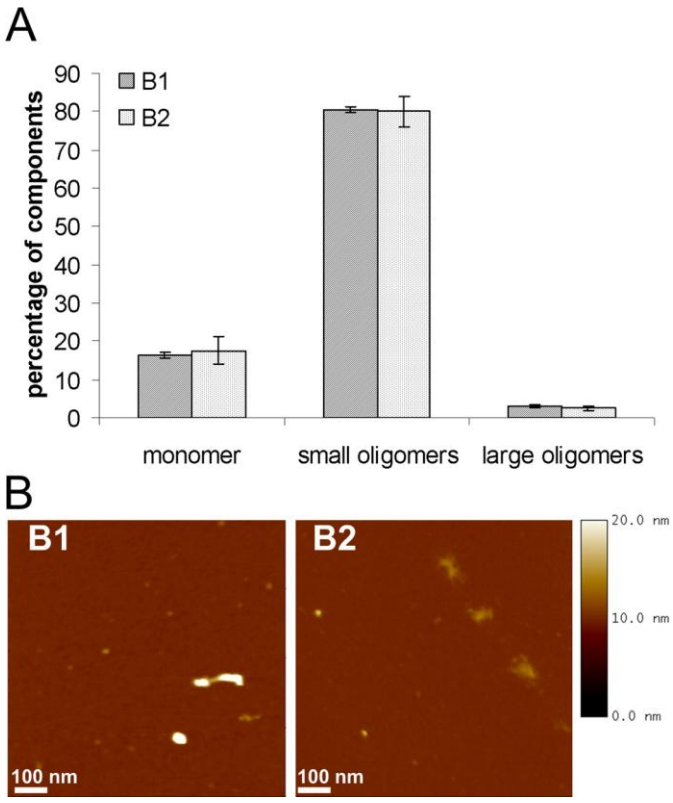

Figure 2: Characterization of α-syn oligomer types B1 and B2 generated with stirring bars. ***A)*** Single-particle analysis revealed two oligomeric forms generated with stirring bars. The influence of ferrous chloride has been worked out (type B1 without ferrous chloride and type B2 with ferrous chloride). ***B)*** AFM images (1μm²) of two oligomeric forms generated with stirring bars. Oligomers appeared as heterogeneous population with particles from 3 to 23nm in height using section analysis. Oligomer type B1 appeared in a more compact spherical form than oligomer type B2. AFM images are representative examples of several AFM images of independent oligomer preparations.

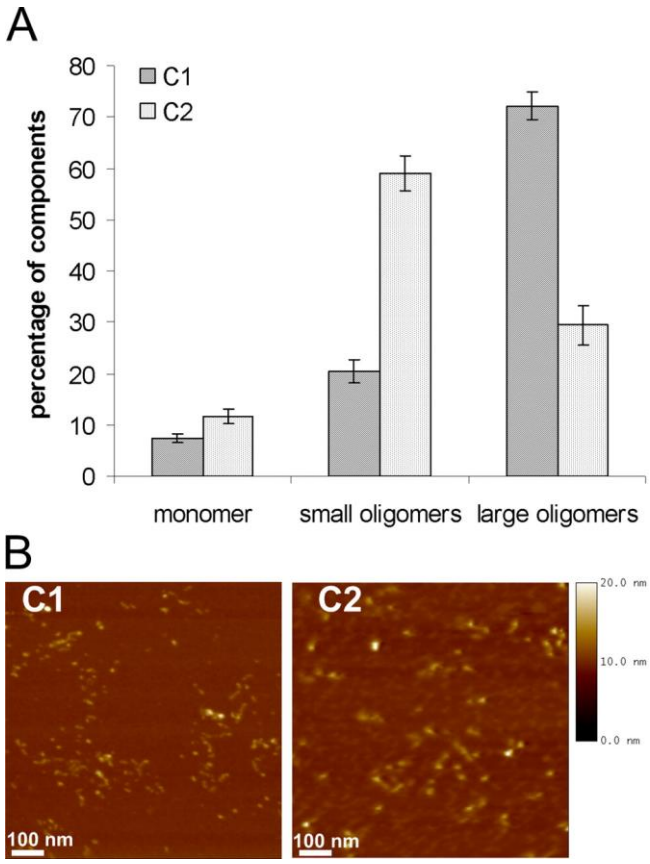

Figure 3: Characterization of α-syn oligomers (types C1 and C2). ***A)*** Single-particle analysis of two oligomeric α-syn forms generated by overnight incubation and ultrafiltration. The influence of ferrous chloride has been analyzed (type C1 without ferrous chloride and type C2 with ferrous chloride). ***B)*** AFM images (1μm²) of two oligomeric α-syn forms generated by overnight incubation and ultracentrifugation. Images showed globular and protofibrillar oligomer structures 4-10nm in height. Using AFM analysis, there were no significant morphological differences detectable between oligomer type C1 and oligomer type C2. AFM images are representative examples of several AFM images of independent oligomer preparations.

Characterization of type B oligomers

Type B oligomers were generated using stirring bars to facilitate ethanol evaporation. Applying FIDA for oligomer type B characterization, we found, in contrast to the type A preparation, a higher conversion rate (80%) from monomers to small oligomers. This type B oligomer contained low monomeric percentages and only a small portion of large oligomeric particles. Additionally, there was no significant influence of iron on particle composition when comparing the FIDA analysis of the B1 and B2 oligomer preparations (Fig. 2 A).

Structural insight into type B oligomers was given by AFM analysis. Height images showed that type B oligomers appeared as a heterogeneous population (Fig. 2 B). Also by stirring, globular structures have been detected, but no annular structures have been observed in any preparation. In contrast to FIDA analysis, we saw an influence of iron on oligomer formation: iron-free prepared B1 oligomers appeared in a more compact spherical shape, whereas B2 oligomers prepared with iron showed up as amorphous structures.

Finally, the data demonstrate that type B oligomers were heterogeneous, globular oligomers, with low amounts of monomers and a majority of small oligomeric particles.

Characterization of type C oligomers

The third kind of oligomers, type C oligomers, were prepared similar to the previous preparations and combined with an ultrafiltration step after the aggregation process.

With FIDA analysis we observed only in type C preparations an effect of iron administration: type C2 oligomers contained three times more small oligomeric forms than iron-free preparations (C1). Additionally, oligomer types C1 and C2 also differed in the proportion of large particles. Here, large particles were present to a higher amount when compared with oligomer types A and B. Type C oligomers showed the lowest portion of monomers (Fig. 3 A) among our three oligomer types, A, B, and C.

In contrast to the confocal fluorescence technique FIDA, the AFM analysis did not illustrate morphological differences in particle composition between oligomer types C1 and C2. Both oligomer types appeared as spherical particles with homogenous distribution of globular and protofibrillar structures (Fig. 3 B). No annular structures like in the preparation type A were observed.

In summary, each of our novel protocols ended up in a heterogeneous oligomer population. We showed that changes in the aggregation protocols can lead to distinct forms of oligomers. We used these different oligomers to study the cellular responses to exogenously added oligomers.

Increase in intracellular calcium mediated by type A1 and A2 oligomers

It has been suggested that abnormal intracellular calcium homeostasis plays a crucial role in the pathogenesis of neurodegenerative disorders (Mattson and Chan,

2001). Moreover, we found that iron-induced oligomers were able to form pores in a synthetic bilayer pore-forming assay (M. Kostka, T. Högen, K. Danzer, and A. Giese, unpublished observation). Similarly, Volles *et al.* (Volles *et al.*, 2001; Volles and Lansbury, 2002) have shown pore-forming activity of α-syn protofibrils using synthetic vesicles. Therefore, we asked whether we could detect a calcium dysregulation in cells treated with type A oligomers. In contrast to monomer samples, oligomer types A1 and A2 evoked a rapid increase within seconds in calcium-dependent fluorescence in fluo-4-loaded singular SH-SY5Y cells using confocal microscopy (Fig. 4) and in an FLIPR (supplemental Fig. 3 A). The increase in intracellular calcium of singular SH-SY5Y cells is also demonstrated on a time lapse video (supplemental movie 1). As positive controls, we used the channel-forming polypeptide ionophore gramicidin and the chelating calcium ionophore ionomycin, which allows calcium to diffuse passively through cellular membranes (Fig. 4 and supplemental Fig. 3). To investigate whether the observed increase in intracellular calcium was dependent on cellular α-syn-expression levels, we compared mock-transfected SH-SY5Y cells expressing endogenous α-syn with cells stably overexpressing α-syn[wt] or mutant α-syn[A30P/A53T]. These cell lines exhibited comparable α-syn expression levels compared with the endogenous control as shown in supplemental Figure 2. Again, type A1 and A2 oligomers evoked a clear increase in calcium-dependent fluorescence compared with monomer and respective solvent controls. No clear differences in the calcium signal increase between mock-transfected SH-SY5Y cells and α-syn-overexpressing SH-SY5Y cells have been observed (supplemental Fig. 3). These data suggest that only the exogenously applied oligomers are responsible for the elevation of intracellular calcium and that the intracellular α-syn does not contribute to the effect in the time window investigated here.

To demonstrate also for primary neurons an elevation of intracellular calcium induced by type A oligomers, we performed the same experiments as described above for SH-SY5Y cells. Using confocal microscopy, we confirmed also in primary neurons a significant increase in intracellular calcium (Fig. 5). A time lapse video of singular neurons shows also the calcium influx effect (supplemental movie 2). This was further confirmed by FLIPR measurements (supplemental Fig. 4).

To support pore formation as a possible mechanism responsible for the calcium influx, we measured the membrane potential. Indeed, oligomer types A1 and A2 showed a depolarization of the membrane potential in primary cortical neurons as also shown for gramicidin (Fig. 6).

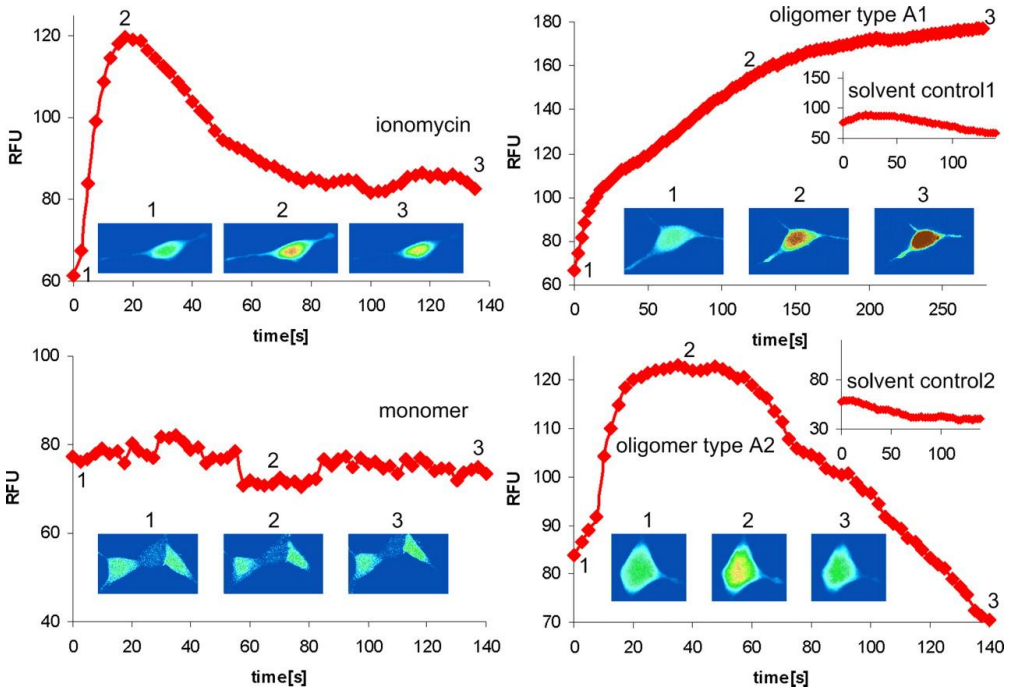

Figure 4: [Ca²⁺] elevation by α-syn oligomer types A1 and A2 in SH-SY5Y cells. Traces show [Ca²⁺]-dependent fluorescence of single SH-SY5Y cells overexpressing α-syn[wt] in response to 6µM ionomycin, 0.1mg/ml monomer, and 0.1mg/ml oligomer types A1 and A2 with respective solvent controls. Oligomer types A1 and A2 evoked a clear increase in intracellular [Ca²⁺]. Fluorescence records illustrating typical responses to different treatments starting at the time point of application are shown. The inset images of the cell were captured at the times indicated during the trace and are depicted on a pseudocolor scale with "warmer" colors on a rainbow scale corresponding to higher fluorescence. The inset images show representatives of a single cell.

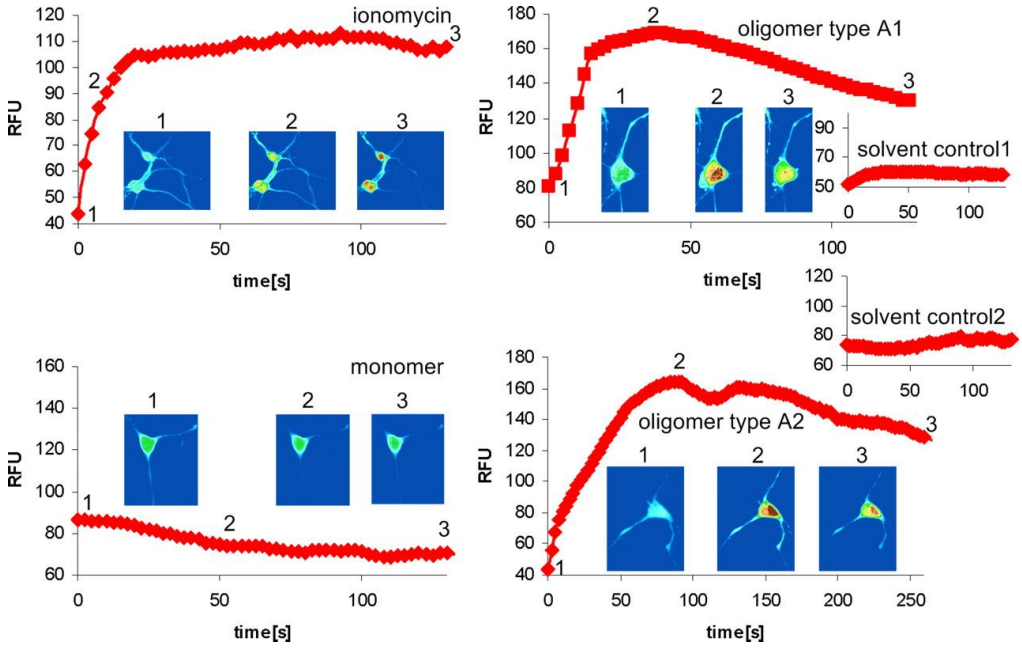

Figure 5: [Ca²⁺] elevation by α-syn oligomer types A1 and A2 in primary neurons. Traces show [Ca²⁺]-dependent fluorescence of single cortical neurons in response to 6µM ionomycin, 0.1mg/ml monomer, and 0.1mg/ml oligomer types A1 and A2 with respective solvent controls. Oligomer types A1 and A2 evoked a clear increase in intracellular [Ca²⁺]. Fluorescence records illustrating typical responses to the different treatments starting at the time point of application are shown. The inset images show pseudocolor representatives of a single cell, captured at the times indicated by the trace.

Oligomer type A-induced calcium ion influx from extracellular sources

To discriminate whether the observed increase in intracellular calcium induced by oligomers types A1 and A2 resulted from influx of extracellular calcium or emptying of intracellular calcium stores, we reduced the extracellular calcium concentration to very low levels by using calcium-free buffer. In the absence of extracellular calcium, the treatment of endogenous α-syn SH-SY5Y cells (Fig. 7 A) completely abrogated the oligomer type A1- and A2-induced intracellular calcium increase. As expected, application of the channel-forming polypeptide gramicidin also no longer elicited an increase in intracellular calcium. Only ionomycin-induced calcium signals were detectable. Thus, the increase of intracellular calcium levels induced by oligomer types A1 and A2 and gramicidin resulted from extracellular sources, whereas the remaining ionomycin signal response was mediated by both influx of extracellular calcium and intracellular calcium release.

To rule out the possibility that endogenous calcium-permeable plasma membrane ion channels were affected by oligomers types A1 and A2, we added 20μM cobalt, a nonspecific calcium-channel blocker, to endogenous α-syn SH-SY5Y cells, before application of 7μM oligomer type A1. Signal response in the presence of cobalt was of a comparable magnitude to that obtained in the absence of cobalt (Fig. 7 B), suggesting that calcium influx through cobalt-sensitive calcium channels does not contribute to oligomer type A1- and A2-induced increase in intracellular calcium.

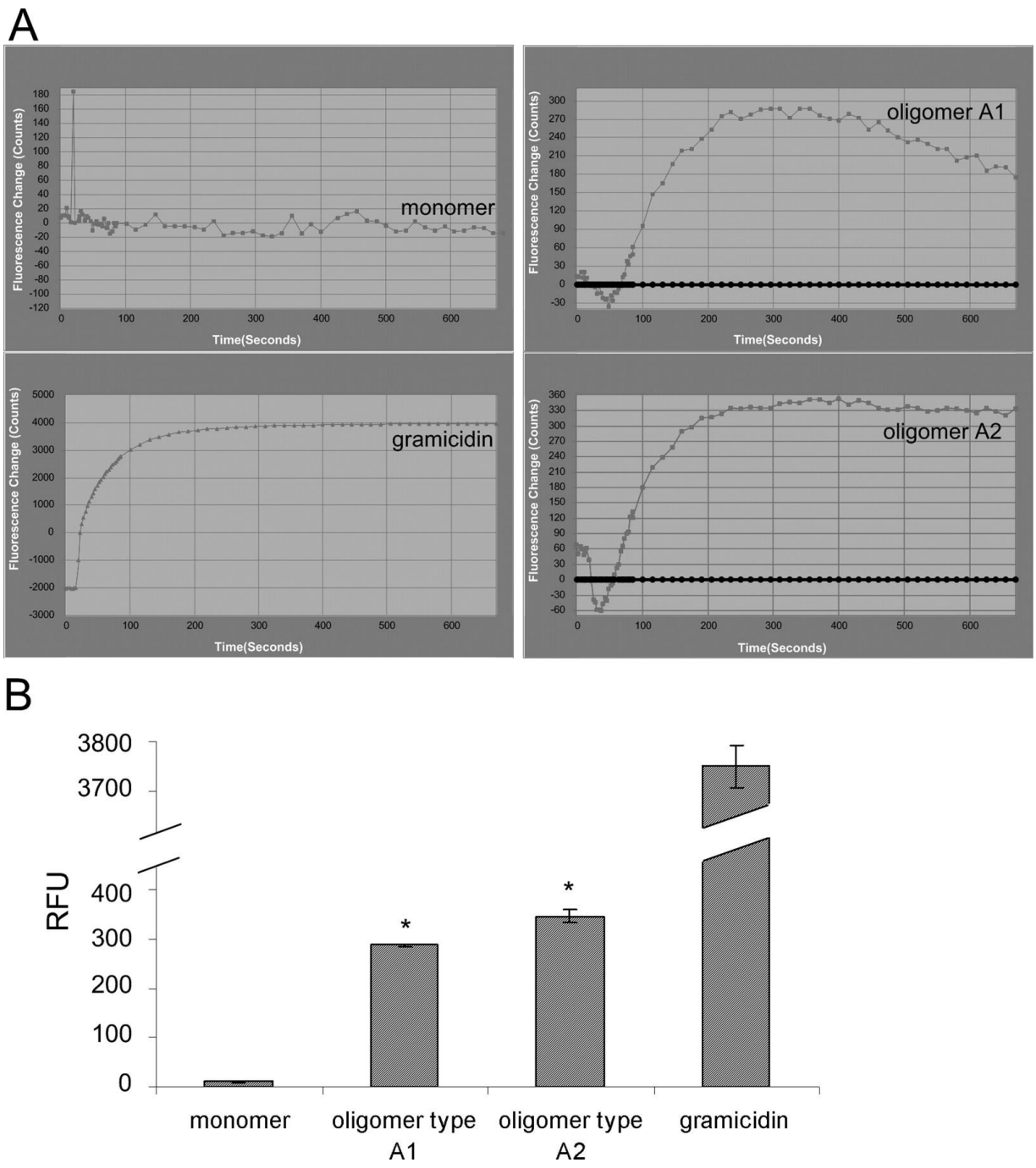

Figure 6: Depolarization of membrane potential induced by oligomer types A1 and A2. ***A)*** Kinetic plots illustrating typical signal responses to application of 0.1µg/µl α-syn monomer, oligomer types A1 and A2, and 500µg/ml gramicidin as a positive control. Oligomer types A1 and A2 showed a clear depolarization of membrane potential. Each trace shows the negative control corrected mean fluorescence of 1.25 x 10^5 primary neurons. ***B)*** Quantification of fluorescence intensity in response to oligomer types A1 and A2 induced depolarization in primary neurons compared with solvent control. Values are mean ± SEM; $n = 3$; $^*p < 0.002$, one-sample t test against hypothetical value 0. A1-treated neurons: $\Delta = 286.8$ (95% CI, 277.4-296.2); A2 treated neurons: $\Delta = 345.2$ (95% CI, 286.2-404.2).

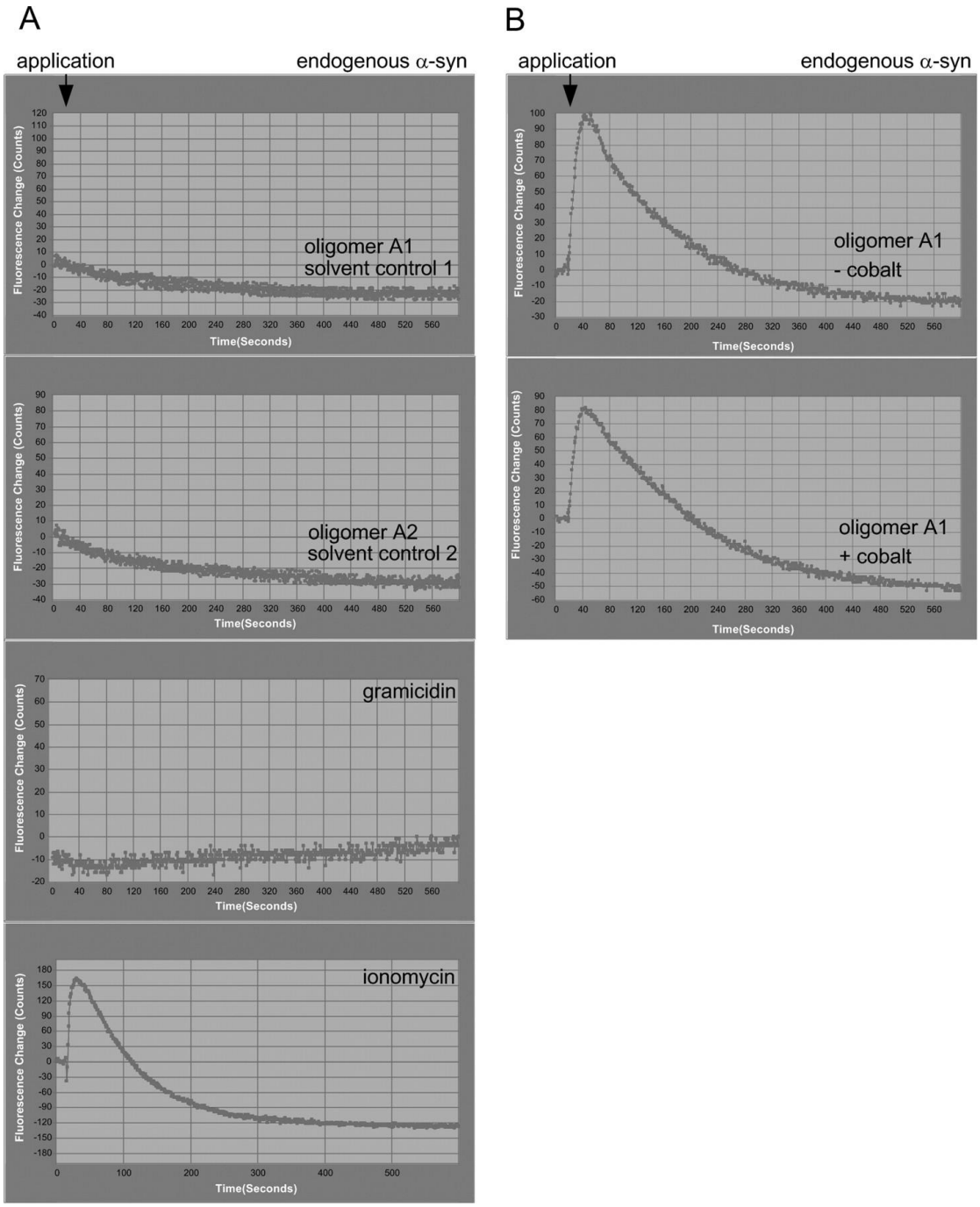

Figure 7: α-Syn oligomer types A1 and A2 induced intracellular [Ca^{2+}] increase *via* influx of extracellular [Ca^{2+}] sources. ***A)*** Kinetic plots illustrating typical signal responses to application of 0.1µg/µl α-syn oligomer types A1 and A2 and positive controls, 1.5µM ionomycin, and 500 µg/ml gramicidin in [Ca^{2+}]-free extracellular buffer. Each trace shows the mean fluorescence of 6000 mock-transfected SH-SY5Y cells expressing endogenous α-syn. Intracellular [Ca^{2+}] signals evoked by oligomers type A1, A2, and gramicidin were completely abolished when cells were incubated in [Ca^{2+}]-free extracellular buffer, whereas ionomycin-induced [Ca^{2+}] signals were persistent. ***B)*** [Ca^{2+}] signals evoked by oligomer types A1 and A2 are not reduced by cobalt, a nonspecific Ca^{2+} channel blocker. Each trace shows the typical mean fluorescence of 6000 mock-transfected SH-SY5Y cells after addition of type A1 oligomers in the presence and absence of cobalt. Type A oligomers showed a clear calcium channel-independent increase in intracellular [Ca^{2+}]. This experiment was repeated two times and showed similar results.

Toxicity of type A oligomers

To investigate whether type A oligomers have toxic properties, we examined caspase-3 activation and determined cell number reduction after oligomer type A1 and A2 treatment. Because there were no biologically relevant differences in calcium response seen in SH-SY5Y cells expressing endogenous or elevated levels of α-syn, we performed toxicity assays only in mock-transfected cells and in mutant α-syn[A53T]-overexpressing cells.

Immunofluorescence staining for caspase-3 after oligomer type A1 treatment showed, for both mock-transfected and mutant α-syn [A53T]-expressing SH-SY5Y cells, a significant ($p < 0.05$) increase in cleaved caspase-3 activity. Also, treatment with oligomer type A2 resulted in a significant increase of caspase-3 activity in both cell lines, whereas the increase in caspase-3 activity seemed to be slightly higher in mutant α-syn[A53T]-overexpressing cells than in cells with endogenous levels of α-syn (Fig. 8 A). Treatment with oligomer type A1 caused, in both cell lines, a significant reduction in cell number, whereas mutant α-syn [A53T]-overexpressing cells seemed to be more affected in cell number reduction than mock-transfected cells. Although there was a lower caspase activation compared with the mock-transfected cells, there was a stronger cell number reduction in this cell line. This discrepancy might be explained by nonapoptotic cell death. We observed a strong and significant cell number reduction in mutant α-syn[A53T]-overexpressing cells treated with type A2 oligomers. This is in accordance with the caspase-3 results. Although the cell number reduction in mock-transfected cells treated with A2 oligomers is not statistically significant ($p = 0.56$) compared with solvent control 2, type A2 oligomers seem to reduce cell number also in mock-transfected cells (Fig. 8 B).

In contrast to type A oligomers, our other types of oligomers, types B and C, did not increase the level of intracellular calcium (data not shown). Moreover, we also did not detect a caspase activation or cell number reduction for oligomer types B and C. Thus, type A oligomers were the only type of oligomers with annular structures and a calcium influx effect with a induction of cell death.

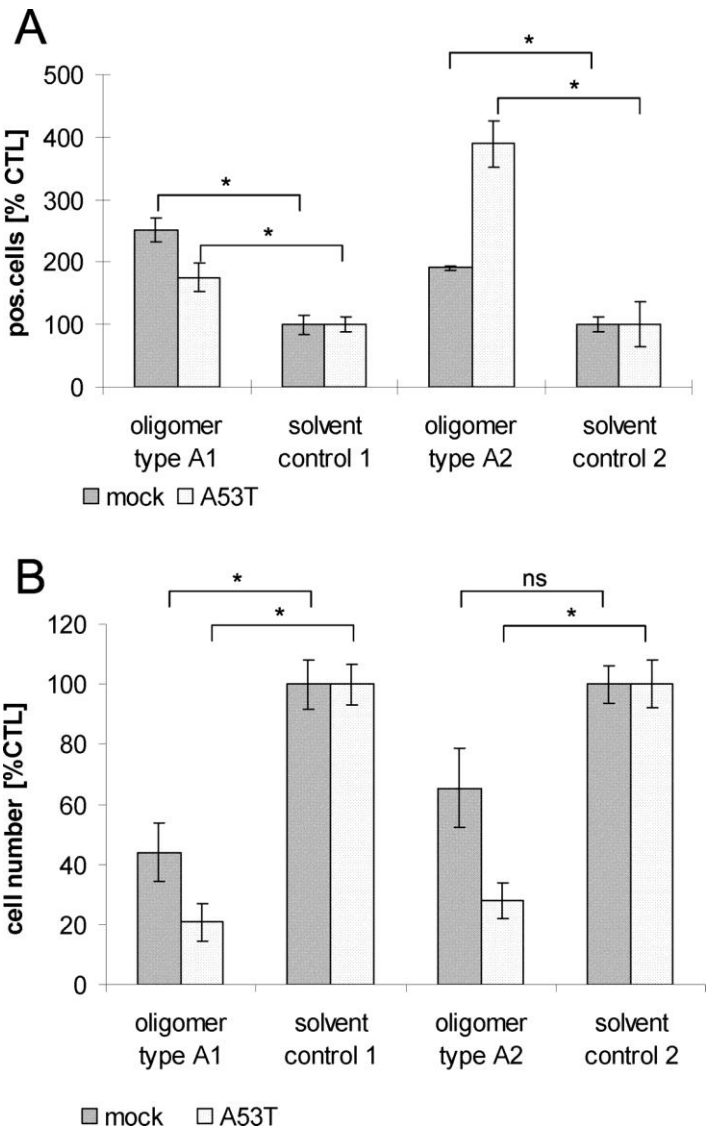

Figure 8: Toxicity of α-syn oligomer types A1 and A2. ***A)*** Quantification of caspase-3 activation normalized to corresponding solvent controls; values are the mean ± SEM; $n = 3$. Treatment of mock-transfected SH-SY5Y cells or cells overexpressing α-syn mutant A53T with 0.1 mg/ml oligomer types A1 and A2 led to a significant activation of caspase-3 [unpaired t test, $^*p < 0.05$ compared with data from corresponding solvent controls; oligomer type A1 treated: mock, Δ= 151 (95% CI, 83.3-218.6); α-syn[A53T], Δ= 75.8 (95% CI, 5.8-145.9); oligomer type A2 treated: mock, Δ= 90.9 (95% CI, 54.6-127.2); α-syn[A53T], Δ= 288.9 (95% CI, 147.3-430.5)]. ***B)*** Quantification of cell number reduction normalized to corresponding solvent controls. Values are shown as mean ± SEM; $n = 3$. Oligomer type A1 evoked, on both mock-transfected and stably overexpressing mutant α-syn[A53T] SH-SY5Y cell lines, a significant reduction in cell number. Oligomer type A2 led, on overexpressing mutant α-syn[A53T] SH-SY5Y cells, to a significant reduction in cell number [unpaired t test, $^*p < 0.05$ compared with data from corresponding solvent controls; oligomer type A1 treated: mock, Δ= -56 (95% CI, -91.5 to -20.5); α-syn [A53T], Δ= -79.3 (95% CI, -104.9 to -53.62); oligomer type A2 treated: mock, Δ= -34.6 (95% CI, -75.6 to -6.5); α-syn[A53T], Δ= -72.1 (95% CI, -99.4 to -44.7). Both oligomer types mediated their toxicity after 24h. ns, Not significant.

Seeding characteristics of type B oligomers

It has been shown previously that aggregation of α-syn is a nucleation-dependent process in which preformed aggregates function as seeds (Wood *et al.*, 1999). To analyze whether exogenously added oligomers have the propensity to seed cytosolic α-syn, we treated SH-SY5Y cells stably overexpressing α-syn mutant [A53T] and mock-transfected cells with endogenous levels of α-syn with Alexa-488-conjugated type B oligomers. Immunofluorescence staining showed colocalization of Alexa-488-conjugated type B oligomers (green) and the total amount of α-syn (red) in overlaid images. We found yellow-colored aggregates within cells after oligomer type B treatment in both α-syn mutant [A53T] and mock-transfected cells. Confocal images demonstrated that cells treated with Alexa-488-conjugated type B2 oligomers displayed a reduction in cytoplasmic α-syn staining and an increase in yellow-colored intracellular aggregates (seeding), whereas solvent control-treated cells showed homogenous cytoplasmic staining of α-syn (Fig. 9). Thus, exogenously added type B oligomers have entered the cell and seeded aggregation of cytosolic α-syn with a resulting increased protein aggregation in one local area.

Notably, the oligomer types B1 and B2 did not cause an increase in intracellular calcium (data not shown). This supports the idea that the type B oligomers are different from the type A oligomers. Thus, oligomer types B and A differ not only in their biophysical properties, but this difference also translates into different cellular effects.

Seeding characteristics of type C oligomers

Because type C oligomers also seemed to have different biophysical characteristics compared with oligomer types A and B, we assumed also different biological effects on cells. First, we investigated again the effect on calcium homeostasis in neuroblastoma cells. In none of our assays did type C oligomers cause an increase in intracellular calcium (data not shown).

We also investigated the seeding ability of type C oligomers as described for type B oligomers. Type C2 Alexa-488 oligomers induced as well a remarkable reduction in cytoplasmic staining of α-syn and a tremendous seeding effect in both α-syn mutant [A53T] and mock-transfected cells with endogenous levels of α-syn (Fig. 10), whereas corresponding solvent control-treated cells showed a homogeneous α-syn staining. Also, type C1 oligomers induced aggregate formation in both SH-SY5Y cell lines, whereas the seeding effect of type C2 oligomers was stronger. Also, in primary neurons, we were able to demonstrate a reduction in cytoplasmic α-syn staining and a tremendous "yellow" aggregate formation near the nucleus after oligomer type C2 treatment. Corresponding solvent control-treated neurons showed a homogeneous cytoplasmic staining of α-syn (Fig. 10 C). Thus, also type C oligomers had the propensity to seed cytosolic α-syn by accumulation of intracellular α-syn within one local area after exogenous

application in both SH-SY5Y cell lines and primary neurons.

Notably, type A oligomers had in none of our approaches any seeding propensity (data not shown).

All together, our data provide evidence that several different types of oligomers can be formed under various conditions, which differ in shape, morphology, and size. Consequently, these different types of oligomers have distinct biological effects on cells (summarized in Table 1).

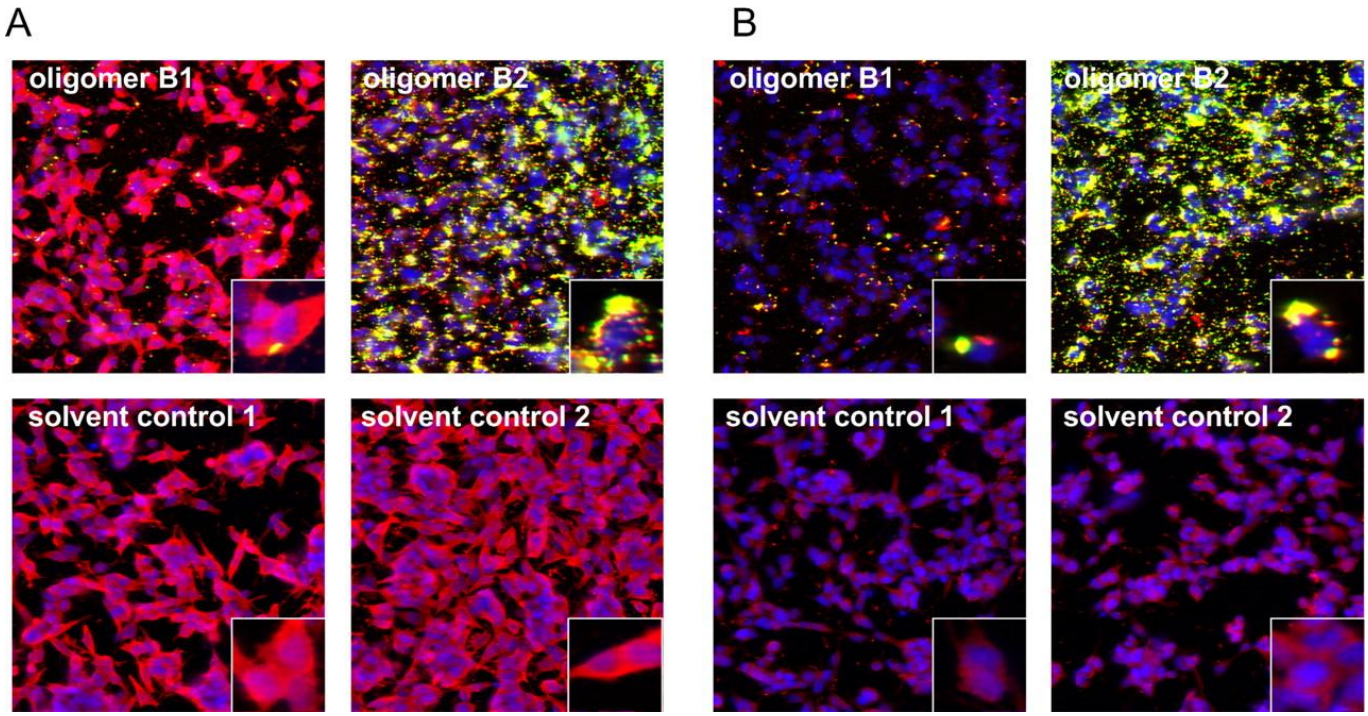

Figure 9: Seeding effect of α-syn oligomer types B1 and B2. Immunocytochemical staining of α-syn with ASY-1 antibody (in red) after treatment with 0.1mg/ml Alexa-488-labeled oligomer types B1 and B2 (in green) or solvent controls is shown. ***A and B)*** Confocal images showed a reduction in cytoplasmic staining of α-syn and an increase in cell-associated aggregates (seeding) in SH-SY5Y stably overexpressing α-syn[A53T] ***(A)*** or mock-transfected SH-SY5Y with endogenous expression of α-syn ***(B)*** when treated with oligomer type B2. Oligomer type B2 had a higher potential to seed aggregate formation than oligomer type B1. This experiment was repeated two times and showed similar results.

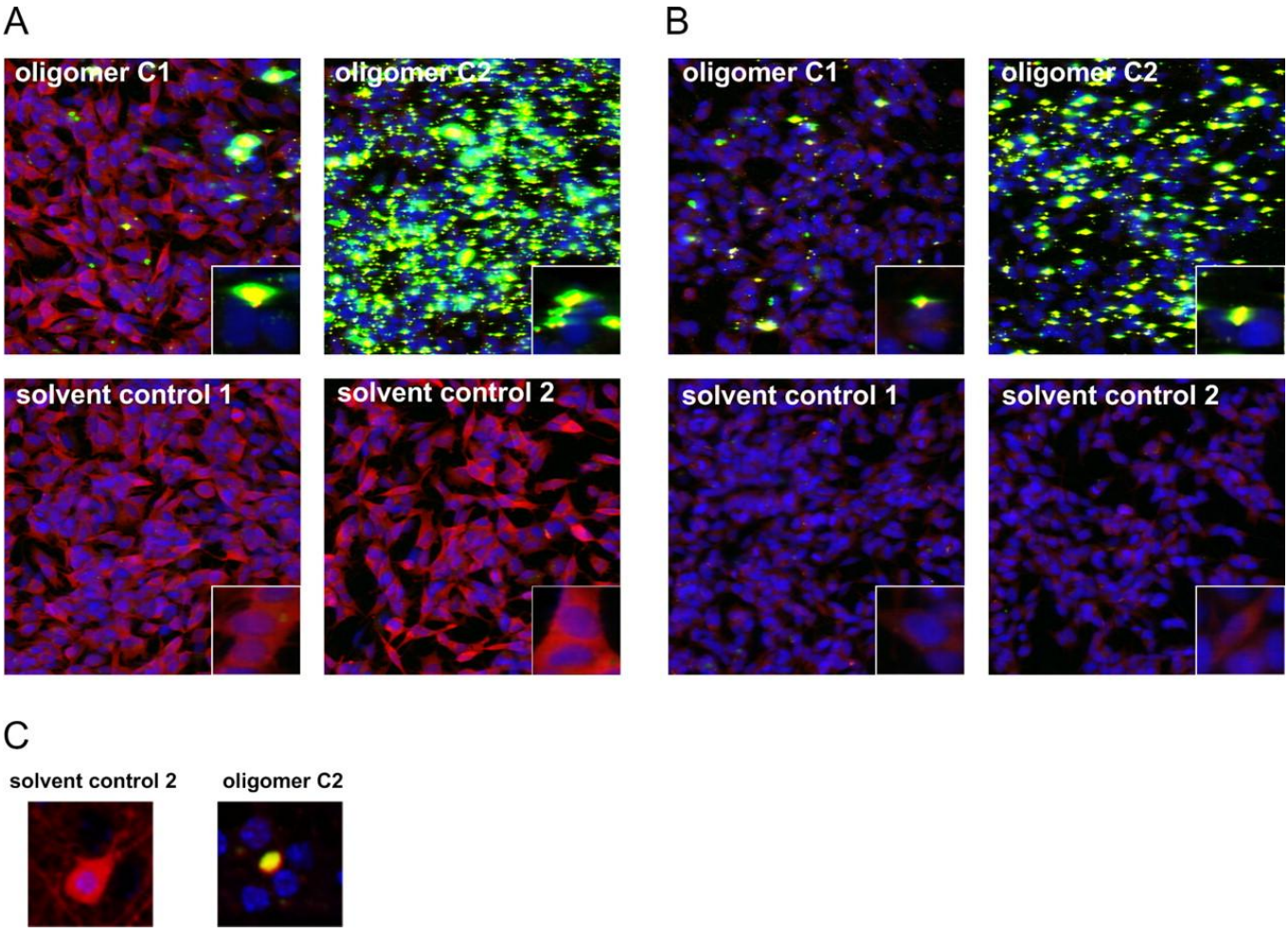

Figure 10: Seeding effect of α-syn oligomer types C1 and C2. Immunocytochemical staining of α-syn with ASY-1 antibody (in red) after treatment with 0.1mg/ml Alexa-488 labeled oligomers type C1 and C2 (in green) or solvent controls is shown. ***A and B)*** Confocal images showed a reduction in cytoplasmic staining of α-syn and an increase in cell-associated aggregates (seeding) in SH-SY5Y stably overexpressing α-syn mutant A53T ***(A)*** or mock-transfected SH-SY5Y cells ***(B)*** treated with oligomer type C2. Oligomer type C2 had a higher potential to trigger aggregate formation than oligomer type C1. This experiment was repeated two times and showed similar results. ***C)*** Also, primary cortical neurons showed a decrease in cytoplasmic staining of α-syn (red) and remarkable cell-associated α-syn aggregate formation (yellow).

1.7. Discussion

Table 1: Different types of α-syn oligomers

Oligomer type	Annular structures	Particles >5 nm in height	Calcium influx	Cell death	Caspase activation	Seeding
A1	+	−	+	+	+	−
A2	+	−	+	+	+	−
B1	−	+	−	−	−	+
B2	−	+	−	−	−	++
C1	−	+	−	−	−	+
C2	−	+	−	−	−	++

Overview of different types of α-syn oligomers with their respective characteristics and biological effects.

In this study we have shown that, depending on aggregation conditions, heterogeneous populations of α-syn oligomers are forming, which can be differentiated based on their biophysical properties and cellular effects. Type A oligomers induced an increased membrane permeability and trigger cell death. Type B and C oligomers were able to enter cells directly and to seed intracellular α-syn aggregation.

Many protocols of oligomer preparation have been described in the literature, but all were characterized with different methods, making it difficult to compare the different approaches. Here, we directly compared various types of oligomers by two single-particle analysis methods, AFM and FIDA, and cellular readouts. The influence of iron on *in vitro* aggregation of α-syn has been reported by Uversky *et al.* (2001). These findings formed the basis for our present work.

Characterization of our type A oligomers with AFM revealed spherical oligomers from 2 to 6nm in height. This is consistent with observations of other groups (Conway *et al.*, 2000; Rochet *et al.*, 2000; Volles *et al.*, 2001; Hoyer *et al.*, 2004; Apetri *et al.*, 2006), although these studies were performed with far higher protein concentrations. Wood *et al.* (1999) had previously determined 28μM as the critical concentration for α-syn aggregation. Our approaches used four times less protein. This was possible because of the application of the highly sensitive FIDA analysis in contrast to the standard techniques used in the other studies. The method of oligomer generation used by Jensen *et al.* (2000) required protein concentrations 10-fold higher than our approaches and resulted mostly in fibrils after 7 days of incubations. In contrast, our samples still consisted mainly of oligomers and monomers at this time point, with no fibrils yet apparent. Prolonged incubation, however, lead to fibril formation (supplemental Fig. 5), suggesting that our oligomers were on pathway to fibrils.

Kayed and Glabe (2006) described the generation of homogeneous oligomer populations using a greatly differing protocol

starting with seedless stock solutions. In contrast, our oligomer preparations turned out to be heterogeneous mixtures: FIDA data demonstrated that almost 50% of α-syn contained in type A oligomers was in the monomeric form. An obvious explanation for the relatively high proportion of monomers in the type A preparations is an equilibrium between monomers and type A oligomers. After ultrafiltration to separate the monomer fraction and the oligomer type A fraction, monomers reappeared in the oligomer fraction (data not shown). The α-syn monomers were, however, not seen by AFM, most probably because the monomers were washed off during the AFM sample preparation.

In addition to the generation and biophysical characterization of different oligomer types, we also investigated their biological effects after application to cells. We found that two types of our oligomers (B and C) entered into cells and seeded intracellular α-syn aggregation. Our other type of oligomers (type A) did not enter into cells. Instead, they seemed to act at the cellular membrane where they initiated an elevation of intracellular calcium. This increase in intracellular calcium occurred only in the presence of calcium in the extracellular buffer, suggesting that this effect is attributable to an influx from extracellular sources. We also showed that this calcium influx is independent of cobalt-sensitive calcium channels. This is in contrast to the study by Adamczyk and Strosznajder (2006), who suggested that α-syn induces a calcium influx *via* N-type voltage-dependent Ca^{2+} channels. Their study differs greatly in two aspects. First, their model system is comprised of rat synaptoneurosomes, and second, they used monomeric α-syn for their investigations. Therefore, the data of Adamczyk and Strosznajder (2006) are not directly comparable with our data.

Several mechanisms have been suggested to underlie the increase in intracellular calcium induced by amyloidogenic proteins: increase in membrane permeability (Demuro *et al.*, 2005), insertion into the membrane and formation of a pore (Kawahara *et al.*, 2000; Arispe, 2004; Lashuel and Lansbury, 2006), and a direct interaction with membrane components to destabilize the membrane structure (Muller *et al.*, 1995; Mason *et al.*, 1996; Avdulov *et al.*, 1997; Green *et al.*, 2004). Although we cannot exclude an increase in membrane permeability or mechanisms destabilizing the membrane structure, our data support the amyloid pore hypothesis suggested by Lashuel and Lansbury (2006). They demonstrated with synthetic vesicles a pore-forming mechanism of α-syn protofibrils (Volles *et al.*, 2001; Volles and Lansbury, 2002; Lashuel *et al.*, 2002a). The influx of extracellular calcium observed in our experiments suggests that α-syn pore formation occurs also in living cells. In addition, the calcium influx pattern of bacterial toxin gramicidin closely resembled the α-syn oligomer type A-induced calcium influx. Thus, the pore forming mechanism mediated by oligomers type A could be similar to that of membrane-spanning pores formed by known protein toxins (e.g., hemolysin, latroxin, and aerolysin) (Valeva *et al.*, 1997; Orlova *et al.*, 2000; Wallace *et al.*, 2000). Moreover, we

also found a change in membrane potential in primary neurons after oligomer type A treatment. The observed depolarization could be the consequence of ion fluxes through pores in the membrane. Intriguingly, only type A oligomers contained annular structures. Recently, Tsigelny *et al.* (2007) showed, by using molecular modeling and molecular dynamics simulations, that α-syn can form pentamers and hexamers forming a ring-like structure that can incorporate in the membrane. Direct evidence for the existence of amyloid pore-like structures *in vivo* has been provided by the extraction of annular α-syn structures from postmortem brain tissues from a multiple-system atrophy patient (Pountney *et al.*, 2005). Our annular type A oligomers, 45nm in diameter, were similar to those extracted oligomers that ranged from 30 to 50nm in diameter

These results suggest a disruption of cellular ion homeostasis followed by caspase activation and cell death *via* membrane spanning pores as one possible pathogenic mechanism of α-syn oligomers that might also occur *in vivo*. A disruption of calcium homeostasis has been proposed for several related amyloidogenic oligomers, including amyloid ß-peptide, prion, islet amyloid polypeptide, polyglutamine, and lysozyme (Demuro *et al.*, 2005). Even prefibrillar aggregates of nondisease-related proteins have been shown to be internalized into cells followed by a rise of free calcium levels (Bucciantini *et al.*, 2004). These findings strengthen the idea of a common mechanism of disruption of calcium homeostasis mediated by different prefibrillar aggregates of disease-related and nondisease-related proteins.

Our data demonstrate that oligomer type A-evoked increase in intracellular calcium was similar in cells overexpressing α-syn[wt, A30P, A53T], and cells expressing only an endogenous level of α-syn. This suggests that intracellular α-syn does not contribute under these experimental conditions to the pore formation, although other studies have shown that cells expressing mutant α-syn[A53T] have a higher plasma membrane permeability (Furukawa *et al.*, 2006).

In contrast, oligomer types B and C did not increase intracellular calcium (data not shown), but these oligomers could directly enter the cell and promote intracellular aggregate formation.

Effects of extracellular oligomers on cells might play an important role, also under pathophysiological conditions, because intriguing findings have shown previously that α-syn aggregates could be secreted from cells and therefore possibly insult neighboring cells (Lee *et al.*, 2005). However, because α-syn is an intracellular protein, the *in vivo* situation can still differ from this model, because there could also be other mechanisms involved not considered in this study.

Previous studies have shown that monomeric α-syn and prefibrillar aggregates from nondisease-related proteins can translocate into cells, although the mechanism of aggregate internalization to date remains unclear (Bucciantini *et al.*, 2004; Ahn *et al.*, 2006). We were able to confirm that oligomer types B and C could also be internalized into cells and

deploy then their seeding properties. A previous study has shown that membrane-bound α-syn can seed intracellular α-syn (Lee *et al.*, 2002). The seeding effect observed in our study could be similar to the effect shown by Lee *et al.* (2002). Oligomer types B and C might resemble nucleating species as described also in cell-free studies (Hoyer *et al.*, 2002). Seeding could also be one underlying mechanism for the ascending progression of α-syn pathology within the brains of Parkinson's patients (Braak *et al.*, 2003).

In our experimental setup, oligomer types B and C did not induce caspase activation or cell loss (data not shown). This correlates with the lack of an increase in intracellular calcium. We hypothesize that, although oligomer types B and C seed intracellular aggregation of α-syn, the resulting progression in aggregate formation in cell culture models is so fast because of the high levels of α-syn overexpression that the nucleating species immediately end up as large aggregates, bypassing the toxic oligomeric intermediates. Therefore, it might well be that oligomers with seeding properties could still trigger toxic neurodegenerative processes in synucleinopathies, where α-syn is present at physiological concentrations.

In conclusion, this study suggests that the aggregation process of α-syn results in distinct populations of oligomeric forms with different cellular effects. The cellular effects of α-syn oligomers described here in cell culture could resemble events that take place in Parkinson's patients. However, additional studies are needed to characterize the pathophysiologically relevant oligomeric forms in the brains of Parkinson's patients. Preventing the early events in oligomer formation might be a novel approach for the development of effective drugs for the treatment of Parkinson's disease and other synucleinopathies.

1.8. Supplemental materials

1.8.1. Supplemental figures

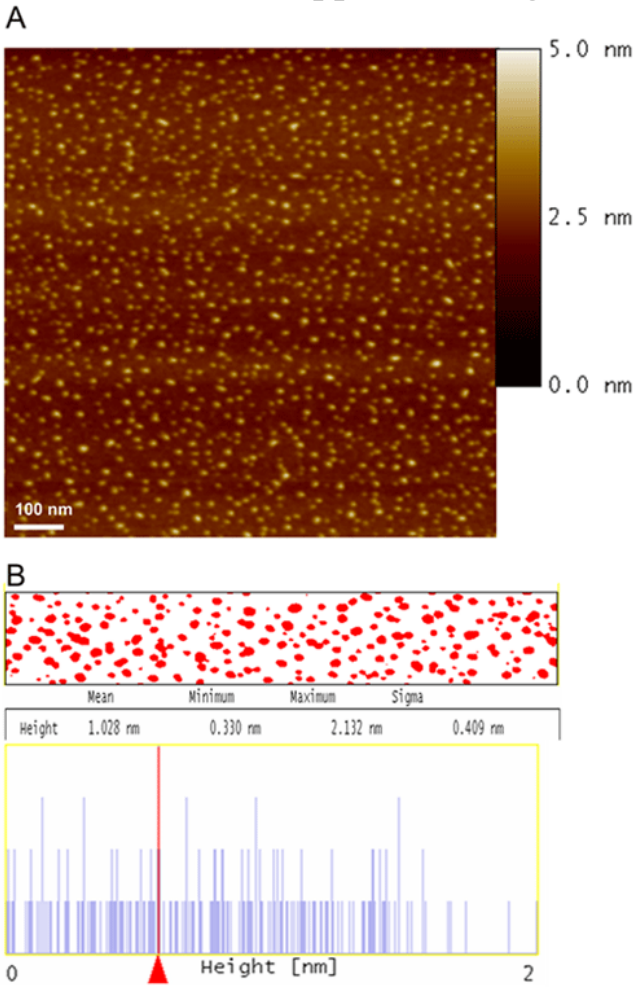

Supplemental figure 1: AFM image of monomeric α-syn.
A) The lyophilized protein was freshly dissolved in 50mM sodium phosphate buffer at a concentration of 1nM. The corresponding height images (1μm²) showed almost exclusively particles of 0.8 -1nm in height. ***B)*** Size distribution of monomeric α-syn. Quantitative size distribution analysis of α-syn particles reveal average heights of 1nm indicating that monomeric species had adsorbed on muscovite mica surface. Particle analysis was performed by the NanoScope data processing software (Digital Instruments, Santa Barbara, CA, USA) corrected for tilting and bowing of the substrate.

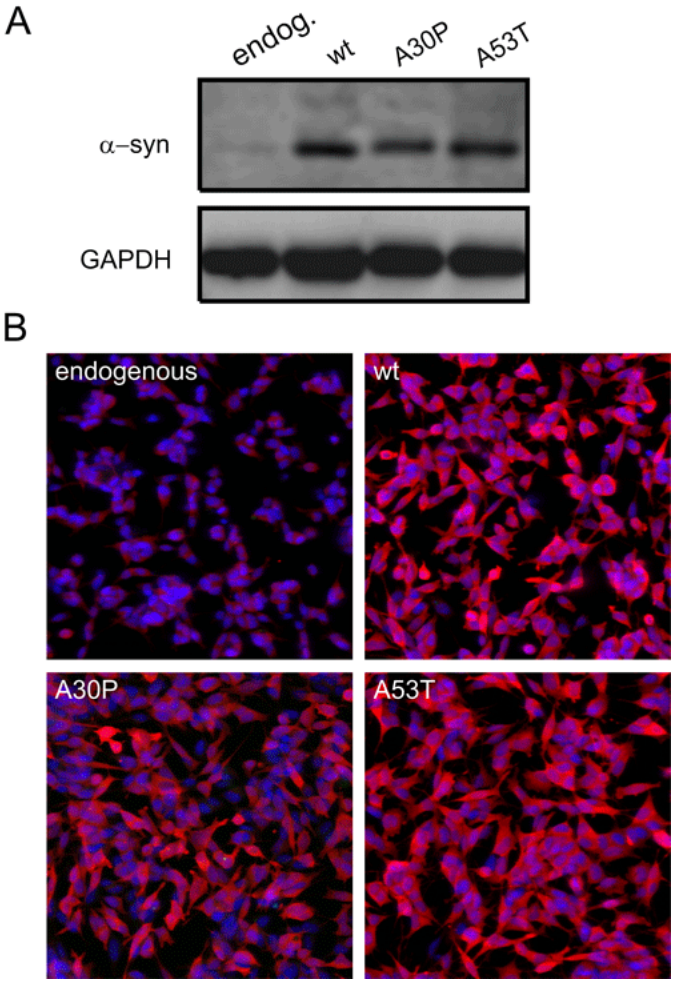

Supplemental figure 2: Expression levels of α-syn in SH-SY5Y cells.
A) Mock transfected and SH-SY5Y cells overexpressing α-syn[wt, A30P, A53T] were lysed, and proteins were resolved by 4-12% SDS PAGE. Lysates were Western blotted using polyclonal α-syn antibody ASY-1. Equal protein loading was verified using an anti GAPDH antibody (loading control). ***B)*** Laser confocal microscope images of mock transfected and SH-SY5Y cells overexpressing α-syn[wt, A30P, A53T]. Cells were immunostained with the α-syn antibody ASY-1 (red).

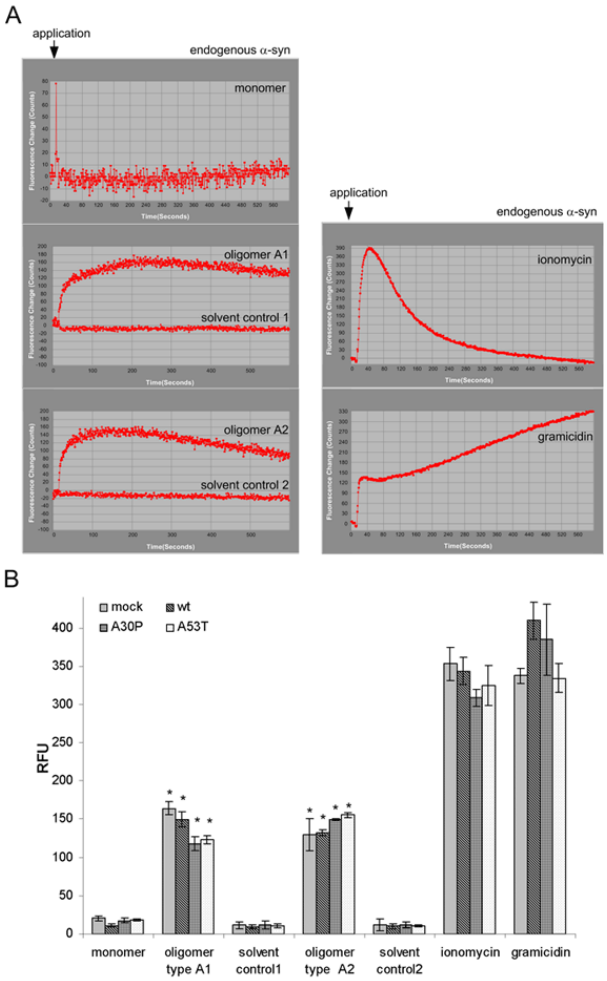

Supplemental figure 3: [Ca^{2+}] elevation by α-syn oligomers type A1 and A2 in SH-SY5Y cells.
A) Kinetic plots illustrating typical signal responses to application of 0.1µg/µl α-syn monomer, oligomers type A1 and A2, and 1.5µM ionomycin and 500µg/ml gramicidin as positive controls. Oligomers type A1 and A2 evoked a clear increase in intracellular calcium. Each trace shows the negative control corrected mean fluorescence of 6000 mock transfected SH-SY5Y cells expressing endogenous level of α-syn. ***B)*** Quantification of [Ca^{2+}] elevation in mock transfected SH-SY5Y cells, cells overexpressing α-syn[wt, A30P, A53T] induced by different treatments. All cell lines showed a clear increase of intracellular [Ca^{2+}] after oligomer treatment compared to the respective solvent controls and α-syn monomeric form. Values are the mean ± SEM; n=3; *P < 0.0001. Bonferroni adjusted p-value for pair wise comparisons versus corresponding solvent controls. Oligomer type A1 treated: mock: Δ=153 (95% CI: 126.6-179.3); α-syn[wt]: Δ=140.8 (95% CI: 114.5-167.1); α-syn[A30P]: Δ=106.6 (95% CI: 80.3-132.9); α-syn[A53T]: Δ=112.5 (95% CI: 86.13-138.8). Oligomer type A2 treated: mock: Δ=118.6 (95% CI: 78.85-158.4); α-syn[wt]: Δ=122.1 (95% CI: 82.31-161.9); α-syn[A30P]: Δ=137.7 (95% CI: 97.96-177.5); α-syn[A53T]: Δ=145.4 (95% CI: 105.6-185.2). The experiments were repeated 4 times, all experiments showed similar results.

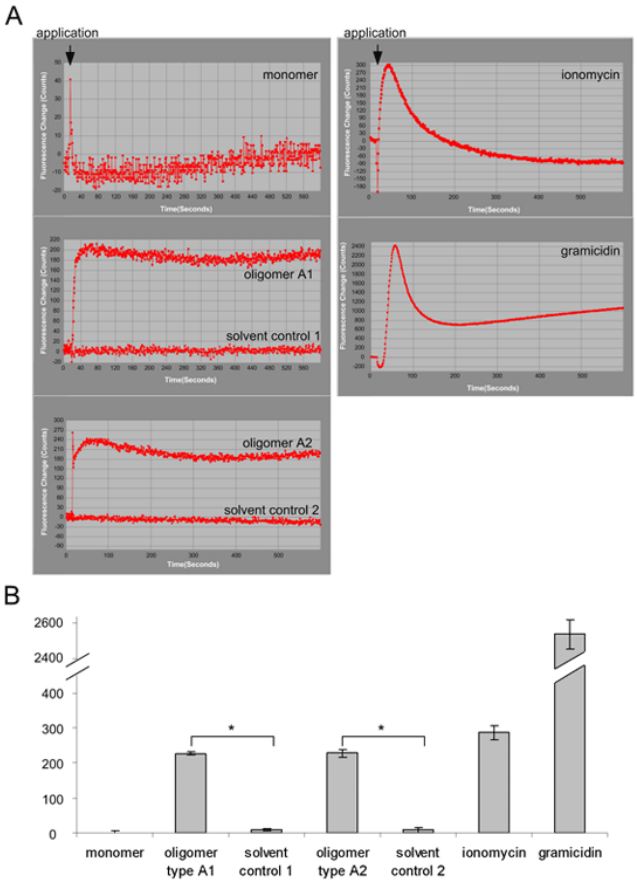

Supplemental figure 4: [Ca^{2+}] elevation by α-syn oligomers type A1 and A2 in primary cortical neurons.
A) Kinetic plots illustrating typical signal responses to application of 0.1µg/µl α-syn monomer, oligomers A1 and 2, and 1.5µM ionomycin and 500µg/ml gramicidin as positive controls. Both oligomer types A1 and A2 increased intracellular [Ca^{2+}] to the same extend compared to the respective solvent controls and α-syn monomeric form. Each trace shows the negative control corrected mean fluorescence of 1.25 x 10^5 primary neurons. ***B)*** Quantification of [Ca^{2+}] elevation induced by different treatments. Values are the mean ± SEM; n=3; *P < 0.0001, unpaired t test. Oligomer type A1 treated neurons: Δ= 218.5 (95% CI: 201.0-235.9); Oligomer type A2 treated neurons: Δ= 219.5 (95% CI: 181.7-257.2).

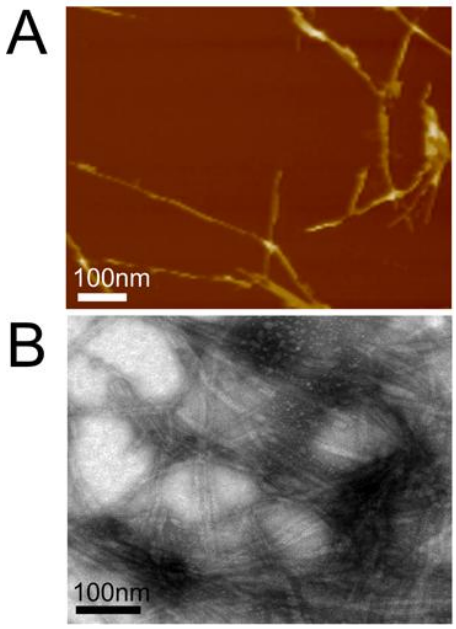

Supplemental figure 5: α-syn fibrils.
A) AFM image of α-syn fibrils. Fibrils of the A type after 1 week prolonged incubation (15 days) in 50mM sodium phosphate buffer. ***B)*** Negatively stained transmission electron micrographs of α-syn fibrils after 15 days incubation of approach type A.

1.8.2. Supplemental videos

Two 10-fold accelerated time laps videos performed on a confocal microscope with equipped with a Leica 63x objective are attached as supplemental materials. The videos are available:

- on the enclosed CD at the end of the manuscript (in the folder Article 1/Supplemental materials)
- or online at http://www.jneurosci.org/cgi/content/full/27/34/9220.

Supplemental Video 1 and Supplemental Video 2 show Fluo-4 AM Ca^{2+} imaging in response to α-syn oligomers of a SHSY cell and a primary neuron, respectively.

1.9. Acknowledgments

We are grateful to P. Kahle and C. Haass for providing α-syn plasmids and to F. Gillardon for suggestions concerning this manuscript. We also thank S. Eder for exquisite technical support for calcium measurements. The excellent technical assistance of P. Anding, S. Finger, W. Lemmer, and M. Palchauchdhuri is gratefully acknowledged.

2. Electrophysiological characterisation of microglia (article 2)

Original Paper

Cellular Physiology and Biochemistry

Cell Physiol Biochem 2009;24:141-152 Accepted: June 24, 2009

Characterisation of K^+ Currents in the C8-B4 Microglial Cell Line and their Regulation by Microglia Activating Stimuli

Simon Moussaud[1,2], Elisabeth Lamodière[1,2], Catherine Savage[2] and Henning J. Draheim[2]

[1]University of Burgundy, INSERM U866, [2]CNS Research Boehringer Ingelheim Pharma GmbH & Co KG, Biberach

2.1. Résumé en français

Les microglies sont les seules cellules immunitaires résidantes du cerveau. A ce titre, elles sont fortement impliquées dans la neuroprotection et la neurodégénération. En effet, leur activation induit la neuroinflammation *via* la production de cytokines et chimiokines, ainsi que la formation de stress oxydatif *via* la production d'oxyde nitrique et d'espèces réactives de l'oxygène. De plus, l'activation induit chez les microglies un profond changement de la régulation de l'homéostasie du potassium.

Dans le présent article, nous nous sommes intéressés à ce phénomène électrophysiologique encore peu étudié et à son implication dans l'activation microgliale. Pour ce faire, nous avons caractérisé et étudié les courants et les canaux potassiques présents chez les microglies. Comme modèle *in vitro*, nous avons utilisé des microglies primaires de souriceaux nouveaux-nés et nous les avons comparées à la lignée cellulaire murine d'origine microgliale C8-B4. En utilisant la technique du patch-clamp, nous avons mesuré de forts courants potassiques entrants et sortants. Ces courants potassiques étaient tout deux voltage-dépendants. D'ailleurs, aucun courant potassique calcique-dépendant n'a pu être identifié. Par l'utilisation combinée de techniques de caractérisation biophysique, pharmacologique et de biologie moléculaire, nous avons réussi à identifier les canaux ioniques responsables de ces flux potassiques sortants et entrants comme étant respectivement le canal Kv1.3 et le canal Kir2.1.

Nous nous sommes ensuite intéressés à la régulation de ces canaux et à leur lien avec l'activation des microglies. Nos données montrent que les courants potassiques sont en effet profondément modifiés à la suite de l'activation des microglies par le LPS, l'IFN-γ, le TGF-β ou le

GM-CSF. Le courant potassique entrant, présent pour les potentiels inférieurs au potentiel membranaire, diminue alors qu'un important courant voltage-dépendant sortant apparaît dans les potentiels positifs.

Nous avons montré que la quantité totale des canaux ne varie pas en réponse à l'activation. Cependant, les courants potassiques sont fortement réduits par l'action d'inhibiteurs de protéine kinase, ce qui suggère que la régulation des courants potassiques ne se fait pas par la synthèse *de novo* de canaux mais plutôt par l'activation des canaux déjà existants par phosphorylation.

Bien que nous ayons observé des différences mineures entre les microglies primaires et la lignée cellulaire C8-B4, la lignée C8-B4 est, d'après nos résultats, une alternative valable et utile à l'utilisation de microglies primaires pour réaliser des études électrophysiologiques. La lignée cellulaire C8-B4 serait par exemple idéale pour la recherche par criblage de bloqueurs du canal Kv1.3 en vue de développer de nouveaux immunosuppresseurs.

2.2. Foreword

The problems with the use of primary microglia are that they are difficult and time-consuming to isolate and that one has to sacrifice animals. For these ethical and practical reasons, we were interested in using the C8-B4 microglial cell line instead of the primary microglia in our high cell-consuming assays. However, little was published about this cell line and, consequently, we decided to compare the C8-B4 cells to primary microglia. The authors' lab concentrates important technology and know-how in electrophysiology. Therefore, we performed this electrophysiology-oriented comparative study of the C8-B4 microglial cell line and primary microglia. Moreover, with this study, we shed light on ion channels properties of microglia in response to activation.

2.3. Abstract

Microglia are the intrinsic immune cells of the brain. As such, they are crucially involved in neuro-protection as well as neuro-degeneration. Their activation leads to the induction of cytokine and chemokine release, the production of reactive oxygen species and nitric oxide and an increased outward potassium conductance.

In this study, we focus our interest on potassium currents and channels in the C8-B4 murine microglial cell line and compare them with those of primary cultured microglia from neo-natal mice. Using the whole cell patch-clamp technique, we have recorded prominent inward and outward rectifying voltage-dependent potassium currents but no calcium-activated potassium currents. Using pharmacological, biophysical and molecular approaches, we demonstrate that Kv1.3 and Kir2.1 channels underlie outward and inward rectifying potassium currents, respectively.

In contrast to primary cultured microglia, we observe that an outward rectifying potassium current is already present in unstimulated C8-B4 cells. However, as seen in primary

microglia, this current increases after treatment with LPS, IFN-γ, TGF-β and GM-CSF and is suppressed by treatment with protein kinase inhibitors.

Our study indicates that the C8-B4 cell line shows similar though not identical potassium channel properties compared to primary cultured microglia. We demonstrate that despite some differences, they are a useful tool to study potassium currents in microglial activation mechanisms by means of electrophysiological methods without the need for preparation of cells as primary culture.

2.4. Introduction

Neuro-inflammation plays a crucial role in numerous neuro-pathologies (e.g. ischemia, hypoxia, AIDS dementia, chronic pain) and neurodegenerative diseases (e.g. Parkinson's disease, Alzheimer's disease, multiple sclerosis, amyotrophic lateral sclerosis, Huntington's disease, Creutzfeldt-Jacob disease) (Gao and Hong, 2008; Tambuyzer *et al.*, 2008).

As guardians of the CNS, microglial cells are at the front line of all these pathologies. Microglia are a cell population of myeloid-monocytic origin that colonize the brain at different "developmental windows" (Kettenmann and Verkhratsky, 2008; Tambuyzer *et al.*, 2008). Microglia steadily survey their environment and can migrate and adopt different phenotypes in response to a multitude of stimuli. Microglia are usually beneficial. For example, they promote neuron survival by secreting growth factors (e.g. neurotrophin, nerve growth factor, brain-derived neurotrophic factor, glial cell derived neurotrophic factor, insulin-like growth factor 1) and anti-inflammatory cytokines (e.g. transforming growth factor beta, interleukin 1 receptor antagonist, interleukin 10). They scavenge toxins, unwanted inflammatory cells and cellular debris, and elicit neuro-plasticity by producing various proteases (Hanisch and Kettenmann, 2007). Yet in several pathological conditions, microglia can be detrimental due to exaggerated pro-inflammatory activity. Indeed, microglia can injure neurons through secretion of abnormal amounts of pro-inflammatory and pro-apoptotic cytokines (e.g. interleukin 1 beta, interleukin 6, tumor necrosis factor alpha) and through production of glutamate, reactive oxygen species and nitric oxide (Block *et al.*, 2007). The research fields of different neuro-pathologies associated with inflammatory processes share the same big challenge: to modulate microglia activation in order to increase their beneficial effects whilst avoiding their damaging effects on neurons (Liu, 2006; McCarty, 2006).

Potassium (K^+) channels are involved in the regulation of membrane potential, cell volume and intracellular ion concentrations. Interestingly in immune cells, K^+ channels are also implicated in cell activation processes (Chandy *et al.*, 2004). In microglia, K^+ current properties differ profoundly depending on the cellular state of activation (Draheim *et al.*, 1999; Eder, 1998; Eder, 2005; Fischer *et al.*, 1995; Norenberg *et al.*, 1994; Pannasch *et al.*, 2006; Prinz *et al.*, 1999; Schilling *et al.*, 2000; Schilling *et al.*,

2001; Schilling and Eder, 2003). Moreover, K^+ channels are linked to microglial activation processes like proliferation, migration, release of interleukin-1β and production of reactive oxygen species (Eder, 2005; Fordyce *et al.*, 2005; Kaushal *et al.*, 2007; Khanna *et al.*, 2001; Li *et al.*, 2008; Wu *et al.*, 2009). Thus K^+ channels are a potential target in view of modulation of microglial behaviour.

The presence of voltage-dependent and calcium-activated K^+ currents in microglia is well documented (Eder, 1998; Eder, 2005; Kaushal *et al.*, 2007; Khanna *et al.*, 2001; Kettenmann *et al.*, 1993) but the molecular identities of the K^+ channels involved are still not clear. The Kir2.1 channel was identified as being responsible for voltage-dependent inward rectifying currents (Eder, 1998). Kv1.3 and Kv1.5 voltage-gated channels are the most frequently proposed possibilities for the voltage-dependent outward K^+ current (Pannasch *et al.*, 2006; Kotecha and Schlichter, 1999). But the distinction between the two channels is difficult to unravel for three reasons. Firstly, both have similar electrophysiological and pharmacological characteristics. Secondly, both were found in myeloid cells. Finally, they can form heteromers with hybrid properties (Vincente *et al.*, 2006; Villalonga *et al.*, 2007).

However, the vast majority of experiments were performed using primary cultured microglia from neo-natal rodents. Strikingly, the little electrophysiological data available on microglial cell lines (Bocchini *et al.*, 1992; Schilling *et al.*, 2000) or on *in situ* microglia (Boucsein *et al.*, 2000; Kotecha and Schlichter, 1999; Schilling and Eder, 2007) shows inconsistencies in K^+ channel properties when compared to that of primary cultured microglia. Isolation of primary microglia is both difficult and time consuming and the various protocols used to prepare them are a source of discrepancy. Thus, microglial cell lines have often been used in the literature as microglial models. The C8-B4 microglia cell line is a spontaneous immortalized cell line derived from an 8-day mouse cerebellum organ culture. Consistent with primary microglia, C8-B4 cells have a similar ramified morphology and behave in a similar way in response to stimuli by producing large amounts of nitric oxide and glutamate. Furthermore, they express classical microglial markers, such as F4/80, CD11b, CD16/32 and CD45 low (Alliot and Pessac, 1984; Alliot *et al.*, 1996; Beauvillain *et al.*, 2008; Xu *et al.*, 2008).

Thus, we asked whether the C8-B4 cell line is a suitable surrogate model to study ion channel activity in microglia. Using electrophysiology and molecular biology, we investigated K^+ channels in C8-B4 cells with regards to their identity, modulation and function in microglial activation. We show that this cell line displays similar though not identical electrophysiological properties to primary cultured microglia from neo-natal rodents.

2.5. *Materials and Methods*

Cell culture and microglia treatment

The murine microglial cell line C8-B4 (ATCC, CRL-2540, Manassas, USA) was maintained at 37°C in 10% CO_2 in Dulbecco's modified Eagle's medium with 4.5g/L glucose supplemented with 10% foetal bovine serum and 4mM L-glutamine (Invitrogen, Karlsruhe, Germany). Cells were split once a week and tested frequently for mycoplasma contamination. Primary microglia were isolated from 4-day old C57BL6 mice as described by Draheim *et al.* (1999). Purity of primary microglia was controlled by flow cytometry using antibodies against CD11b (AbDserotec, Düsseldorf, Germany) and *Griffonia simplicifolia* isolectin B_4 (Invitrogen) and was routinely in excess of 95%. For experiments, cells were seeded on glass cover-slips in 24-well plates ($2x10^4$cells/ml).

16 hours before measurement, the medium was changed and cells were treated with 100µM 4',5,7-trihydroxyisoflavone (genistein); 100µM 1-(5-isoquinolinesulfonyl)-2-methylpiperazine (H-7); 1µg/ml lipopolysaccharide (LPS) from *E. coli* strain K235 (all from Sigma, Munich, Germany); 100ng/ml murine recombinant interferon gamma (IFN-γ); 10ng/ml human recombinant transforming growth factor beta 1 (TGF-β); or 100ng/ml murine recombinant granulocyte and macrophage colony stimulating factor (GM-CSF). All cytokines were purchased from R&D systems, Wiesbaden-Nordenstadt, Germany which guarantees them to be endotoxin free. For electrophysiological experiments, apamin, charybdotoxin, α-dendrotoxin, margatoxin, 1-[(2-chlorophenyl)diphenylmethyl]-1H-pyrazole (TRAM-34), 4-aminopyridine (4-AP), 5,6-dichloro-1-ethyl-1,3-dihydro-2H-benzimidazole-2-one (DC-EBIO) and barium chloride (all from Sigma) were diluted in bath solution and applied directly to the cells by superfusion.

Electrophysiology

Whole-cell membrane currents were measured according to Hamill *et al.* (1981) using an EPC-9 patch clamp amplifier (HEKA, Lambrecht/Pfalz, Germany). Data acquisition and storage were carried out with TIDA software (HEKA) on a Compaq computer. Patch electrodes of 3-8MΩ were made with a micropipette puller (P97, Sutter, Novato, USA) from borosilicate glass capillaries (outer diameter 1.5mm and inner diameter 0.84mm; WPI, Sarasota, USA) and then fire-polished with a pipette forge (List-medical, Darmstadt/Eberstadt, Germany). The electrodes were filled with the following solution: 140mM KCl, 20mM NaCl, 2mM $MgCl_2$, 2.5mM $CaCl_2$, 10mM HEPES and 5mM EGTA. In some cases, a modified pipette solution containing 4.5mM $CaCl_2$ was also used to reach an intracellular free Ca^{2+} concentration of 1µM. Both solutions were adjusted to pH 7.35 with KOH. The extracellular solution contained: 5.5mM KCl, 140mM NaCl, 1mM $MgCl_2$, 1.8mM $CaCl_2$, 10mM HEPES and 35mM glucose. The pH of the bath solution was adjusted to pH 7.4 with NaOH. All experiments were performed at room temperature (20-22°C) and results are given as mean ± S.E.M., unless otherwise stated.

Western Blot analysis

C8-B4 cells were lysed and the protein concentration of each lysate was determined using a BCA protein quantification kit (Pierce, Rockford, USA). Proteins (30µg per lane) were separated on 4-12% polyacrylamide minigels (Invitrogen) and subsequently transferred to nitrocellulose membranes using a semi-dry transfer system (Bio-Rad, Munich, Germany). After blocking in buffer containing 20mmol/L Tris, pH 7.4, 500mmol/L NaCl, 0.1% Tween 20, and 5% bovine serum albumin for 90min, the membranes were incubated

overnight at 4°C with rabbit polyclonal antibodies against Kv1.3 or Kv1.5 (1:500; Alomone Labs, Jerusalem, Israel) and with a mouse monoclonal antibody against Glyceraldehyde 3-phosphate dehydrogenase (GAPDH; 1:1000; Sigma) for the loading control. Specificity of the antibodies used was challenged with pre-incubation with the control antigen. Furthermore, as positive control for Kv1.5 immuno-reactivity, 20ng of epitope-GST fusion protein was loaded in parallel to the samples. Infrared fluorescent dye-conjugated secondary antibodies (1:5000; Li-Cor, Bad Homburg, Germany) and the Odyssey infrared imaging system were used for two-colour multiplexed detection.

Immuno-fluorescence

Cells were fixed using a 4% formaldehyde solution in phosphate-buffered saline. After washing, cells were permeabilized and non-specific binding sites were blocked using 0.005% saponin and 1% bovine serum albumin in phosphate-buffered saline. Primary antibodies were incubated overnight at 4°C and secondary antibodies for 1h at room temperature. The following primary antibodies were used; rabbit anti-Kv1.3 (1:100; Alomone Labs), rabbit anti-Kir2.1 (1:100; Abcam, Cambridge, UK) and rat anti-CD11b/Mac1 (1:100; AbDserotec). Alexa 488 or 647 fluorophore-conjugated anti-immunoglobulin G were used as secondary antibodies (1:1000; Invitrogen). After a final washing step, the cover-slides were mounted and visualized using a DM IRBE inverted confocal microscope (Leica, Wetzlar, Germany).

Reverse transcription polymerase chain reaction

Total RNA was extracted from C8-B4 cells using the RNeasy Mini Kit (Qiagen, Hilden, Germany). To avoid genomic DNA (gDNA) contamination, RNA was treated with DNase (Qiagen). Moreover, as a control, untranscribed RNA was also tested by PCR. Complementary DNA (cDNA) was synthesised with reverse transcriptase and random hexamer primers $p(dN)_6$ (Applied Biosystems, Foster City, USA). The cDNA was then used as a template for PCR reactions using gene-specific primers (Table 1). Amplification was carried out in a thermocycler (PeqLab Biotechnologies, Erlangen, Germany) using Taq-DNA polymerase (New England Biolabs, Frankfurt am Main, Germany). The amplified DNA fragments were loaded in 1.2% agarose gels containing 0.5µg/ml ethidium bromide (Invitrogen).

Data analysis and statistics

Data analysis and statistics were performed with GraphPad Prism 5.0 software (San Diego, USA). The statistical significance of differences between experimental groups was calculated by one-way analysis of variance test followed by Dunnett's post test. Differences were considered to be statistically significant with *P< 0.01.

Table 1: Primers used in reverse transcription PCR

Gene	Accession no.	Forward primer (5'- 3')	Reverse primer (5' - 3')	Length (bp)
GAPDH	NM_008084.2	CCATCACCATCTTCCAGGAGC	GAAGGCCATGCCAGTGAGCT	481
Kir 2.1	NM_008425.3	CAACAGTGCAGGAGCCGCTTTG	GCATTGAGTTGTCATGGCAGTCG	812
Kv 1.1	NM_010595.3	TCCAGGTTGCTTGCACCGTGTG	GGCTTCAGAGCCAGAAGGTTCAG	636
Kv 1.2	NM_008417.4	TAGAGCACACCTCCAGGACCTGC	TTCCAGACAGAAGCTGACGATGG	867
Kv 1.3	NM_008418.2	GTACTTCTTCGACCGCAACCGAC	TTGTCGTTCAGCCAGCTCAGTGC	615
Kv 1.4	NM_021275.3	CTTAGGATCATTCGTCTGGTCCGAG	GGACAGTGGCAGGTGGAGAGAAC	661
Kv 1.5	NM_145983.2	ATTGCCATCGTGTCGGTCTTGG	AGCCTGCTCCTCGTGGTCTGTCT	839

2.6. *Results*

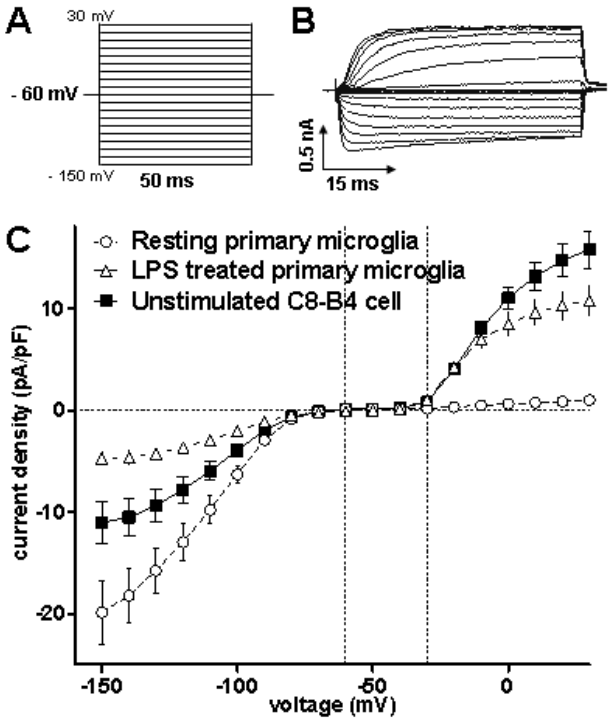

Figure 1: Comparison of voltage-dependent K^+ currents in primary microglia and the C8-B4 cell line. ***A)*** Cells were patched in whole cell configuration and held at a holding potential of -60mV. Voltage-dependent currents were elicited with 50ms voltage steps from -150mV to +30mV in 10mV increments. ***B)*** Representative recording of K^+ currents from a single C8-B4 cell. ***C)*** 20 independent current measurements were averaged to construct current-to-voltage curves. K^+ currents in resting primary microglia (○) in comparison to primary microglia treated for 16h with 1µg/ml LPS (△) or to unstimulated C8-B4 cells (■). Values are given as mean ± S.E.M.; n=20.

C8-B4 cells show microglia-like K^+ currents

Using the patch clamp technique, K^+ fluxes across the cell membrane of a single cell can be measured. C8-B4 cells were patched in whole cell configuration and held at a holding potential of -60mV. The K^+ current intensity was recorded at voltage steps from -150mV to +30mV in 10mV increments (Fig. 1 A). Under these conditions, two prominent voltage-dependent K^+ currents were observed (Fig. 1 B).

Between a holding potential of -150mV and -80mV, a strong inward K^+ current was measured. Then, between the equilibrium potential of K^+ and approximately -30mV, the cells had no measurable current. Finally from -30mV to +30mV, a prominent outward K^+ current was registered (Fig. 1 C).

The inward rectifying K^+ current seen in C8-B4 microglia was similar to the one seen in primary cultured microglia from neo-natal mice (Fig. 1 C). But in comparison to resting primary microglia, unstimulated C8-B4 cells also display a significant voltage-dependent outward K^+ current. It is noteworthy that a similar outward K^+ current was observed in primary microglia treated for 16 hours with 1µg/ml LPS (Fig.1 C).

Calcium-activated K+ currents

Calcium-activated K+ currents were investigated in order to determine whether C8-B4 cells have functional calcium-activated K+ channels. To block SK and IK channel activities, TRAM-34 (3µM) or apamin (100nM) were used. Calcium-activated currents were triggered by challenging the cells with 1µM intracellular free calcium and/or 100µM DC-EBIO application. Neither DC-EBIO application nor 1µM intracellular free calcium stimulation were able to activate K+ currents (data not shown). We only observed that DC-EBIO and TRAM-34 at high concentrations slightly decreased voltage-gated K+ current amplitudes. Thus, no significant calcium-activated K+ current was observed in C8-B4 microglia.

The voltage-dependent inward rectifying K+ current

The inward rectifying K+ current was found in all measured unstimulated C8-B4 cells. This current was elicited by hyperpolarisation and started at a threshold potential of approximately -80mV (Fig. 1 C). The density of this current had a mean value of -10.5±2pA/pF (n=20) at a holding potential of -140mV. Thus, in unstimulated C8-B4 cells, the inward rectifying K+ current was weaker than in resting primary microglia but larger than in activated primary microglia.

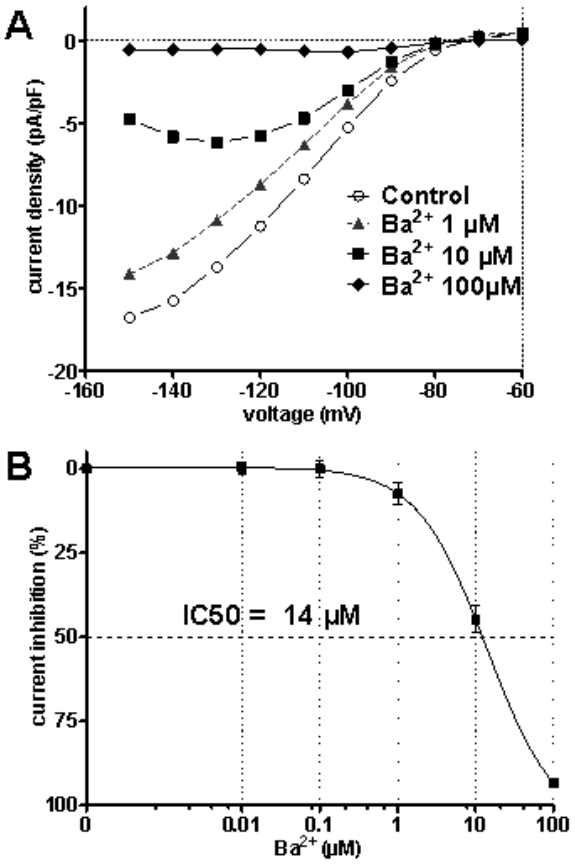

Figure 2: Characterisation of the voltage-dependent inward rectifying K+ current. The inward rectifying K+ current of C8-B4 cells was measured after application of increasing barium concentrations (0, 0.01, 0.1, 1, 10 and 100µM). ***A)*** Example of a K+ inward rectifying current measurement performed on a C8-B4 cell by voltage clamp before (○) and after application of barium at 1µM (▲), 10µM (■) and 100µM (◆). ***B)*** Dose-response curve comprising of the average of 13 independent measurements at a holding potential of -140 mV. The half maximal inhibitory concentration of barium was measured at 14µM.

To better characterise the inward rectifying K^+ current, the K^+ channel blocker barium chloride was applied in the bath solution at the following concentrations: 0, 0.01, 0.1, 1, 10 and 100µM (Fig. 2 A). The inward rectifying K^+ current of C8-B4 cells showed a high sensitivity to barium ions. The blockade was fully reversible and dependent on the barium concentration. At a concentration of 100µM, the inhibition was nearly complete and a half maximal inhibitory concentration (IC50) of 14µM was measured (Fig. 2 B). All these characteristics are in line with the assumption that Kir2.1 channels underlie the inward rectifying K^+ current of C8-B4 cells.

Pharmacological characterisation of the voltage-dependent outward rectifier K^+ channels

All measured C8-B4 cells displayed an outward K^+ current even without any prior treatment. This current was voltage-dependent and started at a threshold potential of approximately -30mV. The density of this current had a mean value of 14.7±2pA/pF (n=20) at a holding potential of +20mV in unstimulated cells (Fig. 1 C).

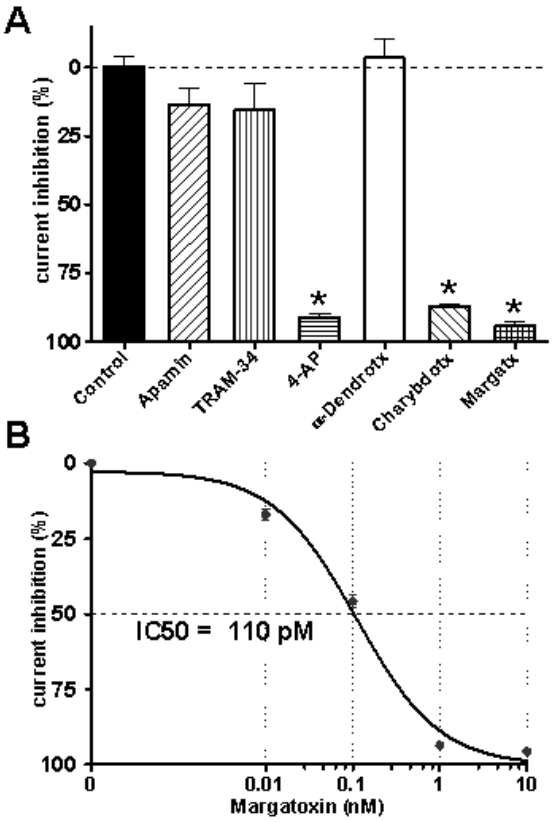

Figure 3: Pharmacological characterisation of the voltage-dependent outward K^+ current. The outward K^+ currents were elicited by depolarisation of the membrane from -60mV to +20mV for 50ms. ***A)*** The outward K^+ current density was measured before and after application of bath solution alone (control) or with the following: 100nM apamin, 3µM TRAM-34, 1mM 4-aminopyridine, 300nM α-dendrotoxin, 100nM charybdotoxin or 100nM margatoxin. Values are given as mean ± S.E.M.; n=5; * P< 0.01. ***B)*** Outward K^+ current density was measured before and after application of increasing concentrations of margatoxin (0.01, 0.1, 1, and 10nM). The results of 11 independent experiments were averaged and the half maximal inhibitory concentration value of margatoxin on C8-B4 was determined to be 110pM.

To identify the nature of the involved channel, a pharmacological profile of the outward K^+ current was established. Different classical channel blockers were applied *via* the bath solution to single cells patched in the whole cell configuration. The outward K^+ current was measured before and after application to calculate the relative inhibition as a percentage (Fig. 3 A).

The outward K^+ current of C8-B4 microglia showed no significant sensitivity to apamin (100nM) and TRAM-34 (3µM), excluding the implication of calcium-activated K^+ channels of the SK or IK family. Addition of 4-aminopyridine at a concentration of 1mM almost completely blocked the outward K^+ current (91±1%). Therefore the outward K^+ current of C8-B4 cells can be attributed to a voltage-gated channel of the shaker-related family (Kv1.x) (Grissmer *et al.*, 1994). α-Dendrotoxin (300nM), a potent Kv1.1, Kv1.2 and Kv1.6 channel blocker, had no effect on the outward K^+ current and thereby excluded the implication of the aforementioned three channels. Charybdotoxin and margatoxin, both at a concentration of 100nM, were able to block the K^+ outward current by 87±1% and 96±1%, respectively. All these results are a good hallmark for the implication of either Kv1.3 and/or Kv1.5 channels.

To distinguish between Kv1.3 homomeric, Kv1.5 homomeric and Kv1.3/5 heteromeric channels, margatoxin sensitivity of C8-B4 cells was studied (Draheim *et al.*, 1999; Garcia-Calvo *et al.*, 1993; Vincente *et al.*, 2006; Villalonga *et al.*, 2007).

The dose-response inhibition of margatoxin on the outward K^+ current was determined by sequential application of increasing concentrations of margatoxin (Fig. 3 B). The density of the outward K^+ current was measured after each application. In response to increasing margatoxin concentrations, the outward K^+ current decreased. The inhibition described a sigmoidal curve with an IC50 value of 110pM which corresponds to the value of a pure Kv1.3 homomere channel (Gutman *et al.*, 2005).

Biophysical characterisation of the voltage-dependent outward K^+ current

Kv1.3 and Kv1.5 channels have different inactivation kinetics. Whereas Kv1.1, Kv1.2 and Kv1.5 channels are constantly open in response to a long depolarisation, Kv1.3 channels present a time-dependent inactivation. Furthermore, this inactivation recovers slowly. Therefore Kv1.3 activity presents a use dependent decrease in response to repeated depolarizing pulses called cumulative inactivation (Grissmer *et al.*, 1994; Schilling *et al.*, 2000; Vincente *et al.*, 2006; Villalonga *et al.*, 2007).

To examine the inactivation kinetics of the outward K^+ current of C8-B4 microglia, cells were patched in whole cell configuration. The holding potential was set from -60mV to +20mV for 1s (Fig. 4 A). In response to this voltage step, voltage-dependent K^+ channels opened, generating a large K^+ efflux (Fig. 4 B). Less than 30ms after the onset of the stimulation, maximal amplitude was reached. Current amplitude then decreased slowly

following an inverse hyperbolic time course. Thus, the involved channel has a very fast opening kinetic followed by a slow time-dependent inactivation.

After the 5s pause at physiological holding potential, the second electrical pulse failed to produce the same current amplitude as the first one and, pulse after pulse, the peaks became progressively smaller (Fig. 4 B). The K^+ current decay fit a two-phase exponential curve. After a rapid decrease phase, the intensity of the current reached a plateau corresponding to 25% of its initial value (Fig. 4 C). Taken together, these data show that the outward K^+ current of C8-B4 cells has a cumulative inactivation kinetic in accordance with the biophysical characteristics of Kv1.3 channels but not of Kv1.5 channels (Gutman *et al.*, 2005).

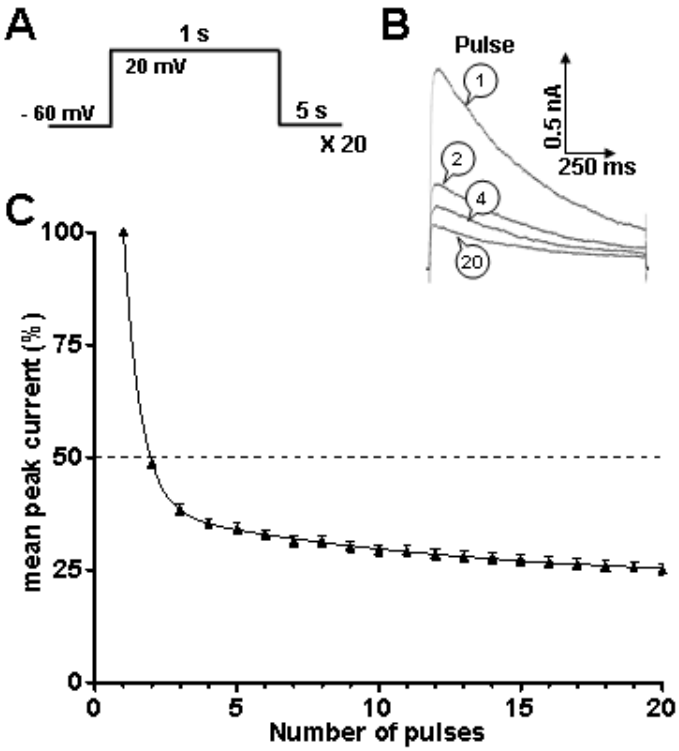

Figure 4: The outward K^+ current of C8-B4 cells is cumulatively inactivated. ***A)*** K^+ currents of single cells were recorded at depolarizing voltage steps of +20mV (duration 1s). This voltage step was repeated 20 times and each record was spaced from the next by a 5s pause at a holding potential of -60mV. ***B)*** Example of a current measurement. The peak amplitude of the outward K^+ current decreased pulse after pulse. ***C)*** Extinction kinetic of the outward K^+ currents of C8-B4 microglia in response to a train of 20 depolarizing pulses. Values are given as mean ± S.E.M.; n=30.

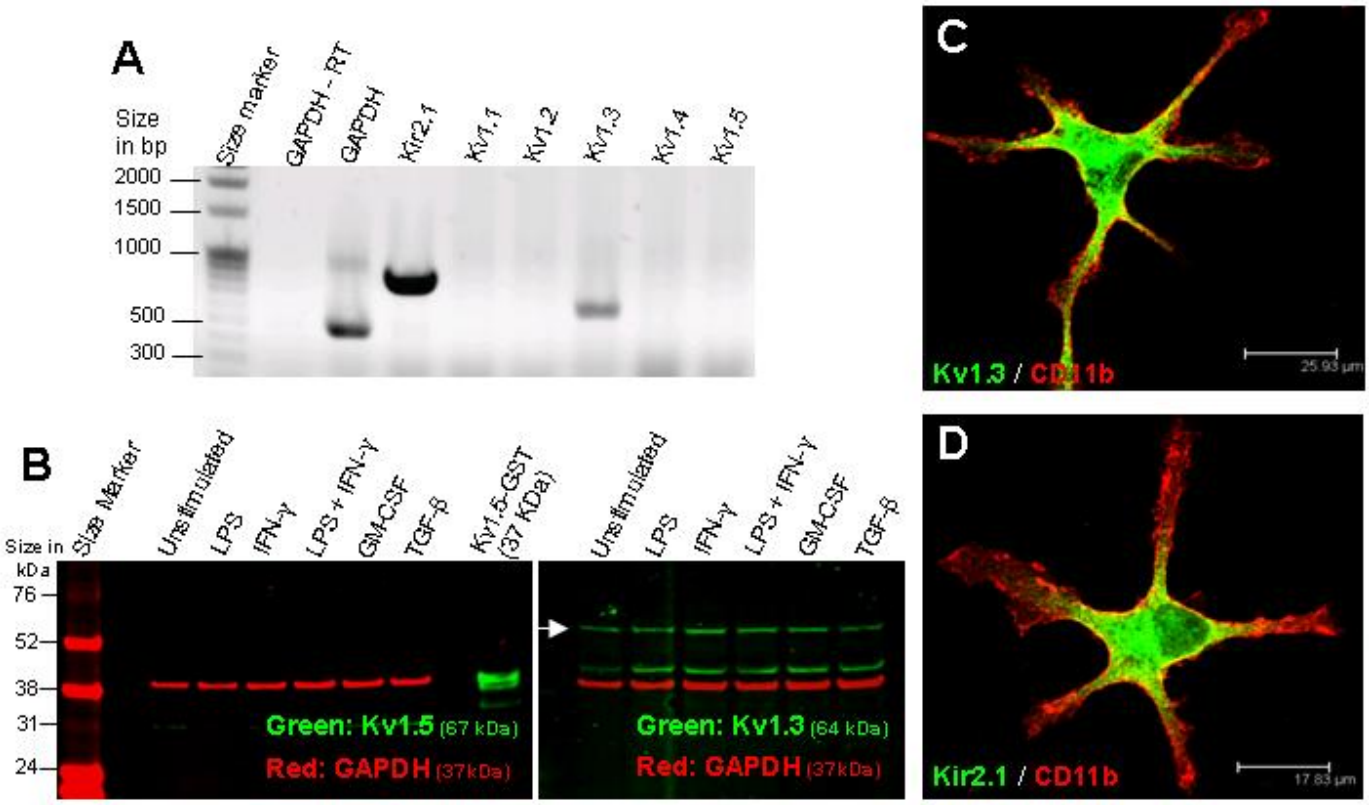

Figure 5: Molecular characterisation of K⁺ channels in C8-B4 microglia. ***A)*** Ethidium bromide-stained gel showing reverse transcription PCR amplified products of GAPDH, Kir2.1, Kv1.1, Kv1.2, Kv1.3, Kv1.4 and Kv1.5, from 2µg of mRNA extracted from unstimulated C8-B4 microglia. GAPDH expression was used as a positive control (lane GAPDH) and gDNA contamination was excluded by performing reverse transcription PCR on untranscribed mRNA with the GAPDH specific primers (lane GAPDH-RT). ***B)*** Western blot analysis of C8-B4 cell lysates. Prior to lysis, cells were incubated for 16 hours with fresh medium alone (unstimulated), or with fresh medium supplemented with the following: 1µg/ml LPS, 100ng/ml IFN-γ, a combination of both, 100ng/ml GM-CSF or 10ng/ml TGF-β. In the left panel, GAPDH was labelled in red and Kv1.5 in green. In the right panel, GAPDH is labelled in red and Kv1.3 in green (bands are marked with the arrow). ***C and D)*** Confocal immuno-fluorescence pictures of unstimulated C8-B4 microglia. The red stain indicates anti-CD11b antibodies whilst the green stain indicates anti-Kv1.3 antibodies and anti-Kir2.1 antibodies, respectively. The cells display the characteristic ramified shape seen in resting microglia.

Molecular characterisation of K⁺ channels

To compare our electrophysiological results and verify the presence of K⁺ channels, molecular experiments were conducted on C8-B4 microglia. First of all, the expression of the Kv1.1, Kv1.2, Kv1.3, Kv1.4, Kv1.5 and Kir2.1 channels was tested by reverse transcription PCR on unstimulated C8-B4 cells (Fig. 5 A) using gene-specific primers (Table 1). Bands at the expected size were found for Kv1.3 and Kir2.1 demonstrating the expression of both genes in C8-B4. In contrast, no expression of Kv1.1, Kv1.2, Kv1.4 and Kv1.5 genes was seen.

Subsequently, a closer look at the protein level was taken using antibodies against Kir2.1, Kv1.3 and Kv1.5 channels. Western blot analysis revealed the presence of Kv1.3 protein and the absence of Kv1.5 protein in both unstimulated and stimulated C8-B4 cells (Fig. 5 B). Following on from this, confocal immuno-fluorescence pictures

confirmed the presence of Kv1.3 and Kir2.1 channels in C8-B4 cells and gave us information about their cellular localisation (Fig. 5 C and D). Both channels had similar localisation, being predominantly in the cell body and partially co-localised with CD11b at the plasma membrane. Furthermore a punctate staining of the cytoplasm was observed suggesting vesicle localisation.

Regulation of inward and outward rectifying K^+ currents and their role in cell activation

To investigate the regulation of inward and outward rectifying K^+ currents, C8-B4 cells were activated *in vitro*. Classical microglial activators known to influence the inward and outward K^+ currents in primary cultured microglia were tested (Eder, 1998). As pro-inflammatory stimuli, the lymphokine IFN-γ and the potent immune reaction elicitor LPS from *E. coli* K 235 were used. Furthermore, a combination of LPS and IFN-γ was also used for maximal pro-inflammatory stimulation. Two other cytokines were also tested on C8-B4 cells. The first, GM-CSF, is a key growth factor of myeloid lineage which strongly induces microglial proliferation. The second, TGF-β, is known for its neuro-protective and anti-inflammatory effects. Finally, to investigate the effect of protein kinases on the regulation of inward and outward K^+ currents, C8-B4 cells were exposed to the tyrosine kinase inhibitor genistein, and the serine/threonine kinase inhibitor H-7.

To compare unstimulated and stimulated C8-B4 microglia, cells were incubated for 16 hours with the previously mentioned substances or with fresh medium alone as a control (Fig. 6). The cells were patched to measure their K^+ currents. Similar to previous observations in primary cultured microglia (Draheim *et al.*, 1999; Eder, 1998; Eder, 2005; Fischer *et al.*, 1995; Fordyce *et al.*, 2005; Norenberg *et al.*, 1994, Pannasch *et al.*, 2006; Prinz *et al.*, 1999; Schilling *et al.*, 2000; Schilling *et al.*, 2001; Schilling and Eder, 2003), C8-B4 cells changed their voltage-gated inward and outward rectifying currents in response to various activating stimuli (Fig. 6). Activated C8-B4 cells displayed larger outward K^+ currents than unstimulated cells (Fig. 6 A). Treatment with LPS, IFN-γ or both together led to a 59%-73% increase in amplitude of the outward K^+ current. In contrast, GM-CSF and TGF-β treatments induced a more than 2-fold increase in amplitude of the outward K^+ current (Fig. 6 A).

The regulation of the inward rectifying K^+ current regulation was more complex (Fig. 6 B). TGF-β was the only substance to increase the amplitude of the inward rectifying K^+ current. On the other hand, LPS or IFN-γ treatment provoked a 23% and 34% decrease, respectively. Interestingly, when LPS and IFN-γ were combined, their effect on inward rectifying K^+ currents appeared to be cumulative, with a larger decrease of 52% being observed.

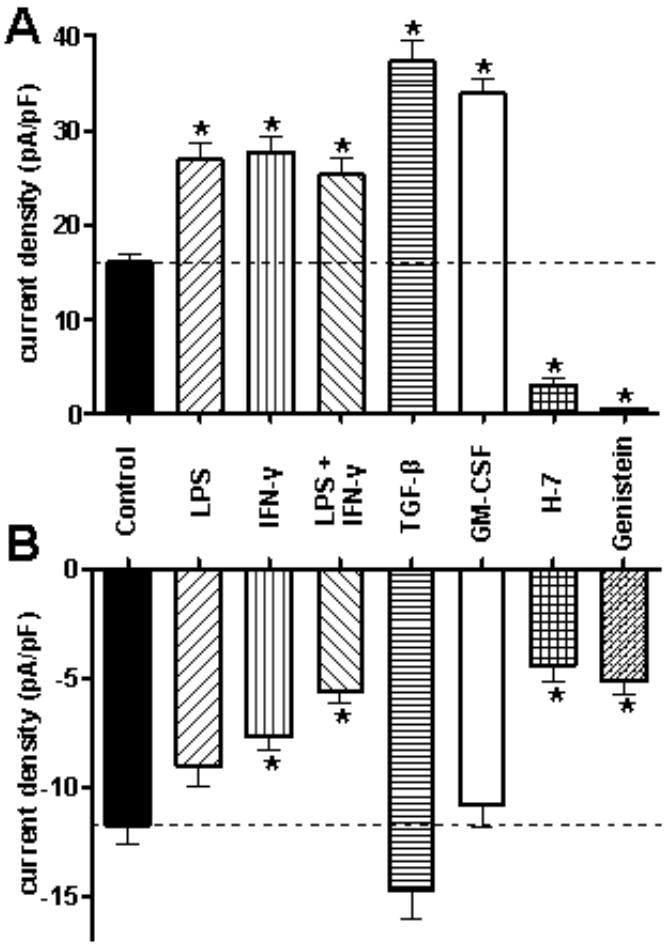

Figure 6: Inward and outward rectifying K+ currents are modulated in response to cell activation and protein kinase activity. Cells were incubated for 16 hours with fresh medium alone (control) or with fresh medium supplemented with the following: 1µg/ml LPS, 100ng/ml IFN-γ, a combination of both, 100ng/ml GM-CSF, 10ng/ml TGF-β, 100µM H-7 or 100µM genistein. After treatment, C8-B4 cells were patched in the whole cell configuration. The results of 70 measurements were averaged in these histograms. ***A)*** The outward K^+ current intensity was measured during a 50ms voltage step to +20mV. ***B)*** The inward K^+ current intensity was measured during a 50ms voltage step to -140mV. Values are given as mean ± S.E.M.; n=70; * P< 0.01.

To determine whether the increase of outward K^+ current seen after cell activation was due to additional activity of another K^+ channel or to an increase of Kv1.3 channel activity, the pharmacological and biophysical characterisations previously performed on unstimulated cells were repeated for each stimulatory condition (Table 2).

Unstimulated and activated microglia showed virtually identical pharmacological profiles. They were both insensitive to apamin (100nM), TRAM-34 (3µM) and α-dendrotoxin (300nM) application. Additionally they were both sensitive to 4-aminopyridine (1mM), charybdotoxin (100nM) and margatoxin (100nM). Furthermore, the margatoxin IC50 values were all in the same range and close to those of Kv1.3 homomeric channels (Gutman *et al.*, 2005). Finally, the outward K^+ currents in all measured cells had the same cumulative inactivation kinetic. Thus, the properties of the outward K^+ current of activated C8-B4 cells can also be attributed to a pure Kv1.3 homomeric channel activity.

To clarify whether the increase of outward K^+ current seen after cell activation was due to an increase of Kv1.3 channel quantity, a western blot analysis was carried out. Unexpectedly, western blot analysis revealed no significant difference in Kv1.3 protein expression between the different conditions (Fig. 5 B).

Given that Kv1.3 channel quantity stayed constant, regulation through phosphorylation mechanisms were investigated. Treatment with two protein kinase inhibitors, namely genistein and H-7,

drastically reduced the outward K^+ currents by 81% and 97%, respectively (Fig. 6 A). Protein kinase inhibition also affected the inward rectifying K^+ current, though to a lesser extent (Fig. 6 B). These results are in line with phospho-regulation of Kv1.3 activity.

2.7. Discussion

As the resident immune cells of the brain, microglia are the focal point of many neuro-pathologies. K^+ channels have been ascertained to be involved in microglial activation mechanisms. Thus far they have been studied mostly in primary cultured microglia and never been observed in the microglial cell line C8-B4.

The first aim of this study was to examine the electrophysiological characteristics of the C8-B4 cell line in comparison with primary microglia, with the focus of our interest being the identification of K^+ channels present in these cells. Additionally, we investigated the regulation of these K^+ channels in response to microglial activation.

Several previous reports described the presence of calcium-activated K^+ currents in primary cultured microglia, which were attributed to SK or BK channels (Eder, 2005; Kaushal *et al.*, 2007; Khanna *et al.*, 2001) while others did not (Draheim *et al.*, 1999). Intriguingly, in acute hippocampal slices, Schilling *et al.* did not detect calcium-activated K^+ currents in primary murine microglia. However when the brain slices were cultured, calcium-activated K^+ currents appeared (Schilling and Eder, 2007). In this study, C8-B4 microglia did not show any calcium-activated K^+ currents.

Consistent with what has been described in primary cultured microglia (Draheim *et al.*, 1999; Eder, 1998; Eder, 2005; Fischer *et al.*, 1995; Fordyce *et al.*, 2005; Norenberg *et al.*, 1994; Kettenmann *et al.*, 1990; Kettenmann *et al.*, 1993; Pannasch *et al.*, 2006; Prinz *et al.*, 1999; Schilling *et al.*, 2000; Schilling *et al.*, 2001; Schilling and Eder, 2003), C8-B4 cells functionally express voltage-dependent K^+ currents. Two distinct voltage-activated currents, inward and outward rectifying K^+ currents, were recorded. Both currents appeared to be identical to the ones described in primary microglia. However, in contrast with primary cultured microglia, the outward K^+ current in C8-B4 microglia was already present in unstimulated cells. As a control, we incubated primary cultured microglia from neo-natal mice with C8-B4-conditioned medium. C8-B4-conditioned medium did not induce the appearance of an outward K^+ current (data not shown). Thus, the presence of a constitutive outward K^+ current can not be explained by artefact stimulation, such as a contamination or the presence of endotoxins or paracrine and autocrine stimulation. It is noteworthy that similar constitutive outward

K^+ currents were described in bone-marrow macrophages and in the J774.1, and RAW 264.7 cell lines (Gallin and Sheehy, 1985; Kettenmann *et al.*, 1990; Vincente *et al.*, 2006; Villalonga *et al.*, 2007) and that C8-B4 cells were described to be "pre-activated" (Alliot *et al.*, 1996; Xu *et al.*, 2008).

Our assumption is that this constitutive outward K^+ current might be linked to the continual proliferation of the C8-B4 cell line. This idea correlates with the fact that outward K^+ currents are induced by proliferation. It is well known that primary cultured microglia patched on an astrocyte-layer (Schmidtmayer *et al.*, 1994) or incubated with astrocyte-conditioned medium also display an outward K^+ current (Fischer *et al.*, 1995; Schilling *et al.*, 2001). Indeed, astrocyte-conditioned medium contains GM-CSF and TGF-β, both cytokines that are involved in microglial proliferation and deactivation, respectively, and are known to up-regulate the outward K^+ current of primary cultured microglia (Fischer *et al.*, 1995; Schilling *et al.*, 2000).

More recently, Schiling *et al.* demonstrated that murine microglia patched in acute brain slices displayed both inward and outward rectifying voltage-dependent K^+ currents (Schilling and Eder, 2007). Furthermore, Draheim *et al.* noticed differences in the occurrence of inward and outward rectifying voltage-dependent K^+ currents between embryonic and neo-natal as well as between rat and mouse cultured microglia (Draheim *et al.*, 1999; Prinz *et al.*, 1999).

By using electrophysiological, pharmacological, biophysical and molecular methods, we identified the channels underlying the K^+ currents observed. Concerning the inward rectifying current, its electrophysiological and pharmacological properties were close to the Kir2.1 voltage-gated channel (Eder, 1998). Furthermore, Kir2.1 transcript and protein expression were detected in C8-B4 cells.

The outward K^+ channel identification was more complex due to the number of potential candidates. The pharmacological profile of the outward K^+ current gave evidence for voltage-gated K^+ channels of the shaker-related family. Indeed, the outward K^+ current was 4-AP, charybdotoxin and margatoxin sensitive. But α-dendrotoxin, at high concentration, failed to have a significant effect. These results exclude Kv1.1, Kv1.2 and Kv1.6 as the channels underlying the outward currents.

To distinguish between pure Kv1.3 homomeric channels, pure Kv1.5 homomeric channels, and Kv1.3/5 heteromeric channels, margatoxin sensitivity and the channel closing kinetic were investigated. Margatoxin had an IC50 value of 110pM which is in accordance with the sensitivity of pure Kv1.3 homomeric channels (Draheim *et al.*, 1999; Grissmer *et al.*, 1994; Gutman *et al.*, 2005; Vincente *et al.*, 2006). Further evidence for the presence of Kv1.3 channels in C8-B4 cells was the fast, time-dependent inactivation and the cumulative inactivation kinetic of the outward K^+ current.

Table 2: Comparison of activated and unstimulated C8-B4 microglia

	Unstimulated	LPS	IFN-γ	LPS + IFN-γ	TGF-β	GM-CSF
Cumulative inactivation	yes	yes	yes	yes	yes	yes
Apamin (100nM) inhibition in %	14 ±6	8 ±2	7 ±6	9 ±5	12 ±5	12 ±5
TRAM-34 (3µM) inhibition in %	15 ±10	19 ±5	26 ±5	23 ±4	25 ±3	26 ±6
4-Aminopyridine (1mM) inhibition in %	91 ±1	92 ±2	94 ±1	93 ±0.5	93 ±1	93 ±0.5
Dendrotoxin (300nM) inhibition in %	- 4 ±7	2 ±4	3 ±4	-1 ±4	8 ±6	5 ±2
Charybdotoxin (100nM) inhibition in %	87 ±1	91 ±2	92 ±2	89 ±1	90 ±1	92 ±1
Margatoxin (100nM) inhibition in %	96 ±1	97 ±0.5	97 ±1	98 ±0.5	98 ±1	97 ±1
Margatoxin IC50	110 pM	107 pM	104 pM	106 pM	99 pM	115 pM

% inhibition of the outward K^+ current at +20mV after substance application, ± S.E.M.

Thus, from a functional point of view, we provide strong evidence for pure Kv1.3 channels being responsible for the outward K^+ currents of unstimulated C8-B4 microglia.

To confirm our electrophysiological experiments and to look at the presence of non functional K^+ channels, molecular methods were also used. Reverse transcription PCR analysis provided details on expression of K^+ channels. Kv1.3 and Kir2.1 but no Kv1.1, Kv1.2, Kv1.4 and Kv1.5 transcripts were detected in unstimulated C8-B4 microglia. Western blot analysis and confocal microscopy immuno-fluorescence measurements confirmed the presence of Kv1.3 and Kir2.1 channels in C8-B4 microglia. The confocal immuno-fluorescence analyses gave clues to the localisation of Kv1.3 and Kir2.1 channels. Both were co-localised with CD11b at the plasma membrane. Some Kv1.3 and Kir2.1 fluorescence was also found in the cytoplasm in vesicle-like punctate staining.

The fact that Kv1.5 activity is not recorded by patch-clamping and not found by molecular techniques is an interesting though not surprising discovery. The presence and the activity of Kv1.3 and Kv1.5 channels in primary cultured microglia are well documented and discussed. Kv1.5-like currents have been measured in rat microglia (Kotecha and Schlichter, 1999) but not in murine microglia (Draheim *et al.*, 1999; Schilling *et al.*, 2000; Schilling and Eder, 2007). Furthermore, even if Kv1.5 was detected in cultured rat microglia by molecular methods, no Kv1.5-like currents were measured (Fordyce *et al.*, 2005; Khanna *et al.*, 2001). Kotecha and Schlichter observed transitory Kv1.5 activity *in situ* in rat microglia and demonstrated that when the cells were maintained in culture, this Kv1.5 activity disappeared with time and was replaced by Kv1.3 activity in proliferating microglia (Kotecha and Schlichter, 1999). Recently, Kv1.1 and Kv1.2 channels were also detected at the molecular level in the BV-2 cell line and in primary rat microglia (Fordyce *et al.*, 2005; Li *et al.*, 2008; Wu *et al.*, 2008). In our opinion, these apparent differences reflect the

discrepancies between the models used and the Kv channel redundancy.

In order to compare C8-B4 cells with primary cultured microglia, we also investigated the regulation of inward and outward rectifying currents with regard to the microglial activation state. As has been described in primary microglia (Draheim *et al.*, 1999; Eder, 1998; Eder, 2005; Fischer *et al.*, 1995; Fordyce *et al.*, 2005; Norenberg *et al.*, 1994; Pannasch *et al.*, 2006; Prinz *et al.*, 1999; Schilling *et al.*, 2000; Schilling *et al.*, 2001; Schilling and Eder, 2003), both voltage-dependent K^+ currents were modulated in response to cytokines or bacterial components. Meanwhile the inward rectifying K^+ current was reduced in presence of IFN-γ and/or LPS.

LPS, IFN-γ, TGF-β and GM-CSF treatments provoked prominent increases in amplitude of the outward K^+ current in C8-B4 cells. Interestingly, the outward K^+ current seemed to be regulated on a gradient. LPS and/or IFN-γ treatments turned the outward K^+ current to its intermediate level, whereas GM-CSF or TGF-β treatments turned it to the maximal level.

In addition, we demonstrated that the up-regulation of the outward K^+ current amplitudes seen in stimulated C8-B4 cells was due to increased Kv1.3 homomeric channel activity and not to the activation of a different channel type. Strikingly, the increased amplitude of the outward K^+ currents seen in stimulated C8-B4 were not linked to global channel quantity up-regulation. These results are in apparent contradiction with a transcriptional regulation of the Kv1.3 channel. Paradoxically, in LPS activated rat primary microglia, Fordyce *et al.* observed an increased amplitude of the outward K^+ current and an enhanced Kv1.3 transcript quantity without any change in Kv1.3 protein expression (Fordyce *et al.*, 2005).

Finally, we demonstrated that the tyrosine kinase inhibitor genistein and the serine/threonine kinase inhibitor H-7 strongly down-regulated the outward K^+ current of C8-B4 cells. In current publications, H-7 but not genistein was found to down-regulate the outward K^+ current of primary cultured microglia (Schilling *et al.*, 2000; Schilling and Eder, 2003). This difference in kinase inhibitor sensitivity might reflect a signalling pathway difference in the regulation of the K^+ currents in C8-B4 cells compared to primary cultured microglia. Nonetheless, the fact that the outward K^+ current is abolished by protein kinase inhibitors and that Kv1.3 was also found in the cytoplasm of C8-B4 cells in vesicle-like structures suggests that Kv1.3 activity modulation is not only transcriptional but also linked to post-translational regulation processes, such as phosphorylation and sequestration.

All our observations question the role of the outward K^+ current occurrence as marker of "activated" microglia and reinforce the role of outward K^+ currents in microglia activation and proliferation. Nevertheless, more investigations are needed to better understand the function of this current. It will be interesting to further investigate the differences between *in situ* and *in vitro* microglia, as well as between different species and developmental stages.

However, in the brain, Kv1.3 channels are essentially found in microglia and their inhibition dramatically blocks microglial pro-inflammatory activities and proliferation. Here, we have shown that the C8-B4 cell line has similar electrophysiological properties to *in vivo* and *in situ* primary microglia. In comparison to these other models, C8-B4 cells are much simpler to use. Furthermore, due to their lack of calcium-activated K^+ currents, C8-B4 microglia may be a useful tool for research on Kv1.3 or Kir2.1 in microglia. In consequence, C8-B4 cells may be a suitable surrogate model in screening scenarios that use automated patch-clamp, fluorescence or impedance assays to identify small molecules interacting with the Kv1.3 channel.

2.8. Acknowledgments

This work was supported by the CNS Research department from Boehringer Ingelheim. The authors are grateful to Pr. Chluba J., Pr. Pugin A., Dr. Kostka M. and Pr. Hengerer B.. The excellent technical assistance of Linn D., Longden T., Anding P., Finger S. and Palchaudhuri M. are gratefully acknowledged.

3. A new method to isolate microglia of aged animals (article 3)

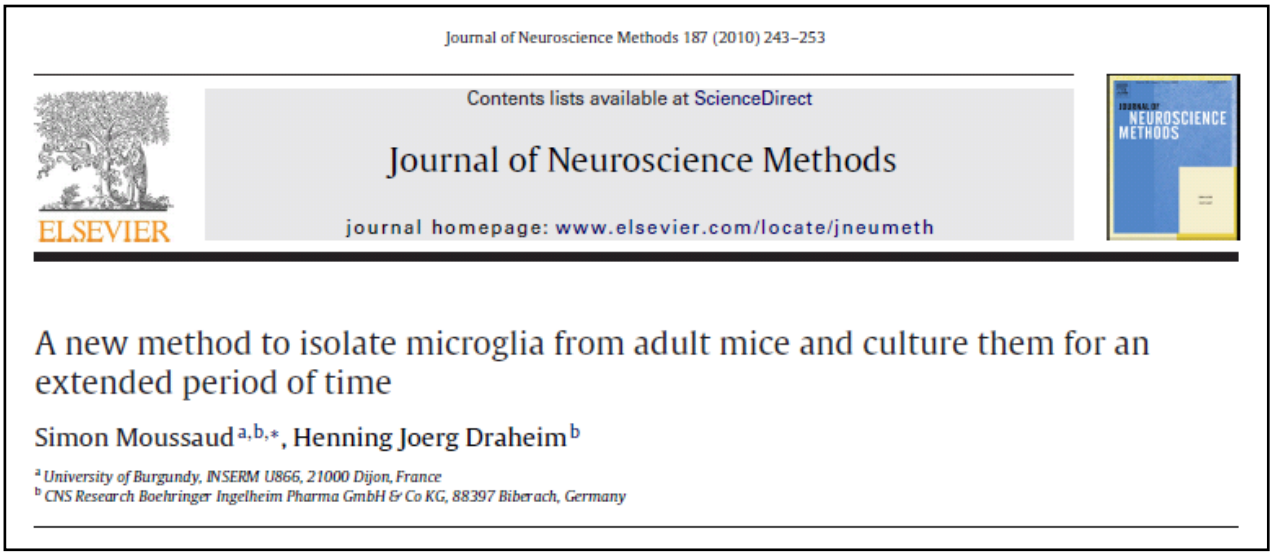

Journal of Neuroscience Methods 187 (2010) 243–253

Contents lists available at ScienceDirect

Journal of Neuroscience Methods

journal homepage: www.elsevier.com/locate/jneumeth

A new method to isolate microglia from adult mice and culture them for an extended period of time

Simon Moussaud [a,b,*], Henning Joerg Draheim [b]

[a] University of Burgundy, INSERM U866, 21000 Dijon, France
[b] CNS Research Boehringer Ingelheim Pharma GmbH & Co KG, 88397 Biberach, Germany

3.1. Résumé en français

En tant que principales cellules immunocompétentes du cerveau, les microglies sont impliquées dans les processus de neuroprotection et de neurodégénération. En conséquence, les microglies jouent un rôle dans de nombreuses neuropathologies et intéressent par là même de nombreux chercheurs.

Actuellement, pour l'étude *in vitro* de la neuroinflammation et des microglies, la majorité des chercheurs ont recours à des lignées cellulaires d'origine microgliale ou à des cultures primaires de microglies préparées à partir de cerveaux de rongeurs nouveaux-nés. Cependant, ces modèles *in vitro* ne sont pas idéaux dans le cas de la recherche sur des maladies neurodégénératives liées à l'âge comme les maladies d'Alzheimer et de Parkinson, car ils ne reflètent pas les processus de vieillissement pourtant si importants dans ces pathologies.

Jusqu'ici, seuls quelques rares articles décrivant des microglies adultes dans un environnement *in vitro* ont été publiés et ceux-ci se sont restreints à utiliser des microglies *ex vivo* qui en réalité n'arrivent à survivre que brièvement *in vitro*. En effet, jusqu'à présent, il n'existait pas de méthode fiable pour isoler des microglies à partir de tissus nerveux adultes et pour les cultiver *in vitro* pendant une période prolongée.

Avec cet article, nous publions une nouvelle méthode permettant de combler cette lacune technique. En suivant notre protocole, il est possible d'isoler, puis de cultiver une population quasi pure de microglies primaires issues de cerveaux de souris adultes ou même âgées. Notre méthode est basée sur la combinaison d'une purification des cellules par centrifugation sur gradient de densité discontinu, suivie d'un processus de sélection en culture. A la fin de la procédure, les microglies se concentrent à la surface du milieu de culture en formant une couche de cellules non adhérentes. Les microglies peuvent ainsi être aisément et

successivement récoltées. De plus, cette méthode présente l'avantage d'être simple à réaliser et de fournir des microglies d'une pureté élevée et avec des rendements conséquents. Un autre avantage est que ces microglies adultes primaires sont capables de proliférer *in vitro* et peuvent ainsi être maintenues *in vitro* pendant une longue durée.

De plus, dans cet article, nous avons soigneusement caractérisé ces microglies adultes en utilisant diverses techniques, comme la cytométrie de flux, l'immunofluorescence, le patch-clamp et l'ELISA multispoté à détection par électroluminescence. En parallèle, nous avons aussi comparé les microglies primaires en provenance d'adultes aux microglies primaires en provenance de nouveaux-nés, ainsi qu'à la lignée cellulaire d'origine microgliale C8-B4. Nous avons ainsi pu observer que les microglies primaires d'adultes présentent des différences subtiles mais intéressantes avec les microglies de nouveaux-nés.

3.2. Foreword

This article is the result of a long and difficult investigative work. Our first aim was just to isolate microglia from adult brains and to keep them in culture. At first sight, this idea seems to be simple, but in reality it is very challenging due to numerous technical difficulties. Actually, in the literature, no prior protocol existed for adult microglia culture. In consequence, we took inspiration from the existing primary culture techniques and developed our own method. Part of our protocol has been first presented in September 2009 at the Euroglia meeting in Paris. Considering the great interest that it generated, we decided to write the following publication of the preparation method, which found broad response in the microglia research field.

3.3. Abstract

As the major immuno-competent cells of the brain, microglia are highly implicated in neuro-protection as well as in neuro-degeneration. Therefore, they are of key interest for research on numerous CNS diseases.

Currently, to model inflammation in the brain, microglial cell lines or primary microglia prepared from embryonic or neo-natal rodents are widely used. However, these *in vitro* microglial models are not suitable for research in the field of neuro-degenerative diseases where aging is a crucial parameter. Only a few *in vitro* studies on aged microglia have been published so far, most of which use *ex vivo* microglia which can not be kept in culture for prolonged periods of time.

In the present study, we provide a new approach which allows the isolation and culture of an almost pure population of microglia from adult mouse brains. The isolation is based on a procedure which combines density separation and a subsequent culture selection process. After these steps, microglia form a non-adherent floating cell layer that can be easily and repeatedly harvested and replated. This method is simple and allows for a comparatively high yield and purity of adult microglial cells.

The collected primary adult microglia proliferate and can be kept in culture for extended periods of time. We compared the primary adult microglia to primary microglia from neo-natal mice as well as to the C8-B4 microglial cell line. We found that adult microglia have similar, but not identical, immuno-phenotypic, functional and electrophysiological characteristics to the other *in vitro* models.

3.4. Introduction

Microglial cells are the sentries of the brain. They are at the front line in numerous neuro-pathologies including ischemia, chronic pain, Alzheimer's disease, Parkinson's disease, multiple sclerosis, amyotrophic lateral sclerosis, Huntington's disease and brain tumours (Tambuyzer *et al.*, 2008).

Microglia account for approximately 12% of cells in the central nervous system (CNS) (Block *et al.*, 2007). They are derived from early embryonic myeloid-monocytic cells that colonise the brain (Ajami *et al.*, 2007). Microglia continually monitor their micro-environment (Nimmerjahn *et al.*, 2005) and are implicated in neuro-plasticity, host defence, homeostasis, wound healing, debris scavenging, peripheral immune cells recruitment and immune response regulation (Aloisi, 2001). In response to a multitude of stressors, they have the capacity to migrate and undergo morphological and functional change.

As the major immuno-competent cells of the brain, they are critically involved in neuro-protection as well as in neuro-degeneration. Microglia are usually beneficial and support neuron survival through secretion of growth factors and anti-inflammatory cytokines (e.g. transforming growth factor beta, interleukin (IL)-1 receptor antagonist, IL-10) (Colton, 2009). Yet, in several pathological conditions, microglia can be deleterious due to inappropriate pro-inflammatory activity. Indeed, microglia can elicit neurotoxicity through secretion of abnormal amounts of pro-inflammatory and pro-apoptotic cytokines and chemokines (e.g. IL-1β, IL-6, IL-12, tumour necrosis factor alpha (TNF-α)) and through production of excitatory amino acids, eicosanoids, reactive oxygen species and nitric oxide (NO) (Block *et al.*, 2007).

Mounting evidence highlights the linkage between aging, microglial dysfunction, increased neuro-inflammation and neuro-degenerative pathologies (Tansey *et al.*, 2008; Gao and Hong, 2008). Aging leads to microglial senescence and the loss of beneficial microglial effects on neurons (Streit and Xue, 2009). Moreover, aged microglia release increased amounts of pro-inflammatory cytokines and lower levels of the anti-inflammatory cytokine IL-10 (Ye and Johnson, 2001; Xie *et al.*, 2003; Sierra *et al.*, 2007). Furthermore, activated microglia and increased levels of cytokines are found in the brains of patients suffering from neuro-degenerative diseases, and IL-1 is known to actively contribute to Alzheimer's and Parkinson's pathologies (Schulte *et al.*, 2002; Griffin, 2006).

Presently, microglial cell lines or primary microglia isolated from embryonic (Gingras *et al.*, 2007) or neo-natal animals (Giulian and Baker, 1986; Floden and Combs, 2007) are widely used as *in vitro* microglial models. However, microglial cell lines are not a perfect model (Horvath *et al.*, 2008) and embryonic or neo-natal primary microglia are not completely mature (Draheim *et al.*, 1999) and behave differently to adult microglia (Sierra *et al.*, 2007). In consequence, these *in vitro* microglial models might not be suitable models for research in the field of neuro-degenerative diseases where aging is crucial.

The culture of microglia prepared from adult animals is challenging and actually the only alternative to the direct *in vivo* study of aged microglia is the *ex vivo* approach first described by Sedgwick *et al.* (1991). This *ex vivo* isolation of microglia from adult brains is based on separation steps using a discontinuous gradient density centrifugation. This isolation methodology has been improved and optimized with the addition of fluorescence activated or immuno-magnetic cell sorting steps (Ford *et al.*, 1995; Guillemin *et al.*, 1997; De Groot *et al.*, 2000; Frank *et al.*, 2006; Cardona *et al.*, 2006; De Haas *et al.*, 2007). Recently, Yip *et al.* (2009) described a simpler method based on the high adherence of microglia which allows the isolation of *ex vivo* adult primary microglia without gradient density centrifugation step. However, these different methods are limited to the direct use of the collected cells, for example for RNA or protein extraction (Cardona *et al.*, 2006) or for steady state observation by flow cytometry (Ford *et al.*, 1995). Indeed, although the aforementioned methods are efficient and rapid, they are impractical for long term culture experiments because *ex vivo* microglia are difficult to keep in culture due to extensive cell death.

With the ultimate goal to culture aged microglia, we developed and optimized procedures into a new approach which opens the possibility of the isolation and culture of an essentially pure population of microglia from adult mouse brains.

The resulting primary microglia isolated from adult mice are able to proliferate and can therefore be kept in culture for a long period of time. These cells show the morphological, molecular and electrophysiological characteristics of microglia. They have typical microglial potassium (K^+) currents and channels. They are positive for microglial markers, such as CD11b, F4/80 and *Griffonia simplicifolia* isolectin B_4 (IB_4). They are also capable of phagocytosis and can produce NO and cytokines, such as TNF-α, IL-1β, IL-10 and IL-12 in response to pro-inflammatory stimuli. But in comparison to primary cultured microglia of neo-natal mice or to C8-B4 microglial cell line, adult microglia appear to be more reactive.

3.5. Materials and Methods

Primary microglia from adult mice

8-month-old female C57BL/6J@Rj mice (Charles River Laboratories, Sulzfeld, Germany) were deeply anesthetized and perfused in the left ventricle with ice-cold Ringer solution (B. Braun, Melsungen, Germany) supplemented with 2units/ml heparin (Sigma, Munich, Germany) at an approximate hydrostatic pressure of 1 meter of water to wash out all contaminating blood cells from the brain. After 5min perfusion the brain was aseptically removed and carefully freed from the meninges. Brains not appearing appropriately exsanguinated were discarded. Then, the brain of one animal was transferred to a small Petri dish containing 5ml of enzymatic solution and finely minced with a scalpel. The enzymatic solution (Huettner and Baughman, 1986) contained 116mM NaCl, 5.4mM KCl, 26mM $NaHCO_3$, 1mM NaH_2PO_4, 1.5mM $CaCl_2$, 1mM $MgSO_4$, 0.5mM EDTA, 25mM glucose, 1mM cysteine and 20units/ml papain (all from Sigma). Next, the tissue was incubated at 37°C, 5% CO_2 and continuously stirred. After a 90min incubation the digested CNS was transferred to a 50ml-conical tube and the enzymatic reaction was quenched by the addition of 20ml of 20% heat-inactivated foetal bovine serum (FBS) in Hank's balanced salt solution (HBSS) (Invitrogen, Karlsruhe, Germany). After centrifugation at 200g for 7min at room temperature, the pellet was resuspended in 2ml of 0.5mg/ml DNase I (Roche, Mannheim, Germany) in HBSS and incubated for 5min at room temperature. Then, the tissues were gently disrupted with fire-polished Pasteur pipettes of decreasing diameters. Finally, the homogenate was filtered through a 70µm-cell strainer (Becton Dickinson, Heidelberg, Germany) into a new 50ml-conical tube. After rinsing the filter with HBSS, the resulting cell suspension was centrifuged again at 200g for 7min at room temperature. Then, a discontinuous gradient density centrifugation step using Percoll (GE healthcare, Freiburg, Germany) was performed; the cells were resuspended in 20ml of 20% stock isotonic Percoll (SIP = v/v ratio: 9/10 Percoll + 1/10 HBSS 10X) in HBSS. The cell suspension was carefully overlaid with 20ml pure HBSS and centrifuged at 200g for 20min with slow acceleration and no brake. Next, the material at the interphase – which contained myelin and cell debris – was discarded, whereas the pellet – which contained mixed glial cells – was washed once in HBSS before being resuspended in Dulbecco's modified Eagle's/F12 medium with GlutaMAX™I (DMEM/F12) supplemented with 10% FBS, 100units/ml penicillin, 100µg/ml streptomycin (all from Invitrogen) and 5ng/ml of carrier-free murine recombinant granulocyte and macrophage colony stimulating factor (GM-CSF) (415-ML/CF, R&D systems, Wiesbaden-Nordenstadt, Germany). The cell suspension from one mouse brain was plated in a T75-cell culture flask (Becton Dickinson) coated with poly-L-lysine (Sigma) and maintained in culture at 37°C in a 95% air/ 5% CO_2 humidified incubator. The medium was changed twice a week until the cells became confluent (after approximately 2 weeks).

When full confluence of the cell layer was reached, microglia detached from the bottom of the flask and migrated to the medium-air interphase where they were able to float and proliferate. To isolate a nearly pure microglial cell population, the supernatant of the flask of mixed glia was collected without any prior shaking and subsequently centrifuged at 200g for 7 min. The resulting pellet could be replated and kept in culture for several weeks or frozen and stored. Before the start of experiments, microglia were cultured for at least 3 days in medium without GM-CSF. For

electrophysiological and immunofluorescence experiments cells with an *in vitro* age between 15 and 32 days *in vitro* (DIV) were seeded on glass cover-slips in 24-well plates ($3x10^4$cells/well).

Primary microglia from neo-natal mice

Primary microglia were isolated from 4-day-old C57BL/6J@Rj mice as described by Draheim *et al.* (1999) with some modifications. In brief, whole brains of neo-natal mice were taken, and blood vessel and meninges were carefully removed. Then, the whole brains of 5 mice were pooled together. From this point, the same protocols as for adult mice were followed for the mechanical and enzymatic digestion as well as for the cell culture.

After obtaining a confluent cell layer, neo-natal primary microglia were harvested by vigorous shaking of the flask.

Microglial cell line

The murine microglial cell line C8-B4 (ATCC, CRL-2540, Manassas, USA) (Alliot *et al.*, 1996) was maintained in DMEM/F12 medium supplemented with 10% FBS, 100units/ml penicillin and 100µg/ml streptomycin (all from Invitrogen) at 37°C in a 95% air/ 5% CO_2 humidified incubator. Cells were split once a week and tested frequently for mycoplasma contamination.

Flow cytometry

The purity and the immuno-phenotype of the microglial cell preparations were assessed by flow cytofluorometry. Cells were harvested and resuspended in 1% bovine serum albumin (BSA) + 2.5% goat serum in phosphate-buffered saline (PBS). For intracellular markers, cells were previously fixed and permeabilized following supplier's instructions (Leucoperm, AbDserotec, Düsseldorf, Germany). After a washing step cells were incubated for 20min with anti-CD16/CD32 monoclonal antibodies (MCA2305EL, AbDserotec) to saturate Fc receptors. Then, cells were stained for 1 hour with fluorescence-labelled primary antibodies and/or with Alexa 488, or Alexa 647-conjugated *Griffonia simplicifolia* isolectin B_4 (IB_4) at 5µg/ml (Invitrogen). We used Alexa 488, FITC or Alexa 647-conjugated primary antibodies against: CD4, CD11b, CD11c, CD34, CD45, CD68, CD80, CD86, MOMA, F4/80, Gr-1, epidermal growth factor receptor (EGF-R) (for references, see Table 1), galactocerebroside (GalC) (4600-0004, AbDserotec), ER-TR7 (MCA2402, AbDserotec), Ki-67 (sc-7846, Santa Cruz, Heidelberg, Germany), glial fibrillary acidic protein (GFAP) (A-21294, Invitrogen), neuron nuclei (NeuN) (MAB377, Millipore, Schwalbach, Germany). For some experiments cells were simultaneously stained against two different markers with two different labels. As negative controls, the same staining procedure was repeated in parallel with the corresponding isotype control antibodies (AbDserotec). The samples were analysed on a flow cytofluorometer (LSRII, Becton Dickinson) and data analysis was performed using FlowJo software (Tree Star Inc., Ashland, USA).

Immuno-fluorescence and phagocytosis measurement

Microglia were incubated for 24 hours in pure medium or medium supplemented with 1µg/ml lipopolysaccharide (LPS) from *E. coli* strain K235 (Sigma). For phagocytosis measurement, 4µl per ml medium of red fluorescence-labelled latex beads of 2µm diameter (L3030, Sigma) were added to cells for 60min at 37°C prior to fixation. After a washing step with PBS, cells were fixed for 20min using a 2% formaldehyde solution in PBS. After washing, cells were permeabilized and non-specific binding sites were blocked using a solution containing 0.05% saponin, 1% BSA and 5% goat serum in PBS. Then, fluorescence-labelled primary antibodies and/or fluorescence-labelled IB_4 were

incubated overnight at 4°C. For immuno-fluorescence experiments, the following Alexa 488, FITC or Alexa 647-conjugated primary antibodies were used: anti-CD11b, anti-GalC, anti-F4/80, anti-CD68 and anti-MOMA (for references, see section *Flow cytometry*). After a final washing step with PBS, the cover-slips were mounted on microscope slides. Cells were visualised using a DM IRBE inverted confocal microscope (Leica, Wetzlar, Germany) and z-stacking was performed to localise the fluorescent beads (see supplementary material 2). Control stainings were also performed with isotype antibodies and did not reveal non-specific staining.

NO and cytokine production

C8-B4 cells, neo-natal primary microglia, or adult primary microglia (DIV 26), were seeded in 24-well plates (600µl medium per well) at a concentration of 10^5 cells per well and incubated for 24 hours in DMEM/F12 medium without phenol red supplemented with 10% FBS, 100units/ml penicillin and 100µg/ml streptomycin (all from Invitrogen) and with the following substances: 1µg/ml LPS, 100ng/ml murine recombinant interferon gamma (IFN-γ), LPS and IFN-γ together, or 5ng/ml GM-CSF. Both cytokines were purchased from R&D systems and were guaranteed to be endotoxin-free. After 24 hours incubation with the substances, culture media were collected and tested. NO production was quantified by measuring nitrite levels using a Griess assay (G4410, Sigma). Cytokine secretion was quantified by using a multiplex electrochemiluminescence immuno-assay (MS6000 Mouse TH1/TH2- 9 Tissue Culture Kit K11013B-1, Meso Scale Discovery, Gaithersburg, USA). For these experiments, each condition was repeated in separate quadruplicates (NO production) or triplicates (cytokine secretion) and each probe was measured in independent quadruplicates (NO production) or duplicates (cytokine secretion). The values are given as mean ± S.E.M. and normalised to cell number.

Electrophysiology

Whole-cell membrane currents were measured according to Hamill *et al.* (1981) and as described by Moussaud *et al.* (2009). Briefly, data acquisition was carried out with an EPC-9 patch clamp amplifier and TIDA software (HEKA, Lambrecht/Pfalz, Germany). Patch electrodes of 3-8MΩ were made with a micropipette puller (P97, Sutter, Novato, USA) from borosilicate glass capillaries (1B150-F3, WPI, Sarasota, USA) and fire-polished with a pipette forge (List-medical, Darmstadt/Eberstadt, Germany). Electrodes were filled with the following solution: 140mM KCl, 20mM NaCl, 2mM $MgCl_2$, 2.5mM $CaCl_2$, 10mM HEPES and 5mM EGTA. The extracellular solution contained 5.5mM KCl, 140mM NaCl, 1mM $MgCl_2$, 1.8mM $CaCl_2$, 10mM HEPES and 35mM glucose. 16 hours before measurement, the medium was changed and cells received fresh medium alone (negative control) or supplemented with the following substances: 5ng/ml or 100ng/ml GM-CSF, or 1µg/ml LPS, or 100ng/ml IFN-γ, or LPS and IFN-γ together. For pharmacological characterisations margatoxin and barium chloride (both from Sigma) were diluted in bath solution and applied directly to the cells by superfusion in the measuring chamber during the measurement.

Statistics and data analysis

Data analysis and statistics were performed with GraphPad Prism 5.0 software (San Diego, USA). The statistical significance of differences between experimental groups was calculated by one-way analysis of variance test followed by Dunnett's post test. Differences were considered to be statistically significant with *P< 0.05, **P< 0.01 and ***P< 0.001. Results are given as mean ± S.E.M. unless otherwise stated.

Table 1: Immuno-phenotype characterisation by flow cytometry

Specificity	Marker	Other names	Supplier	Ref.	Adult primary microglia	Neo-natal primary microglia	C8-B4 microglial cell line
Immune and myeloid cells	**IB_4**	*Griffonia simplicifolia* isolectin B_4	Invitrogen	I21411/I32450	**46 735**	**25 648**	**7 854**
	CD4	T4	BD	553651	**(24)**	**(24)**	**(25)**
	CD11b	Mac1, CR3, OX42	AbDserotec	MCA711F	**231**	**279**	**650**
	CD16/32	Fc receptor γ II and III	AbDserotec	MCA2305EL	**111**	**162**	**180**
	CD45	LCA	AbDserotec	MCA1031A647	**325**	**267**	**671**
	CD68	KiM7, ED1, macrosialin	AbDserotec	MCA1957A647T	**11 152**	**2 092**	**3 494/19 183**
	F4/80		AbDserotec	MCA497A647	**819**	**596**	**1885**
	MOMA	monocyte/macrophage marker	AbDserotec	MCA519F	**1507**	**810**	**2471**
Dendritic and antigen presenting cells	**CD11c**	CR4	AbDserotec	MCA1369A488T	**(18)**	**(14)**	**(37)**
	CD80	B7-1	AbDserotec	MCA2462A647T	**66**	**38**	**134**
	CD86	B7-2	AbDserotec	MCA2463A488T	**(30)**	**(17)**	**943**
Precursor and stem cell marker	**Gr-1**	Ly-6G	AbDserotec	MCA2387A647T	**(21)**	**(13)**	**(26)**
	CD34		AbDserotec	MCA1825A647T	**(33)**	**(20)**	**(43)**
	EGF-R	Epidermial growth factor receptor	AbDserotec	MCA1784F	**(24)**	**(23)**	**(24)**

Values are presented as mean fluorescent intensity (MFI) of each marker. Values in brackets were considered as negative (MFI of marker ≈ MFI of isotype control). Values without brackets were considered as positive (MFI of marker > MFI of isotype control).

3.6. Results

Principle of the isolation of primary microglia from adult mice

Figure 1 represents a flow chart of the procedure used to isolate primary microglia from adult mice. Under deep narcosis mice were perfused in order to wash out all contaminating blood cells from the brain (Fig. 1, step 1-2). Next, to convert the brain to a cell suspension, the tissue was finely minced and incubated in a papain solution and subsequently in a DNAse I solution. Then, using Pasteur pipettes and a cell strainer, the tissue was gently mechanically disrupted (Fig. 1, step 3). Next, to remove debris and dead cells, a discontinuous gradient density centrifugation step was performed. After centrifugation living glial cells were pelleted and finally plated on a poly-L-lysine coated cell culture flask (Fig. 1, step 4 and 5).

The poly-L-lysine coated flask allowed for a rapid attachment of glial cells. After 4 days *in vitro*, the medium was changed to remove the remaining debris and cells started to recover and grow. After approximately 2 weeks, the mixed glial culture formed a tight feeder-layer of a not fully known composition (Fig. 1, step 6, A). The feeder-layer presence is a key point for survival and proliferation of microglia. Once full confluency was reached, microglia detached from the bottom of the flask and migrated to the medium-air interphase (Fig. 1, step 6, B). From this point, to isolate an almost pure microglia cell population, it sufficed to collect and centrifuge the supernatant of the mixed glial culture flask. After centrifugation primary microglia of adult mice could be replated on a new dish. They immediately lost their floating properties and, after attaching to the bottom of the dish, adopted a classical ramified microglial morphology (Fig. 1, step 7, C). Interestingly, 46% of the freshly isolated adult primary microglia were positive for the proliferation marker Ki-67 (data not shown).

Furthermore, after separation from the feeder-layer, microglia continued to proliferate slowly and survived for extended periods of time, raising the possibility of sustained microglial cultures. Moreover, it is possible to freeze the freshly isolated adult primary microglia and store them for later use.

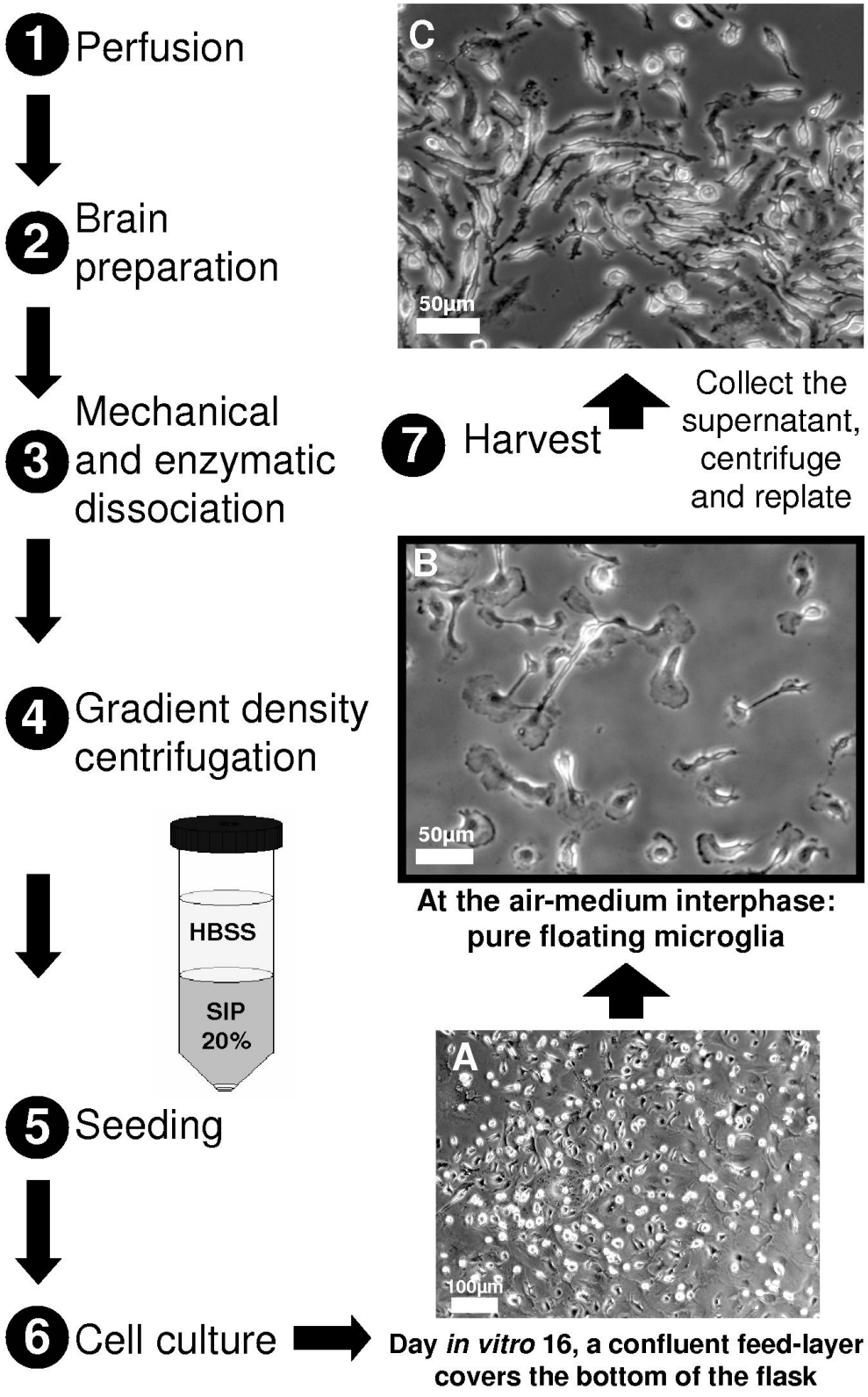

Figure 1: The different protocol steps to isolate microglia from an adult mouse are outlined and illustrated in this schematic procedure workflow.

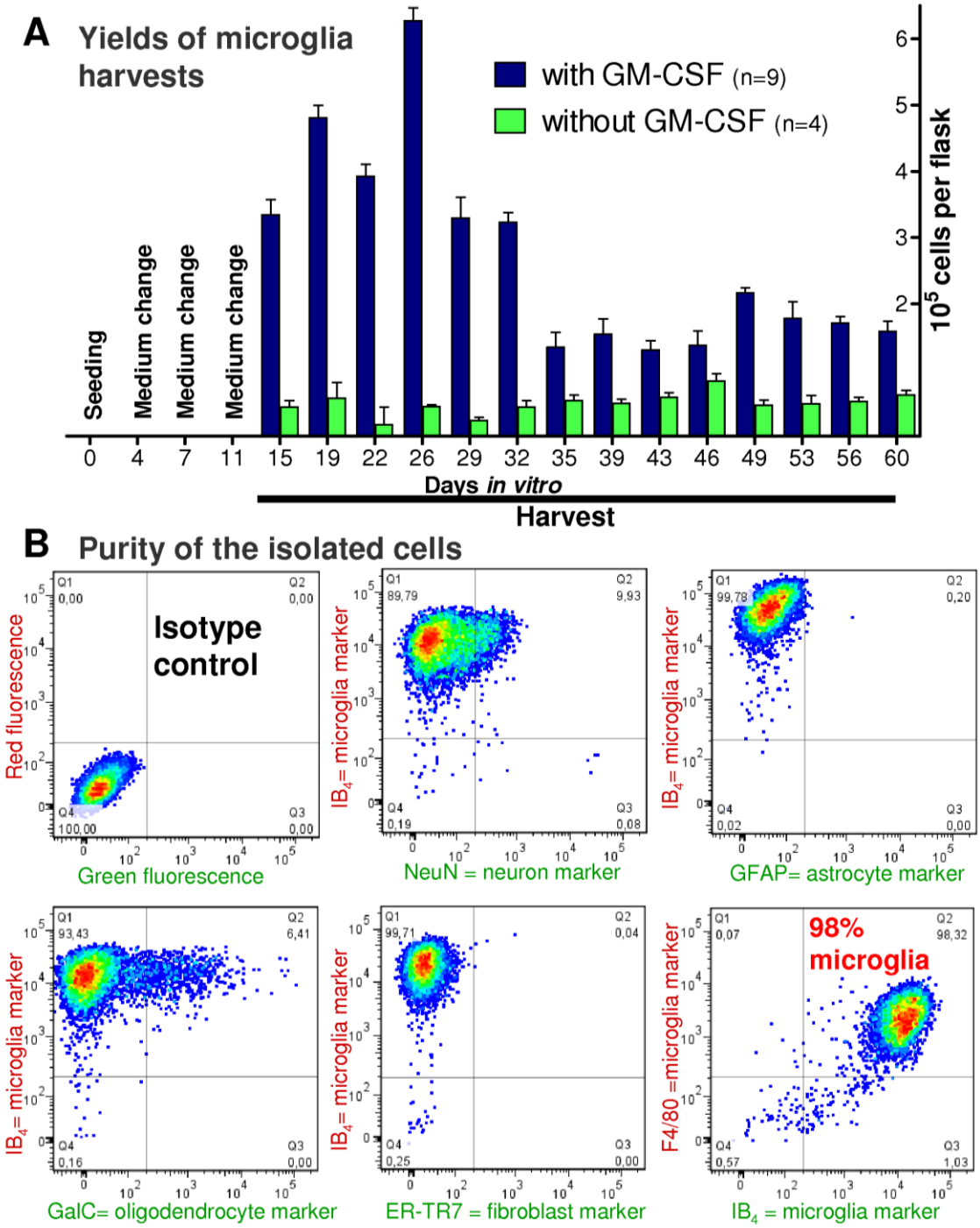

Figure 2: Quantity and purity of the collected cells. Graph ***A)*** summarizes the harvest yields at different time points of mixed glial culture flasks without (green) and with 5ng/ml GM-CSF (blue). Values are given as mean ± S.E.M.; n=9 for with GM-CSF and n=4 for without GM-CSF. ***B)*** Flow cytometry purity 2D plots. To quantify the purity of the isolated cells fluorescence activated cell sorting was performed. Cells were stained with IB_4 and with anti-F4/80, anti-GFAP, anti-NeuN, anti-ER-TR7 or anti-GalC antibodies as microglia, astrocyte, neuron, fibroblast and oligodendrocyte markers, respectively. More than 98% were double positive for the both microglial markers F4/80 and IB_4.

Yield and purity of the adult primary microglia

Similar to the neo-natal primary microglia isolation method (Giulian and Baker, 1986; Floden and Combs, 2007), each mixed glial culture flask could be harvested twice a week for more than one month (Fig. 2 A). Following the addition of 5ng/ml of the growth factor GM-CSF, the yield was drastically improved. Without GM-CSF, the yields were between 17 500 and about 83 500 cells per flask per harvest (Fig. 2 A, n=4) with a mean value of 49 000 cells. In contrast, with GM-CSF, the yields varied from about 130 000 to 627 400 cells (Fig. 2 A, n=9) with a mean value of 269 000 cells per flask per harvest. It is noteworthy that with GM-CSF the yield curve first rapidly increased until it reached its maximum at around day *in vitro* 26 and then decreased before it stabilized to a plateau. Therefore, although it is possible to harvest microglia for much longer, in this study the culture flasks were only harvested until an *in vitro* age threshold of 32 days.

To evaluate the purity of the harvested cells, flow cytometry analysis was performed after cell type specific immuno-staining (Fig. 2 B). The collected cells were stained with anti-NeuN, anti-GFAP, anti-GalC, anti-ER-TR7 and anti-F4/80 antibodies to detect neurons, astrocytes, oligodendrocytes, fibroblasts and microglia, respectively. In addition, cells were incubated with *Griffonia simplicifolia* isolectin B_4 (IB_4) which binds to immune cells. As shown on the 2 dimension plots (Fig. 2 B), more than 98 % of the cells were double positive for the microglial markers IB_4 and F4/80. Despite that the vast majority of cells were negative for NeuN, GFAP, ER-TR7 and GalC immuno-reactivity, a few positive events for the oligodendrocyte marker GalC were also observed. However, these positive events were also positive for the microglial marker IB_4. Immuno-fluorescence staining (Fig. 3 D) confirmed that the few GalC positive cells were not contaminating oligodendrocytes but microglia which had phagocytosed oligodendrocytes debris.

Immuno-phenotype of the adult primary microglia

To gain further insight into the properties of adult primary microglia, their marker expression was characterised by flow cytometry and directly compared to those of other *in vitro* microglial models, namely the murine cell line C8-B4 and primary microglia isolated from neo-natal mice.

Antibodies against classical immune/myeloid cell markers (CD4, CD11b, CD16/32, CD45, CD68, MOMA, F4/80, IB_4), activated antigen presenting cell and dendritic cell markers (CD11c, CD80, CD86), or stem/progenitor cell markers (EGF-R, Gr-1, CD 34) were used. The results of this marker screening are summarised in table 1 (for raw data, see supplementary material 1).

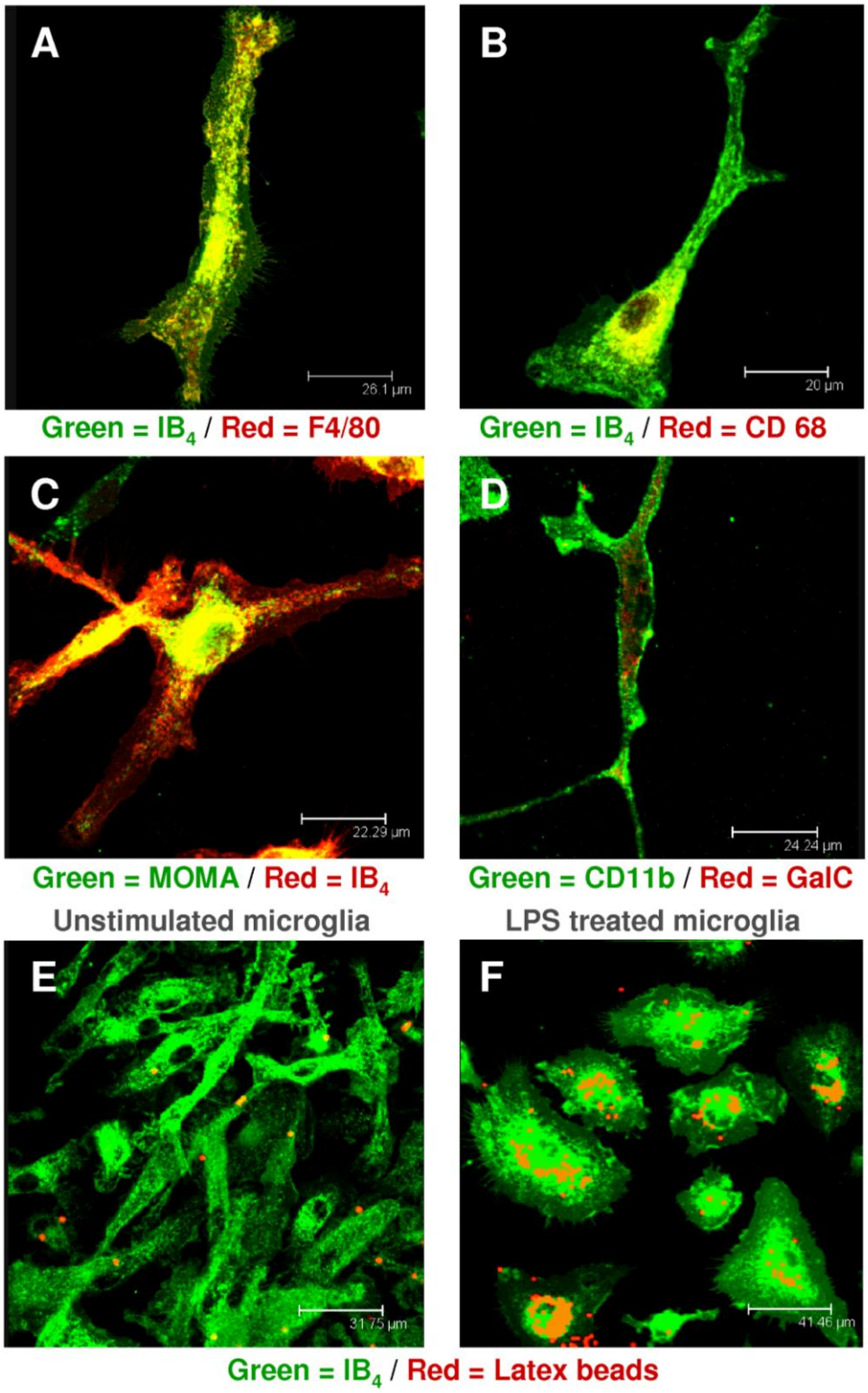

Figure 3: Immuno-fluorescence pictures of adult primary microglia ***(A-F)*** performed with a confocal microscope. The adult microglia were stained in green with anti-MOMA ***(C)*** and anti-CD11b ***(D)*** antibodies and with IB_4 ***(A, B, E and F)*** and in red with anti-F4/80 ***(A)***, anti-CD68 ***(D)*** and anti-GalC ***(D)*** antibodies and with IB_4 ***(C)***. To visualise phagocytosis in response to LPS pre-treatment, cells were incubated one hour with fluorescent latex beads prior to fixation ***(E and F)***.

The adult primary microglia expressed virtually the same markers as neo-natal primary microglia (Table 1). They were both positive (mean fluorescent intensity (MFI) value > 100) for IB_4, CD11b, CD16/32, CD45, CD68, MOMA, F4/80; negative (MFI value identical to isotype control) for CD4, CD11c, CD86, EGF-R, Gr-1 and CD34; and slightly positive for CD80 (MFI value of isotype control < MFI value of CD80 < 100). For some markers minor intensity variations between the neo-natal and the adult primary microglia were noted. However, these differences were not significant except for CD68; adult microglia expressed this marker at higher levels (MFI = 11152) compared to the neo-natal primary microglia (MFI = 2092). Surprisingly, in the C8-B4 cell line two distinct populations could be distinguished on the basis of their CD68 expression (MFI = 3492 and 19183), whereas in both newborn and adult primary microglia only one homogeneous population was observed (supplementary material 1).

Contrary to the C8-B4 cells, adult microglia were found to be negative for the CD86 marker. Furthermore, they were negative for CD11c and showed only low intensity for CD80 (Table 1). All these results indicate that adult microglia are not differentiated in an activated antigen presenting phenotype.

In order to clarify whether precursor or dedifferentiated cells were present in the preparation, antibodies against the precursor and stem cell markers CD34, Gr-1 and EGF-R were used. The adult microglia were negative for all markers tested. Taken together, these data demonstrate that the adult microglia display markers of mature myeloid cells (Table 1).

Immuno-fluorescence and phagocytosis

Immuno-fluorescence experiments (Fig. 3) confirmed the expression pattern of adult primary microglia witnessed to flow cytometry data (Table 1) and brought additional information about the localisation of the markers. Cells showed a clear intracellular staining for MOMA and CD68 antigens and a plasma membrane staining for IB_4, CD11b and F4/80 antigens (Fig. 3). A few CD11b positive cells also displayed a weak intracellular GalC staining indicating that some microglia had phagocytosed oligodendrocyte cell debris (Fig. 3 D).

After LPS treatment adult microglia undergo morphological transformations. The cells adopted a flat and round form instead of being elongated with arborescent long processes (Fig. 3). Furthermore, when fluorescence-labelled latex beads were added, the cells were able to phagocytose them and phagocytosis was greatly increased after LPS stimulation (Fig. 3 E and F and supplementary material 2).

Comparison of cytokine and NO production

To compare the functional activity of adult primary microglia to neo-natal microglia as well as to the C8-B4 cell line, NO production and cytokine secretion were measured under different conditions. To trigger pro-inflammatory responses, the potent immune reaction elicitor LPS from *E.coli*

K235 and the lymphokine IFN-γ were used separately and in combination. As negative control, cells were incubated with medium alone. Moreover, as a second control to investigate the potential effect of GM-CSF on microglial activation, cells were incubated in medium with 5ng/ml GM-CSF. After a 24-hour incubation, the supernatants were collected and the cytokine secretion and NO production were quantified with a multiplex electrochemiluminescence immuno-assay and a Griess assay, respectively (Fig. 4).

As seen in neo-natal microglia, adult microglia were able to secrete NO, TNF-α, KC, IL-1β, IL-10 and IL-12 after stimulation with LPS and/or IFN-γ. In contrast, medium alone or with 5ng/ml GM-CSF did not trigger the production of detectable amounts of NO or cytokines, indicating that the adult microglia are not pro-inflammatorily pre-activated by the *in vitro* culture conditions.

It is noteworthy that like it was described by Kawanokuchi *et al.* (2006) we were not able to detect microglial IFN-γ secretion in any tested cell preparation (data not shown).

Interestingly, in all *in vitro* models investigated, prominent NO production was only registered after simultaneous stimulation with LPS and IFN-γ. But when IFN-γ or LPS were given separately, only a negligible NO production was detected (Fig. 4). These results are in line with the idea that iNOS induction is fully attained only when NF-κB and STAT-1 cell signalling pathways are simultaneously activated (Mir *et al.*, 2008).

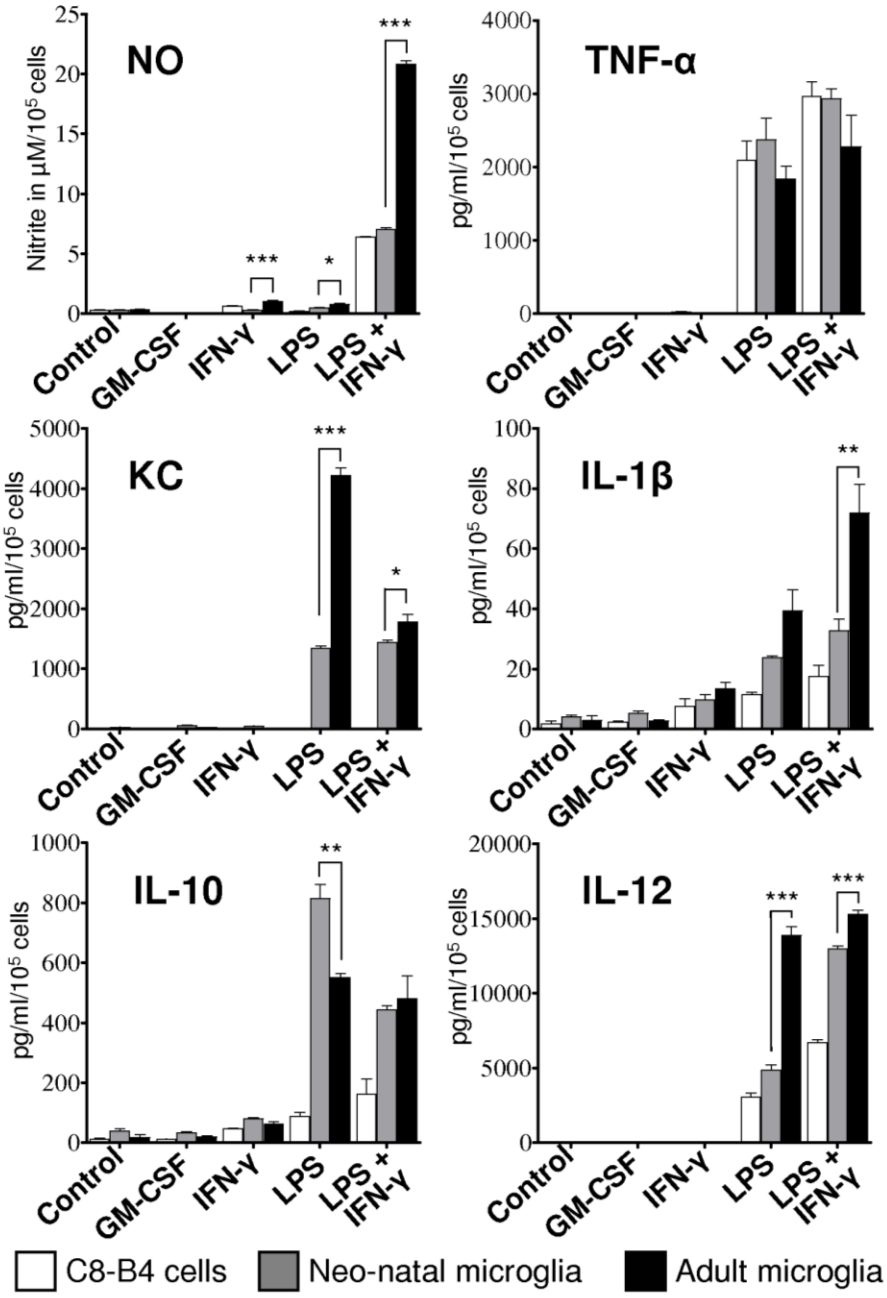

Figure 4: Functional characterisation of the adult microglia in comparison with other microglial models. The NO production and cytokine secretion of C8-B4 cell line (white bars) as well as primary microglia of neo-natal (grey bars) and adult (black bars) mice were quantified after a 24-hr. incubation with fresh medium alone (control) or with GM-CSF, IFN-γ, LPS or with LPS and IFN-γ together. NO production and cytokine levels in the supernatant were quantified using a Griess assay and a multiplex immuno-array, respectively. Values are normalised to cell number and given as mean ± S.E.M.; n=4 for NO and n=3 for cytokine measurements; *P< 0.05, **P< 0.01 and ***P< 0.001.

Interesting differences appeared after comparison of the NO, cytokine and chemokine production in the different microglial models. With regard to the NO production, adult microglia had a more than 2 fold higher production compared to the other microglial models. Concerning the cytokine and chemokine secretion, primary microglia, in contrast to C8-B4 cells, were able to produce KC (a homolog of human Gro-α/CXCL1) and significant higher amounts of IL-1β, IL-10 and IL-12 in response to LPS. TNF-α appeared to be the only cytokine for which all three *in vitro* models had a similar quantitative and qualitative profile. These observations point to important differences in the response to pro-inflammatory activating stimuli at least

between primary microglia and the C8-B4 cell line (Fig. 4).

A direct comparison between adult and neo-natal microglia unveiled other interesting differences. After pro-inflammatory stimulation adult microglia produced higher amounts of IL-1β, IL-12 and KC compared to neo-natal microglia but similar or lower amounts of TNF-α and IL-10. Even if these differences were not significant in all cases, they are consistent with the idea that adult microglia produce more pro-inflammatory cytokines and less anti-inflammatory cytokines in response to pro-inflammatory stimuli (Fig. 4).

Electrophysiological characterisation

Microglia are known to express specific voltage-dependent potassium currents which differ depending on their activation state (Kettenmann *et al.*, 1993; Eder, 2005). To examine whether the microglia isolated from adult mice functionally express these voltage-dependent K^+ currents, the whole cell patch clamp technique was applied (Fig. 5). After a 16-hour incubation with fresh pure medium or supplemented with 5ng/ml or 100ng/ml GM-CSF, 100ng/ml IFN-γ, 1µg/ml LPS, or LPS and IFN-γ together, cells were patched in whole-cell configuration and held at a holding potential of -60mV. The K^+ current density was recorded at voltage steps from -150mV to +30mV in 10mV increments (Fig. 5).

As seen in neo-natal microglia or C8-B4 cells, two prominent K^+ currents were observed in the adult primary microglia (Fig. 5).

Between a holding potential of -150mV and -80mV, a prominent inward K^+ current was measured in adult primary microglia. This current was more prominent in unstimulated cells (Fig. 5 C and D) than in LPS treated microglia (Fig. 5 A, B and F) and was highly barium chloride sensitive (Fig. 5 D). This inwardly rectifying K^+ current seen in adult primary microglia had identical properties to the one seen in primary neo-natal microglia and C8-B4 cells (Eder, 2005; Moussaud *et al.*, 2009) suggesting Kir2.1 potassium channels being responsible for the K^+ current.

Between -80mV and +30mV, the unstimulated adult microglia showed no detectable current (Fig. 5 C and D). In contrast, cells treated with LPS, IFN-γ, or high doses of GM-CSF, had a prominent outward K^+ current from -30mV to +30mV (Fig. 5 A, B and E). This inducible outward K^+ current was identical to the one observed in neo-natal microglia and C8-B4 cells (Moussaud *et al.*, 2009). It displayed cumulative inactivation (data not shown) and was sensitive to picomolar concentrations of margatoxin (Fig. 5 B). These observations strongly suggest that the Kv1.3 homomere channel is the voltage-gated channel underlying the outward K^+ current. Taken together, these electrophysiological data on adult murine microglia are consistent with the previously published data on neo-natal murine microglia (Moussaud *et al.*, 2009).

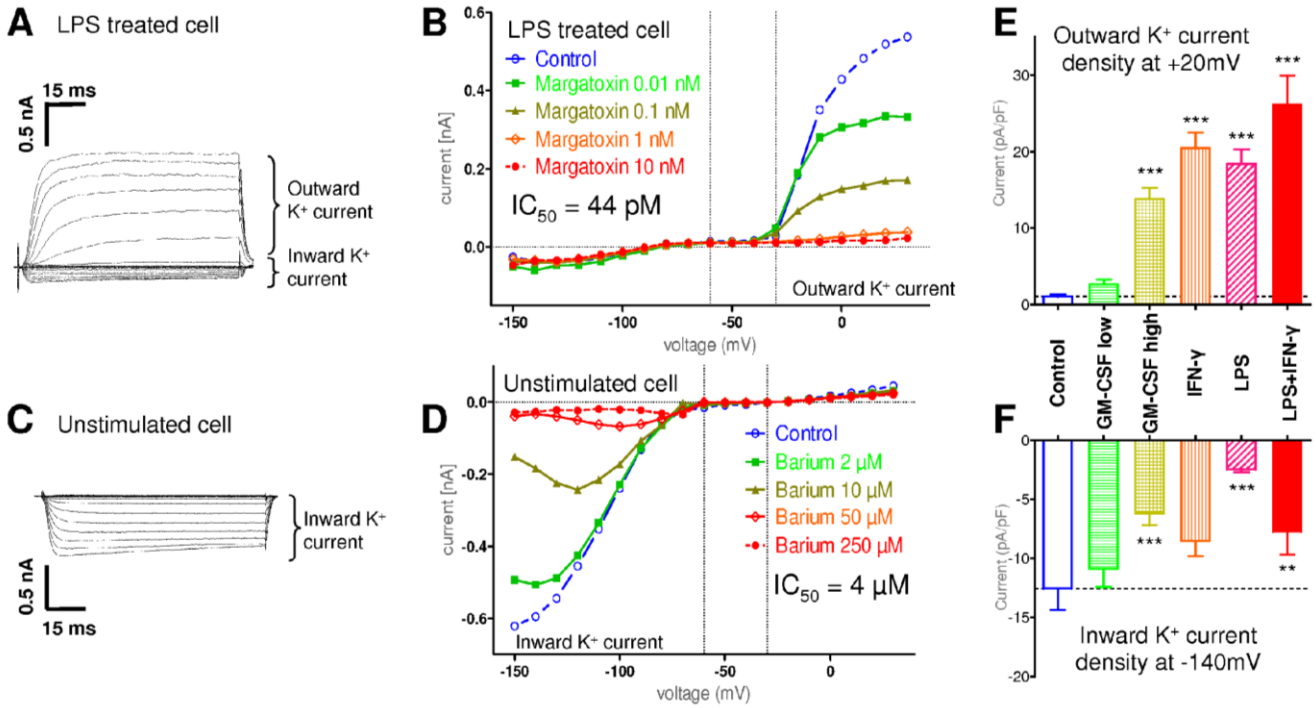

Figure 5: Electrophysiological and pharmacological characterisation of voltage-dependent K+ currents in adult microglia. Cells were patched in the whole-cell configuration. Voltage-dependent currents were elicited with 50ms voltage steps from -150mV to +30mV in 10mV increments. Representative recordings of K+ currents from single adult primary microglia cells unstimulated ***(C)*** and LPS treated ***(A)***. Current voltage relationship curves of K+ currents in adult primary microglia unstimulated ***(D)*** and LPS treated ***(B)***. Two different K+ currents, an inward current from -80 to -150mV and an outward current from -30 to +30mV, were registered. The outward K+ current was not present in unstimulated cells but was induced after treatment with microglial activators ***(E)***. The inward K+ current was also modulated after treatment (F) and was blocked at low barium concentrations ***(D)***. On the other hand, the outward K+ current was sensitive to margatoxin ***(B)***. For E and F values are given as mean ± S.E.M.; n=16; *P< 0.05, **P< 0.01 and ***P< 0.001.

3.7. Discussion

In this study we provide a simple and effective method for isolating essentially pure primary microglia from adult murine brains enabling us to culture them for extended time periods. To the authors' knowledge this is a novel technique, as all previous methods (Sedgwick *et al.*, 1991; Ford *et al.*, 1995; Guillemin *et al.*, 1997; De Groot *et al.*, 2000; Frank *et al.*, 2006; Cardona *et al.*, 2006; De Haas *et al.*, 2007), although being more rapid, are restricted to an acute *ex vivo* isolation of adult microglia for immediate use and not for long-term *in vitro* experiments.

The first step of our method consists in producing and culturing a mixed glial cell population devoid of dead cells and myelin debris. Indeed, the absence of cellular and myelin debris and the presence of other glial cell types are crucial for this preparation. The feeder-layer appears to promote microglial survival after the stressful isolation procedure, and helps to sustain the *in vitro* microglial proliferation through trophic support (Alliot *et al.*, 1991).

Once the glial cells have reached confluency, microglia are isolated from the mixed glial culture in a similar way to the neo-natal primary microglia isolation method (Giulian and Baker, 1986; Floden and Combs, 2007). However, in the herein described method there is no need to shake the culture flask because microglia detach by themselves from the bottom of the flask and migrate to the air-medium interphase where they float and proliferate (Fig. 1 B). Thus, an essentially pure primary microglial cell population can be easily isolated by collecting the cell supernatant (Fig. 2). Then, cells can be either kept in culture for extended time periods and used for functional assays, or they can be frozen and stored for later use.

Neo-natal primary microglia isolated with the classical Giulian and Baker (1986) method have a limited life span in culture (Kaneko *et al.*, 2009). In contrast, adult primary microglia slowly proliferate and survive for a long period of time. For example, cell survival has been observed for over 2 years in culture for one of the adult microglia preparations. This surprisingly long life span and the self-renewal capability of these cells is not yet fully explainable. Although it is tempting to speculate about a hidden stem-cell like population within the adult microglia preparations, all cells were negative for all tested stem-cell markers and displayed mature myeloid-cell markers (Table1). However, the prolonged life span of adult microglia appears to be linked to their microglial nature as well as to their age and to the presence of FBS and the growth factor GM-CSF. Consistent with these speculations, microglia were previously described to constitute a stable pool of cells which have the ability of self-renewal *in vivo* as well as *in vitro* (Alliot *et al.*, 1991; Ajami *et al.*, 2007). Furthermore, Rozovsky *et al.* (1998) described a 4-fold enhancement of *in vitro* microglial

proliferation with age. Additionally, GM-CSF has often been described to support the survival and proliferation of myeloid cells (Lee *et al.*, 1994; Kloss *et al.*, 1997; Chitta *et al.*, 2008). Interestingly, Guillemin *et al.* (1997) and others observed that microglia differ from macrophages in their proliferation upon GM-CSF treatment. In terms of the involvement of the feeder-layer, it is also well known that astrocytes are able to produce GM-CSF (Malipiero *et al.*, 1990; Lee *et al.*, 1994). In the herein described method, GM-CSF addition to the medium was not crucial but very useful because it drastically increased the yield of the preparation and it helped sustain the survival and proliferation of microglia *in vitro* (Fig. 2 A). However, GM-CSF in combination with IL-4 was also previously shown to induce monocyte differentiation into dendritic cells (Chitta *et al.*, 2008). Similarly, treatment with GM-CSF has been shown to play a role in the differentiation of microglia into CD11c positive cells (Fischer and Reichmann, 2001). Nonetheless, Esen and Kielian (2007) demonstrated that the dose of GM-CSF was crucial to induce these effects. These findings correlate with our observation that GM-CSF at low concentrations had neither effects on differentiation into a dendritic cell phenotype (Table 1) nor on inflammatory activation of the cells (Fig. 4) nor on outward K^+ current induction (Fig. 5).

Our desire to isolate microglia from adult brains and culture them formed the starting point for this study. Next, we were interested in the characterisation of the adult primary microglia and their direct comparison with neo-natal microglia as well as with the microglial cell line C8-B4.

To this end, flow cytometry and immuno-fluorescence were first used to determine the antigenic phenotype of the cells. The adult microglia shared the commonly described immuno-epitopes of microglia (Beauvillain *et al.*, 2008). More than 98% of the cells were positive for microglial/myeloid cell markers, such as CD11b, CD16/32, MOMA, IB_4 and F4/80 (Fig. 2, Table 1 and supplementary material 1). Moreover, they expressed only low levels of the pan-leukocyte marker CD45 which in turn is a hallmark of microglial cells (Sedgwick *et al.*, 1991; Carson *et al.*, 1998). In contrast, they neither express the distinguishing marker to identify immature and mature dendritic cells CD11c, nor the activated antigen presenting cell marker CD86 nor progenitor/stem cell markers, such as Gr-1, CD34 and EGF-R. The only minor difference between neo-natal and adult microglia immunophenotypes was expression of CD68. CD68 is a lysosomal myeloid marker also known as ED1 in rats. Both ages of primary microglia were positive for CD68 but adult microglia displayed a higher level than neo-natal microglia. These observations are consistent with the previous report of an enhanced microglial expression of CD68 in aging brains (Kullberg *et al.*, 2001). Intriguingly, in C8-B4 cells, two distinct populations could be distinguished based on their level of CD68.

To further investigate the differences between adult and neo-natal microglia as well as C8-B4 cells, their functional responses to

various stimuli were studied. To induce a response to pro-inflammatory stimuli, the potent immune elicitor LPS and the lymphokine IFN-γ were used separately and in combination. Furthermore, the response of the cells to GM-CSF treatment was also evaluated.

From an electrophysiological point of view, adult primary microglia had virtually identical characteristics to neo-natal cells. The untreated cells had the classical membrane current profile with no detectable outward K^+ current and a large inward K^+ current at potentials negative to -80mV. Conversely, treatment with GM-CSF (but only at high concentration), IFN-γ and/or LPS was able to induce a prominent outward K^+ current and in some cases, a reduced inward K^+ current (Fig. 4). Both voltage-dependent K^+ currents had similar features to those observed in neo-natal microglia or in C8-B4 cells with exception that C8-B4 cells show a Kv1.3 current already in the unstimulated state (Moussaud *et al.*, 2009). After electrophysiological and pharmacological characterisations, the Kir2.1 channel was suspected to be the possible molecular correlate for the inward K^+ current. For the outward K^+ current, its cumulative inactivation and high margatoxin sensitivity clearly indicated that voltage-gated Kv1.3 homomeric channels were responsible for this current.

In terms of NO production and cytokine/chemokine secretion, adult microglia behave similarly to neo-natal primary microglia with minor, yet interesting, differences. Medium alone or with GM-CSF was not able to trigger NO or cytokine and chemokine production suggesting that the cultured adult primary microglia are in a quiescent state. However, in response to LPS and/or IFN-γ, adult microglia produced generally larger amounts of pro-inflammatory cytokines (IL-1β, IL-12 and KC) than neo-natal microglia or C8-B4 cells (Fig. 5). On the other hand, in response to the same stimuli, adult microglia produced similar levels of TNF-α and smaller amounts of the anti-inflammatory IL-10 cytokine than neo-natal microglia. Interestingly, a similar age-mediated imbalance in microglial response has also been previously described in coronal brain sections and in mixed glial culture as well as in isolated microglia (Ye and Johnson, 2001; Xie *et al.*, 2003; Sierra *et al.*, 2007). Concerning NO production, although subsequent studies failed to find any NO production by adult microglia even in response to LPS and IFN-γ (Brannan and Roberts, 2004) or reported a similar or reduced microglial NO production with age in response to LPS (Rozovsky *et al.*, 1998; Xie *et al.*, 2003), we found that adult microglia clearly produce more NO than neo-natal microglia. In our opinion, these apparent discrepancies might reflect differences in the culture medium and in the nature and purity of the LPS used. An other explanation is the higher suitability for long term experiments of the cells from the herein described method, in comparison to the previously used methods.

However, even if it is consistent with *in vivo* observations, the pro-inflammatory over-response of the adult microglia compared to the neo-natal microglia is not fully understood and the possible explanations are numerous

(up-regulation of STAT-1, NF-κB or TLR signal pathways, epigenetic changes, reduced feedback loops…). But knowing that microglia are the main source of cytokines and of reactive oxygen and nitrogen species in the brain and that the aforementioned secretory products induce inflammation, nitrosative and oxidative stress and subsequently neuronal dysfunction when not well-balanced (Park *et al.*, 2007), we can speculate that the increased NO production and pro-inflammatory cytokines secretion in aged microglia might give a rise in neuro-toxicity and thereby contribute to brain injury in aged-related neurodegenerative diseases.

However, these speculations need further investigation to confirm their biological relevance and the methodology described herein lays the ground for further in depth inquiry into microglial changes with regard to age, brain region or pathological condition.

3.8. Acknowledgments

The authors would like to thank the CNS Research department of Boehringer Ingelheim for financial support; Pr. Chluba J., Pr. Pugin A., Dr. Lamodière E., Dr. Longden T., Dr. Schwamborn J. and Pr. Hengerer B. for intellectual contributions and editorial help; and Beyrle U., Linn D., Schad J., Morton L., Lemmer E., Krell M. for excellent technical assistance. Part of this data has been presented in abstract form at the Euroglia meeting (Paris, sept 8th to 12th 2009).

3.9. Supplemental materials

3.9.1. Supplemental material 1

The supplemental material 1 (see below) groups all the flow cytometry raw data presented in table 1. The data are given in the form of histograms where the blue peak corresponds to the isotype control, whereas the red peak corresponds to the immune-stained cells.

3.9.1. Supplemental material 2

The supplemental material 2 is a z-stacking video performed with a confocal microscope, showing unstimulated and LPS-activated adult primary microglia, which have phagocytosed red fluorescent latex beads. This video is available on the enclosed CD at the end of the manuscript (in the folder Article 3/Supplemental materials) or online at:
http://www.sciencedirect.com/science?_ob=ArticleURL&_udi=B6T04-4Y7P4GM-1&_user=10&_coverDate=03%2F30%2F2010&_rdoc=1&_fmt=high&_orig=search&_sort=d&_docanchor=&view=c&_acct=C000050221&_version=1&_urlVersion=0&_userid=10&md5=7cf44b967dde0f125d72be09dc84e08c.

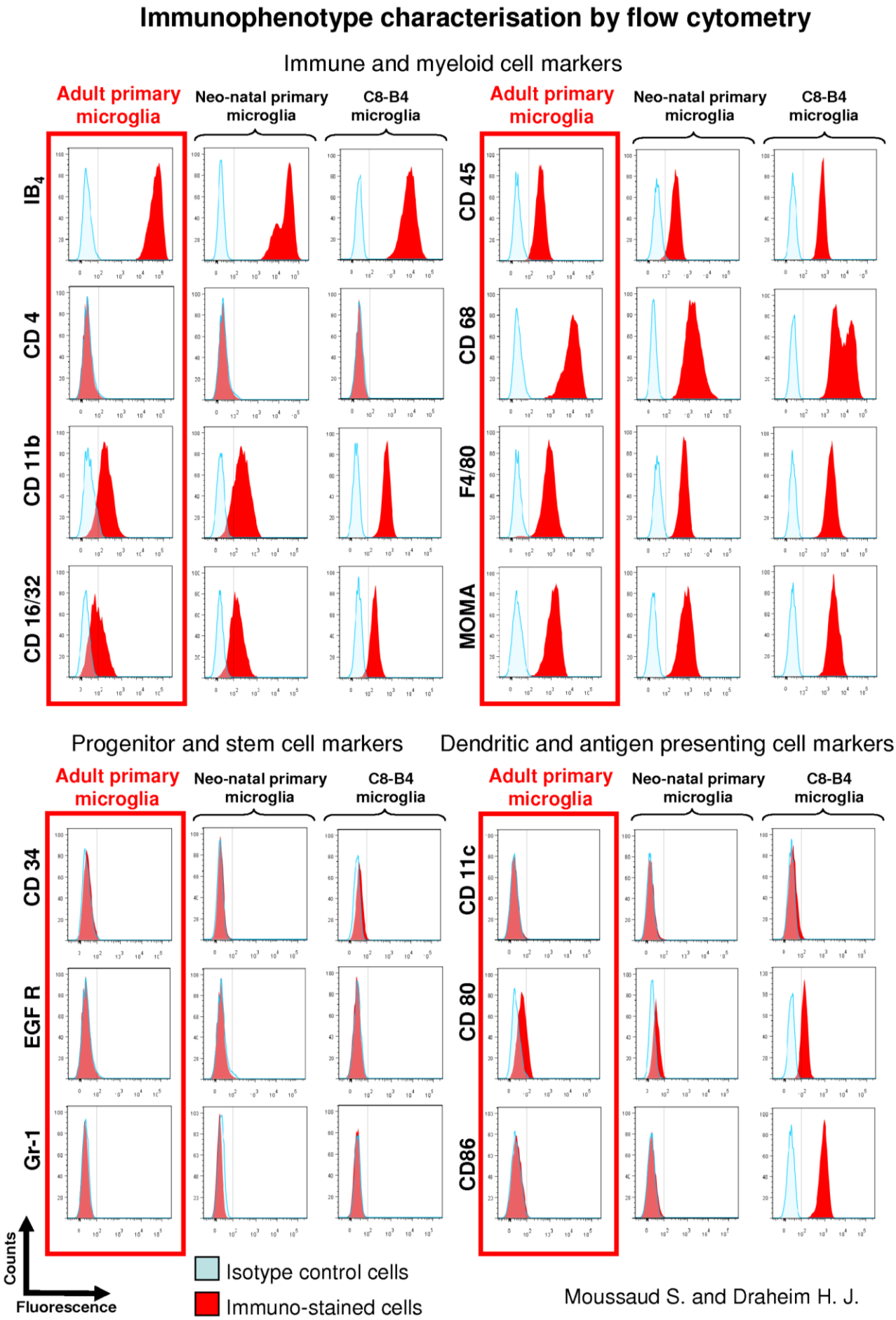
Immunophenotype characterisation by flow cytometry
Immune and myeloid cell markers
Adult primary microglia
Neo-natal primary microglia
C8-B4 microglia
IB4
CD 4
CD 11b
CD 16/32
CD 45
CD 68
F4/80
MOMA
Progenitor and stem cell markers
Dendritic and antigen presenting cell markers
CD 34
EGF R
Gr-1
CD 11c
CD 80
CD86
Counts
Fluorescence
Isotype control cells
Immuno-stained cells
Moussaud S. and Draheim H. J.

IV. Final conclusions and perspectives

A comparison of Parkinson's and Alzheimer's diseases shows disconcerting parallels and intriguing mechanistic similarities suggesting that both diseases result from similar schemes. For example, appearance of both diseases is mainly sporadic and age-related but sometimes also linked with hereditary genetic mutations. Both diseases are characterised by neural transmission failures, programmed cell death dysregulation, abnormal intracellular calcium homeostasis, mitochondrial dysfunction, oxidative stress, protein catabolism dysfunction, formation of proteinous aggregates, microglial activation and chronic neuroinflammation.

In both diseases, the major component of the proteinous inclusions is a specific small protein, namely α-synuclein for Parkinson's disease and Aβ for Alzheimer's disease. Moreover, mutations on the genes coding for both proteins induce genetic inheritance. Both proteins have the ability to form oligomers and larger aggregates in β-sheets structures (Bucciantini *et al.*, 2002; Lashuel *et al.*, 2002; Kayed *et al.*, 2003) and, similarly to prion proteins, they are neurotoxic and they can somehow interact with microglia.

1. α-synuclein

The central role of α-synuclein aberrant aggregation in the pathogenesis of Parkinson's disease and other synucleinopathies is presently widely accepted. However, the association between α-synuclein abnormal polymerisation and neurotoxicity is still far from being fully understood. The identification of the different oligomeric forms of α-synuclein protein, their molecular dissection and their biological effects is an exciting and challenging endeavor that should lead to a better understanding of neurodegeneration.

To investigate α-synuclein oligomers, we developed three new protocols for *in vitro* oligomer preparation (see article 1). In contrast to previous methods, our approaches presented the advantages of using low concentrations of α-synuclein and mainly lead to formation of oligomers rather than fibrils.

Then, using FIDA and AFM, we biophysically characterised six different types of α-synuclein oligomer preparations (noted A1, A2, B1, B2, C1 and C2). We demonstrated that each preparation contained heterogeneous populations of α-synuclein polymers ranging from monomer to small fibrils. However, α-synuclein was predominantly found in the form of small oligomers and monomers, whereas the presence of fibrils was insignificant except with prolonged incubation. Interestingly, within the same preparations as well as between the different preparations, α-synuclein oligomers presented various proportions, shapes, morphologies and sizes. For instance, intriguing annular structures were detected only in type A oligomers. A possible explanation for the presence of heterogeneous polymeric entities is that α-synuclein polymerisation is a dynamic, reversible and evanescent process showing rapid and fragile equilibrium between each step of polymerisation. This hypothesis may also explain why α-synuclein oligomers are so difficult to visualise by classical methods, such as Western blot or size exclusion chromatography.

Next, we investigated the bioactivity of each α-synuclein oligomer preparation on cultured neurons. We observed that the different types of preparations could be also differentiated based on their cellular effects. For instance, only type A oligomers induced Ca^{2+} influxes and subsequently triggered cell death by caspase-mediated apoptosis. Consistent with

previous reports, we hypothesised that the cell membrane integrity was challenged by the action of pore forming α-synuclein oligomers, leading to intracellular Ca^{2+} influxes and membrane potential changes (Volles *et al.*, 2001 and 2002; Lashuel *et al.*, 2002; Demuro *et al.*, 2005). This putative pore forming α-synuclein oligomers are probably linked to the intriguing annular structures that were only found in type A oligomers.

In contrast, type B and C oligomers provoked neither a Ca^{2+} influx, caspase activation, nor cell loss, but were able to translocate into cells and seed intracellular α-synuclein aggregation, thus eliciting the formation of large intracellular aggregates. This seeding effect of B and C oligomers might play an important role under pathophysiological conditions. Indeed, if these α-synuclein oligomers are secreted, they could theoretically provoke the spread of the synucleinopathy to neighboring neurons and consequently lead to Parkinson's disease progression in the brain.

Thus, we were able to demonstrate that distinct types of α-synuclein oligomers triggered toxic neurodegenerative processes in different ways. On one hand, membrane pore formation led to the disruption of cellular ion homeostasis, followed by caspase activation and finally leading to cell death. On the other hand, the seeding effect induced of aggregation of intracellular α-synuclein. Both are possible pathogenic mechanisms of α-synuclein oligomers that might also occur *in vivo,* but additional studies are required to firmly confirm these first *in vitro* observations.

In conclusion, our findings are clearly in line with the hypothesis that the toxic effects of α-synuclein are rather due to the prefibrillar oligomeric forms rather than to the large α-synuclein fibrillar aggregates like in Lewy bodies (Goldberg and Lansbury, 2000; Lashuel *et al.*, 2002). As a consequence, development of novel drugs targeting α-synuclein should prevent the oligomer formation to effectively block its toxic effects. Nonetheless, the exact function of α-synuclein is still not fully defined and considerable work is still required to unequivocally find out if inhibiting α-synuclein oligomerisation could be valuable as a therapeutic strategy in humans to prevent Parkinson's disease and other synucleinopathies (Bodner *et al.*, 2006).

2. Electrophysiology of microglia

The traditional view of microglia being the bad guy in neurodegenerative diseases may not be the entire truth because inflammation has also neurotrophic and neuroprotective effects. Therefore, microglia cannot be simply considered as harmful for neurons. In fact, microglial activation is not a straightforward bipolar response but rather a gradual process that provokes complex functional, morphological and electrophysiological changes. In order to identify putative targets to modulate microglial activation and, more generally, in order to study the electrophysiological characteristics of microglial ion channels, we focused our interest on K^+ channels of murine microglia (see article 2 and 3).

Using the whole cell patch-clamp technique, we recorded K^+ currents in different *in vitro* microglial models, namely in neo-natal and in adult primary microglia as well as in the C8-B4 microglial cell line. We identified two types of voltage-activated K^+ currents: one outward and one inward rectifying K^+ current. In neo-natal and adult primary microglia, the untreated resting cells exhibited no detectable outward K^+ current but a large inward K^+ current at potentials negative to -80mV. Conversely, a prominent outward K^+ current at potentials positive to -30mV and a curtailed inward K^+ current were recorded upon cell activation. In contrast to primary cultured microglia, the outward K^+ current in C8-B4 microglia was already present in unstimulated cells. These results are in line with previous descriptions of C8-B4 cells as being "pre-activated" cells (Alliot *et al.*, 1996; Xu *et al.*, 2008).

Then, using pharmacological, biophysical and molecular approaches, we clearly demonstrated that, in murine microglia, homomeric Kv1.3 and Kir2.1 channels underlay the outward and the inward rectifying K^+ currents, respectively. Additionally, we investigated the regulation of these K^+ channels in response to microglial activation. The presence of growth factors, cytokines and/or bacterial components modulated the activity of both voltage-dependent K^+ channels. In particular, Kv1.3 activity was directly linked to microglial activation in response to treatments with LPS, IFN-γ, TGF-β and GM-CSF. However, there was no increase in global channel quantity or activation of additional channel types after microglial activation. Actually, we were able to demonstrate that inhibiting by protein kinases hampered the outward

K^+ current was, suggesting that up-regulation of the outward K^+ current probably involved post-translational mechanisms, such as phosphorylation and sequestration of Kv1.3 channels.

In the brain, Kv1.3 is mainly found in microglia and its inhibition has been ascertained to be immunosuppressive in lymphocytes (Chandy *et al.*, 2004). Consistently with our observations, Menteyne *et al.* (2009) identified Kv1.3 as being responsible for the outward K^+ current in microglia. Interestingly, these observations were performed in accute hippocampal slices prepared after *status epilepticus*, suggesting a possible role of Kv1.3 in epilepsy (Avignone *et al.*, 2008; Menteyne *et al.*, 2009). In another recent publication, retinal ganglion cell degeneration in an *in vivo* model was successfully rescued by Kv1.3 knock-down and pharmacological blockage (Koeberle and Schlichter, 2010). Taken together, these results highlight the role of Kv1.3 in microglial activation and support the idea that Kv1.3 represents an interesting target to rescue neurons by modulating microglial behavior. However, it is still unclear how Kv1.3 is involved in microglial activation mechanisms and further investigations are needed for a better understanding Kv1.3 functions. We observed that blocking Kv1.3 with margatoxin did not affect the LPS and IFN-γ induced NO production from microglia, suggesting that Kv1.3 does not act as a general inhibitor of microglial activation (data not shown). Our assumption is that Kv1.3 activity might be linked to Ca^{2+} signalling and predominantly acts on microglial proliferation and motility. This hypothesis correlates with the fact that outward K^+ currents are induced during microglial proliferation in response to astrocyte-conditioned medium and GM-CSF treatment.

Aside from cannabinoid receptors, cytokine receptors and P2X and iCRAC channels, Kv1.3 could be a valuable therapeutic target for modulating microglial behaviour in order to decrease its deleterious effects and to increase its beneficial effects. Nonetheless, several questions still need an answer. For example, do *in situ* human microglia have the same electrophysiological characteristics as cultured murine microglia and do they functionally express Kv1.3? What are the exact consequences of Kv1.3 blockage in humans and does it exert detrimental side effects? Finally, is it possible to find a brain-permeable molecule that specifically blocks Kv1.3 and not its homologues and targets microglia but not other immune cells?

3. In vitro *modelling of aged microglial functions*

Recent evidence suggest that aging and/or pathological conditions induce changes in microglial function, leading to exacerbation of their deleterious effects and in parallel, to the reduction of their protective effects on neurons (Ye and Johnson, 2001; Xie *et al.*, 2003; Sierra *et al.*, 2007; Streit and Xue, 2009). This hypothesis of microglial dysfunction may play a pivotal role in the induction of age-related neurodegenerative disorders. However, the knowledge on age-related changes in microglia remains elusive due to the lack of suitable *in vitro* models for studying microglial cells derived from aged brains. For this purpose, we developed a novel method for isolating and culturing primary microglia from aged mice. This simple and effective method for isolating essentially pure primary microglia from adult murine brains enabled us to directly compare *in vitro* adult mature primary microglia with the commonly used neo-natal microglia and with immortalized microglial cells (see article 3).

We found that adult microglia expressed common microglial/myeloid cell markers, such as CD11b, CD16/32, $CD45^{low}$, MOMA, IB_4 and F4/80. In contrast, they express neither dendritic/activated antigen presenting cell markers, nor progenitor/stem cell markers. Neo-natal and adult microglia immunophenotypes only differed in the level of expression of the lysosomal myeloid marker CD68, consistent with previous reports of an enhanced microglial expression of CD68 in brains of aged persons and Parkinson's patients (Kullberg *et al.*, 2001; Croisier *et al.*, 2005).

Except for this subtle variation of the expression level of the CD68 marker, we did not find any fundamental immunophenotype differences between adult and neo-natal primary microglia. Surprisingly, we observed that adult microglia have the rare ability to self-renew and to survive during virtually unlimited periods of time *in vitro*. Such a feature is usually reserved to progenitor/stem cells. Actually, a few studies described that microglia present several properties common to stem cells, such as expression of CD34 (Block *et al.*, 2007) and nestin, leading to the idea that they could be used as a source of stem cells (Yokoyama *et al.*, 2004). However, we did not find any expression of the progenitor/stem cells markers CD34, Gr-1 and

EGF-R. Nonetheless, taken together, our findings give weight to the theory that microglia form an autonomous immune cell population that is able to self-sustain in the brain throughout life.

But, as mentioned in the introduction, the question of the real nature and origin of microglial cells, in particular during adulthood, is still debated (Ajami *et al.*, 2007; Davoust *et al.*, 2008). A major issue is that the clear distinction between "true resident" microglial cells, "bone marrow-derived" microglia, infiltrated monocytes and perivascular and meningeal macrophages is presently not possible, due to the lack of an unequivocal marker to distinguish between them. Such a marker or a method will be of great interest and will undoubtedly lead to a better understanding of the mechanisms of self-renewal of microglial cells during physiological and pathophysiological conditions or, perhaps, even lead to the identification of different microglia subtypes.

By comparing NO production and cytokine/chemokine secretion, we found other interesting differences between neo-natal and adult primary microglia. We observed that in response to LPS and/or IFN-γ stimulation, adult microglia produced larger amounts of NO and pro-inflammatory cytokines (IL-1β, IL-12 and KC) and smaller amounts of the anti-inflammatory IL-10 cytokine in comparison to neo-natal microglia. Strikingly, a similar age-mediated imbalance in microglial response has also been described *ex vivo* and *in vivo* (Ye and Johnson, 2001; Xie *et al.*, 2003; Sierra *et al.*, 2007, Streit and Xue, 2009).

This decreased anti-inflammatory cytokine secretion combined with increases in the secretion of NO and pro-inflammatory cytokines suggest that aging might propel microglial neurotoxic effects and that these age-related microglial changes might contribute to brain injury in aged-related neurodegenerative diseases.

The exact reasons for these age-mediated changes in microglia are not fully defined and further in depth investigations are needed. Nonetheless, our results might suggest an intrinsic cause for the pro-inflammatory over-response of aged microglia, such as up-regulation of STAT-1, NF-κB or TLR signalling pathways, epigenetic changes or reduced feedback loops.

4. Microglia and Parkinson's disease

More and more researchers have recognised the possible involvement of neuroinflammation in Parkinson's pathogenesis (Long-Smith *et al.*, 2005; Block *et al.*, 2007; Tambuyzer *et al.*, 2008). Nonetheless, influence of glial cells on Parkinson's disease onset and progression is a research field that merits further investigations. For example, the consequences of *park* genes mutations (see Table1 in introduction) on glial function are poorly studied. In Alzheimer's disease, it has been demonstrated that Aβ and microglia interact. Aβ activated microglia and microglia were able to clear the Aβ plaques by phagocytosis (Block *et al.*, 2007). In a similar way, several research groups, including us, have addressed the question whether α-synuclein interacts with microglia (Croisier *et al.*, 2005; Zhang *et al.*, 2005; Gao *et al.*, 2008).

Similarly to what has been observed on neurons, we found that type A α-synuclein oligomers induced strong Ca^{2+} influxes into microglia cells, whereas α-synuclein monomers did not (Figure 1 A and B).

In addition, using fluorescent labelling, we were able to track α-synuclein oligomers after incubation with microglia. As shown in figure 1 C, large amounts of α-synuclein were found in microglial cells in the form of vesicular inclusions, suggesting that microglia actively phagocytosed α-synuclein.

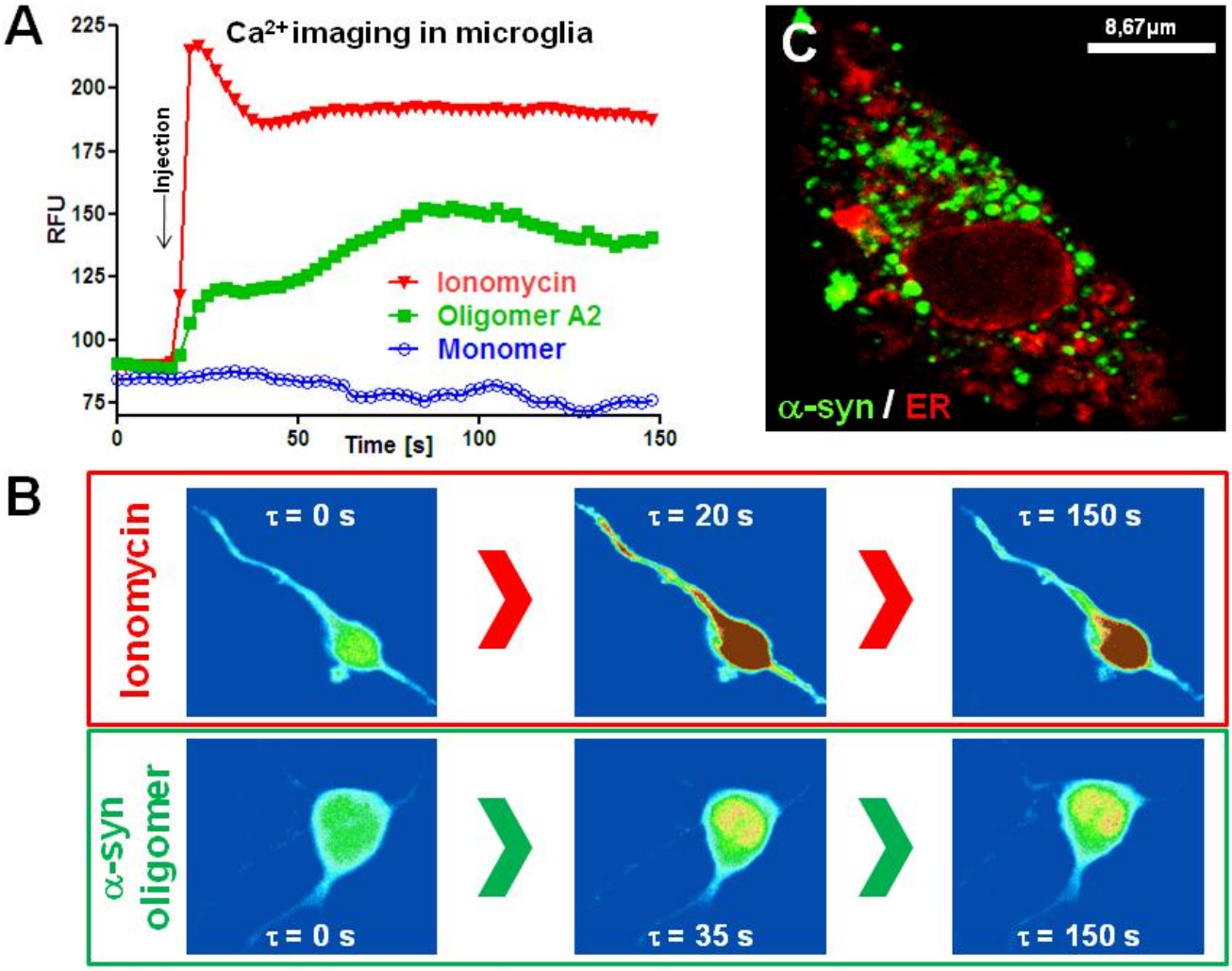

Figure 1: Microglia and α-synuclein oligomers.

***A)* Type A α-synuclein oligomers also induce [Ca^{2+}] elevation on primary microglial cells.** Traces show [Ca^{2+}]-dependent fluorescence (Fluo-4 AM) of single primary microglia in response to 0,1mg/ml oligomers type A2 (green), 6µM ionomycin (as positive control, in red) and 0,1mg/ml monomer in solvent (as negative control, in blue). ***B)* Fluorescence images of single microglia illustrating the responses to different treatments**. Records were captured at different time points and are depicted on a pseudocolor scale with warmer colors on a rainbow scale corresponding to higher fluorescence. ***C)* Microglia actively phagocytose α-synuclein.** Immuno-fluorescence picture of primary microglia performed with a confocal microscope. Prior to fixation, cells were incubated for 24h with 0,01mg/ml Alexa488 labelled type A2 α-synuclein oligomers. Then, anti-calreticulin antibodies were used to stain the endoplasmic reticulum in red. Large amounts of α-synuclein (in green) were found in the form of spherical green inclusion in microglia.

Finally, we investigated whether the presence of α-synuclein was able to activate microglial cells, as mentioned in previous reports (Zhang *et al.*, 2005; Gao *et al.*, 2008). Indeed, an important effect of α-synuclein on microglial activation was seen by measuring cytokine release. For example, α-synuclein induces the secretion of TNF-α from microglia (Figure 2 A). However, unfortunately, control experiments to detect the purity of our recombinant α-synuclein protein revealed a small but non negligible presence of endotoxin. Although this contamination is probably too low to induce microglial activation by itself, the quality and the relevance of our results are subject to doubt and may be not valid.

As a consequence, we tried different ways to get around this technical problem. For example, we collected cell supernatants of α-synuclein-expressing dopaminergic neurons in which considerable amounts of α-synuclein were detected. Subsequently, we challenged microglial cells with this conditioned medium or conditioned medium from other cell types as a control. Surprisingly, only the conditioned medium from the α-synuclein-expressing neurons was able to induce microglial activation, indicating that α-synuclein, or at least a secretion product of dopaminergic neurons, was able to activate microglia (Figure 2 B).

However, α-synuclein is probably not the only vector for microglial dysfunction and other *park* genes may have an influence on glial cells. For example, we discovered recently that LRRK2 (leucin-rich repeat kinase 2) protein was expressed in microglia and that its expression was up-regulated upon microglial activation (Figure 3 A). In addition, LRRK2 pharmacological inhibition evoked a reduced cytokine secretion (Figure 3 B). Previous studies of LRRK2 were mainly focused on neurons, where it was generally expected to act. In contrast, our results suggest that LRRK2 may also act on microglia and that Parkinson-inducing LRRK2 mutations could also have an effect on microglial function.

In conclusion, although further in depth investigations are required to give an exact insight into the role of microglia in Parkinson's pathogenesis, we have identified three possible reasons why microglia are over-activated in Parkinson's disease, namely aged-related changes, α-synuclein and LRRK2 influences.

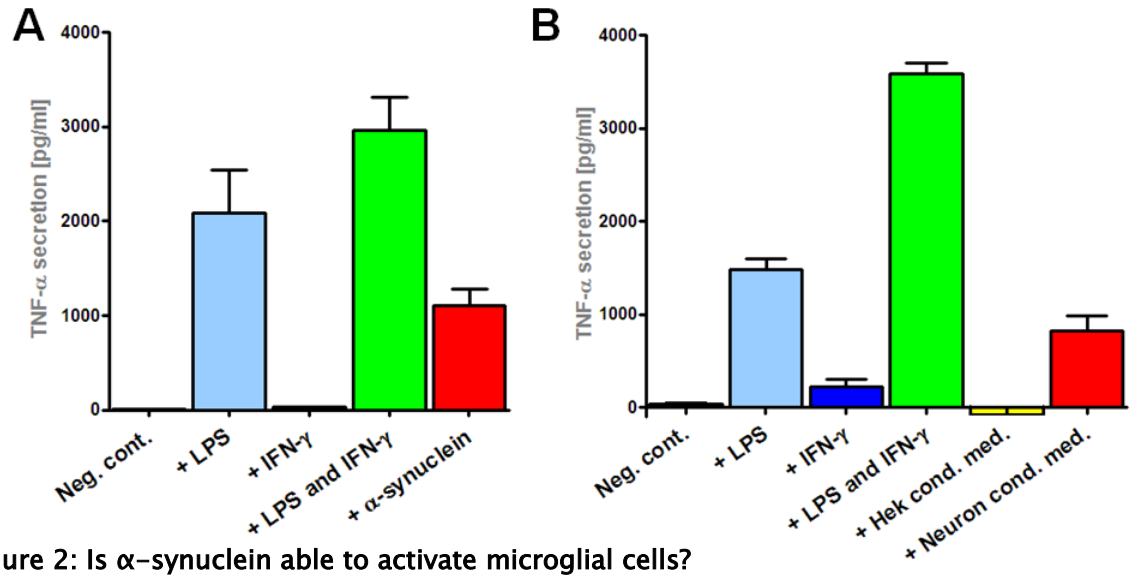

Figure 2: Is α-synuclein able to activate microglial cells?

Microglial TNF-α secretion was quantified in response to 24h incubation with 3,6mg/l recombinant α-synuclein ***(A)*** or with 25% (v/v) conditioned medium from α-synuclein-expressing Bem17 neurons ***(B)***. Fresh medium alone (Neg. cont.) or with 25% Hek (v/v) conditioned medium from normal Hek cells were used as negative controls, whereas LPS (1µg/ml) and/or IFN-γ (100ng/ml) treatments were used as positive controls. Recombinant α-synuclein ***(A,* red bar*)*** and conditioned medium from α-synuclein-expressing dopaminergic neurons ***(B,* red bar*)*** were able to induce TNF-α secretion, whereas conditioned medium from Hek cells were not ***(B,* yellow bar*)***. TNF-α levels in the supernatant were quantified using a multiplex immuno-array ***(A)*** or using a classical ELISA ***(B)***. Values are given as mean ± S.E.M, n=3.

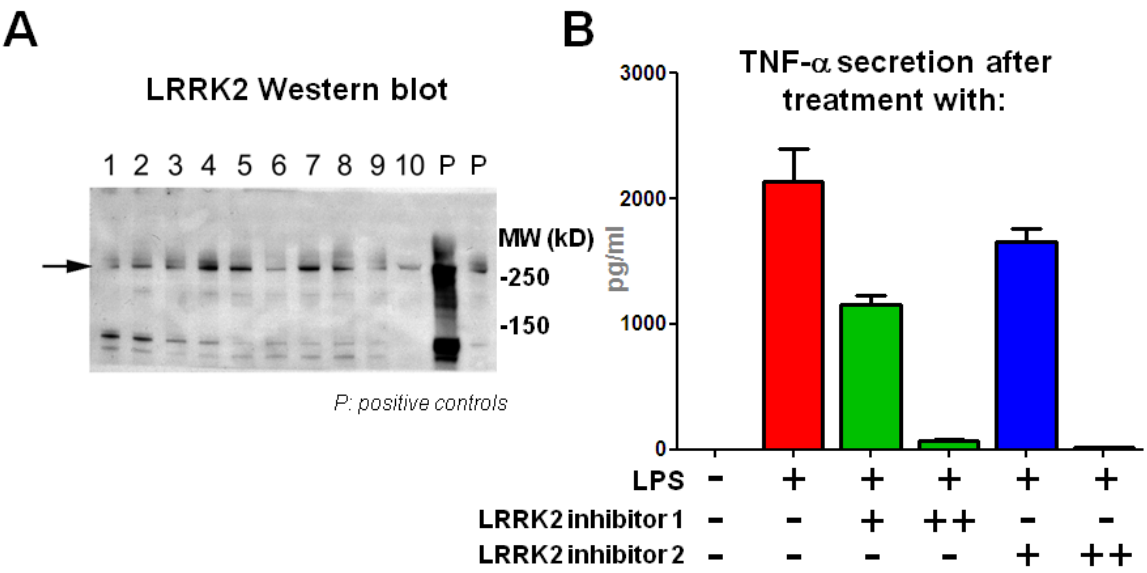

Figure 3: LRRK2 and microglia: a novelty.

A) Western blot analysis of lysates coming from murine RAW 264.7 macrophages (lane 1-4), C8-B4 microglia (lane 5-8) and primary microglia (lane 9 and 10). Prior to lysis, cells were incubated for 24h with fresh medium alone or supplemented with LPS (1µg/ml) and/or IFN-γ (100ng/ml). LRRK2 is expressed in microglia and macrophages and its expression is modulated upon cell activation (bands corresponding to LRRK2 are marked with the arrow). ***B)*** Cytokine secretion of murine microglia was quantified in response to LRRK2 pharmacological inhibition and after a 24h incubation with fresh medium alone (control) or supplemented with LPS (1µg/ml) and/or IFN-γ (100ng/ml). TNF-α levels in the supernatant were quantified using a multiplex immuno-array. Values are given as mean ± S.E.M.; n=3.

5. Future directions

Although research on neurodegenerative disorders highlights promising results ptoviding new hope for Parkinson's patients, the distance between the lab bench to the human patients is huge. Indeed, before concrete development of therapeutic interventions to cure Parkinson's disease, fundamental questions and major issues have to be solved.

The major issue is that the specific factors causing Parkinson's disease are still not unequivocally identified.

Another problem is that research on Parkinson's disease is hampered by the lack of a suitable animal model that acurately mimics all features of human Parkinson's disease. Indeed, despite of extensive efforts, no current animal model presents dopaminergic neurons degeneration in response to α-synucleinopathy, microglial activation and aging.

Another imperative need is the availability of an effective and reliable test for early diagnosis of Parkinson's disease, because therapeutic strategies to halt or prevent Parkinson's disease have little chance of success if they are started too late in the progression of the disease. PET imaging and the search for reliable markers in blood or cerebrospinal fluid are presently in discussion (Gerhard *et al.*, 2005). In this regard, the question whether it is possible to use α-synuclein abnormal polymerisation or neuroinflammation and microglial activity as source of biomarkers for early diagnostic can be addressed.

More generally, we are convinced that research on neurodegenerative disorders will greatly benefit from a better knowledge of glial cells.

For instance, recently, an INSERM team successfully cured two boys that had a rare and lethal genetic neurodegenerative disease, the X-linked adrenoleukodystrophy, by performing a gene therapy where microglia were used as vector for the transgene (Cartier *et al.*, 2009). These prodigious results raise the possibility to use microglia as vector for transgene expression in the brain for curing other pathologies?

Neuropathic pain, brain tumour, epilepsy and neuroregeneration after ischemia or spinal cord lesion are other possible therapeutic applications for research on glial cells.

As a final conclusion, we believe that the future of research on the interactions between neurons, microglia, reactive astrocytes, oligodendrocytes, the blood-brain barrier and lymphocytes during pathophysiological conditions will undoubtedly shed light on the highly sophisticated communication between the CNS and the immune system and contribute to struggle against neuropathologies.

V. References

Abbott NJ, Patabendige AA, Dolman DE, Yusof SR, Begley DJ (2009) Structure and function of the blood-brain barrier. *Neurobiol Dis* 37:13-25.

Abeliovich A, Schmitz Y, Farinas I, Choi-Lundberg D, Ho WH, Castillo PE, Shinsky N, Verdugo JM, Armanini M, Ryan A, Hynes M, Phillips H, Sulzer D, Rosenthal A (2000) Mice lacking α-synuclein display functional deficits in the nigrostriatal dopamine system. *Neuron* 25:239-252.

Adamczyk A, Strosznajder JB (2006) α-synuclein potentiates Ca^{2+} influx through voltage-dependent Ca^{2+} channels. *Neuroreport* 17:1883-1886.

Ahn KJ, Paik SR, Chung KC, Kim J (2006) Amino acid sequence motifs and mechanistic features of the membrane translocation of α-synuclein. *J Neurochem* 97:265-279.

Ajami B, Bennett JL, Krieger C, Tetzlaff W, Rossi FM (2007) Local self-renewal can sustain CNS microglia maintenance and function throughout adult life. *Nat Neurosci* 10:1538-1543.

Alliot F, Pessac B (1984) Astrocytic cell clones derived from established cultures of 8-day postnatal mouse cerebella. *Brain Res* 306:283-291.

Alliot F, Lecain E, Grima B, Pessac B (1991) Microglial progenitors with a high proliferative potential in the embryonic and adult mouse brain. *Proc Natl Acad Sci U S A* 88:1541-1545.

Alliot F, Marty MC, Cambier D, Pessac B (1996) A spontaneously immortalized mouse microglial cell line expressing CD4. *Brain Res Dev Brain Res* 95:140-143.

Aloisi F (2001) Immune function of microglia. *Glia* 36:165-179.

Apetri MM, Maiti NC, Zagorski MG, Carey PR, Anderson VE (2006) Secondary structure of α-synuclein oligomers: characterization by raman and atomic force microscopy. *J Mol Biol* 355:63-71.

Arispe N (2004) Architecture of the Alzheimer's A β P ion channel pore. *J Membr Biol* 197:33-48.

Ascherio A, Chen H, Weisskopf MG, O'Reilly E, McCullough ML, Calle EE, Schwarzschild MA, Thun MJ (2006) Pesticide exposure and risk for Parkinson's disease. *Ann Neurol* 60:197-203.

Auluck PK, Chan HY, Trojanowski JQ, Lee VM, Bonini NM (2002) Chaperone suppression of α-synuclein toxicity in a Drosophila model for Parkinson's disease. *Science* 295:865-868.

Avdulov NA, Chochina SV, Igbavboa U, Warden CS, Vassiliev AV, Wood WG (1997) Lipid binding to amyloid β-peptide aggregates: preferential binding of cholesterol as compared with phosphatidylcholine and fatty acids. *J Neurochem* 69:1746-1752.

Avignone E, Ulmann L, Levavasseur F, Rassendren F, Audinat E (2008) *Status epilepticus* induces a particular microglial activation state characterized by enhanced purinergic signaling. *J Neurosci* 28:9133-9144.

Beauvillain C, Donnou S, Jarry U, Scotet M, Gascan H, Delneste Y, Guermonprez P, Jeannin P, Couez D (2008) Neonatal and adult microglia cross-present exogenous antigens. *Glia* 56:69-77.

Bennett MC (2005) The role of α-synuclein in neurodegenerative diseases. *Pharmacol Ther* 105:311-331.

Block ML, Zecca L, Hong JS (2007) Microglia-mediated neurotoxicity: uncovering the molecular mechanisms. *Nat Rev Neurosci* 8:57-69.

Bocchini V, Mazzolla R, Barluzzi R, Blasi E, Sick P, Kettenmann H (1992) An immortalized cell line expresses properties of activated microglial cells. *J Neurosci Res* 31:616-621.

Bodner RA, Outeiro TF, Altmann S, Maxwell MM, Cho SH, Hyman BT, McLean PJ, Young AB, Housman DE, Kazantsev AG (2006) Pharmacological promotion of inclusion formation: a therapeutic approach for Huntington's and Parkinson's diseases. *Proc Natl Acad Sci U S A* 103:4246-4251.

Bonifati V, Rizzu P, Squitieri F, Krieger E, Vanacore N, van Swieten JC, Brice A, van Duijn CM, Oostra B, Meco G, Heutink P (2003) DJ-1(PARK7), a novel gene for autosomal recessive, early onset parkinsonism. *Neurol Sci* 24:159-160.

Boucsein C, Kettenmann H, Nolte C (2000) Electrophysiological properties of microglial cells in normal and pathologic rat brain slices. *Eur J Neurosci* 12:2049-2058.

Braak H, Del TK, Rub U, de Vos RA, Jansen Steur EN, Braak E (2003) Staging of brain pathology related to sporadic Parkinson's disease. *Neurobiol Aging* 24:197-211.

Braak H, Ghebremedhin E, Rub U, Bratzke H, Del TK (2004) Stages in the development of Parkinson's disease-related pathology. *Cell Tissue Res* 318:121-134.

Brannan CA, Roberts MR (2004) Resident microglia from adult mice are refractory to nitric oxide-inducing stimuli due to impaired NOS2 gene expression. *Glia* 48:120-131.

Bucciantini M, Giannoni E, Chiti F, Baroni F, Formigli L, Zurdo J, Taddei N, Ramponi G, Dobson CM, Stefani M (2002) Inherent toxicity of aggregates implies a common mechanism for protein misfolding diseases. *Nature* 416:507-511.

Bucciantini M, Calloni G, Chiti F, Formigli L, Nosi D, Dobson CM, Stefani M (2004) Prefibrillar amyloid protein aggregates share common features of cytotoxicity. *J Biol Chem* 279:31374-31382.

Cabin DE, Shimazu K, Murphy D, Cole NB, Gottschalk W, McIlwain KL, Orrison B, Chen A, Ellis CE, Paylor R, Lu B, Nussbaum RL (2002) Synaptic vesicle depletion correlates with attenuated synaptic responses to prolonged repetitive stimulation in mice lacking α-synuclein. *J Neurosci* 22:8797-8807.

Cardona AE, Huang D, Sasse ME, Ransohoff RM (2006) Isolation of murine microglial cells for RNA analysis or flow cytometry. *Nat Protoc* 1:1947-1951.

Carson MJ, Reilly CR, Sutcliffe JG, Lo D (1998) Mature microglia resemble immature antigen-presenting cells. *Glia* 22:72-85.

Cartier N, *et al.* (2009) Hematopoietic stem cell gene therapy with a lentiviral vector in X-linked adrenoleukodystrophy. *Science* 326:818-823.

Chandy KG, Wulff H, Beeton C, Pennington M, Gutman GA, Cahalan MD (2004) K^+ channels as targets for specific immunomodulation. *Trends Pharmacol Sci* 25:280-289.

Chartier-Harlin MC, Kachergus J, Roumier C, Mouroux V, Douay X, Lincoln S, Levecque C, Larvor L, Andrieux J, Hulihan M, Waucquier N, Defebvre L, Amouyel P, Farrer M, Destee A (2004) α-synuclein locus duplication as a cause of familial Parkinson's disease. *Lancet* 364:1167-1169.

Chitta S, Santambrogio L, Stern LJ (2008) GMCSF in the absence of other cytokines sustains human dendritic cell precursors with T cell regulatory activity and capacity to differentiate into functional dendritic cells. *Immunol Lett* 116:41-54.

Colton CA (2009) Heterogeneity of Microglial Activation in the Innate Immune Response in the Brain. *J Neuroimmune Pharmacol* 4:399-418.

Conway KA, Lee SJ, Rochet JC, Ding TT, Williamson RE, Lansbury PT, Jr. (2000) Acceleration of oligomerization, not fibrillization, is a shared property of both α-synuclein mutations linked to early-onset Parkinson's disease: implications for pathogenesis and therapy. *Proc Natl Acad Sci U S A* 97:571-576.

Croisier E, Moran LB, Dexter DT, Pearce RK, Graeber MB (2005) Microglial inflammation in the parkinsonian *substantia nigra*: relationship to α-synuclein deposition. *J Neuroinflammation* 2:14.

Danzer KM, Haasen D, Karow AR, Moussaud S, Habeck M, Giese A, Kretzschmar H, Hengerer B, Kostka M (2007) Different species of α-synuclein oligomers induce calcium influx and seeding. *J Neurosci* 27:9220-9232.

Dauer W, Przedborski S (2003) Parkinson's disease: mechanisms and models. *Neuron* 39:889-909.

Davidson WS, Jonas A, Clayton DF, George JM (1998) Stabilization of α-synuclein secondary structure upon binding to synthetic membranes. *J Biol Chem* 273:9443-9449.

Davoust N, Vuaillat C, Androdias G, Nataf S (2008) From bone marrow to microglia: barriers and avenues. *Trends Immunol* 29:227-234.

Davson H (1976) Review lecture. The blood-brain barrier. *J Physiol* 255:1-28.

de Groot CJ, Montagne L, Janssen I, Ravid R, Van D, V, Veerhuis R (2000) Isolation and characterization of adult microglial cells and oligodendrocytes derived from postmortem human brain tissue. *Brain Res Brain Res Protoc* 5:85-94.

de Haas AH, Boddeke HW, Brouwer N, Biber K (2007) Optimized isolation enables *ex vivo* analysis of microglia from various central nervous system regions. *Glia* 55:1374-1384.

de Rijk MC, Launer LJ, Berger K, Breteler MM, Dartigues JF, Baldereschi M, Fratiglioni L, Lobo A, Martinez-Lage J, Trenkwalder C, Hofman A (2000) Prevalence of Parkinson's disease in Europe: A collaborative study of population-based cohorts. Neurologic Diseases in the Elderly Research Group. *Neurology* 54:S21-S23.

Demuro A, Mina E, Kayed R, Milton SC, Parker I, Glabe CG (2005) Calcium dysregulation and membrane disruption as a ubiquitous neurotoxic mechanism of soluble amyloid oligomers. *J Biol Chem* 280:17294-17300.

Dev KK, van der PH, Sommer B, Rovelli G (2003) Part I: parkin-associated proteins and Parkinson's disease. *Neuropharmacology* 45:1-13.

Dev KK, Hofele K, Barbieri S, Buchman VL, van der PH (2003) Part II: α-synuclein and its molecular pathophysiological role in neurodegenerative disease. *Neuropharmacology* 45:14-44.

Djukic M, Mildner A, Schmidt H, Czesnik D, Bruck W, Priller J, Nau R, Prinz M (2006) Circulating monocytes engraft in the brain, differentiate into microglia and contribute to the pathology following meningitis in mice. *Brain* 129:2394-2403.

Doty RL, Bromley SM, Stern MB (1995) Olfactory testing as an aid in the diagnosis of Parkinson's disease: development of optimal discrimination criteria. *Neurodegeneration* 4:93-97.

Draheim HJ, Prinz M, Weber JR, Weiser T, Kettenmann H, Hanisch UK (1999) Induction of potassium channels in mouse brain microglia: cells acquire responsiveness to pneumococcal cell wall components during late development. *Neuroscience* 89:1379-1390.

Dutta G, Zhang P, Liu B (2008) The lipopolysaccharide Parkinson's disease animal model: mechanistic studies and drug discovery. *Fundam Clin Pharmacol* 22:453-464.

Eder C (1998) Ion channels in microglia (brain macrophages). *Am J Physiol* 275:C327-C342.

Eder C (2005) Regulation of microglial behavior by ion channel activity. *J Neurosci Res* 81:314-321.

El-Agnaf OM, Salem SA, Paleologou KE, Curran MD, Gibson MJ, Court JA, Schlossmacher MG, Allsop D (2006) Detection of oligomeric forms of α-synuclein protein in human plasma as a potential biomarker for Parkinson's disease. *FASEB J* 20:419-425.

Esen N, Kielian T (2007) Effects of low dose GM-CSF on microglial inflammatory profiles to diverse pathogen-associated molecular patterns (PAMPs). *J Neuroinflammation* 4:10.

Esposito E, Di M, V, Benigno A, Pierucci M, Crescimanno G, Di GG (2007) Non-steroidal anti-inflammatory drugs in Parkinson's disease. *Exp Neurol* 205:295-312.

Fischer HG, Eder C, Hadding U, Heinemann U (1995) Cytokine-dependent K^+ channel profile of microglia at

immunologically defined functional states. *Neuroscience* 64:183-191.

Fischer HG, Reichmann G (2001) Brain dendritic cells and macrophages/microglia in central nervous system inflammation. *J Immunol* 166:2717-2726.

Floden AM, Combs CK (2007) Microglia repetitively isolated from *in vitro* mixed glial cultures retain their initial phenotype. *J Neurosci Methods* 164:218-224.

Ford AL, Goodsall AL, Hickey WF, Sedgwick JD (1995) Normal adult ramified microglia separated from other central nervous system macrophages by flow cytometric sorting. Phenotypic differences defined and direct *ex vivo* antigen presentation to myelin basic protein-reactive $CD4^+$ T cells compared. *J Immunol* 154:4309-4321.

Fordyce CB, Jagasia R, Zhu X, Schlichter LC (2005) Microglia Kv1.3 channels contribute to their ability to kill neurons. *J Neurosci* 25:7139-7149.

Frank MG, Wieseler-Frank JL, Watkins LR, Maier SF (2006) Rapid isolation of highly enriched and quiescent microglia from adult rat hippocampus: immunophenotypic and functional characteristics. *J Neurosci Methods* 151:121-130.

Furukawa K, Matsuzaki-Kobayashi M, Hasegawa T, Kikuchi A, Sugeno N, Itoyama Y, Wang Y, Yao PJ, Bushlin I, Takeda A (2006) Plasma membrane ion permeability induced by mutant α-synuclein contributes to the degeneration of neural cells. *J Neurochem* 97:1071-1077.

Gallin EK, Sheehy PA (1985) Differential expression of inward and outward potassium currents in the macrophage-like cell line J774.1. *J Physiol* 369:475-499.

Gandhi S, Muqit MM, Stanyer L, Healy DG, bou-Sleiman PM, Hargreaves I, Heales S, Ganguly M, Parsons L, Lees AJ, Latchman DS, Holton JL, Wood NW, Revesz T (2006) PINK1 protein in normal human brain and Parkinson's disease. *Brain* 129:1720-1731.

Gao HM, Hong JS (2008) Why neurodegenerative diseases are progressive: uncontrolled inflammation drives disease progression. *Trends Immunol* 29:357-365.

Gao HM, Kotzbauer PT, Uryu K, Leight S, Trojanowski JQ, Lee VM (2008) Neuroinflammation and oxidation/nitration of alpha-synuclein linked to dopaminergic neurodegeneration. *J Neurosci* 28:7687-7698.

Garcia-Calvo M, Leonard RJ, Novick J, Stevens SP, Schmalhofer W, Kaczorowski GJ, Garcia ML (1993) Purification, characterization, and biosynthesis of margatoxin, a component of Centruroides margaritatus venom that selectively inhibits voltage-dependent potassium channels. *J Biol Chem* 268:18866-18874.

Gasser T, Muller-Myhsok B, Wszolek ZK, Oehlmann R, Calne DB, Bonifati V, Bereznai B, Fabrizio E, Vieregge P, Horstmann RD (1998) A susceptibility locus for Parkinson's disease maps to chromosome 2p13. *Nat Genet* 18:262-265.

Gerhard A, Pavese N, Hotton G, Turkheimer F, Es M, Hammers A, Eggert K, Oertel W, Banati RB, Brooks DJ (2006) *In vivo* imaging of microglial activation with [11C](R)-PK11195 PET in idiopathic Parkinson's disease. *Neurobiol Dis* 21:404-412.

Gingras M, Gagnon V, Minotti S, Durham HD, Berthod F (2007) Optimized protocols for isolation of primary motor neurons, astrocytes and microglia from embryonic mouse spinal cord. *J Neurosci Methods* 163:111-118.

Giulian D, Baker TJ (1986) Characterization of ameboid microglia isolated from developing mammalian brain. *J Neurosci* 6:2163-2178.

Godoy MC, Tarelli R, Ferrari CC, Sarchi MI, Pitossi FJ (2008) Central and systemic IL-1 exacerbates neurodegeneration and motor symptoms in a model of Parkinson's disease. *Brain* 131:1880-1894.

Goedert M (2001) α-synuclein and neurodegenerative diseases. *Nat Rev Neurosci* 2:492-501.

Goldberg MS, Lansbury PT, Jr. (2000) Is there a cause-and-effect relationship between α-synuclein fibrillization and Parkinson's disease? *Nat Cell Biol* 2:E115-E119.

Goldman SM, Tanner CM, Oakes D, Bhudhikanok GS, Gupta A, Langston JW (2006) Head injury and Parkinson's disease risk in twins. *Ann Neurol* 60:65-72.

Gosavi N, Lee HJ, Lee JS, Patel S, Lee SJ (2002) Golgi fragmentation occurs in the cells with prefibrillar α-synuclein aggregates and precedes the formation of fibrillar inclusion. *J Biol Chem* 277:48984-48992.

Green JD, Kreplak L, Goldsbury C, Li B, X, Stolz M, Cooper GS, Seelig A, Kistler J, Aebi U (2004) Atomic force microscopy reveals defects within mica supported lipid bilayers induced by the amyloidogenic human amylin peptide. *J Mol Biol* 342:877-887.

Griffin WS (2006) Inflammation and neurodegenerative diseases. *Am J Clin Nutr* 83:470S-474S.

Grissmer S, Nguyen AN, Aiyar J, Hanson DC, Mather RJ, Gutman GA, Karmilowicz MJ, Auperin DD, Chandy KG (1994) Pharmacological characterization of five cloned voltage-gated K^+ channels, types Kv1.1, 1.2, 1.3, 1.5, and 3.1, stably expressed in mammalian cell lines. *Mol Pharmacol* 45:1227-1234.

Guillemin G, Boussin FD, Croitoru J, Franck-Duchenne M, Le GR, Lazarini F, Dormont D (1997) Obtention and characterization of primary astrocyte and microglial cultures from adult monkey brains. *J Neurosci Res* 49:576-591.

Gutman GA, Chandy KG, Grissmer S, Lazdunski M, McKinnon D, Pardo LA, Robertson GA, Rudy B, Sanguinetti MC, Stuhmer W, Wang X (2005) International Union of Pharmacology. LIII. Nomenclature and molecular relationships of voltage-gated potassium channels. *Pharmacol Rev* 57:473-508.

Haasen D, Wolff M, Valler MJ, Heilker R (2006) Comparison of G-protein coupled receptor desensitization-related β-arrestin redistribution using confocal and non-confocal imaging. *Comb Chem High Throughput Screen* 9:37-47.

Halliday GM, McCann H (2010) The progression of pathology in Parkinson's disease. *Ann N Y Acad Sci* 1184:188-195.

Hamill OP, Marty A, Neher E, Sakmann B, Sigworth FJ (1981) Improved patch-clamp techniques for high-

resolution current recording from cells and cell-free membrane patches. *Pflugers Arch* 391:85-100.

Hamza TH, Zabetian CP, Tenesa A, Laederach A, Montimurro J, Yearout D, Kay DM, Doheny KF, Paschall J, Pugh E, Kusel VI, Collura R, Roberts J, Griffith A, Samii A, Scott WK, Nutt J, Factor SA, Payami H (2010) Common genetic variation in the HLA region is associated with late-onset sporadic Parkinson's disease. *Nat Genet* 42:781-785.

Hanisch UK, Kettenmann H (2007) Microglia: active sensor and versatile effector cells in the normal and pathologic brain. *Nat Neurosci* 10:1387-1394.

Hernan MA, Takkouche B, Caamano-Isorna F, Gestal-Otero JJ (2002) A meta-analysis of coffee drinking, cigarette smoking, and the risk of Parkinson's disease. *Ann Neurol* 52:276-284.

Hickey WF, Vass K, Lassmann H (1992) Bone marrow-derived elements in the central nervous system: an immunohistochemical and ultrastructural survey of rat chimeras. *J Neuropathol Exp Neurol* 51:246-256.

Hicks AA, Petursson H, Jonsson T, Stefansson H, Johannsdottir HS, Sainz J, Frigge ML, Kong A, Gulcher JR, Stefansson K, Sveinbjornsdottir S (2002) A susceptibility gene for late-onset idiopathic Parkinson's disease. *Ann Neurol* 52:549-555.

Hirsch EC, Breidert T, Rousselet E, Hunot S, Hartmann A, Michel PP (2003) The role of glial reaction and inflammation in Parkinson's disease. *Ann N Y Acad Sci* 991:214-228.

Horvath RJ, Nutile-McMenemy N, Alkaitis MS, De Leo JA (2008) Differential migration, LPS-induced cytokine, chemokine and NO expression in immortalized BV-2 and HAPI cell lines and primary microglial cultures. *J Neurochem* 107:557-569.

Hoyer W, Antony T, Cherny D, Heim G, Jovin TM, Subramaniam V (2002) Dependence of α-synuclein aggregate morphology on solution conditions. *J Mol Biol* 322:383-393.

Hoyer W, Cherny D, Subramaniam V, Jovin TM (2004) Rapid self-assembly of α-synuclein observed by *in situ* atomic force microscopy. *J Mol Biol* 340:127-139.

Huettner JE, Baughman RW (1986) Primary culture of identified neurons from the visual cortex of postnatal rats. *J Neurosci* 6:3044-3060.

Hunot S, Dugas N, Faucheux B, Hartmann A, Tardieu M, Debre P, Agid Y, Dugas B, Hirsch EC (1999) FcepsilonRII/CD23 is expressed in Parkinson's disease and induces, *in vitro*, production of nitric oxide and tumor necrosis factor-α in glial cells. *J Neurosci* 19:3440-3447.

Imbimbo BP (2009) An update on the efficacy of non-steroidal anti-inflammatory drugs in Alzheimer's disease. *Expert Opin Investig Drugs* 18:1147-1168.

Inoue K (2008) Purinergic systems in microglia. *Cell Mol Life Sci* 65:3074-3080.

Jakobsen LD, Jensen PH (2003) Parkinson's disease: α-synuclein and parkin in protein aggregation and the reversal of unfolded protein stress. *Methods Mol Biol* 232:57-66.

Jenner P, Olanow CW (2006) The pathogenesis of cell death in Parkinson's disease. *Neurology* 66:S24-S36.

Jensen PH, Islam K, Kenney J, Nielsen MS, Power J, Gai WP (2000) Microtubule-associated protein 1B is a component of cortical Lewy bodies and binds α-synuclein filaments. *J Biol Chem* 275:21500-21507.

Kaneko YS, Nakashima A, Mori K, Nagatsu T, Nagatsu I, Ota A (2009) Lipopolysaccharide extends the lifespan of mouse primary-cultured microglia. *Brain Res* 279:9-20.

Kask P, Palo K, Ullmann D, Gall K (1999) Fluorescence-intensity distribution analysis and its application in biomolecular detection technology. *Proc Natl Acad Sci U S A* 96:13756-13761.

Kask P, Palo K, Fay N, Brand L, Mets U, Ullmann D, Jungmann J, Pschorr J, Gall K (2000) Two-dimensional fluorescence intensity distribution analysis: theory and applications. *Biophys J* 78:1703-1713.

Kaushal V, Koeberle PD, Wang Y, Schlichter LC (2007) The Ca^{2+}-activated K^+ channel KCNN4/KCa3.1 contributes to microglia activation and nitric oxide-dependent neurodegeneration. *J Neurosci* 27:234-244.

Kawahara M, Kuroda Y, Arispe N, Rojas E (2000) Alzheimer's β-amyloid, human islet amylin, and prion protein fragment evoke intracellular free calcium elevations by a common mechanism in a hypothalamic GnRH neuronal cell line. *J Biol Chem* 275:14077-14083.

Kawanokuchi J, Mizuno T, Takeuchi H, Kato H, Wang J, Mitsuma N, Suzumura A (2006) Production of interferon-γ by microglia. *Mult Scler* 12:558-564.

Kayed R, Head E, Thompson JL, McIntire TM, Milton SC, Cotman CW, Glabe CG (2003) Common structure of soluble amyloid oligomers implies common mechanism of pathogenesis. *Science* 300:486-489.

Kayed R, Sokolov Y, Edmonds B, McIntire TM, Milton SC, Hall JE, Glabe CG (2004) Permeabilization of lipid bilayers is a common conformation-dependent activity of soluble amyloid oligomers in protein misfolding diseases. *J Biol Chem* 279:46363-46366.

Kayed R, Glabe CG (2006) Conformation-dependent anti-amyloid oligomer antibodies. *Methods Enzymol* 413:326-344.

Kennedy DW, Abkowitz JL (1997) Kinetics of central nervous system microglial and macrophage engraftment: analysis using a transgenic bone marrow transplantation model. *Blood* 90:986-993.

Kettenmann H, Hoppe D, Gottmann K, Banati R, Kreutzberg G (1990) Cultured microglial cells have a distinct pattern of membrane channels different from peritoneal macrophages. *J Neurosci Res* 26:278-287.

Kettenmann H, Banati R, Walz W (1993) Electrophysiological behavior of microglia. *Glia* 7:93-101.

Kettenmann H, Verkhratsky A (2008) Neuroglia: the 150 years after. *Trends Neurosci* 31:653-659.

Khanna R, Roy L, Zhu X, Schlichter LC (2001) K^+ channels and the microglial respiratory burst. *Am J Physiol Cell Physiol* 280:C796-C806.

Kiefer R, Lindholm D, Kreutzberg GW (1993) Interleukin-6 and transforming growth factor-β 1 mRNAs are induced in rat facial nucleus following motoneuron axotomy. *Eur J Neurosci* 5:775-781.

Kim YS, Joh TH (2006) Microglia, major player in the brain inflammation: their roles in the pathogenesis of Parkinson's disease. *Exp Mol Med* 38:333-347.

Kitada T, Asakawa S, Hattori N, Matsumine H, Yamamura Y, Minoshima S, Yokochi M, Mizuno Y, Shimizu N (1998) Mutations in the parkin gene cause autosomal recessive juvenile parkinsonism. *Nature* 392:605-608.

Kloss CU, Kreutzberg GW, Raivich G (1997) Proliferation of ramified microglia on an astrocyte monolayer: characterization of stimulatory and inhibitory cytokines. *J Neurosci Res* 49:248-254.

Koeberle PD, Schlichter LC (2010) Targeting K(V) channels rescues retinal ganglion cells *in vivo* directly and by reducing inflammation. *Channels (Austin)* 4:337-346.

Kotecha SA, Schlichter LC (1999) A Kv1.5 to Kv1.3 switch in endogenous hippocampal microglia and a role in proliferation. *J Neurosci* 19:10680-10693.

Kreutzberg GW (1996) Microglia: a sensor for pathological events in the CNS. *Trends Neurosci* 19:312-318.

Kruger R, Kuhn W, Muller T, Woitalla D, Graeber M, Kosel S, Przuntek H, Epplen JT, Schols L, Riess O (1998) Ala30Pro mutation in the gene encoding α-synuclein in Parkinson's disease. *Nat Genet* 18:106-108.

Kullberg S, Aldskogius H, Ulfhake B (2001) Microglial activation, emergence of ED1-expressing cells and clusterin upregulation in the aging rat CNS, with special reference to the spinal cord. *Brain Res* 899:169-186.

Lang AE, Lozano AM (1998) Parkinson's disease. Second of two parts. *N Engl J Med* 339:1130-1143.

Lang AE, Lozano AM (1998) Parkinson's disease. First of two parts. *N Engl J Med* 339:1044-1053.

Langston JW, Forno LS, Tetrud J, Reeves AG, Kaplan JA, Karluk D (1999) Evidence of active nerve cell degeneration in the *substantia nigra* of humans years after 1-methyl-4-phenyl-1,2,3,6-tetrahydropyridine exposure. *Ann Neurol* 46:598-605.

Langston JW (2002) Parkinson's disease: current and future challenges. *Neurotoxicology* 23:443-450.

Lannuzel A, Ruberg M, Michel PP (2008) Atypical parkinsonism in the Caribbean island of Guadeloupe: etiological role of the mitochondrial complex I inhibitor annonacin. *Mov Disord* 23:2122-2128.

Lashuel HA, Hartley D, Petre BM, Walz T, Lansbury PT, Jr. (2002) Neurodegenerative disease: amyloid pores from pathogenic mutations. *Nature* 418:291.

Lashuel HA, Petre BM, Wall J, Simon M, Nowak RJ, Walz T, Lansbury PT, Jr. (2002) α-synuclein, especially the Parkinson's disease-associated mutants, forms pore-like annular and tubular protofibrils. *J Mol Biol* 322:1089-1102.

Lashuel HA, Grillo-Bosch D (2005) *In vitro* preparation of prefibrillar intermediates of amyloid-β and α-synuclein. *Methods Mol Biol* 299:19-33.

Lashuel HA, Lansbury PT, Jr. (2006) Are amyloid diseases caused by protein aggregates that mimic bacterial pore-forming toxins? *Q Rev Biophys* 39:167-201.

Lavedan C, Dehejia A, Pike B, Dutra A, Leroy E, Ide SE, Root H, Rubenstein J, Boyer RL, Chandrasekharappa S, Makalowska I, Nussbaum RL, Polymeropoulos MH (1998) Contig map of the Parkinson's disease region on 4q21-q23. *DNA Res* 5:19-23.

Lawson LJ, Perry VH, Dri P, Gordon S (1990) Heterogeneity in the distribution and morphology of microglia in the normal adult mouse brain. *Neuroscience* 39:151-170.

Lee HJ, Choi C, Lee SJ (2002) Membrane-bound α-synuclein has a high aggregation propensity and the ability to seed the aggregation of the cytosolic form. *J Biol Chem* 277:671-678.

Lee HJ, Patel S, Lee SJ (2005) Intravesicular localization and exocytosis of α-synuclein and its aggregates. *J Neurosci* 25:6016-6024.

Lee SC, Liu W, Brosnan CF, Dickson DW (1994) GM-CSF promotes proliferation of human fetal and adult microglia in primary cultures. *Glia* 12:309-318.

Leroy E, Boyer R, Auburger G, Leube B, Ulm G, Mezey E, Harta G, Brownstein MJ, Jonnalagada S, Chernova T, Dehejia A, Lavedan C, Gasser T, Steinbach PJ, Wilkinson KD, Polymeropoulos MH (1998) The ubiquitin pathway in Parkinson's disease. *Nature* 395:451-452.

Levin J, Bertsch U, Kretzschmar H, Giese A (2005) Single particle analysis of manganese-induced prion protein aggregates. *Biochem Biophys Res Commun* 329:1200-1207.

Lewy FH (1912) *Handbuch der Neurologie* 3:920-933.

Li F, Lu J, Wu CY, Kaur C, Sivakumar V, Sun J, Li S, Ling EA (2008) Expression of Kv1.2 in microglia and its putative roles in modulating production of proinflammatory cytokines and reactive oxygen species. *J Neurochem* 106:2093-2105.

Liu B (2006) Modulation of microglial pro-inflammatory and neurotoxic activity for the treatment of Parkinson's disease. *AAPS J* 8:E606-E621.

Liu S, Ninan I, Antonova I, Battaglia F, Trinchese F, Narasanna A, Kolodilov N, Dauer W, Hawkins RD, Arancio O (2004) α-Synuclein produces a long-lasting increase in neurotransmitter release. *EMBO J* 23:4506-4516.

Long-Smith CM, Sullivan AM, Nolan YM (2009) The influence of microglia on the pathogenesis of Parkinson's disease. *Prog Neurobiol* 89:277-287.

Malipiero UV, Frei K, Fontana A (1990) Production of hemopoietic colony-stimulating factors by astrocytes. *J Immunol* 144:3816-3821.

Manyam BV, Sanchez-Ramos JR (1999) Traditional and complementary therapies in Parkinson's disease. *Adv Neurol* 80:565-574.

Maroteaux L, Campanelli JT, Scheller RH (1988) Synuclein: a neuron-specific protein localized to the nucleus and presynaptic nerve terminal. *J Neurosci* 8:2804-2815.

Masliah E, Rockenstein E, Veinbergs I, Mallory M, Hashimoto M, Takeda A, Sagara Y, Sisk A, Mucke L (2000) Dopaminergic loss and inclusion body formation

in α-synuclein mice: implications for neurodegenerative disorders. *Science* 287:1265-1269.

Mason RP, Trumbore MW, Pettegrew JW (1996) Molecular membrane interactions of a phospholipid metabolite. Implications for Alzheimer's disease pathophysiology. *Ann N Y Acad Sci* 777:368-373.

Mattson MP, Chan SL (2001) Dysregulation of cellular calcium homeostasis in Alzheimer's disease: bad genes and bad habits. *J Mol Neurosci* 17:205-224.

McCarty MF (2006) Down-regulation of microglial activation may represent a practical strategy for combating neurodegenerative disorders. *Med Hypotheses* 67:251-269.

McGeer PL, Itagaki S, McGeer EG (1988) Expression of the histocompatibility glycoprotein HLA-DR in neurological disease. *Acta Neuropathol* 76:550-557.

McGeer PL, Yasojima K, McGeer EG (2002) Association of interleukin-1 β polymorphisms with idiopathic Parkinson's disease. *Neurosci Lett* 326:67-69.

McGeer PL, Schwab C, Parent A, Doudet D (2003) Presence of reactive microglia in monkey *substantia nigra* years after 1-methyl-4-phenyl-1,2,3,6-tetrahydropyridine administration. *Ann Neurol* 54:599-604.

McLean PJ, Hyman BT (2002) An alternatively spliced form of rodent α-synuclein forms intracellular inclusions *in vitro*: role of the carboxy-terminus in α-synuclein aggregation. *Neurosci Lett* 323:219-223.

McNaught KS, Olanow CW (2003) Proteolytic stress: a unifying concept for the etiopathogenesis of Parkinson's disease. *Ann Neurol* 53 Suppl 3:S73-S84.

Menteyne A, Levavasseur F, Audinat E, Avignone E (2009) Predominant functional expression of Kv1.3 by activated microglia of the hippocampus after *Status epilepticus*. *PLoS ONE* 4:e6770.

Mir M, Tolosa L, Asensio VJ, Llado J, Olmos G (2008) Complementary roles of tumor necrosis factor α and interferon γ in inducible microglial nitric oxide generation. *J Neuroimmunol* 204:101-9.

Moussaud S, Lamodiere E, Savage C, Draheim HJ (2009) Characterisation of K^+ currents in the C8-B4 microglial cell line and their regulation by microglia activating stimuli. *Cell Physiol Biochem* 24:141-152.

Moussaud S, Draheim HJ (2010) A new method to isolate microglia from adult mice and culture them for an extended period of time. *J Neurosci Methods* 187:243-253.

Muller WE, Koch S, Eckert A, Hartmann H, Scheuer K (1995) β-Amyloid peptide decreases membrane fluidity. *Brain Res* 674:133-136.

Najim al-Din AS, al-Kurdi A, Dasouki M, Wriekat AL, al-Khateeb M, Mubaidin A, al-Hiari M (1994) Autosomal recessive ataxia, slow eye movements and psychomotor retardation. *J Neurol Sci* 124:61-66.

Nimmerjahn A, Kirchhoff F, Helmchen F (2005) Resting microglial cells are highly dynamic surveillants of brain parenchyma *in vivo*. *Science* 308:1314-1318.

Norenberg W, Gebicke-Haerter PJ, Illes P (1994) Voltage-dependent potassium channels in activated rat microglia. *J Physiol* 475:15-32.

Nuscher B, Kamp F, Mehnert T, Odoy S, Haass C, Kahle PJ, Beyer K (2004) α-synuclein has a high affinity for packing defects in a bilayer membrane: a thermodynamics study. *J Biol Chem* 279:21966-21975.

Okochi M, Walter J, Koyama A, Nakajo S, Baba M, Iwatsubo T, Meijer L, Kahle PJ, Haass C (2000) Constitutive phosphorylation of the Parkinson's disease associated α-synuclein. *J Biol Chem* 275:390-397.

Orlova EV, Rahman MA, Gowen B, Volynski KE, Ashton AC, Manser C, van HM, Ushkaryov YA (2000) Structure of α-latrotoxin oligomers reveals that divalent cation-dependent tetramers form membrane pores. *Nat Struct Biol* 7:48-53.

Paisan-Ruiz C, *et al.* (2004) Cloning of the gene containing mutations that cause PARK8-linked Parkinson's disease. *Neuron* 44:595-600.

Pankratz N, Nichols WC, Uniacke SK, Halter C, Murrell J, Rudolph A, Shults CW, Conneally PM, Foroud T (2003) Genome-wide linkage analysis and evidence of gene-by-gene interactions in a sample of 362 multiplex Parkinson disease families. *Hum Mol Genet* 12:2599-2608.

Pannasch U, Farber K, Nolte C, Blonski M, Yan CS, Messing A, Kettenmann H (2006) The potassium channels Kv1.5 and Kv1.3 modulate distinct functions of microglia. *Mol Cell Neurosci* 33:401-411.

Park JY, Lansbury PT, Jr. (2003) β-synuclein inhibits formation of α-synuclein protofibrils: a possible therapeutic strategy against Parkinson's disease. *Biochemistry* 42:3696-3700.

Park KW, Lee HG, Jin BK, Lee YB (2007) Interleukin-10 endogenously expressed in microglia prevents lipopolysaccharide-induced neurodegeneration in the rat cerebral cortex *in vivo*. *Exp Mol Med* 39:812-819.

Parkinson J (2002) An essay on the shaking palsy. 1817. *J Neuropsychiatry Clin Neurosci* 14:223-236.

Polymeropoulos MH, Lavedan C, Leroy E, Ide SE, Dehejia A, Dutra A, Pike B, Root H, Rubenstein J, Boyer R, Stenroos ES, Chandrasekharappa S, Athanassiadou A, Papapetropoulos T, Johnson WG, Lazzarini AM, Duvoisin RC, Di IG, Golbe LI, Nussbaum RL (1997) Mutation in the α-synuclein gene identified in families with Parkinson's disease. *Science* 276:2045-2047.

Pountney DL, Voelcker NH, Gai WP (2005) Annular α-synuclein oligomers are potentially toxic agents in α-synucleinopathy. Hypothesis. *Neurotox Res* 7:59-67.

Prinz M, Kann O, Draheim HJ, Schumann RR, Kettenmann H, Weber JR, Hanisch UK (1999) Microglial activation by components of gram-positive and -negative bacteria: distinct and common routes to the induction of ion channels and cytokines. *J Neuropathol Exp Neurol* 58:1078-1089.

Raivich G, Bohatschek M, Kloss CU, Werner A, Jones LL, Kreutzberg GW (1999) Neuroglial activation repertoire in the injured brain: graded response, molecular mechanisms and cues to physiological function. *Brain Res Brain Res Rev* 30:77-105.

Ramirez A, Heimbach A, Grundemann J, Stiller B, Hampshire D, Cid LP, Goebel I, Mubaidin AF, Wriekat AL, Roeper J, Al-Din A, Hillmer AM, Karsak M, Liss B,

Woods CG, Behrens MI, Kubisch C (2006) Hereditary parkinsonism with dementia is caused by mutations in ATP13A2, encoding a lysosomal type 5 P-type ATPase. *Nat Genet* 38:1184-1191.

Rochet JC, Conway KA, Lansbury PT, Jr. (2000) Inhibition of fibrillization and accumulation of prefibrillar oligomers in mixtures of human and mouse α-synuclein. *Biochemistry* 39:10619-10626.

Rozovsky I, Finch CE, Morgan TE (1998) Age-related activation of microglia and astrocytes: *in vitro* studies show persistent phenotypes of aging, increased proliferation, and resistance to down-regulation. *Neurobiol Aging* 19:97-103.

Schilling T, Quandt FN, Cherny VV, Zhou W, Heinemann U, DeCoursey TE, Eder C (2000) Upregulation of Kv1.3 K^+ channels in microglia deactivated by TGF-β. *Am J Physiol Cell Physiol* 279:C1123-C1134.

Schilling T, Nitsch R, Heinemann U, Haas D, Eder C (2001) Astrocyte-released cytokines induce ramification and outward K^+ channel expression in microglia *via* distinct signalling pathways. *Eur J Neurosci* 14:463-473.

Schilling T, Eder C (2003) Effects of kinase inhibitors on TGF-β induced upregulation of Kv1.3 K^+ channels in brain macrophages. *Pflugers Arch* 447:312-315.

Schilling T, Eder C (2007) Ion channel expression in resting and activated microglia of hippocampal slices from juvenile mice. *Brain Res* 1186:21-28.

Schmidtmayer J, Jacobsen C, Miksch G, Sievers J (1994) Blood monocytes and spleen macrophages differentiate into microglia-like cells on monolayers of astrocytes: membrane currents. *Glia* 12:259-267.

Schulte T, Schols L, Muller T, Woitalla D, Berger K, Kruger R (2002) Polymorphisms in the interleukin-1 α and β genes and the risk for Parkinson's disease. *Neurosci Lett* 326:70-72.

Sedgwick JD, Schwender S, Imrich H, Dorries R, Butcher GW, ter M, V (1991) Isolation and direct characterization of resident microglial cells from the normal and inflamed central nervous system. *Proc Natl Acad Sci U S A* 88:7438-7442.

Sierra A, Gottfried-Blackmore AC, McEwen BS, Bulloch K (2007) Microglia derived from aging mice exhibit an altered inflammatory profile. *Glia* 55:412-424.

Singleton AB, *et al.* (2003) α-Synuclein locus triplication causes Parkinson's disease. *Science* 302:841.

Spillantini MG, Schmidt ML, Lee VM, Trojanowski JQ, Jakes R, Goedert M (1997) α-synuclein in Lewy bodies. *Nature* 388:839-840.

Strauss KM, Martins LM, Plun-Favreau H, Marx FP, Kautzmann S, Berg D, Gasser T, Wszolek Z, Muller T, Bornemann A, Wolburg H, Downward J, Riess O, Schulz JB, Kruger R (2005) Loss of function mutations in the gene encoding Omi/HtrA2 in Parkinson's disease. *Hum Mol Genet* 14:2099-2111.

Streit WJ, Xue QS (2009) Life and Death of Microglia. *J Neuroimmune Pharmacol* 4:371-379.

Takahashi T, Yamashita H, Nakamura T, Nagano Y, Nakamura S (2002) Tyrosine 125 of α-synuclein plays a critical role for dimerization following nitrative stress. *Brain Res* 938:73-80.

Tambuyzer BR, Ponsaerts P, Nouwen EJ (2008) Microglia: gatekeepers of central nervous system immunology. *J Leukoc Biol* 85:352-370.

Tansey MG, Frank-Cannon TC, McCoy MK, Lee JK, Martinez TN, McAlpine FE, Ruhn KA, Tran TA (2008) Neuroinflammation in Parkinson's disease: is there sufficient evidence for mechanism-based interventional therapy? *Front Biosci* 13:709-717.

Tsigelny IF, Bar-On P, Sharikov Y, Crews L, Hashimoto M, Miller MA, Keller SH, Platoshyn O, Yuan JX, Masliah E (2007) Dynamics of α-synuclein aggregation and inhibition of pore-like oligomer development by β-synuclein. *FEBS J* 274:1862-1877.

Ueda K, Fukushima H, Masliah E, Xia Y, Iwai A, Yoshimoto M, Otero DA, Kondo J, Ihara Y, Saitoh T (1993) Molecular cloning of cDNA encoding an unrecognized component of amyloid in Alzheimer disease. *Proc Natl Acad Sci U S A* 90:11282-11286.

Uversky VN, Li J, Fink AL (2001) Metal-triggered structural transformations, aggregation, and fibrillation of human α-synuclein. A possible molecular NK between Parkinson's disease and heavy metal exposure. *J Biol Chem* 276:44284-44296.

Valente EM, *et al.* (2004) Hereditary early-onset Parkinson's disease caused by mutations in PINK1. *Science* 304:1158-1160.

Valeva A, Pongs J, Bhakdi S, Palmer M (1997) Staphylococcal α-toxin: the role of the N-terminus in formation of the heptameric pore -- a fluorescence study. *Biochim Biophys Acta* 1325:281-286.

Vicente R, Escalada A, Villalonga N, Texido L, Roura-Ferrer M, Martin-Satue M, Lopez-Iglesias C, Soler C, Solsona C, Tamkun MM, Felipe A (2006) Association of Kv1.5 and Kv1.3 contributes to the major voltage-dependent K^+ channel in macrophages. *J Biol Chem* 281:37675-37685.

Villalonga N, Escalada A, Vicente R, Sanchez-Tillo E, Celada A, Solsona C, Felipe A (2007) Kv1.3/Kv1.5 heteromeric channels compromise pharmacological responses in macrophages. *Biochem Biophys Res Commun* 352:913-918.

Volles MJ, Lee SJ, Rochet JC, Shtilerman MD, Ding TT, Kessler JC, Lansbury PT, Jr. (2001) Vesicle permeabilization by protofibrillar α-synuclein: implications for the pathogenesis and treatment of Parkinson's disease. *Biochemistry* 40:7812-7819.

Volles MJ, Lansbury PT, Jr. (2002) Vesicle permeabilization by protofibrillar α-synuclein is sensitive to Parkinson's disease-linked mutations and occurs by a pore-like mechanism. *Biochemistry* 41:4595-4602.

Wallace AJ, Stillman TJ, Atkins A, Jamieson SJ, Bullough PA, Green J, Artymiuk PJ (2000) *E. coli* hemolysin E (HlyE, ClyA, SheA): X-ray crystal structure of the toxin and observation of membrane pores by electron microscopy. *Cell* 100:265-276.

Weintraub D, Comella CL, Horn S (2008) Parkinson's disease--Part 1: Pathophysiology, symptoms, burden, diagnosis, and assessment. *Am J Manag Care* 14:S40-S48.

Weintraub D, Comella CL, Horn S (2008) Parkinson's disease--Part 2: Treatment of motor symptoms. *Am J Manag Care* 14:S49-S58.

Weintraub D, Comella CL, Horn S (2008) Parkinson's disease--Part 3: Neuropsychiatric symptoms. *Am J Manag Care* 14:S59-S69.

Whitton PS (2007) Inflammation as a causative factor in the aetiology of Parkinson's disease. *Br J Pharmacol* 150:963-976.

Wolff M, Haasen D, Merk S, Kroner M, Maier U, Bordel S, Wiedenmann J, Nienhaus GU, Valler M, Heilker R (2006) Automated high content screening for phosphoinositide 3 kinase inhibition using an AKT 1 redistribution assay. *Comb Chem High Throughput Screen* 9:339-350.

Wood SJ, Wypych J, Steavenson S, Louis JC, Citron M, Biere AL (1999) α-synuclein fibrillogenesis is nucleation-dependent. Implications for the pathogenesis of Parkinson's disease. *J Biol Chem* 274:19509-19512.

Wooten GF, Currie LJ, Bovbjerg VE, Lee JK, Patrie J (2004) Are men at greater risk for Parkinson's disease than women? *J Neurol Neurosurg Psychiatry* 75:637-639.

Wu CY, Kaur C, Sivakumar V, Lu J, Ling EA (2009) Kv1.1 expression in microglia regulates production and release of proinflammatory cytokines, endothelins and nitric oxide. *Neuroscience* 158:1500-1508.

Xie Z, Morgan TE, Rozovsky I, Finch CE (2003) Aging and glial responses to lipopolysaccharide *in vitro*: greater induction of IL-1 and IL-6, but smaller induction of neurotoxicity. *Exp Neurol* 182:135-141.

Xu X, Kim JA, Zuo Z (2008) Isoflurane preconditioning reduces mouse microglial activation and injury induced by lipopolysaccharide and interferon-γ. *Neuroscience* 154:1002-1008.

Yavich L, Tanila H, Vepsalainen S, Jakala P (2004) Role of α-synuclein in presynaptic dopamine recruitment. *J Neurosci* 24:11165-11170.

Ye SM, Johnson RW (2001) An age-related decline in interleukin-10 may contribute to the increased expression of interleukin-6 in brain of aged mice. *Neuroimmunomodulation* 9:183-192.

Yip PK, Kaan TK, Fenesan D, Malcangio M (2009) Rapid isolation and culture of primary microglia from adult mouse spinal cord. *J Neurosci Methods* 183:223-37.

Yokoyama A, Yang L, Itoh S, Mori K, Tanaka J (2004) Microglia, a potential source of neurons, astrocytes, and oligodendrocytes. *Glia* 45:96-104.

Zarranz JJ, Alegre J, Gomez-Esteban JC, Lezcano E, Ros R, Ampuero I, Vidal L, Hoenicka J, Rodriguez O, Atares B, Llorens V, Gomez TE, del ST, Munoz DG, de Yebenes JG (2004) The new mutation, E46K, of α-synuclein causes Parkinson and Lewy body dementia. *Ann Neurol* 55:164-173.

Zemanova L, Schenk A, Hunt N, Nienhaus GU, Heilker R (2004) Endothelin receptor in virus-like particles: ligand binding observed by fluorescence fluctuation spectroscopy. *Biochemistry* 43:9021-9028.

Zhang W, Wang T, Pei Z, Miller DS, Wu X, Block ML, Wilson B, Zhang W, Zhou Y, Hong JS, Zhang J (2005) Aggregated alpha-synuclein activates microglia: a process leading to disease progression in Parkinson's disease. *FASEB J* 19:533-542.

Zimprich A, *et al.* (2004) Mutations in LRRK2 cause autosomal-dominant parkinsonism with pleomorphic pathology. *Neuron* 44:601-607.

Zlokovic BV (2008) The blood-brain barrier in health and chronic neurodegenerative disorders. *Neuron* 57:178-201.

VI. Appendices

The enclosed CD contains my publications with supplemental materials, my PhD report and my curriculum vitae.